Organometallic and Metal-amide Precursors for Transition Metal and Lanthanide Cluster Complexes with Interesting Electronic and Magnetic Properties

A thesis submitted to The University of Manchester for the degree of Doctor of Philosophy in the Faculty of Engineering and Physical Sciences

Daniel Nathan Woodruff

2012

The School of Chemistry

Table of Contents

List of Figures

List of Schemes

List of Tables

Abstract

This project exploited the Brönsted basicity of the organometallic/metal-amide compounds, $MnCp_2$ and $Ln[N(SiMe_3)_2]_3{\cdot}LiCl(THF)_3$ (Ln = Gd, Tb and Dy) in attempts to synthesize polymetallic cluster compounds via deprotonation of X-H (X = N or S) bond containing pro-ligands. The chemical, electronic and magnetic properties of the resulting compounds were studied with a variety of methods.

The reaction of $Ln[N(SiMe_3)_2]_3{\cdot}LiCl(THF)_3$ (Ln = Gd, Tb and Dy) with EtSH yields a series of $[\{Ln(N(SiMe_3)_2)(\mu_2\text{-}SEt)_2\}_4(\mu_3\text{-}SEt)][Li(THF)_4]$ "Ln_4" squares in which the terbium and dysprosium analogues show SMM behaviour in zero field, with the dysprosium analogue displaying a fast relaxation process which can be "switched off" by the application of a 2000 Oe external field.

Reactions of $MnCp_2$ with $Me_3SiNP(NHR)_3$ (R = ^{n}Pr, Cy, ^{t}Bu) afforded a series of compounds; $[CpMn\{Me_3SiN{=}P(NH^nPr)_2(\mu\text{-}N^nPr)\}]_2$, $[Mn\{Me_3SiN{=}P(NHCy)_2(NCy)\}_2]$ and $[CpMn\{Me_3SiN{=}P(NH^tBu)_2(N^tBu)\}]$. Q-band EPR studies of these complexes reveal that altering the R group attached to the ligand causes a variation in coordination geometry around the manganese centers and as such alters the electronic properties of the manganese centres present in each complex.

In order to avoid the synthesis of potentially unstable organometallic/metal-amide precursors, one pot synthetic methodologies were developed to allow the isolation a series of μ_8-oxo centred Li_7M cubes $[ML_{i7}(\mu_8\text{-}O)(\mu\text{-}hpp)_6]^+$ (M = Co, Mn and Zn). Addition of stiochiometric amounts of water to the initial reaction mixture produced the Li_7M cubes in high yields.

Extension of the one pot synthetic strategy to the use of $DyCl_3$ and $YbCl_3$ in reactions with Li-TMP (TMP = 2,2,6,6-tetramethylpipiridine) afforded the lanthanide dimers $[Ln(TMP)_2(\mu\text{-}OEt)]_2$ (Ln = Dy and Yb) in which the EtO^- ligands were formed via *in situ* ether cleavage and the dysprosium analogue shows SMM behaviour under a 7000Oe applied field.

Declaration

No portion of the work referred to in the thesis has been submitted in support of an application for another degree or qualification of this or any other university or other institute of learning.

Copyright Statement

Acknowledgments

Firstly I would like to thank both Dr. Richard Layfield and Prof. Richard Winpenny for their continued support and guidance throughout my PhD and for giving me the opportunity to pursue a PhD in inorganic chemistry. I would also like to thank Prof. Eric McInnes and Prof. David Collison for their advice and useful insights into my work and for treating me with patience when I couldn't quite grasp a few things. My thanks also go to Dr. Floriana Tuna and Dan Sells for all their help with SQUID and EPR, and Dr. Robin Pritchard and Dr. Chris Muryn for teaching me crystallography and putting up with my stupid questions. I would also like to thank everyone in the office and lab for making it and incredibly enjoyable and interesting place to work.

My most heartfelt thanks go to my family and friends, especially my mother and father, Bruce and Jean Woodruff who have always believed in me, supported me and given me the drive to always do the best I can and I'd like to thank my brother, Dean Woodruff, who has always been there if I needed anything. I would also like to thank my grandparents who have always believed in me. Thanks to my friends Ben and Joe who have always managed to steer me in the right direction and make every opportunity for fun a good one. All my other friends who are too many to mention, I would also like to thank, for making the time I'm away from lab, the most enjoyable I could imagine.

Finally I would like to thank Sophia Solomon, whom without I would not be where I am today. She has always believed in me and put up with what at times seems like an endless stream of stupidity on my part better than I could ever have believed anyone could. For her and everyone in my life, I am very grateful for everything.

Chapter 1: Introduction

1.1 Rationale for submitting an alternative format thesis

The thesis author has been extremely fortunate in having the opportunity and ability to publish his results in peer reviewed journals over the course of his research. The timely publication of results is critical in this field for two main reasons. Firstly the field of magnetically interesting molecules is ever changing and so getting up-to-date research in the public domain is of high importance. Secondly the research is equipment intensive and access to sought after national services (e.g. EPSRC National EPR Facility) is dependent on high quality research, demonstrated by publication in high impact journals. It has therefore been preferable to publish during the course of the author's research. The published papers cover all of the author's work and are deemed suitable for submission as part of this thesis.

1.2 Organisation of thesis

Chapter one provides a preface to this thesis and describes the relevant author contributions on published and in preparation papers. Chapter two reviews the field of lanthanide single molecule magnets to-date. Chapter three outlines the aims of the research undertaken. Chapters four to seven contain peer-reviewed publications and manuscripts in preparation. Chapter eight provides a summary of the work undertaken and an outlook on future work. Chapter nine contains general experimental considerations. Chapter ten contains references that are cited outside of chapters four to seven.

1.3 Author Contributions

Chapter 4, Paper 1, “Single-molecule magnetism in thiolate-bridged terbium and dysprosium squares” is a draft paper written by the thesis author. Syntheses were performed by thesis author. X-ray crystallography was performed by the thesis author. SQUID measurements were performed by Dr. Floriana Tuna and simulations of data were performed by Dr. Floriana Tuna and in part by the thesis author.

Chapter 5, Paper 2, “Single Molecule Magnets (SMMs) from ether cleavage: A Dy(III) dimer SMM formed from in situ solvent cleavage” is a draft paper written by the thesis author. Syntheses were performed by the thesis author. X-ray crystallography was performed in part by Dr. Robin Pritchard and in part by the thesis author. SQUID measurements were performed by Dr. Floriana Tuna and simulations of data were performed by Dr. Floriana Tuna and in part by the thesis author.

Chapter 6, Paper 3, “Synthesis, Structure and Paramagnetism of Manganese(II) Iminophosphate Complexes” is a full paper written by the thesis author. Syntheses were performed by the thesis author. X-ray crystallography was performed by the thesis author and in part by Dr. Madeleine Helliwel. EPR measurements were performed by Daniel Sells. EPR spectra simulations were performed by the thesis author. ^{1}H and ^{13}C NMR spectra were recorded by the thesis author.

Chapter 7, Paper 4, “Synthesis and structure of cationic guanidinate-bridged bimetallic $\{Li_7M\}$ cubes (M = Mn, Co, Zn) with inverse crown counter anions” is a full paper written by Dr. Richard Layfield and in part by the thesis author. Syntheses were performed by the thesis author. X-ray crystallography was performed in part by Dr. Michael Bodensteiner and in part by the thesis author. EPR measurements and simulations were performed by Daniel Sells. ^{1}H, ^{7}Li and ^{13}C NMR spectra were recorded by the thesis author.

Chapter 2: Review of Lanthanide SMMs

Lanthanide Single Molecule Magnets (SMMs): A Review

1. Introduction

1.1 Overview

A decade has passed since the discovery of Ishikawa's double decker phthalocyaninate lanthanide compounds [1] and their ability to show slow relaxation of magnetization at temperatures up to 40 K. This is the signature of a single molecule magnet (SMM) occurring at temperatures much higher than any previously discovered *d*-block metal containing SMM.[1] As a consequence, interest in lanthanide based SMMs has exploded and has led to a diverse range of complexes exhibiting slow relaxation of magnetisation being isolated, using a huge variety of chemistry. Attempts to increase the height of the barrier to reversal of magnetization, U_{eff}, have been met with varying levels of success with the highest barrier of U_{eff} = 550cm^{-1} belonging to a version of Ishikawa's original [{Pc(OEt$_8$)}$_2$Tb]$^-$ complex (where Pc = phthalocyaninate) in which ethoxide groups are attached to the phthalocyaninate ligand in the 2,3,9,10,16,17,23 and 24 positions.[2]

These new lanthanide SMMs cover a remarkably large range of nuclearities ranging from single lanthanide centers (sometimes called, misleadingly, single ion magnets, SIMS) to polymetallic clusters. The ligands used to form lanthanide SMMs range from classic "hard" *O*- and *N*-donor ligands to the more unconventional and exotic ligands such as radicals, [3] calixarenes [4] and polyoxometallates.[5] This diversity has lead to over one hundred and fifty lanthanide SMMs being reported to date. These complexes form the beginnings of

a library that may allow an insight into the effects both ligand environment as well as local geometry round the metal centre play on the ability of a lanthanide containing molecule to behave as an SMM.

After Ishikawa's initial discovery in 2003, a number of different pathways were taken with a large amount of work being done in the area of changing the properties of the phthalocyaninate ligands attached to the lanthanide metal center to alter the properties of the molecule as a whole.[2,6] Other areas of research included designing specific ligands to create clusters of lanthanide atoms,[7] including *in situ* reactions to form ligands to complex to lanthanide metal centers.[8] However, recently attempts have been made to try and increase the interaction between lanthanide centers either by changing the bridging atoms to try and get a better orbital overlap,[9] or using radical ligands to achieve the same effect.[3,10] Research into more "classical" ligands is still the major focus of the field at present.

Herein we report a comprehensive overview of the field of lanthanide SMMs up to the end of July 2012, including their synthesis, structural and magnetic properties. Compounds will be first split by lanthanide nuclearity and then by complexing ligand chosen. We only include SMMs based exclusively on 4f-metal ions, and do not include the growing body of work on 3d-4f-metal complexes. We have also chosen to include all papers that claim to have made 4f-SMMs for sake of completeness, however we discuss the validity of these claims and suggest criteria for that a complex is an SMM in the concluding section.

1.2 Why Lanthanides?

For a complex to show slow relaxation of magnetization it must have a large thermal energy barrier to relaxation. This arises from a large anisotropy of the magnetic ground state of the

molecule in question. In 3d-metal SMMs the requirements are a significant spin, *S*, in the ground state, and significant easy axis anisotropy of that state, parameterized as an axial zero-field splitting, *D*. The energy barrier, for integer spin systems, is then given by DS^2. For *S* to be sufficiently large it is necessary to bring together multiple paramagnetic metal centres, giving a large spin ground state arising from ferro-magnetic or ferri-magnetic arrangements of the spins. For an SMM the splitting of the ground state *S* into individual M_s levels is the key to an SMM with a high energy barrier. This is often related to the anisotropy of the individual spin centres within the spin cage, and also to the relative orientations of anisotropy axes on the individual centres. The 3d-SMMs with the highest U_{eff} have *S* around 10, and *D* between 0.5 and 0.9 cm^{-1}.[11]

In lanthanide complexes it is the individual ions that are of most interest. The f-orbitals have almost complete degeneracy and this leads to an unquenched orbital moment which must be taken into account when considering the electronic structures of f-elements.[12] The ground states of the ions must be defined in terms of the total angular momentum, *J*, rather than the spin angular momentum only, as in 3d-block ions (notable exceptions include cobalt). For the lanthanides after gadolinium $J = S + L$ for the lowest energy term, and this leads to ground states with large *J* and large magnetic moments. [13,14a] It is the splitting of this ground state term into individual M_J levels that leads to the energy barrier U_{eff} and hence it is the factors that control this splitting are key in deciding the magnitude of U_{eff} in 4f-SMMs.[15]

Although the magnitude of U_{eff} can (usually) be much larger for 4f complexes, quantum tunnelling can severely hinder the ability of a 4f complex to act as a SMM. This is due to quantum tunnelling of the relaxation of magnetisation through the barrier and as such

negating the barrier height. As quantum tunnelling is a low energy process, it can dominate the relaxation of magnetisation in 4f complexes. [14b]

For 4f-elements the spin-orbit coupling energy is larger than the effect of crystal fields and thus instead of the spin-orbit coupling perturbing the crystal field, the opposite is true. This means that the local crystal field in which the lanthanide ion is situated can have a minor but significant effect on the electronic structure of the lanthanide ion. It is the interaction of the crystal field with the ground state that removes the $2J + 1$ degeneracy of the ground state, and the crystal field decides on the ordering and energy gaps between the various M_J states, which in turn influence the magnetic properties of the lanthanide ion. This means that the relaxation behaviour of the 4f-SMMs is strongly dependent on the local crystal field.[12]

The dependence of the magnetic properties of lanthanide ions on the local crystal field has lead to the use of a number of different ligand systems in order to create lanthanide SMMs. It is apparent that the nature of the donor atoms involved are important, as well as the symmetry of the crystal field. Indeed, as will be seen below, which 4f-ion will lead to SMM behaviour can change dramatically with a change of ligand set. This phthalocyanines provide the best example: they are the only family of 4f-SMMs where the Tb(III) complexes show the highest $U_{eff.}$

The continued investigation into lanthanide SMMs is driven by the potential future applications they can be applied to. Quantum computing and information storage are amongst the most significant and continue to entice chemists to synthesize complexes which show SMM behaviour at temperatures at which “everyday” technology can operate. [16e]

2. Monometallic Lanthanide SMMs

Table 1 includes every monometallic lanthanide SMM reported from 2003 to the end of July 2012; the structures of non-trivial ligands featured in these complexes are given in Scheme 1.

Table 1. Monometallic lanthanide SMMs from 2003 to present with the reported values of U_{eff} (cm^{-1})

Compound	Compound Number	U_{eff} (cm^{-1})	Reference
$(^{t}Bu_4N)[Pc_2Tb]$	1	230	1
$(^{t}Bu_4N)[Pc_2Dy]$	2	31	1a + 1b
$[Pc_2Tb]^0$	3	410	17
$[Dy(obPc)_2]$	4	44	6b
$[H][Dy(oCNPc)_2]$	5	40	6a
[Dy(Pc)(TCIPP)]	6	16	18
$[Dy\{Pc(\alpha\text{-}OC_5H_4)_4\}(TCIPP)]$	7	30	18
$[DyH\{Pc(\alpha\text{-}OC_5H_4)_4\}(TCIPP)]$	8	40	18
$[Tb\{Pc^*\}_2]$ slow cooled	9	480	6c
$[Tb\{Pc^*\}_2]$ fast cooled	9	422	6c
$[\{Pc(OEt_8)_2\}Tb]^+(SbCl_6)^-$	10	550	2
$(^{n}Bu_4N)[\{Pc(OEt_8)_2\}Tb]$	11	509	2
$[\{Pc(OEt_8)_2\}Dy](SbCl_6)$	12	55	6d
$(^{n}Bu_4N)[\{Pc(OEt_8)_2\}Dy]$	13	27	6d
$[K(DME)_2][Dy(tmtaa)_2]$	14	20	21
[K(DME)(18-crown-6)][Dy(tmtaa)$_2$]	15	24	21
$[Dy(acac)_3(H_2O)_2]$	16	47	22
$[Dy(bpy)(TTA)_3]$	17	40	23
$[Dy(phen)(TTA)_3]$	18	59	23
$[Dy(phen)(acac)_3]$	19	44	24
$[Dy(NTA)_3(L^1)]$	20	21	25

$[Dy(FTA)_3(L^2)]$	21	38	26
$[Dy(TTA)_3(L^3)]$	22	29	27
$(NEt_4)_3[Dy(dipic)_3]\cdot H_2O$	23	not measurable	28
$(NEt_4)_3[Er(dipic)_3]\cdot H_2O$	24	not measurable	28
$Na[Dy(DOTA)(H_2O)]\cdot 4H_2O$	25	42	29
$[Dy(H_3L^4)_2](NO_3)\cdot EtOH\cdot 8H_2O$	26	42	30
$[Dy(COT'')_2Li(THF)(DME)]$	27	30	31
[Dy(Cp*)(COT)]	28	25	32
[Ho(Cp*)(COT)]	29	5	32
[Er(Cp*)(COT)]	30	225	32
$Na_9[Er(W_5O_{18})_2]\cdot xH_2O$	31	38	5
$Na_9[Ho(W_5O_{18})_2]\cdot xH_2O$	32	not measureable	5a
$K_{13}[Dy(\beta_2\text{-}SiW_{11}O_{39})_2]$	33	not measureable	5a
$K_{13}[Ho(\beta_2\text{-}SiW_{11}O_{39})_2]$	34	not measureable	5a
$K_{13}[Er(\beta_2\text{-}SiW_{11}O_{39})_2]$	35	not measureable	5a
$K_{13}[Yb(\beta_2\text{-}SiW_{11}O_{39})_2]$	36	not measureable	5a
$[Dy(acac)_3(NIT\text{-}2Py)]\cdot 0.5(NIT\text{-}2Py)$	37	15	33e
$[Tb(hfac)_3(NIT\text{-}2Py)]\cdot 0.5(C_7H_{16})$	38	12	33c
$[Dy(hfac)_3(NIT\text{-}2Py)]\cdot 0.5(C_7H_{16})$	39	not measurable	33c
$[Tb(NIT\text{-}2Py\text{-}CO_2^-)_3]\cdot 6H_2O$	40	16	33d
$[Tb(hfac)_3(NITPhOEt)_2]$	41	20	33a
$[Tb(hfac)_3(NITPhSCH_3)_2]$	42	not measurable	33b
$[Tb(TCNQF_4)_2(H_2O)_6](TCNQF_4)\cdot 3H_2O$	43	5	34
$[Tb(hfac)_3(IM\text{-}2Py)]$	44	not measurable	35

[Tb(hfac)$_3$(IM-2thz)]	45	not measurable	35

L^1H_2 = 1,2-diphenylethane-1,2-diamine

Pc = Phthalocyaninate

TCIPP = meso-tetrakis-(4-chlorophenyl)porphyrinate

Pc(α-$OC_5H_4)_4$ = 1,8,15,22-tetrakis(3-pentyloxy)phthalocyaninate

DME = dimethoxyethane

TTA = 2-thenoyltrifluoroacetonate

bpy = 2,2'-bipyridine

phen = 1,10-phenanthroline

hfac = hexafluoro-acetyl acetonate

acac = acetyl acetone

oCNPc = 2, 3, 9, 10, 16, 17, 23,24-octacyanophthalocyanine

Cp* = $C_5Me_5^-$

COT = $C_8H_8^{2-}$

obPc = dianion of 2, 3, 9, 10, 16, 17,23, 24-octabutoxy-phthalocyanine

FTA = 2-furyltrifluoro-acetonate

COT'' = 1,4-bis(trimethylsilyl)cyclooctatetraenyl dianion

Pc* = dianion 2, 3, 9, 10, 16, 17, 23,24-octakis-((S)-2-(dodecyloxy)propoxy)-phthalocyanine

Pc(OEt_8) = dianion of 2, 3, 9, 10, 16, 17, 23,24-octaethoxyphthalocyanine

dipic = pyridine-2,6-dicarboxylate

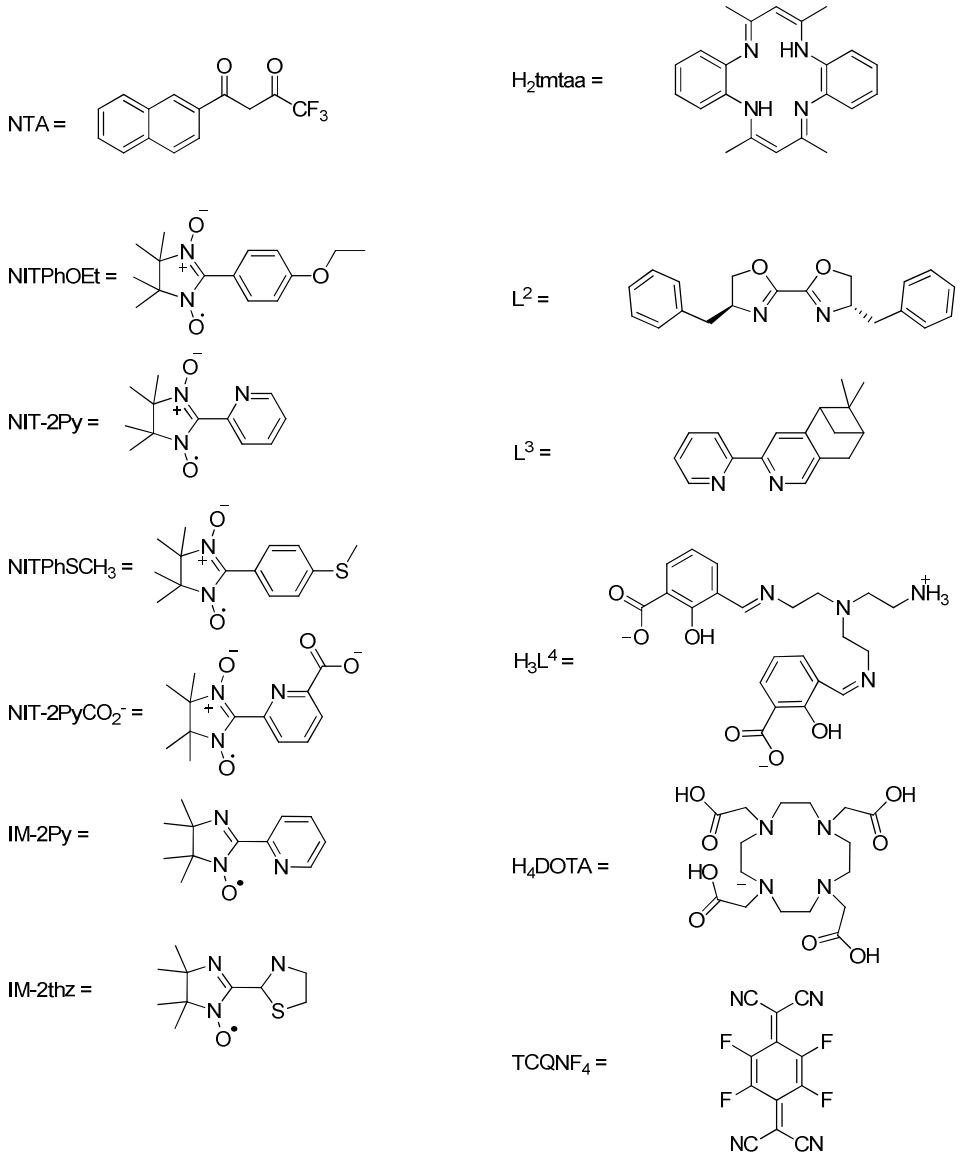

Scheme 1. Chemical structures of non trivial ligands used to produce monometallic lanthanide SMMs.

To date the highest barriers to reversal of magnetization belong to monometallic SMMs, namely phthalocyaninate complexes of lanthanides.[1] The monometallic SMMs also play an important role in our understanding of the effects that ligand field can have on a lanthanide metal centre and whether it shows slow relaxation of magnetization.

2.1 Phthalocyanines

Since the initial report of ($^{t}Bu_4N$)[$LnPc_2$](Ln = Tb, Dy, Ho, Er, Tm and Yb, Pc = phthalocyaninate) (Figure 1) showing SMM behavior,[1] a large amount of research has focused on modifying these molecules to improve their properties and to create derivatives that will bind to surfaces.[1]

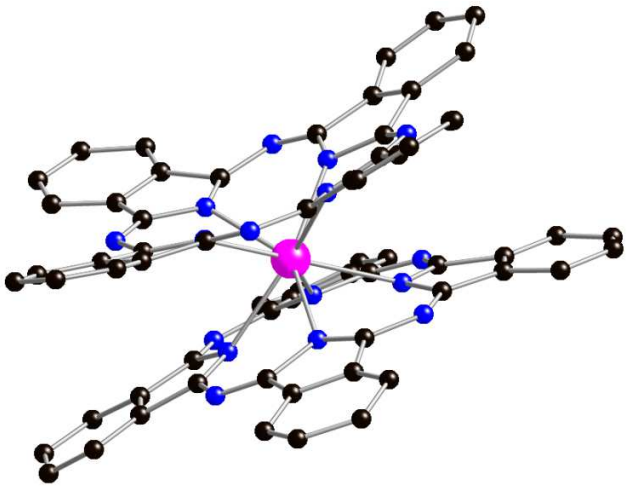

Figure 1. Solid state structure of $[LnPc_2]^-$ (Ln = Tb, Dy, Ho, Er, Tm, Yb). All hydrogen atoms have been omitted for clarity. Black = Carbon, blue = Nitrogen and Magneta = Lanthanide

The $[LnPc_2]^-$ complexes contain one lanthanide centre in the +3 oxidation state sandwiched between to dianions of phthalocyanine with four nitrogen atoms from each Pc^{2-} bonding to the lanthanide metal centre. This gives the lanthanide centre a local coordination environment with C_{4v} symmetry.[1] The symmetry of the environment around the lanthanide centre and the effect it has on the property of the SMM has been the subject of a number of reviews and so will not be discussed further here.[16] The synthesis of this class of compounds requires rigorous purification steps to ensure a magnetically pure sample as $[LnPc_2]^0$ impurities also behave as SMMs.[1]

The Tb(III) and Dy(III) derivatives of (^{t}Bu$_4$N)[LnPc$_2$] (compounds **1** and **2** respectively) show slow relaxation of magnetization as shown by the frequency dependency of the out of phase AC susceptibility (χ_M'') in an oscillating AC field of 3.5G (Figure 2).[1]

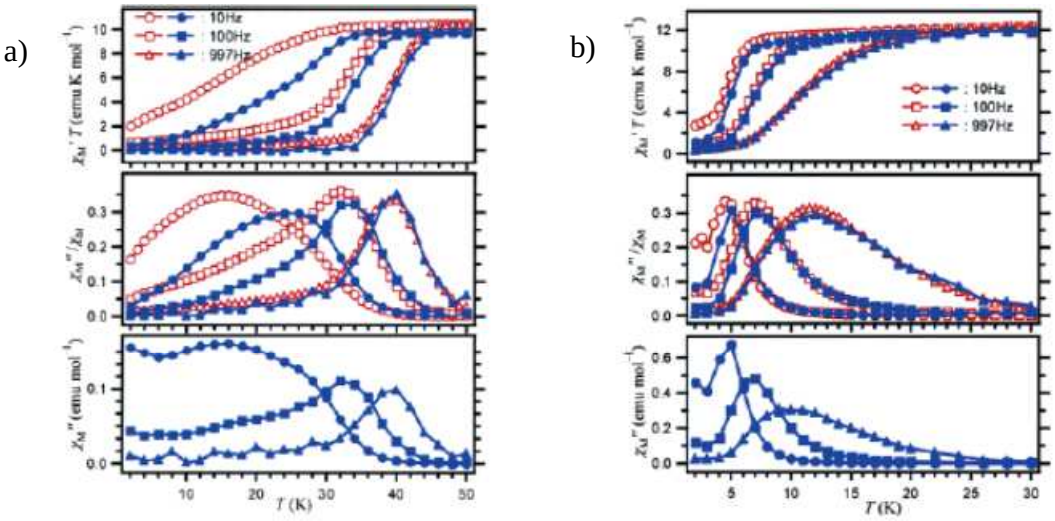

Figure 2. a) Plots of (top) χ_M'*T*, (middle) χ_M''/χ_M and (bottom) χ_M' 'against temperature *T*, where χ_M', χ_M'', and χ_M are in-phase-AC, out-of-phase-AC, and DC molar magnetic susceptibilities, respectively, for a powder sample of 1 (open marks) and that diluted in (^{t}Bu$_4$N)[Pc$_2$Y] (filled marks) measured in a 3.5G AC magnetic field oscillating at indicated frequencies. b) Plots of (top) χ_M'*T*, (middle) χ_M''/χ_M and (bottom) χ_M'' against temperature *T*, for a powder sample of 2 (open marks) and that diluted in (^{t}Bu$_4$N)[Pc$_2$Y] (filled marks) measured in a 3.5G AC magnetic field oscillating at indicated frequencies.

Standard Arrhenius analysis of the data for **1** and **2** using the equation $\tau = \tau_0 \exp(U_{eff}/k_BT)$ (where τ = relaxation time at a given frequency, τ_0 = relaxation time of system in the absence of an oscillating magnetic field, U_{eff} = energy barrier to relaxation of magnetization, k_B = Boltzmann constant and T = temperature) gives U_{eff} values of 230 cm^{-1} and 28 cm^{-1}respectively. The height of the barrier for **1** is almost four times larger than that of [Mn$_6$O$_2$(sao)$_6$(O$_2$CH)$_2$(MeOH)$_4$] (H$_2$sao = 2-hydroxybenzaldehyde oxime) which has U_{eff} = 60 cm^{-1} (the highest value of U_{eff} for a pure 3d metal system).[11]

After this initial discovery, other similar compounds were tested for their ability to show slow relaxation. These include the neutral [$TbPc_2$]**3**,[17] [$Dy(obPc)_2$]**4**,[6b] (obPc = dianion of 2,3,9,10,16,17,23,24-octabutoxyphthalocyanine) and the mono-anionic $[Dy(oCNPc)_2]^-$ **5** [6a] (dianion 2,3,9,10,16,17,23,24-octacyanophthalocyanine) which showed U_{eff} values of 410 cm^{-1}, 44 cm^{-1} and 40 cm^{-1} respectively. Other complexes studied include [Dy(Pc)(TCIPP)] **6**,[18] [Dy{$Pc(\alpha\text{-}OC_5H_4)_4$}(TCIPP)] **7** [18] and [DyH{$Pc(\alpha\text{-}OC_5H_4)_4$}(TCIPP)] **8** [18] ({$Pc(\alpha\text{-}OC_5H_4)_4$} = 1,8,15,22-tetrakis(3-pentyloxy)phthalocyaninate, TCIPP = meso-tetrakis-(4-chlorophenyl)porphyrinate) in which one Pc ligand is replaced with a porphyrin in order to investigate the relationship between twist angle Φ (defined as the rotation angle of one coordination square away from the eclipsed conformation to the other, 45 ° for ideal D_{4d} symmetry) and SMM behaviour. The difference in values of U_{eff} = 16, 30 and 40 cm^{-1} for **6, 7** and **8** respectively can be rationalized by looking at the twist angles of the complexes.[18]

The justification for the almost two-fold increase in U_{eff} from complex **1** to complex **3** has been explained by considering the splitting of the ground state energy levels by the ligand field potential within the complex.[17] The ligand field potential splits the ground multiplet ($^7F_6$) so that the lowest sub-level has the largest J_z value (J_z = ±6) and large energy gaps from the rest of the sublevels (*ca*. 400 cm^{-1}).[19] This condition then leads to a small probability of the transition between J_z = 6 and -6 sub-states, and hence a slow magnetization response.[17]

Other modified forms of the [$LnPc_2$] compounds include [$Tb(Pc^*))_2$] **9** (where Pc* = dianion 2,3,9,10,16,17,23,24-octakis-((S)-2-(dodecyloxy)propoxy)-phthalocyanine), in which long chiral alkyl chain “arms” are attached to the phthalocyanine.[6c] This gives **9** the

ability to act as a liquid crystal at room temperature whilst behaving as an SMM at low temperatures. The rate of cooling of the sample affects the height of the barrier to reversal of magnetization. Quenching a sample quickly to 150 K gives a disordered phase, $\mathbf{9_{dis}}$, which after analysis was found to have U_{eff} = 422 cm^{-1} whilst heating the same sample and cooling at a slower controlled rate gives an ordered crystalline sample, $\mathbf{9_{cr}}$, which has U_{eff} = 480 cm^{-1}.[6c] The differences in U_{eff} for $\mathbf{9_{dis}}$ and $\mathbf{9_{cr}}$ are attributed to changes in the molecular confirmation brought about by the phase change within a given sample. This in turn alters the intensity and symmetry of the off-diagonal anisotropy terms present in the spin Hamiltonian which causes a change in U_{eff}.[6c]

The phthalocyaninate complexes with the largest U_{eff} values (of any SMM) are [{$Pc(OEt)_8$}$_2$Tb][$SbCl_6$] **10** and ($^nBu_4N$)[{$Pc(OEt)_8$}$_2$Tb] **11** which have U_{eff} = 550 and 509 cm^{-1} respectively.[2,6d] This 2.5 fold increase in U_{eff} from **1** to **10** is attributed to a longitudinal contraction of the coordination space of the lanthanide centre caused by a two-electron oxidation of the starting complex. As the HOMO of the [$LnPc_2$] complexes is antibonding,[20] removal of two electrons from the HOMO increase bond strengths within the complex and thus reduces the inter-planar distance between the two Pc ligands. This then increases the multiplet ground state splitting which in turn increases the barrier to reversal of magnetization.[2,6d]

A similar but lower symmetry ligand (compared to Pc) has also been used to isolate two monometallic dysprosium SMMs in the form of [K(DME)2][Dy(tmtaa)$_2$] **14** [21] and [K(DME)(18-crown-6)][Dy(tmtaa)$_2$] **15** [21] (tmtaaH_2 =6,8,15,17-tetramethyldibenzotetraaza[14]annulene, DME = dimethoxyethane). With this ligand the highest symmetry possible at the dysprosium center is only C_{2v} and as such the ground state

level splitting gives rise to smaller barrier to reversal of magnetization with U_{eff} = 20 (**14**) and 24 cm^{-1} (**15**).[21]

2.2 Alcohols, Ketones and Acids

These types of *O*-donor ligands make up a large number of monometallic SMMs, and are normally used to complete a coordination sphere of a monometallic lanthanide complex. The simplest example is $[Dy(acac)_3(H_2O)_2]$ **16** (acac = acetylacetone) [22] which contains three bidentate diketones bound to the dysprosium centre and two capping water molecules. Complex **16** shows frequency dependency of χ_M'' at temperatures up to 15K and has U_{eff} = 47 cm^{-1} with hysteresis being observed up to 2 K.[22]

There are several examples where a single lanthanide center is surrounded by three bidentate diketonates and one bidentate *N*-donor ligand, and subtle changes in the ligand environment of these compounds leads to changes in their magnetic properties. For example the three complexes $[Dy(TTA)_3(bpy)]$ **17**,[23] $[Dy(TTA)_3(phen)]$ **18** [23] and $[Dy(acac)_3(phen)]$ **19** [24] (TTA =2-thenoyltrifluoroacetonate, bpy = 2,2'-bipyridine and phen = 1,10-phenanthroline) all show SMM behaviour and are structurally very similar. However the height of the barriers for these compounds vary with U_{eff} = 40, **17**; 59, **18** and 44 cm^{-1}**19**. These differences can be explained by examination of the crystal structures of **17** – **19**. The coordinating atoms in **17** – **19** each form a slightly distorted polyhedron with local D_{4d} symmetry around the dysprosium centers.[23,24] The level of distortion can be quantified by looking at the twist angle, Φ, (45 ° for ideal D_{4d} symmetry) and the magic angle, α, (angle between the S_8 axis and Dy-L vector, 54.74 ° for ideal D_{4d} symmetry). Compound **18** has Φ

= 42.1 ° and α = 57.2 °, which makes it more symmetric than either **17**(where Φ = 39.7 °) or **19** (where α = 58.3 °); it appears a higher symmetry produces an increased value of U_{eff}.[23,24]

The use of chiral *N*-donor capping ligands in conjunction with β-diketonates has also led to monometallic lanthanide SMMs: $[Dy(NTA)_3(L^1)]$ **20**,[25] $[Dy(FTA)_3(L^2)]$ **21** [26] and $[Dy(TTA)_3(L^3)]$ **22** [27] (NTA = 4,4,4-trifluoro-1-(naphthalen-2-yl)butane-1,3-dione, FTA = 2-furyltrifluoro-acetonate, L^1H_2 = (1S,2S)-1,2-diphenylethane-1,2-diamine, L^2 = (S,S)-2,20-Bis(4-benzyl-2-oxazoline), L^3 = 4,5-pinenebipyridine) all contain chiral bidentate *N*-donor ligands and have U_{eff} = 21 cm^{-1}, 38 cm^{-1} and 29 cm^{-1} respectively.[25-27]

Combining the *N*- and *O*-donor atoms into one ligand has also led to the isolation of SMMs. Pyridine-2,6-dicarboxylate (dipic) has been used to create $[NEt_4]_3[Ln(dipic)_3]\cdot H_2O$ (Ln = Dy, **23** and Er, **24**) [28] in which three tridentate dipic ligands bind to a single lanthanide center. Complexes **23** and **24** show a rise in χ'' at temperatures below 3K, but no maximum is observed and hence the size of U_{eff} cannot be measured.[28]

Other ligands include the octadentate DOTA ligand (H_4DOTA = 1,4,7,10-tetraazacyclododecane-N,N',N'',N'''-tetraacetic acid) in which a *N*-donor macrocycle has four carboxylate "arms" which all bind to a single dysprosium centre in $Na[Dy(DOTA)(H_2O)]\cdot 4H_2O$ **25**.[29] The coordination sphere of **25** is capped by a single water molecule. Complex **25** has U_{eff} = 42 cm^{-1} and recent magnetic studies of single crystals have shown that the magnetic anisotropy axis of **25** lies almost perpendicular to the idealized C_4 symmetry axis, and that the single water molecule bound to the dysprosium center strongly influences the direction of the magnetic anisotropy axis.[29b] Another example is in $[Dy(H_3L^4)_2](NO_3)\cdot EtOH\cdot 8H_2O$ **26** [30] (L^4H_4 = 2,2'-{[(2-aminoethyl)imino]bis[2,1-

ethanediyl-nitriloethylidyne]}bis-2-hydroxy-benzoic acid) in which the nitrogen atoms of the ligand do not take part in the bonding due to their distance from the dysprosium centre. Complex **26** has U_{eff} = 42 cm^{-1}, however if a manganese source is present upon the formation of **26**, a new complex $(NHEt_3)_2[Dy\{Mn(L^4)\}_2](ClO_4)\cdot 2(H_2O)$ is formed in which no SMM behaviour can be observed.[30]

2.3 Organometallics

This class of monometallic SMMs contains only four examples, comprising of $[Dy(COT'')_2Li(THF)(DME)]$ (**27**) [31] (COT'' = 1,4-bis(trimethylsilyl)cyclooctatetraenyl dianion) and [Ln(Cp*)(COT)] (Ln = Dy, **28**; Ho, **29** and Er, **30**; Cp* = $C_5Me_5^-$, COT = $C_8H_8^{2-}$) (Figure 3).[32] Complex **27** has a U_{eff} = 30 cm^{-1} in an applied static field of 600 Oe.

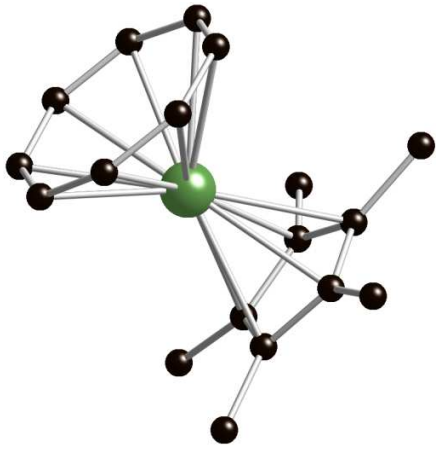

Figure 3. Structure of [Ln(Cp*)(COT)] (Ln = Dy, Ho, Er). All hydrogen atoms omitted for clarity. Green = Ln and Black = Carbon.

Complexes **28** – **30** are similar to Ishikawa's double decker $[LnPc_2]$ complexes in that they are sandwich complexes, however the ligands vary dramatically as can be seen by the nature of the ligand and the "tilt" angle in the complex (8 °) meaning that the Cp* and COT rings

aren't parallel to each other.[32] Also the presence of two dissimilar ligands means that the C_{4v} symmetry of the [$LnPc_2$] complexes is lost. Of note as well is that two conformers exist of **30** in the solid state as is evidenced by the disordered COT ring within the crystal structure (not shown in Figure 3). This then gives rise to two thermal activated relaxation process with U_{eff} = 225 cm^{-1} and 137 cm^{-1}. Only one thermally activated relaxation process is seen for **28** and **29** with U_{eff} = 25 cm^{-1} and 5 cm^{-1} respectively.[32]

2.4 Other Ligands

Monometallic lanthanide SMMs have been created using polyoxometallate ligands to give complexes such as $Na_9[Ln(W_5O_{18})_2]\cdot xH_2O$ (Ln = Er, **31** and Ho, **32**) [5] and $K_{13}[Ln(\beta_2\text{-}SiW_{11}O_{39})_2]$ (Ln = Dy, **33**; Ho, **34**; Er, **35** and Yb, **36**).[5a] Apart from the ligands used, complexes **31** – **36** are very similar in that they are sandwich complexes with two polyoxometallate ligands coordinating to each lanthanide center. Complex **31** is the only compound in this class to show slow relaxation of magnetization at a sufficient temperature for a barrier height to be calculated and has U_{eff} = 38 cm^{-1}. Complexes **32** – **36** show frequency dependency of χ_M'' but only at extremely low temperatures with no peak observed.[5]

More recently some groups have focused on using organic radical ligands to create monometallic lanthanide SMMs. The use of radical ligands mean the magnetic properties of the molecule are no longer the result of purely the lanthanide center but also the spin added to the molecule by the radical ligand.

The radical species successfully used in the formation are nitronyl nitroxide ligand radicals, NIT-X(X = 2Py, 2Py-CO_2^-, $PhSCH_3$, PhOEt) (Figure 4) [33] or the organic radical ligand $TCNQF_4$ ($TCNQF_4$ = tetrafluorotetracyanoquinodimethane radical).[34]

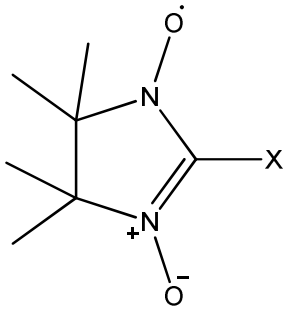

Figure 4. Structure of nitronyl nitroxide radical NIT-X

Complexes containing the NIT-2Py (2Py = 2-pyridyl) all show very similar structures, with each containing a single NIT-2Py radical ligand bound to the lanthanide centre through the nitrogen of the pyridine and the radical oxygen atom of the ligand. The coordination sphere is then completed by either three acac or hfac ligands each being bidentate (acac = acetyl acetonate, hfac = hexafluoro-acetylacetonate) to give $[Dy(acac)_3(NIT\text{-}2Py)]\cdot 0.5NIT\text{-}2Py$, **37** [33e] and $[Ln(hfac)_3(NIT\text{-}2Py)]\cdot 0.5(C_7H_{16})$ (Ln = Tb, **38** and Dy, **39**).[33c] Complexes **37** has U_{eff} = 15 cm^{-1} whilst **39** shows frequency dependency of χ_M'', but no peaks are seen and as such no barrier height can be determined. This is interesting as the only difference between the two complexes is the acetonate used to complete the lanthanide's coordination sphere. However the terbium analogue **38** shows a U_{eff} = 12 cm^{-1}.[33c,e] Addition of a carboxylic acid group to the pyridine ring of the radical ligand gives $[Tb(NIT\text{-}2Py\text{-}CO_2^-)_3]\cdot 6H_2O$, **40**.[33d] In **40** each ligand is tridentate and as such takes up the entire coordination sphere of the terbium ion present in **25** which has U_{eff} = 16 cm^{-1}.

$[Tb(hfac)_3(NIT\text{-}PhOEt)_2]$ (**41**) [33a] and $[Tb(hfac)_3(NIT\text{-}PhSCH_3)_2]$ (**42**) [33b] are almost structurally identical in that they both have two NIT-X ligands bound to the terbium centre via one oxygen atom and three hfac ligands each binding η^2 to the terbium centre to complete the coordination sphere. Despite this they behave differently magnetically. Complex **41** has U_{eff} = 20 cm^{-1} whilst **42** only shows frequency dependency of χ_M'' at very low temperatures (<4 K). This clearly demonstrates the subtle and not so subtle effects ligands can have on a complexes ability to show SMM behaviour.

Using the $TCNQF_4$ radical ligands has allowed the isolation of $[Tb(TCNQF_4)_2(H_2O)_6](TCNQF_4)\cdot 3H_2O$, **43** [34] which has a reported barrier height U_{eff} = 5 cm^{-1}. The terbium center in **43** is bonded to two $TCNQF_4$ ligands *via* one fluorine atom from each ligand. The remainder of the coordination sphere of the terbium ion in **43** is six water molecules. One observation of note is that upon dilution of **43** with the isostructural Y version, the value of U_{eff} decreases. This suggests that the magnetic behaviour seen for **43** is not single ion-based and is most likely due to larger aggregates within the solid state.[34]

Imino nitroxide radicals have also been used to created monometallic SMMs in the form of $[Tb(hfac)_3(IM\text{-}2Py)]$**44** and $[Tb(hfac)_3(IM\text{-}2thz)]$**45** [35] (see Scheme 1 for structures of ligands) in which three η^2 hfac ligands and one η^2 IM-2X ligand bind to a single terbium ion. Neither **44** nor **45** show maxima even at temperatures down to 2 K.[35]

3. Dimetallic 4f-SMMs

Table 2 shows all the dimeric lanthanide SMMs up to the end of July 2012; the non-trivial ligands used in these compounds are shown in Scheme 2.

Table 2. Dimeric lanthanide SMMs from 2003 to present with the reported values of U_{eff} (cm^{-1})

Compound	Compound Number	U_{eff} (cm^{-1})	Reference
$[Tb_2(obPc)_3]$	46	230	36
[(Pc)Tb(Pc)Tb(T(*p*-OMe)PP)]	47	not measurable	37
[(Pc)Y(Pc)Tb(T(*p*-OMe)PP)]	48	not measurable	37
[(Pc)Tb(Pc)Y(T(*p*-OMe)PP)]	49	not measurable	37
[(Pc)Tb(Pc)Tb(obPc)]	50	not measurable	38
[(Pc)Tb(Pc)Y(obPc)]	51	not measurable	38
[(Pc)Y(Pc)Tb(obPc)]	52	not measurable	38
$[Dy_2(ovph)_2(Cl)_2(MeOH)_3]\cdot MeCN$	53	138	39
$[Dy(ovph)_2(NO_3)_2(H_2O)_2]$	54	48	40
$[Dy_2(Hovph)(ovph)(NO_3)_2(H_2O)_4]\cdot(NO_3)\cdot 2MeOH\cdot 3H_2O$	55	1	40
$(NEt_4)_2[Dy_2(L^5)_4]\cdot 0.25(Me_2CO)$	56	9	41
$(NEt_4)_2[Dy_2(L^6)_4]\cdot H_2O\cdot 0.5DMF$	57	49	41
$[Dy_2(L^7)_4]\cdot 2Et_2O\cdot 1.5(Me_2CO)$	58	14	41
$[Dy_2(HL^8)_4(CO_3)]\cdot 4H_2O$	59	12	42
$[Dy_2(L^9)_2(NO_3)_2(MeOH)_2]\cdot 4MeCN$	60	29	42
$[Dy_2(hmi)_2(NO_3)_2(MeOH)_2]$	61	39	44
$[Dy_2(valdien)_2(NO_3)_2]$	62	53	7b
$[Dy_2(L^{10})_3]\cdot(ClO_4)_3\cdot 6MeOH$	63	3	45
$[Dy_2(L^{11})_2(acac)_2(H_2O)]\cdot 2\ CH_2Cl_2$	64	56	47
$[Dy_2(Acc)_4(H_2O)_8]\cdot Cl_6\cdot 5.89H_2O$	65	not measurable	48
$[Dy_2(3\text{-}Htzba)_2(3\text{-}tzba)_2(H_2O)_8]\cdot 4H_2O$	66	38	49
$[Dy_2(L^{12})_6(MeOH)_2(H_2O)_2]$	67	not measurable	50
$[(phen)_2Er_2(HCOO)_{4.2}(NO_3)_{1.8}]$	68	not measurable	51
$[Dy_2(phen)_2(L^{13})_6]\cdot 2H_2O$	69	20	52
$[Dy_2(phen)_2(L^{13})_6]$	70	4	52

$[Dy_2(hfac)_6(H_2O)_2(L^{14})]$	71	11	53
$[Dy_2(HBpz_3)_4(\mu\text{-ox})]\cdot 2MeCN\cdot CH_2Cl_2$	72	29	54
$[(\eta^5\text{-Cp})_2Dy(\mu\text{-Cl})]_2$	73	26	55
$[(\eta^5\text{-Cp})_2(THF)Dy(\mu\text{-Cl})]_2$	74	34	55
$[\{Cp_2Dy(\mu\text{-bta})\}_2]$	75	39	56
$[\{CpMe)_2Dy(\mu\text{-SSiPh}_3)\}_2]$	76	133	9
$[Tb(Phtfac)_3(NITpPy)]_2$	77	18	57
$[Dy(Phtfac)_3(NITpPy)]_2$	78	14	57
$[Dy(hfac)_3(NITpPy)]_2$	79	9	58
$[Dy(hfac)_3(NITmbis)]_2$	80	8	59
$[Tb(hfac)_3(NITpPy)]_2$	82	13	60
$[Tb(hfac)_3(NIT\text{-}5\text{-}Br\text{-}3Py)]_2$	83	20	61
$[K(18\text{-crown-}6)(THF)_2][\{[(Me_3Si)_2N]_2(THF)Tb\}_2(\mu\text{-}\eta^2\text{-}\eta^2\text{-}N_2)]$	84	227	3
$[K(18\text{-crown-}6)][\{[(Me_3Si)_2N]_2(THF)Dy\}_2(\mu\text{-}\eta^2\text{-}\eta^2\text{-}N_2)]$	85	123	10
$[Tb_2(L^{15})(NO_3)_2(DMF)_6]\cdot 2DMF$	86	not measurable	4
$[Dy_2(hfac)_6(H_2O)_4pz]\cdot 2pz$	87	77	62
$[\{Dy(TTA)_3(L^{16})\}_2]\cdot 0.5\ CH_2Cl_2$	88	61	63

pz = pyrazine

$L^{13}H$ = *β*-naphthoic acid

Acc = 1-aminocyclohexanel-carboxylic acid

HPhtfac = 4,4,4-trifluoro-1-phenylbutane-1,3-dione

$L^{12}H$ = *n*-butyric acid

$L^{15}H_4$ = *p*-tert-butylsulfonylcalix[4]arene

$HBpz_3^-$: hydrotris(pyrazolyl)borate

ox = oxalate

btaH = benzotriazole

(T(*p*-OMe)PP) = tetra-*p*-methoxyphenylporphyrinato

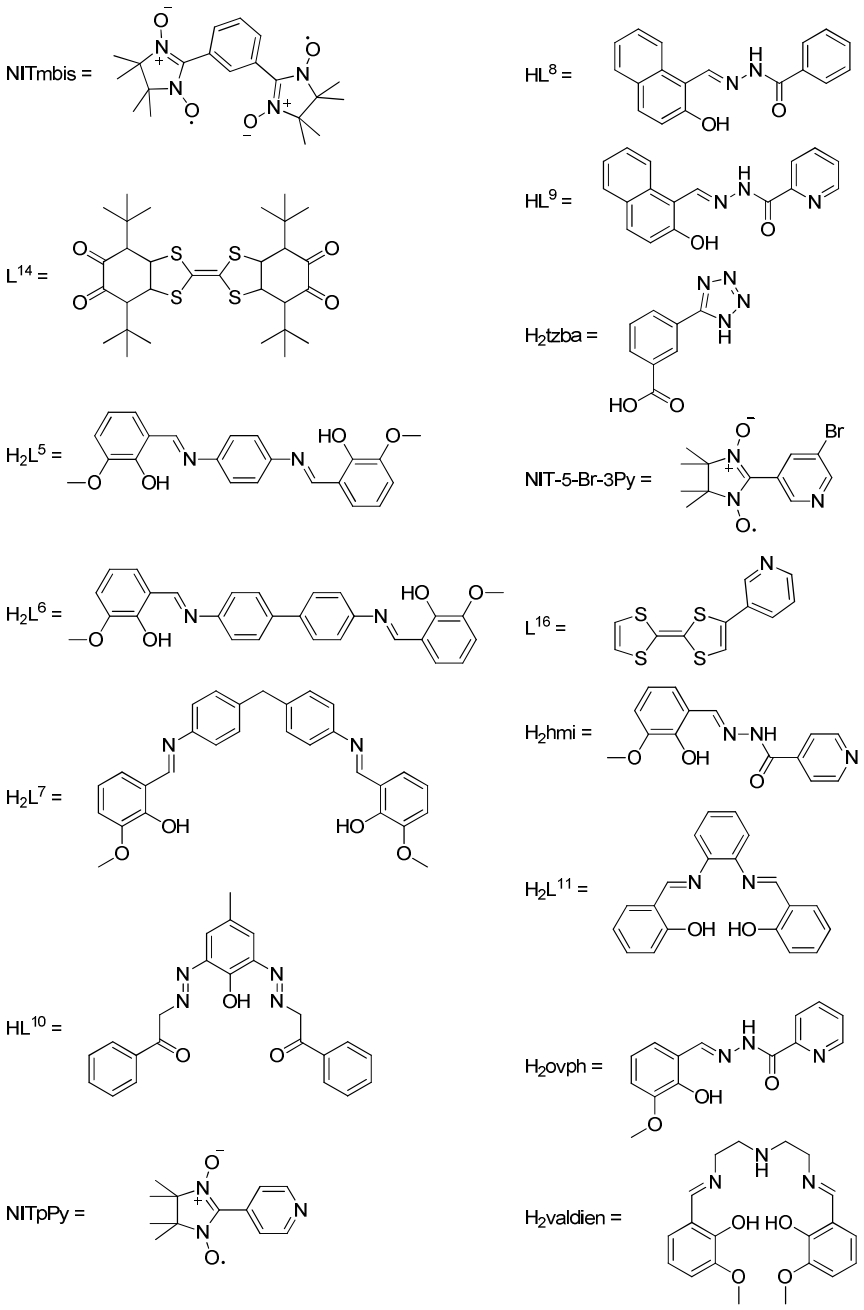

Scheme 2. Chemical structures of non-trivial ligands used to produce dimetallic lanthanide SMMs.

3.1 Phthalocyaninates

Extension of the original double-decker phthalocyaninate complexes by addition of an extra ligand (either phthalocyaninate or porphyrin) has led to the isolation of triple-decker SMMs

$[Tb_2(obPc)_3]$ **46**,[36] $[(Pc)Ln^1(Pc)Ln^2(T(p\text{-}OMe)PP)]$ ($Ln^1 = Ln^2$ = Tb **47**; Ln^1 = Y, Ln^2 = Tb **48**; Ln^1 = Tb, Ln^2 = Y **49**; (T(*p*-OMe)PP) = tetra-*para*-methoxyphenylporphyrinato) [37] and $[(Pc)Ln^1(Pc)Ln^2(obPc)]$ ($Ln^1 = Ln^2$ = Tb **50**; Ln^1 = Tb, Ln^2 = Y **51**; Ln^1 = Y, Ln^2 = Tb **52**).[38] Complex **46** contains two terbium ions sandwiched between three obPc ligands with the twist angle between the outer rings and central ring Φ = 32 °. This gives each terbium ion a pseudo four-fold axis perpendicular to the obPc rings. Complex **46** has U_{eff} = 230 cm^{-1} which is comparable to the double decker complex **1**.[1]

Complex **47** has two Pc ligands that are rotated by nearly 45 ° with respect on one another, giving one terbium ion a square anti-prismatic coordination site. On the other hand, coordinating nitrogen atoms of the central Pc and those of T(*p*-OMe)PP are in eclipsed positions, making a square prismatic coordination site around the second terbium ion. Complex **47** – **49** all show SMM behaviour and despite the two different coordination environments for the two terbium ions in **47**, only one relaxation process is seen for the complex as a whole.[37] This is in contrast to **50** in which two separate independent relaxation processes are observed in the out-of-phase magnetic susceptibility. These are attributed to the different coordination environments for the two terbium ions within the complex, and a weak f-f coupling interaction between the two terbium ions in **50**.[38]

3.2 Alcohols, Ketones and Acids

A large number of lanthanide SMM dimers contain *O*- and *N*-donor ligands. A common occurrence is ligand design to incorporate “pockets” within the ligand that bind specifically to lanthanide ions; there are eleven examples of lanthanide dimer SMMs incorporating ligands designed in this fashion.

The most successful attempt, in terms of the size of U_{eff}, is $[Dy_2(ovph)_2(Cl)_2(MeOH)_3]\cdot MeCN$ **53** (H_2ovph = o-vanillin picolinoylhydrazone) [39] and has U_{eff} = 138 cm^{-1}. Complex **53** has two bridging oxygen atoms (one from each $ovph^{2-}$ ligand) between the dysprosium centers which have different coordination environments (Figure 5).[39]

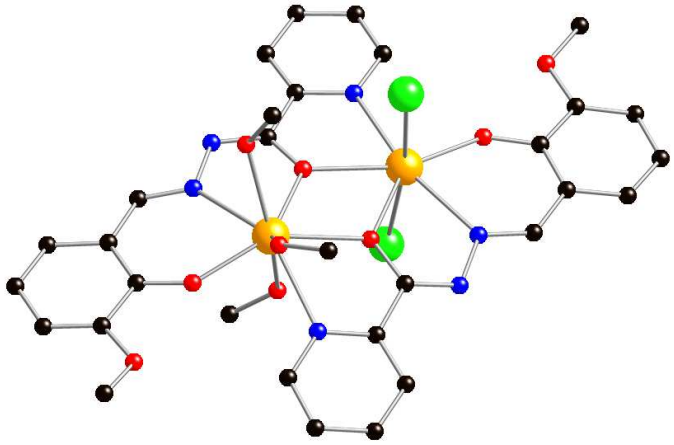

Figure 5. Crystal structure of 51. Hydrogen atoms omitted for clarity. Black = Carbon, Red = Oxygen, Blue = Nitrogen, Orange = Dysprosium and Green = Chlorine

At high temperatures (>11 K), the slow reversal of magnetization of **53** is attributed to the single ion anisotropy of the two individual dysprosium centers. This is supported by the presence of two relaxation times within the high temperature domain.[39]

Other lanthanide dimer SMMs containing the $ovph^{2-}$ ligand show much lower energy barriers with $[Dy_2(ovph)_2(NO_3)_2(H_2O)_2]$ **54** and $[Dy_2(Hovph)(ovph)(NO_3)_2(H_2O)_4]\cdot(NO_3)\cdot 2MeOH\cdot 3H_2O$ **55** [40] having U_{eff} = 1 cm^{-1} and 53 cm^{-1} respectively. In complex **54** two $ovph^{2-}$ ligands coordinate two dysprosium centers in an anti-parallel or "head-to-tail" fashion. The carbonyl oxygen atoms of the ligands bind in their conjugate deprotonated enol form and bridge the two dysprosium ions. The

coordination sphere of each dysprosium ion is then completed by one chelating nitrate ion and one methanol molecule.[40]

In contrast to **54**, the two ovph^{2-} ligands in **55** coordinate to the two dysprosium centers in a parallel fashion with one ligand having undergone a keto-enol tautomerism. The coordination sphere of each dysprosium ion is then completed by one water molecule and one chelating nitrate ion. The differences in the magnetic behaviour of **54** and **55** are attributed to the difference in coordination geometries around the dysprosium ions.[40]

An interesting trio of compounds is $(NEt_4)_2[Dy_2(L^5)_4]0.25(Me_2CO)$ **56**,[41] $(NEt_4)_2[Dy_2(L^6)_4]\cdot H_2O\cdot 0.5DMF$ **57** [41] and $[Dy_2(L^7)_4]\cdot 2Et_2O\cdot 1.5(Me_2CO)$ **58** [41] (DMF = Dimethylformamide, L^5H_2, L^6H_2 and L^7H_2 shown in Scheme 2) in which systematic variations in the ligands allow the comparison of magnetic properties.[41] Comparison of the length of the "linker" ligands (L^5 – L^7) in **56** – **58** shows that an increase in the linker length from 10.8 (L^5) to 14.9 (L^6) to 15.3 Å(L^7) results in a decrease in U_{eff} (70 in **56**; 49 in **57** and 14 cm^{-1} in **58**).[41] The change in SMM behaviour between **56**, **57** and **58** is attributed to small changes in coordination of the dysprosium ions within the complexes rather than due to interactions between the dysprosium centers.

Two complexes which again contain ligands with specific "pockets" to bind to lanthanide ions are $[Dy_2(HL^8)_4(CO_3)]\cdot 4H_2O$ **59** and $[Dy_2(L^9)_2(NO_3)_2(MeOH)_2]\cdot 4MeCN$ **60** (L^8H_2 = N′-((2-hydroxy-1-naphthyl)methylene)benzohydrazide, L^9H_2 shown in Scheme 2) and slight differences in the ligand lead to different reaction.[42] Complex **59** contains two dysprosium ions each bound to two tridentate HL^8 ligands and bridged by two phenoxido atoms (one each from two separate ligands) and by one 2.11-bridging carbonate ion.[43] In contrast **60** contains two L^9 ligands each binding two dysprosium ions in anti-parallel

fashion with the tridentate "pocket" binding to one dysprosium ion and the bidentate "pocket" binding to the other dysprosium ion.[42] Complex **59** has U_{eff} = 12 cm^{-1}, while **60** has U_{eff} = 29 cm^{-1} and the differences in these values are attributed to differences in coordination geometry around the dysprosium ions, brought about by the keto-enol tautomerism seen between HL^8 and L^9.[42]

$[Dy_2(hmi)_2(NO_3)_2(MeOH)_2]$ **61** [44] and $[Dy_2(valdien)_2(NO_3)_2]$ **62** [7b] ($hmiH_2$ = 2-hydroxy-3-methoxyphenyl)methylene (isonicotino)hydrazine, H_2ovph = o-vanillin picolinoylhydrazone) have similar structures but slightly different magnetic properties owing to the different coordination environments around the dysprosium ions within **61** and **62**. Complex **61** contains two dysprosium ions bridged by two phenoxide groups of two hmi^{2-} ligands with the remainder of the coordination sphere of each dysprosium ion occupied by oxygen and nitrogen atoms of the hmi ligand, one methanol molecule and one chelating nitrate ion. Complex **62** has a similar structure with two dysprosium ions being bridged by two phenoxo oxygen atoms (one from each $valdien^{2-}$ ligand) and the remainder of the coordination sphere of each dysprosium being taken up by oxygen and nitrogen atoms of the $valdien^{2-}$ ligand and one chelating nitrate ion. Complex **61** has U_{eff} = 39 cm^{-1} whilst **62** has U_{eff} = 53 cm^{-1}.[7b,44]

Lanthanide dimers with triple helicate architectures have recently been report to show SMM behaviour in the form of $[Dy_2(L^{10})_3]\cdot(ClO_4)_3\cdot 6MeOH$ (**63**) ($L^{10}H$ is shown in Scheme 2).[45] Complex **63** contains three ligands that twist along a pseudo-threefold axis defined by the two dysprosium ions. The two dysprosium ions have the same coordination environment with each one coordinated by six oxygen atoms and three nitrogen atoms of the ligands. Complex **63** shows frequency dependency of out of phase magnetic susceptibility

but no maxima down to temperatures of 2 K. As such, and estimation of $U_{eff} \approx 3$ cm^{-1} was calculated using the method previously used for the calculation of $\tau 0$ for Mn12 acetate .[45,46]

$[Dy_2(L^{11})_2(acac)_2(H_2O)]\cdot 2CH_2Cl_2$ (**64**) (L^{11} = *N*,*N*-bis(salicylidene)-o-phenylenediamine) [47] contains two L^{11} ligands bonded to two dysprosium centers. The first L^{11} ligand encapsulates one dysprosium ion completely, whilst the second has two phenoxide oxygen atoms bridging between the two dysprosium centers. The dysprosium centre bound to the bridging L^{11} ligand is also coordinated to two bidentate acac ligands whilst the encapsulated dysprosium ion is bound to one water molecule. Complex **64** has U_{eff} = 56 cm^{-1} and shows two relaxation processes due to different ligand fields and coordination geometries around the dysprosium centres.[47]

Carboxylic acids have also been used to create lanthanide dimer SMMs in the form of $[Dy_2(Acc)_4(H_2O)_8]\cdot(Cl)_6\cdot 5.89H_2O$ **65**,[48] $[Dy_2(3\text{-}Htzba)_2(3\text{-}tzba)_2(H_2O)_8]\cdot 4H_2O$ **66**,[49] $[Dy_2(L^{12})_6(MeOH)_2(H_2O)_2]$ **67**,[50] $[(phen)_2Er_2(HCOO)_{4.2}(NO_3)_{1.8}]$ **68**,[51] $[Dy_2(phen)_2(L^{13})_6]\cdot 2H_2O$ **69** [52] and $[Dy_2(phen)_2(L^{13})_6]$ **70** [52] (Acc = 1-aminocyclohexanel-carboxylic acid, H_2tzba = 3-(1H-tetrazol-5-yl)benzoic acid, L^{12}H = n-butyric acid and L^{13}H = β-naphthoic acid). Complexes **66** – **70** all have two bridging carboxylate groups between the lanthanide ions with various other *O*- and *N*-donor ligands completing the coordination sphere of lanthanide ions. Complex **70** is the de-hydrated version of **69** and shows different magnetic behaviour. Both **69** and **70** are SMMs but have different barrier heights with U_{eff} = 20 cm^{-1} and 4 cm^{-1} respectively. This has been explained as due to removal of water from **69**causing the coordination environment around the dysprosium ions to change sufficiently that it almost switches off SMM behaviour in **70**.[52]

Complex **65** has four bridging Acc^- ligands between the two dysprosium centers and eight capping water molecules. This is in contrast to **66** which has two bridging 3-$tbza^{2-}$ ligands between the two dysprosium centers and two 3-$tbzaH^-$ capping ligands (one on each dysprosium ion). The coordination sphere of each dysprosium ion in **66** is completed by a total of eight water molecules. Complex **66** has U_{eff} = 38 cm^{-1} whilst **65** only shows a rise in out of phase magnetic susceptibility at low temperatures and no maxima and as such cannot be classified as a true SMM.[48,49] Complex **68** also contains four bridging carboxylate. Despite **68** showing maxima in the out of phase magnetic susceptibility, no barrier height is derived by Liu *et al*.[51] These differences in magnetic behaviour most likely stem from the difference in the coordination geometry of the dysprosium ions present in each complex.

$[Dy_2(hfac)_6(H_2O)_2(L^{14})]$ **71** [53] and $[Dy_2(HBpz_3)_4(\mu\text{-ox})]\cdot 2MeCN\cdot CH_2Cl_2$ **72** [54] (L^{14} shown in Scheme 2 and ox = oxalate) both use tetradentate carboxylic acids to link dysprosium ions through the ligand molecule. Complex **71** contains two dysprosium ions each bound to one carboxylate group of L^6 and three bidentate hfac molecules and has U_{eff} = 11 cm^{-1}.[53] By comparison complex **72** has two dysprosium ions bound to four oxygen atoms of an oxalate ligand with two tridentate $HBpz_3^-$ ligands completing the coordination sphere of each dysprosium ion. Complex **72** has U_{eff} = 29 cm^{-1}.[54] This difference can be attributed to the different ligand environments around the dysprosium ions in **71** and **72**.

3.3 Organometallics

The most common form for organometallic lanthanide SMMs is a dimer with two bridging ligands and two capping ligands. These compounds then allow the effects of low coordination number and symmetry of the lanthanide coordination environment to be

investigated. At present there are only four reported examples of organometallic dimer SMMs, $[[(\eta^5\text{-Cp})_2\text{Dy}(\mu\text{-Cl})]_2$ **73**, $[(\eta^5\text{-Cp})_2(\text{THF})\text{Dy}(\mu\text{-Cl})]_2$ **74**,[55] $[\{\text{Cp}_2\text{Dy}(\mu\text{-bta})\}_2]$ **75** (bta = benzotriazole) [56] and $[\{(\text{MeCp})_2\text{Dy}(\mu\text{-SSiPh}_3)\}_2]$ **76**.[9]

Complexes **73** – **76** all have similar structures and are composed of two dysprosium ions bridged by two ligands with each dysprosium ion coordination sphere being completed by two $\eta^5\text{-Cp}^-$ (or MeCp-) ligands and in the case of **74**, one THF molecule.[55,56] These similarities in structure coupled with the variation in bridging ligand allow a comparison of the magnetic properties of this series of compounds and the effect that the bridging ligand has on them. Looking at the height of the barrier to reversal of magnetization, U_{eff} = 26 (**73**), 34 (**74**) and 39 cm^{-1} (**75**) we can see a small increase in the height of the barrier.[55,56] The only difference between **73** and **74** is the THF molecule making the dysprosium centers formally nine coordinate as opposed to the formally eight coordinate dysprosium centers in **74**. This suggests subtle changes in the ligand environment are affecting the magnetic properties of these complexes.

Complex **76** has the highest barrier in this group with U_{eff} = 133 cm^{-1}. Complex **76** is also the first SMM of any metal where S-bridging ligands have been used.[9] This illustrates a further advantage of the lanthanides: their redox-stability brings a much broader range of ligands than can be used for 3d-metal SMMs. The most remarkable examples are the N_2^{3-} bridged complexes discussed below.

3.4 Radical Ligands

Radical ligands such as nitronyl nitroxide ligand radicals have been successfully used to create lanthanide dimer SMMs in the form of $[\text{Ln}(\text{Phtfac})_3(\text{NITpPy})]_2$ (Ln = Tb,**77** and Dy,

78; HPhtfac and NITpPy are shown in Scheme 2),[57] $[Dy(hfac)_3NITpPy]_2$ **79** [58] and $[Dy(hfac)_3(NITmbis)]_2$ **80** (NITmbis is shown in Scheme 2).[59]

Complexes **77** – **79** contain three bidentate diketone ligands binding to each lanthanide ion. Each lanthanide ion is then bound by the oxygen molecule of one NITpPy radical and the nitrogen atom of the pyridine ring of the other NITpPy radical ligand. Complexes **77**, **78** and **79** have very similar energy barriers of U_{eff} = 18, 14 and 9 cm^{-1} respectively.[57,58] Whilst **77** shows SMM behaviour the analogous $[Tb(hfac)_3NITpPy]_2$ **81** does not.[58]

Altering the position of the pyridine ring on the nitronyl nitroxide ligand such that the radical is on the three position of the pyridine ring, turns on SMM behaviour in $[[Tb(hfac)_3NITpPy]_2$ **82** [60] and $[Tb(hfac)_3NIT\text{-}5\text{-}Br\text{-}3\text{-}Py)]_2$ **83**.[61] Complexes **82** and **83** have similar structures to **77** – **79** and **81** with the only difference being a twist in the NIT-X ligand in order to allow coordination of the pyridine nitrogen to a terbium ion. Complexes **82** and **83** have U_{eff} = 13 cm^{-1} and 20 cm^{-1} respectively.

Recently Long *et al*, have shown that using N_2^{3-} radical bridging ligands can greatly increase the interaction between lanthanide ions within a complex. $[K(18\text{-crown-}6)(THF)_2][\{[(Me_3Si)_2N]_2(THF)Ln\}_2(2.2\text{-}N_2)]$ (Ln = Tb (**84**) and Dy (**85**)) [3,10] are generated by reducing the isostructural N_2^{2-} bridged compounds with potassium graphite in THF. Both **84** and **85** show SMM behaviour and have U_{eff} = 227 cm^{-1} and 123 cm^{-1} respectively with **84** showing magnetic hysteresis at temperatures up to 14K. This is a remarkably high temperature for magnetic hysteresis in an SMM; previous examples with 3d-metals are restricted to around 5 K. It is also surprising that the high temperature hysteresis is seen in

these molecules where the U_{eff} is not as high as in some others. The high temperature hysteresis has been attributed to the increased interaction between lanthanide ions with the complexes caused by the bridging N_2^{3-} radical which has good orbital overlap with the 4f orbitals present in lanthanides.[3,10] This area of chemistry presents a new and exciting approach to SMM synthesis and design.

3.5 Other Ligands

An unusual ligand that has been used to create a terbium dimer is *p*-tert-butylsulfonylcalix[4]arene ($L^{15}H_4$) which forms $[Tb_2(L^{15})(NO_3)_2(DMF)_6]\cdot 2DMF$ **86**.[4] Each terbium ion in **86** is coordinated by three oxygen atoms from the calixerene, three oxygen atoms from DMF molecules and one η^2-nitrate ion. Although **86** shows frequency dependent rises in χ_M" at low temperature, no maximum in the out of phase susceptibility is observed.[4]

N-donor bridging ligands have also been used successful in the creation of a dysprosium based dimer exhibiting SMM behaviour in the form of $[Dy_2(hfac)_6(H_2O)_4(pz)]\cdot 2pz$ **87** (pz = pyrazine).[62] Each dysprosium ion in **87** is coordinated to three bidentate hfac diketones, two water molecules and one nitrogen atom of the central pyrazine ligand. Complex **87** has a respectable value of U_{eff} = 77 cm^{-1}.

Pyridine oxide ligands have also been used as bridging ligands between dysprosium centers in the form of $[\{Dy(TTA)_3(L^{16})\}_2]\cdot 0.5CH_2Cl_2$ **88** [63] which contains two bridging L^{16} ligands between the dysprosium centers and has three bidentate TTA ligands coordinating to each dysprosium centre to complete the coordination sphere of each. Complex **88** has U_{eff} = 61 cm^{-1}.[63]

4. Trimetallic 4f-SMMs

Table 3 shows all reported trimetallic lanthanide SMMs up until the end of July 2012, with all non-trivial ligands used in these complexes shown in Scheme 3.

Table 3. Trimetallic lanthanide SMMs from 2003 to present with the reported values of U_{eff} (cm^{-1})

Compound	Compound Number	U_{eff} (cm^{-1})	Reference
$[Dy_3(\mu_3\text{-}OH)_2(L^{17})_3Cl(H_2O)_5]Cl_3\cdot 4H_2O\cdot 2MeOH\cdot 0.7MeCN$	89	25	64
$[Dy_3(\mu_3\text{-}OH)_2(L^{17})_3(Cl)_2(H_2O)_4]$ $[Dy_3(\mu_3\text{-}OH)_2(L^{17})_3Cl(H_2O)_5]Cl_5\cdot 19H_2O$	90	83	64
$[Dy_3(HSA)_5(SA)_2(phen)_3]$	91	45	66
$[(L^{18}H_2)_2Dy_3(NO_3)_5(DMF)]\cdot DMF$	92	10	67
$[Dy_3(Meosalox)_2(MeosaloxH)_4(OH)(H_2O)]\cdot MeOH\cdot 7H_2O$	93	26	68b
$[Dy_3(Meosalox)_2(MeosaloxH)_4(NO_3)(MeOH)]$ $\cdot MeOH\cdot 0.5H_2O$	94	27	68b
$[Dy_3(Meosalox)_2(MeosaloxH)_4(Cl_3CCO_2)(MeOH)]$ $\cdot MeOH$	95	28	68b
$[Dy_3(Mesalox)_2(MeOsaloxH)_4(EtOH)_2]\cdot(ClO_4)$ $\cdot 1.5EtOH\cdot H_2O$	96	48	68a
$[Dy_3(\mu_3\text{-}OMe)_2(HL^{10})_3(SCN)]$ $\cdot 4MeOH\cdot 2MeCN\cdot 2H_2O$	97	6	69
$[Dy_3(\mu_3\text{-}N_3)(\mu_3\text{-}OH)(H_2L^{10})_3(SCN)_3]\cdot(SCN)$ $\cdot 3MeOH\cdot H_2O$	98	not measurable	69
$[Dy_3(L^{19})(\mu_3\text{-}OH)_2(NO_3)_2(H_2O)_4]\cdot{}_2(NO_3)$ $\cdot 6MeOH\cdot H_2O$	99	<1	70
$[Dy_3(L^{19})(\mu_3\text{-}OH)_2(SCN)_4(H_2O)_2]\cdot 3MeOH\cdot 2H_2O$	100	11	70

L^{17} = anion of ortho-vanillin

H_2SA = salicylic acid

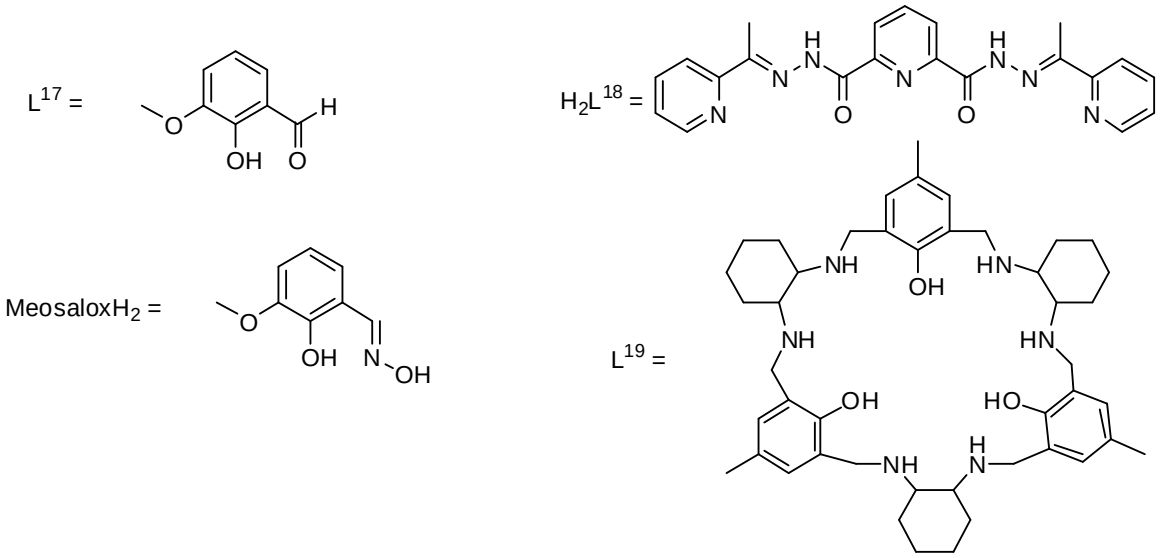

Scheme 3. Chemical structures of non trivial ligands used to produce trimetallic lanthanide SMMs.

4.1 Alcohols, Ketones and Acids

Ortho-vanillin (L^{17}) has been used to create two important Dy_3 triangles show very unusual physics. The compounds have the formulae $[Dy_3(\mu_3\text{-}OH)_2(L^{17})_3Cl(H_2O)_5]Cl_3\cdot 4H_2O\cdot 2MeOH\cdot 0.7MeCN$ **89** [64] and $[Dy_3(\mu_3\text{-}OH)_2(L^{17})_3Cl(H_2O)_5]Cl_5\cdot 19H_2O$ **90**.[64] Both **89** and **90** have two central μ_3-OH at the centre of the Dy_3 triangle with the phenoxide oxygen atom from each ortho-vanillin ligands bridging the edges of the triangle (Figure 6). The methoxy oxygen from one ligand and the aldehyde oxygen from another ligand bind to each dysprosium ion. In **89** the coordination sphere of two dysprosium ions is completed by two water molecule whilst the other dysprosium ion is bound to one water molecule and one chloride anion. Whilst in **90** the coordination sphere of the final dysprosium ion is completed by one chloride anion and either a water molecule or chloride anion (50:50 occupancy/disorder).[64]

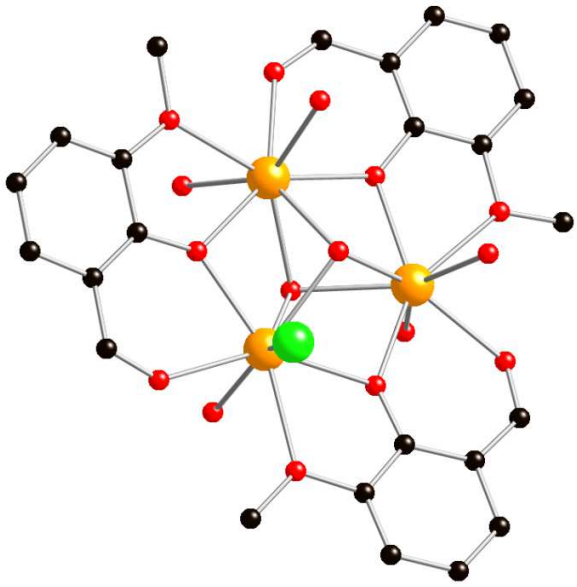

Figure 6. Solid state structure of 89. All hydrogen atoms omitted for clarity. Black = Carbon, Red = Oxygen, Green = Chlorine and Orange = Dysprosium.

Both **89** and **90** show SMM behaviour below 20 K and show a decrease in magnetic susceptibility upon decreasing temperature. This decrease in magnetic susceptibility upon decreasing temperature suggests a non-magnetic ground state for both **89** and **90**, which is unexpected as both systems have odd numbers of unpaired electrons. The magnetic behaviour of **89** and **90** can be explained describing both systems as non-collinear spin systems.[65] The spin anisotropy axes for each dysprosium center in **89/90** are in the plane of the Dy_3 triangle and not perpendicular to each other. In fact the anisotropy axes of each dysprosium center lie at 120° to each other. Coupling this observation with the antiferromagnetic interactions observed between dysprosium centers in **89/90** would lead to the observed non-magnetic ground state of **89/90**.[65] Complexes **89** and **90** have U_{eff} = 25 cm^{-1} and 83 cm^{-1} respectively and were the some of the first compounds to show that the

presence of a large spin ground state is not required for slow relaxation of magnetization to be observed.[64]

Salicylic acid (H_2SA) has been used to create a linear Dy_3 complex $[Dy_3(HSA)_5(SA)_2(phen)_3]$ **91**,[66] (Figure 7) which contains two 2.121 SA^{2-} ligands binding to three dysprosium ions and bridging between the central dysprosium ion and the two terminal dysprosium ions. Three 2.11HAS^- ligands bridge between the central dysprosium ion and the two terminal dysprosium ions, whilst the final HAS^- ligand chelates to one terminal dysprosium ion which has one phen ligand completing the coordination sphere. The other terminal dysprosium ion is bound to two phen ligands to complete the coordination sphere.[66] This means that each dysprosium ion in **91** has a different coordination environment and geometry. The interaction between dysprosium ions in **91** has been shown to be minimal and as such the SMM behaviour of **91**, with U_{eff} = 45 cm^{-1}, is attributed to the single ion anisotropy of each dysprosium centre.[66]

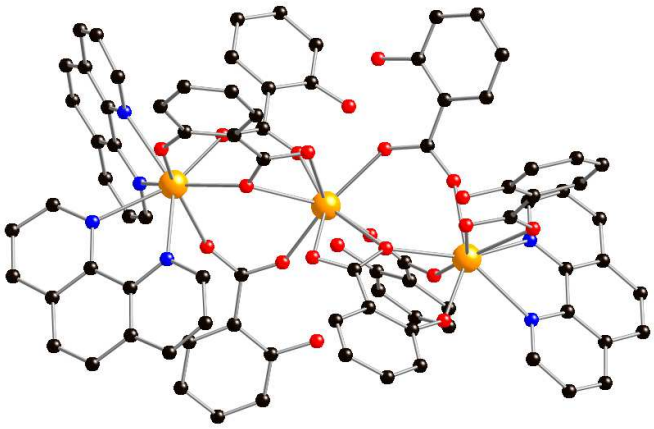

Figure 7. Solid state structure of 91. All hydrogen atoms omitted for clarity. Black = Carbon, Red = Oxygen, Blue = Nitrogen and Orange = Dysprosium

4.2 Schiff Base Ligands

Schiff base ligands have become popular for use in lanthanide complex formation as they provide both *O*- and *N*-donor sites for ligation to lanthanide ions whilst also having the advantage that the steric and electronic properties of Schiff base ligands can be easily tuned. One example is the double helicate complex $[(L^{18}H_2)_2Dy_3(NO_3)_5(DMF)]\cdot DMF$ **92** [67] (L^{18} is shown in Scheme 3) in which "binding pockets" targeted towards lanthanide ions have been constructed into the ligand frame. Each dysprosium ion in **92** is bound in a tridentate "pocket" of two L^{18} ligands, with two dysprosium ions bound to two η^2-nitrate ions and the final dysprosium ion bound to one η^2-nitrate ion and one DMF molecule. Complex **92** shows field-induced SMM behaviour and under a field of 1800Oe has a U_{eff} = 10 cm^{-1}.[67]

Other linear "Dy_3" SMMs have been isolated using the Schiff base ligand $Meosalox^{2-}$ ($MeOsaloxH_2$ = 3-methyloxysalicylaldoxime). Complexes **93** – **96** are very similar, differing only in the ligands attached to the terminal Dy sites (Figure 8, see Table 3 for full formulae).[68] Complexes **93** – **96** all contain two $Meosalox^{2-}$ ligands and four $MeosaloxH^-$ ligands. In each complex two $MeosaloxH^-$ ligands act as tridentate capping ligands for the terminal dysprosium ions, whilst the remaining two $MeosaloxH^-$ and two $Meosalox^{2-}$ligands bridge between the three dysprosium ions via the phenoxide oxygen atoms and oximine nitrogen and oxygen atoms.[68] The central dysprosium ion in each case is nine-coordinate whilst the terminal dysprosium ions are eight-coordinate. Complexes **93** – **96** have U_{eff} = 26, 27, 28 and 48 cm^{-1} respectively. Although the heights of the barrier for **93** – **95** are identical (within error), U_{eff} for **96** is significantly higher. This can be attributed to the ligands attached to the terminal dysprosium ions. In **93** – **95** one anionic (OH, NO_3, Cl_3CCO_2) and one neutral (H_2O or MeOH) ligand are present whilst in **96** two neutral

ligands are present (EtOH). This change in ligand affects the local environment around the terminal dysprosium ions enough to increase the height of U_{eff}.[68]

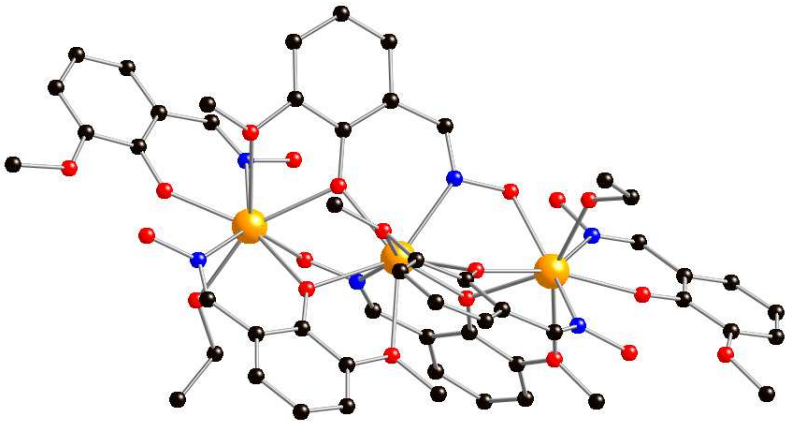

Figure 8. Solid state structure of 96. All hydrogen atoms omitted for clarity. Black = Carbon, Red = Oxygen, Blue = Nitrogen and Orange = Dysprosium

As well as linear Dy_3 SMMs, Schiff base ligands have been recently used to create Dy_3 triangles in the form of $[Dy_3(\mu_3\text{-}OMe)_2(HL^{10})_3(SCN)]\cdot 4MeOH\cdot 2MeCN\cdot 2H_2O$ **97** [69] and $[Dy_3(\mu_3\text{-}N_3)(\mu_3\text{-}OH)(H_2L^{10})_3(SCN)_3]\cdot(SCN)\cdot 3MeOH\cdot H_2O$ **98** [69] ($L^{10}H_3$ is shown in Scheme 2). Complex **97** contains three dysprosium ions coordinated to two central μ_3-OMe ligands, with each edge of the triangle bridged by one phenoxide oxygen atom from each HL^{10} ligand. Two dysprosium atoms are coordinated by two nitrogen atoms and six oxygen atoms of the ligands whilst the final dysprosium ion is also coordinated to the nitrogen atom of one SCN^- ligand.

In contrast, complex **98** contains three dysprosium ions around one central μ_3-OH and a central μ_3-N_3, with the phenoxide oxygen atom from each ligand bridging the edges of the Dy_3 triangle. Each dysprosium ion is then bound to a further two nitrogen atoms and four oxygen atoms from the H_2L^{20} ligands with the coordination sphere being completed by one

SCN^- ligand. Both **97** and **98** show frequency dependency of out-of-phase magnetic susceptibility, but whilst **97** shows maxima within the scanned temperature range, **98** does not. Two maxima are observed in the out of phase susceptibility signal for **97** and for the slow relaxation process a U_{eff} = 6 cm^{-1} can be calculated. The differences in magnetic behaviour between **97** and **98**is attributed to the distinct magnetic anisotropies associated with the different dysprosium sites in **97** and **98**.[69]

4.3 Other Ligands

As well as Schiff base ligands, other mixed *N*- and *O*-donor ligands in the form of a hexaazatriphenolic macrocycle (L^{19}) (Figure 9) have been used to create "Dy_3" triangle SMMs.[70]

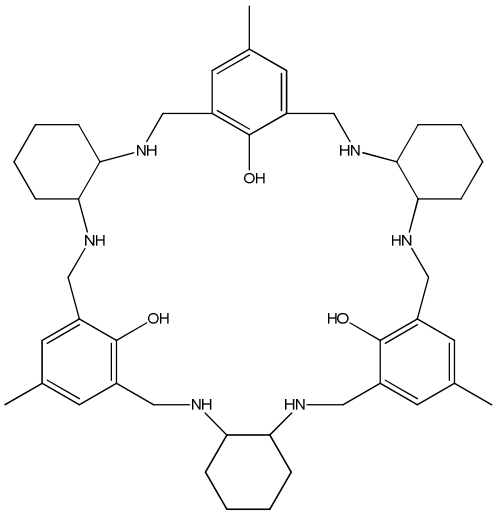

Figure 9. Structure of hexaaza triphenolic macrocycle $L^{18}H_3$

$[Dy_3(L^{19})(\mu_3\text{-}OH)_2(NO_3)_2(H_2O)_4]\cdot(NO_3)_2\cdot 6MeOH\cdot H_2O$ **99** [70] and $[Dy_3(L^{19})(\mu_3\text{-}OH)_2(SCN)_2(H_2O)_2]\cdot 3MeOH\cdot 2H_2O$ **100** [70] are synthesized via reaction of $Dy(NO_3)_3\cdot 6H_2O$ or $Dy(SCN)_3\cdot 6H_2O$ with $L^{19}H_3$ in the presence of base. In both **99** and **100** the macrocycle (L^{19}) encapsulates a "Dy_3" triangle centred on two μ_3-OH ligands. Complex **99** contains

three dysprosium ions in two different coordination environments. All three dysprosium ions are coordinated to two hydroxide oxygen atoms, two phenoxide oxygen atoms and the neighbouring amine nitrogen atoms. The coordination sphere of two dysprosium ions is completed by one water molecule and one monodentate nitrate ion. The coordination sphere of the third dysprosium ion is completed by two water molecules (Figure 10).

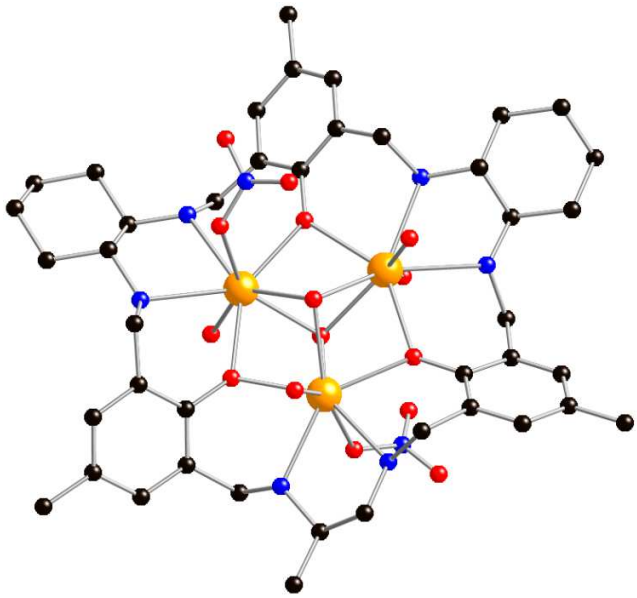

Figure 10. Solid state structure of 99. All hydrogen atoms omitted for clarity. Black = Carbon, Red = Oxygen, Blue = Nitrogen, and Orange = Dysprosium

Complex **100** is almost isomorphous to **99** except that the coordination sphere of two dysprosium ions is completed by one SCN^- ligand and water molecule, whilst the third dysprosium ion is bound to two SCN^- ligands instead of two water molecules.[70] Complex **100** show SMM behaviour under an applied field of 1900 Oe and has U_{eff} = 11 cm^{-1}. Complex 99 only shows a rise in out of phase magnetic susceptibility at low temperatures and so is estimated to have $U_{eff} < 1$ cm^{-1} using a general Debye model. Due to the extremely small value of U_{eff} for **99**, it is debatable as to whether **99** can be considered a "true" SMM,

as barrier heights of less than 1 cm^{-1} can be unreliable to measure. This difference in magnetic behaviour is attributed to the difference in anionic axial ligands between **99** and **100**.[70]

5. Tetrametallic 4f-SMMs

Table 4 shows all reported tetrametallic lanthanide SMMs up until the end of July 2012; non-trivial ligands used in these complexes are shown in Scheme 4.

Table 4. Tetrametallic lanthanide SMMs from 2003 to present with the reported values of U_{eff} (cm^{-1})

Compound	Compound Number	U_{eff} (cm^{-1})	Reference
$[Dy_4(\mu_3\text{-}OH)_4(Acc)_6(H_2O)_7(ClO_4)]\cdot(ClO_4)_7\cdot 11H_2O$	101	not measurable	71
$[Dy_4(\mu_3\text{-}OH)_4(IN)_6(py)(MeOH)_7](ClO_4)_2\cdot py\cdot 4MeOH$	102	28	72
$[Dy_4(\mu_3\text{-}OH)_2(mdeaH)_2(O_2C^tBu)_8]$	103	4	73
$[Dy_4(\mu_3\text{-}OH)_2(L^{17})_4(O_2C^tBu)_4(NO_3)_2]\cdot CH_2Cl_2\cdot 1.5H_2O$	104	3	74
$[Dy_4(\mu_3\text{-}OH)_2(ampdH)_2(O_2C^tBu)_{10}]\cdot 4MeCN$	105	4	75
$[Dy_4(3\text{-}bpp)_3(CO_3)_6(H_2O)_3]\cdot DMSO\cdot 18H2O$	106	4	76
$[Dy_4(L^{18}H_2)_2(L^{18}H)_2(N_3)_4(O)]\cdot 14H_2O$	107	36	7a
$[Dy_4(\mu_4\text{-}OH)(Hhpch^-)_8]\cdot(ClO_4)_3\cdot 2MeCN\cdot MeOH\cdot 4H_2O$	108	64	77
$[Dy_4(HL^{20})_4(MeOH)_4]_2\cdot 7\ CH_2Cl_2\cdot MeOH$	109	11	78
$[Dy_4(\mu_3\text{-}OH)_2(php)_2(O_2CMe)_6(H_2O)_2]\cdot 4MeOH\cdot 2H_2O$	110	not measurable	79
$[Dy_4(\mu_3\text{-}OH)_2(bmh)_2(msh)_4Cl_2]$	111	118	8a
$[Dy_4(\mu_4\text{-}O)(\mu\text{-}OMe)_2(beh)_2(esh)_4]\cdot 3MeOH$	112	16	80
$[Dy_4(L^{21})_4(MeOH)_6]\cdot 2MeOH$	113	120	81
$[Er_4(salen)_6]\cdot 13H_2O$	114	9	82

$[Dy_4(L^{22})_4(HL^{22})_2(C_6H_4NH_2CO_2)_2(MeOH)_4]\cdot 5MeOH$	115	14	83
$[Dy_4(pdmH)_2(pdm)_4(PhCO_2)_2(PhCO_2H)_4]\cdot MeOH\cdot H_2O$	116	not measurable	84
$[Dy_4(dhampH_3)_4(NO_3)_2](NO_3)_2\cdot 3MeOH\cdot H_2O$	117	<1	85
$[Dy_4(\mu_3\text{-}OH)_2(hmmpH)_2(hmmp)_2Cl_4]\cdot 3MeOH\cdot MeCN$	118	not measurable	86
$[Dy_4(\mu_3\text{-}OH)_2(hmmpH)_2(hmmp)_2(N_3)_4]\cdot 4MeOH$	119	5	86
$[Dy_4(\mu_3\text{-}OH)_2(L^{23})_2(acac)_6]\cdot 2(H_2L^{23})\cdot 2MeCN$	120	15	87
$[Dy_4(L^{24})_2(C_6H_5CO_2)_{12}(MeOH)_4]$	121	12	88
$[Dy_4(OH)_4(L^{15})_2(H_2O)_4(MeOH)_4]\cdot 4H_2O$	122	16	89
$[Dy_4(\mu_4\text{-}OH)(PTC4A)_2Cl_3(MeOH)_2(H_2O)_3]\cdot 4.7MeOH\cdot 2H_2O$	123	not measurable	90
$[Dy_4(\mu_3\text{-}OH)_2(\mu\text{-}OH)_2(2,2\text{-}bpt)_4(NO_3)_4(EtOH)_2]$	124	56	92
$(HDAB)_8H_5Li_5[Dy_4As_5W_{10}O_{144}(H_2O)_{10}(gly)_2]\cdot 25H_2O$	125	3	91

3-bpp = 2,6-Di(pyrazole-3-yl)pyridine

OAc = acetate

H_4PTC4A = p-phenylthiacalix[4]arene

HIN = isonicotinic acid

$pdmH_2$ = pyridine-2,6-dimethanol

$ampdH_4$ = 3-amino-3-methylpentane-1,5-diol

Hpiv = pivalic acid

$mdeaH_2$ = N-methyldiethanolamine

HDAB = monoprotonated 1,4-diazabicyclooctane

gly = glycine

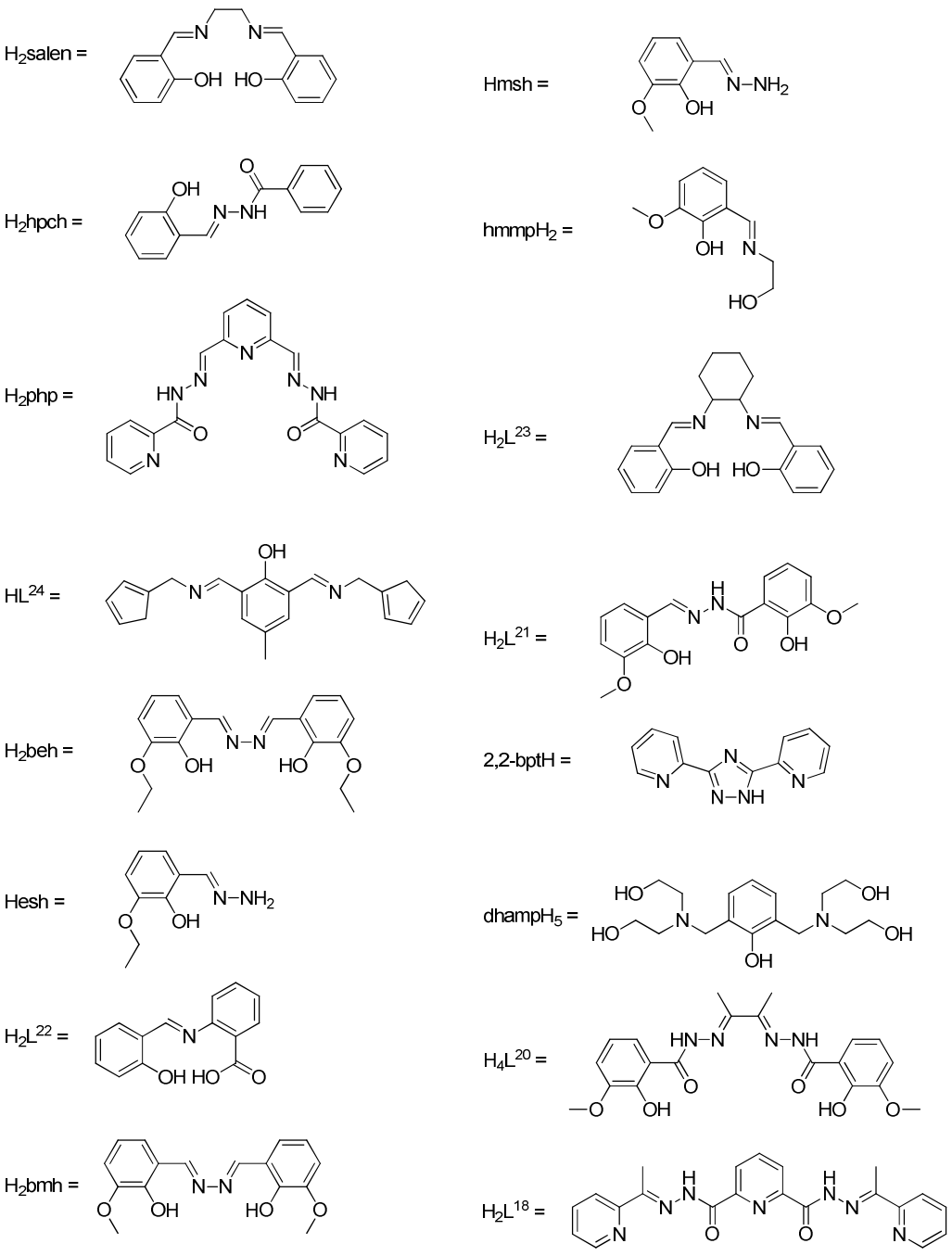

Scheme 4. Chemical structures of non trivial ligands used to produce tetrametallic lanthanide SMMs.

5.1 Alcohols, Ketones and Acids

$[Dy_4(\mu_3\text{-}OH)_4(Acc)_6(H_2O)_7(ClO_4)]\cdot(ClO_4)_7\cdot 11H_2O$ **101** [71] and $[Dy_4(\mu_3\text{-}OH)_4(IN)_6(py)(MeOH)_7](ClO_4)_2\cdot py\cdot 4MeOH$ **102** [72] (Acc = 1-aminocyclohexane-carboxylic acid and HIN = *iso*-nicotinic acid) both have a core tetrahedron of dysprosium ions. Each face of the Dy_4 tetrahedron in **101** is bridged by a μ_3-OH, with each edge of the tetrahedron bridged by a 2.11 Acc ligand. The coordination spheres of three dysprosium ions are completed by two water molecules whilst the coordination sphere of the fourth dysprosium ion is completed by one water molecule and one oxygen atom of a ClO_4^- anion (Figure 11). Complex **101** shows a rise in out of phase magnetic susceptibility at temperatures below 5 K but no maximum.[71]

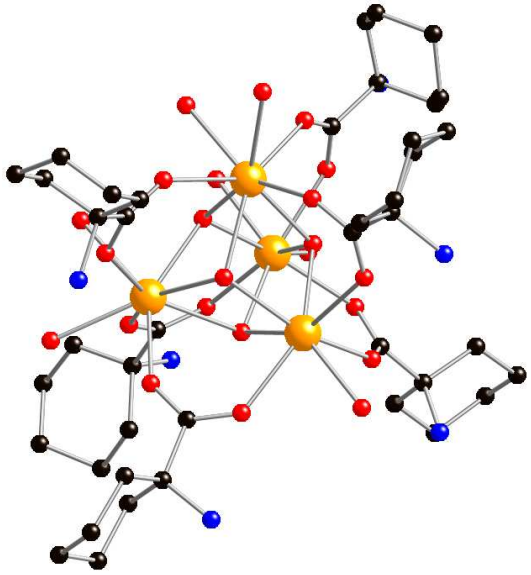

Figure 11. Solid state structure of 101. All hydrogen atoms omitted for clarity. Black = Carbon, Red = Oxygen, Blue = Nitrogen, and Orange = Dysprosium

In contrast **102** has U_{eff} = 28 cm^{-1} despite having a very similar structure to **101**. Again each face of the Dy_4 tetrahedron in **102** is bridged by a μ_3-OH, and each edge of the tetrahedron is

bridged by a 2.11 IN ligand. The coordination sphere of three dysprosium ions is completed by two methanol atoms on each, and the coordination sphere of the fourth dysprosium ion is completed by one methanol and one pyridine ligand.[72] The differences in magnetic behaviour between **101** and **102** can be attributed to differences in coordination environment and geometry of the dysprosium ions present in both.

$[Dy_4(\mu_3\text{-}OH)_2(mdeaH)_2(O_2C^tBu)_8]$ **103**,[73] $[Dy_4(\mu_3\text{-}OH)_2(L^{17})_4(O_2CCMe_2)_4(NO_3)_2]\cdot CH_2Cl_2\cdot 1.5H_2O$ **104** [74] and $[Dy_4(\mu_3\text{-}OH)_2(ampdH)_2(O_2C^tBu)_{10}]\cdot 4MeCN$ **105** [75] ($mdeaH_2$= N-methyldiethanolamine, L^{17} = anion of ortho-vanillin and $ampdH_4$ = 3-amino-3-methylpentane-1,5-diol) all have a $Dy_4(OH)_2$ core with a defect-dicubane architecture. One μ_3-OH sits above the Dy_4 plane and one below. Complex **103** contains two $mdeaH^-$ ligands binding in a 2.211 mode, four bidentate pivalate ligands binding a 2.11 mode, two tridentate pivalates binding in a 2.21 mode and two chelating pivalates (Figure 12). Complex **103** shows SMM behaviour at temperatures below 3 K. Application of a static field had little effect on the magnetic behaviour of **103** suggesting that quantum tunnelling is not very pronounced in **103**. Complex **103** has U_{eff} = 4 cm^{-1} under an applied field of 800 Oe.[73]

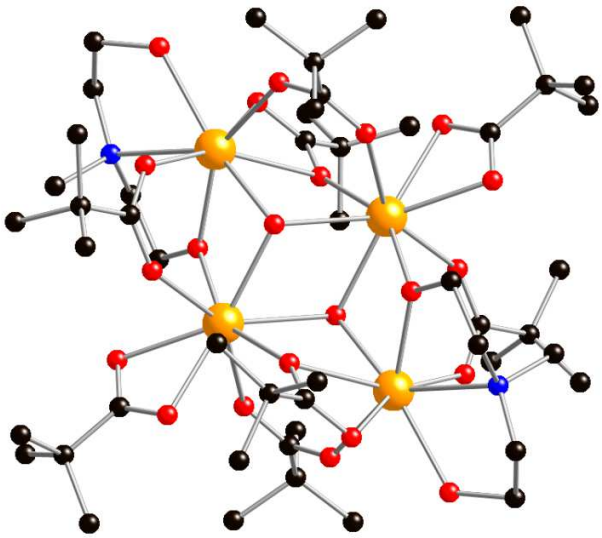

Figure 12. Solid state structure of 103. All hydrogen atoms omitted for clarity. Black = Carbon, Red = Oxygen, Blue = Nitrogen, and Orange = Dysprosium

Complex **104** has the same $Dy_4(OH)_2$ core as **103** and contains four L^{17} ligands binding in a 2.121 mode and four $Me_2HCCO_2^-$ ligands binding in a 2.11 mode. The coordination spheres of two dysprosium ions are completed by one chelating nitrate anion each (Figure 13). Complex **104** has U_{eff} = 3 cm^{-1} which is comparable to the value for **103**. Application of a static field on **104** does not affect the maxima in the out of phase susceptibility measurements and so it is most likely that there is little or no quantum tunnelling in **104** in zero field.[4]

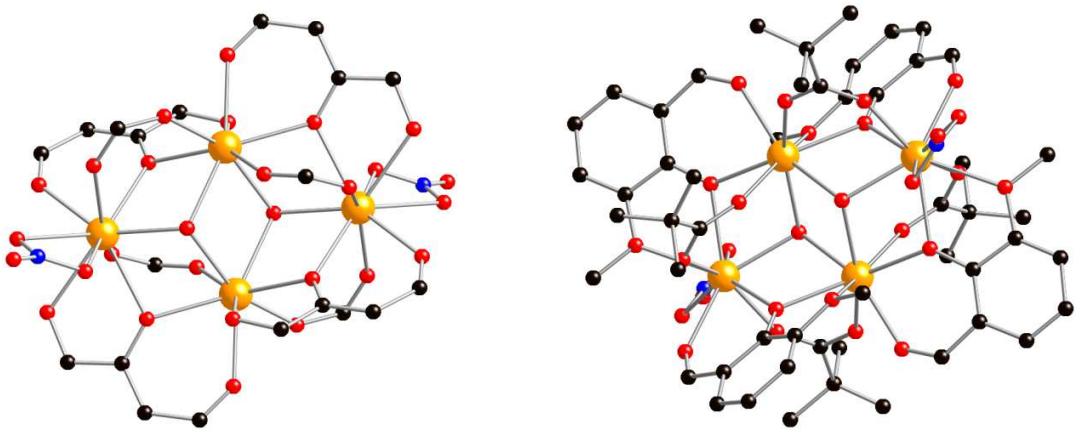

a b

Figure 13. a) Core structure of 104 with peripheral groups removed. b) Solid state structure of 104. All hydrogen atoms omitted for clarity. Black = Carbon, Red = Oxygen, Blue = Nitrogen, and Orange = Dysprosium

Complex **105** has two ampdH ligands binding in a 2.21 mode, four 2.11 pivalates, two 2.21 pivalates, two 1.11-pivalates and two terminal pivalates. Complex **105** has U_{eff} = 4 cm^{-1} which is comparable to the values for both **103** and **104**.[75]

$[Dy_4(3\text{-bpp})_3(CO_3)_6(H_2O)_3]\cdot DMSO\cdot 18H_2O$ **106** [76] contains a triangular based Dy_4 pyramid (Figure 14). The central dysprosium ion is bound to three 2.21 CO_3^{2-} anions and three 3.211 CO_3^{2-} anions. The coordination sphere of the other three dysprosium ions is completed by one 3-bpp ligand on each. The carbonate anions in **106** come from absorption of atmospheric CO_2. Complex **106** shows a rise in out of phase magnetic susceptibility at temperatures below 6 K but no maxima. An energy barrier of U_{eff} = 4 cm^{-1} is estimated, however the crystal structure of 106 reveals a 3D π-π mediated network, meaning the magnetic behaviour observed cannot be unequivocally attributed to a single molecule and not the bulk material. This means that **106** cannot be comprehensively classified as a SMM.

Application of an external static field does not affect the magnetic behaviour and so it is assumed that little or no quantum tunnelling occurs in **106**.[76]

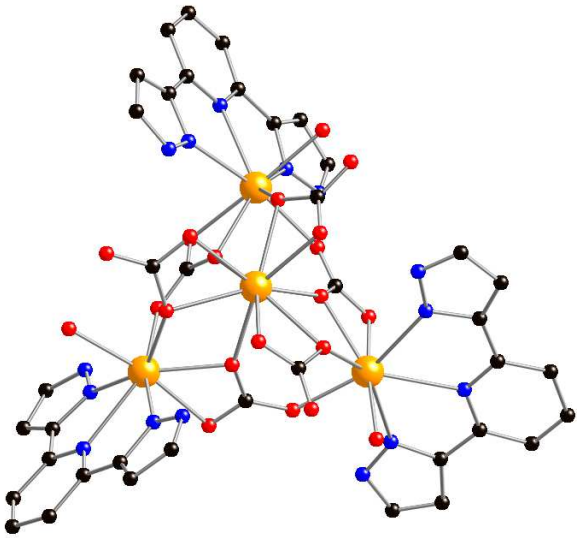

Figure 14. Solid state structure of 106. All hydrogen atoms omitted for clarity. Black = Carbon, Red = Oxygen, Blue = Nitrogen, and Orange = Dysprosium

5.2 Schiff Base Ligands

To date three Dy_4 squares have been reported using Schiff base ligands: $[Dy_4(L^{18}H_2)_2(L^{18}H)_2(N_3)_4(O)]\cdot 14H_2O$**107**,[7a] $[Dy_4(\mu_4\text{-}OH)(Hhpch^-)_8]\cdot(ClO_4)_3\cdot 2MeCN\cdot MeOH\cdot 4H_2O$ **108** [77] and $[Dy_4(HL^{20})_4(MeOH)_4]_2\cdot 7CH_2Cl_2\cdot MeOH$ **109** [78] ($L^{18}H_2$, H_2hpch and $L^{20}H_4$ all shown in Scheme 4). Complex **107** contains four dysprosium ions forming a [2×2] grid centred on a μ_4-O with two L^{18} ligands above the Dy_4O plane and two below the plane. With the bridging azide molecules each dysprosium ion has a N_6O_3 coordination sphere (Figure 15). Complex **107** shows two distinct relaxation processes with U_{eff} = 36 cm^{-1} and 63 cm^{-1}.[7a]

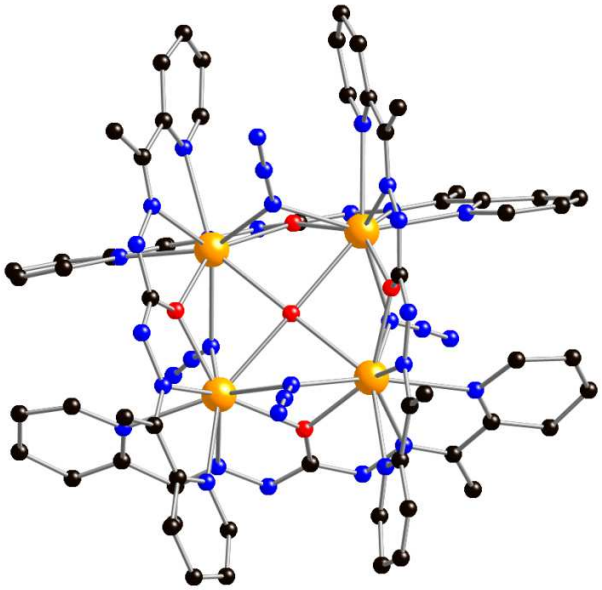

Figure 15. Solid state structure of 107. All hydrogen atoms omitted for clarity. Black = Carbon, Red = Oxygen, Blue = Nitrogen, and Orange = Dysprosium

Complex **108** has a similar structure to **107** and contains four dysprosium ions around a central μ_4-OH as well as eight Hhpch$^-$ ligands. Each pair of Hhpch$^-$ ligands coordinates to two dysprosium ions in an ‘‘head-to-tail’’ fashion with phenoxide oxygen atoms, imine nitrogen atoms and the keto-form carbonyl oxygen atoms. Each phenoxide oxygen atom bridges between two dysprosium ions on each edge of the Dy_4 square (Figure 16). Again **108** shows multiple relaxation processes and under an applied field shows a three-fold increase in barrier height in the thermal relaxation regime. Complex **108** has U_{eff} = 21 cm^{-1} in zero field and U_{eff} = 64 cm^{-1} in a static field of 1000 Oe.[77]

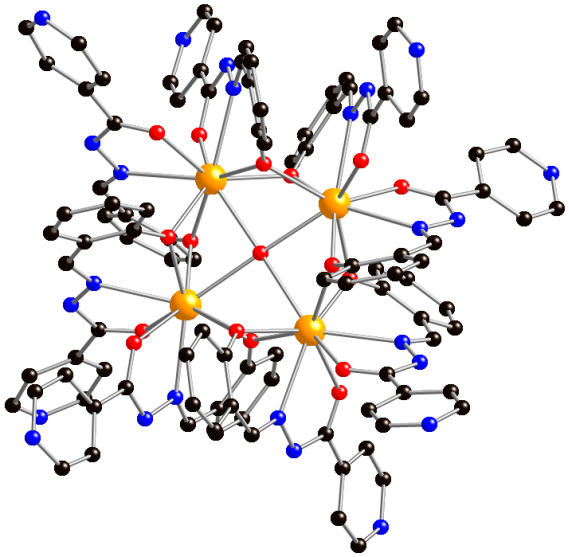

Figure 16. Solid state structure of 108. All hydrogen atoms omitted for clarity. Black = Carbon, Red = Oxygen, Blue = Nitrogen, and Orange = Dysprosium

Complex **109** also shows a [2×2] grid arrangement of dysprosium ions and contains four HL^{20} ligands binding in a 4.421 mode with the coordination sphere of each dysprosium ion completed by one methanol molecule. Complex **109** shows field induced SMM behaviour and has U_{eff} = 11 cm^{-1} under an applied field of 900 Oe.[78]

$[Dy_4(\mu_3\text{-}OH)_2(php)_2(O_2CMe)_6(H_2O)_2]\cdot 4MeOH\cdot 2H_2O$ **110** [79] and $[Dy_4(\mu_3\text{-}OH)_2(bmh)_2(msh)_4Cl_2]$ **111** [8a] (H_2php, H_2bmh and Hmsh shown in Scheme 4) both contain defect-dicubane Dy_4 central cores. Complex **110** contains two μ_3-OH ligands and two php^{2-} ligands bridging in a 3.1211121 modes binding to three dysprosium ions. Two η^2-acetate ligands bind to two dysprosium ions whilst two 2.11 acetate ligands bind to four dysprosium ions. The remaining two η^1-acetate ligands bind to the central two dysprosium ions with one water molecule completing the coordination sphere of each central dysprosium ion (Figure 17). Complex **110** shows field induced frequency dependency of out of phase magnetic

susceptibility under a static field of 1200 Oe but not true SMM behaviour as no maxima are observed, meaning no barrier height can be estimated.[79]

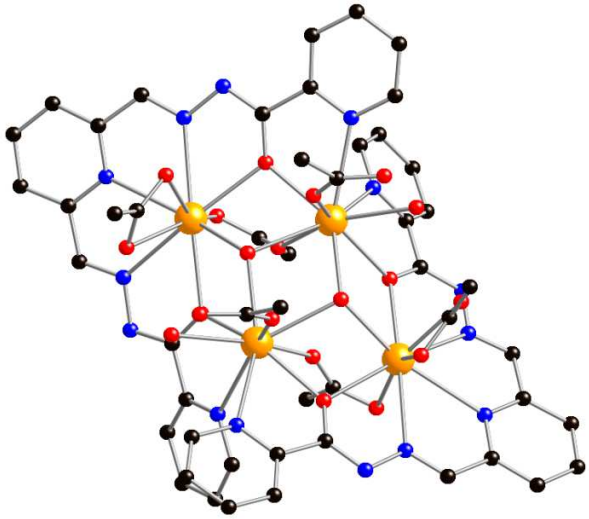

Figure 17. Solid state structure of 110. All hydrogen atoms omitted for clarity. Black = Carbon, Red = Oxygen, Blue = Nitrogen, and Orange = Dysprosium

Complex **111** has a similar Dy_4 core to **110** with two μ_3-OH ligands. Two 2.1111 bmh^{2-} ligands coordinate to the four dysprosium ions whilst four msh^- ligands coordinate in a 2.121 fashion between the four dysprosium ions. The coordination spheres of two dysprosium ions are completed by one chloride anion each (Figure 18).

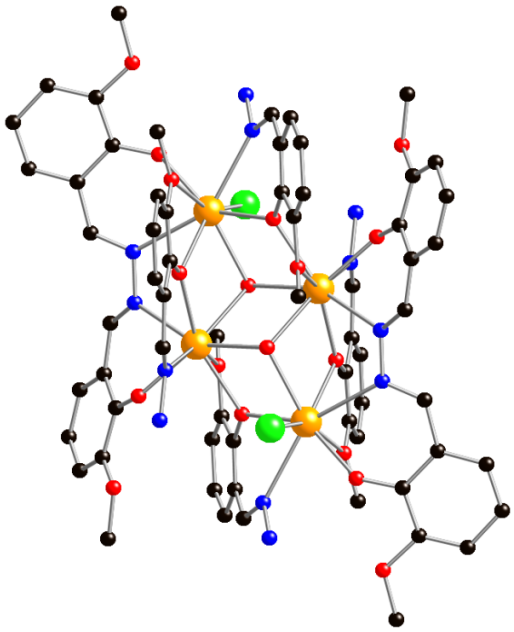

Figure 18. Solid state structure of 111. All hydrogen atoms omitted for clarity. Black = Carbon, Red = Oxygen, Blue = Nitrogen, Green = Chlorine and Orange = Dysprosium

In contrast to **110,** complex **111** has U_{eff} = 118 cm^{-1} in zero static field.[8a] This difference in magnetic behaviour has been attributed to differences in the coordination environment and geometry around the dysprosium ions present in both complexes.

Other Dy_4 cores can be seen when using Schiff base ligands such as a distorted oxo-centered tetrahedron in $[Dy_4(\mu_4\text{-}O)(\mu\text{-}OMe)_2(beh)_2(esh)_4]\cdot 3MeOH$ **112** [80] (H_2beh = bis(2-hydroxy-3-ethoxybenzylidene) hydrazone and Hesh = 3-ethoxysalicylaldehyde hydrazone). Two edges of the Dy_4 tetrahedron are bridged by OMe ligands, two edges are bridged by 2.1111beh^{2-} ligands and the remaining four edges are bridged by four 2.121 meh^- ligands (Figure 19). Complex **112** shows slow relaxation of magnetization at temperatures below 10 K and has U_{eff} = 16 cm^{-1} with only one relaxation process observed.[80]

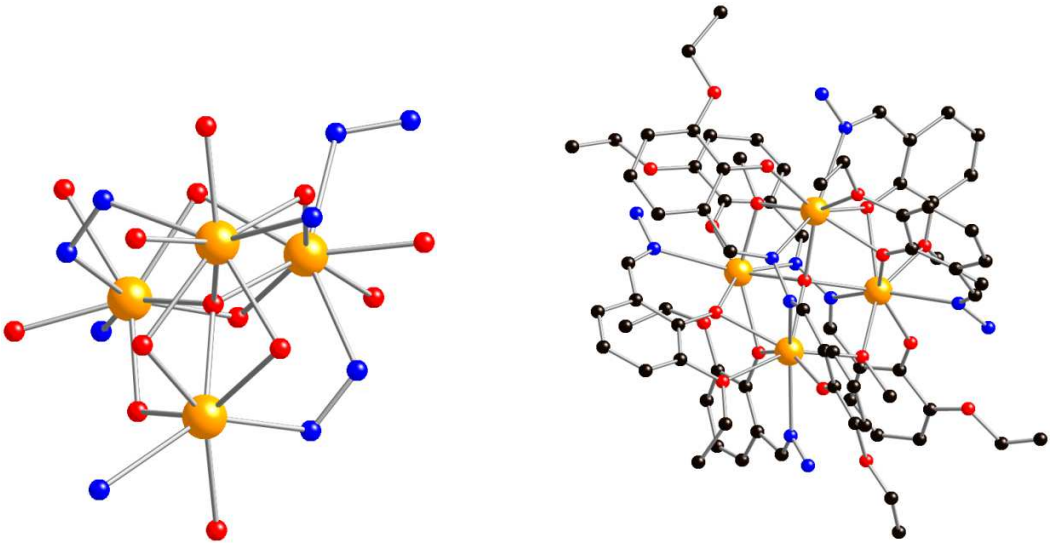

a b

Figure 19. a) Core structure of 112 with all peripheral ligand atoms removed. b) Solid state structure of 112. All hydrogen atoms omitted for clarity. Black = Carbon, Red = Oxygen, Blue = Nitrogen and Orange = Dysprosium

A linear Dy_4 SMM has been synthesized using Schiff base ligands: $[Dy_4(L^{21})_4(MeOH)_6]\cdot 2MeOH$ **113** [81] ($L^{21}H_3$ is shown in Scheme 4). Complex **113** contains four L^{21} ligands with two binding in a 4.121221 mode and two ligands binding in a 2.1211 mode. The coordination sphere of each dysprosium ion is completed by one methanol ligand (Figure 20). Complex **113** shows two relaxation processes with the slower relaxation process having U_{eff} = 120 cm^{-1}.[81]

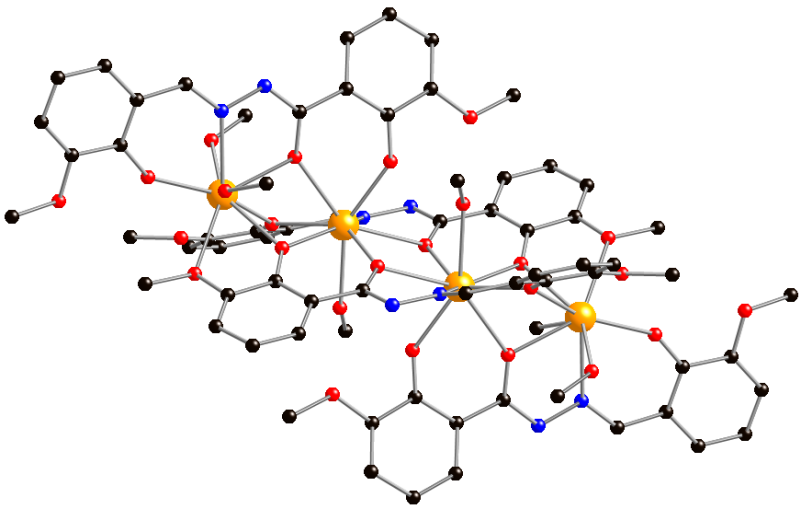

Figure 20. Solid state structure of 113. All hydrogen atoms omitted for clarity. Black = Carbon, Red = Oxygen, Blue = Nitrogen and Orange = Dysprosium

$[Er_4(salen)_6]\cdot 13H_2O$ **114** [82] and $[Dy_4(L^{22})_4(HL^{22})_2(C_6H_4NH_2COO_2)_2(MeOH)_4]\cdot 5MeOH$ **115** [83] **(**salen and $L^{22}H_2$ are shown in Scheme 4) have a "zig-zag" type structure. Complexes **114** – **115** both contain similar Ln_4O_6 cores in which two oxygen atoms bridge between each lanthanide ion to form a "zigzag" chain arrangement of lanthanide ions. Complex **114** contains six salen ligands binding in an 2.2111 mode to give each terminal erbium ion a coordination number of eight and each central erbium ion a coordination number of seven (Figure 21).[82] Complex **114** shows slow relaxation of magnetization in zero field but the one process observed is assigned as due to quantum tunnelling of magnetization. An applied field of 1000 Oe allows maxima to be seen in the out-of-phase magnetic susceptibility measurements and hence a barrier height of $U_{eff} = 9$ cm^{-1} can be extracted.[82]

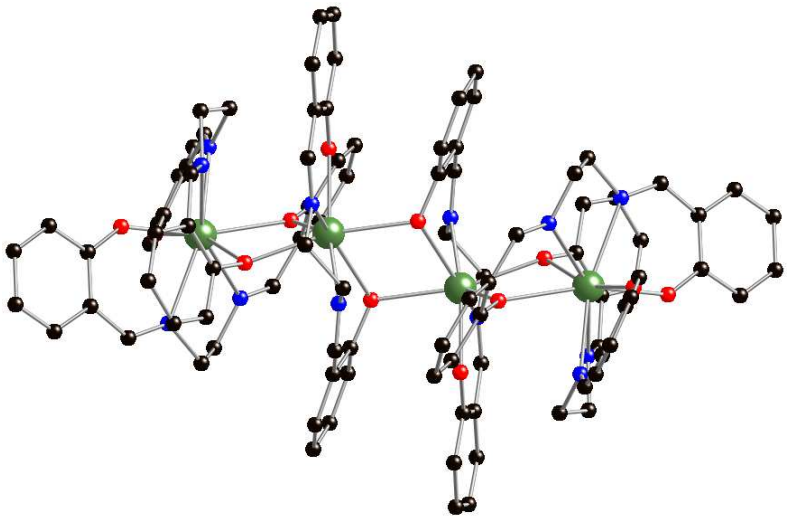

Figure 21. Solid state structure of 114. All hydrogen atoms omitted for clarity. Black = Carbon, Red = Oxygen, Blue = Nitrogen and Green = Erbium

Complex **115** contains two central L^{22} ligands binding in a 3.1211 mode, while two peripheral L^{22} ligands coordinate in a 2.1211 mode and two peripheral zwitterionic tridentate $L^{22}H$ ligands bind in a 2.111 mode. The coordination sphere of the two central dysprosium ions is completed by one methanol molecule each, whilst the coordination sphere of the two outer dysprosium ions is completed by one methanol molecule and one monodentate-$PhNH_2CO_2$ ligand (Figure 22).[83] Complex **115** has U_{eff} = 14 cm^{-1}.

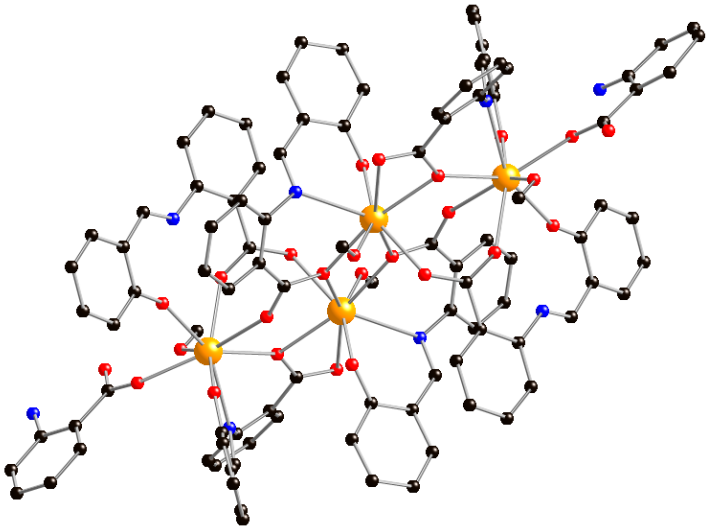

Figure 22. Solid state structure of 116. All hydrogen atoms omitted for clarity. Black = Carbon, Red = Oxygen, Blue = Nitrogen and Orange = Dysprosium

5.3 Other *N*+*O*-donor ligands

Non Schiff base *N*- and *O*-donor ligands have been used to isolate a number of Ln_4 SMMs with different architectures. One architecture is the "zigzag" architecture exhibited by $[Dy_4(pdmH)_2(pdm)_4(PhCO_2)_2(PhCO_2H)_4]\cdot MeOH\cdot H_2O$ **116** [84] and $[Dy_4(dhampH_3)_4(NO_3)_2](NO_3)_2\cdot 3MeOH\cdot H_2O$ **117** [85] ($pdmH_2$ = pyridine-2,6-dimethanol and $dhampH_5$ shown in Scheme 4).

Complex **116** contains four pdm^{2-} ligands binding in a 2.211 mode and two $pdmH^-$ ligands binding a 2.211 mode to the terminal dysprosium ions. The coordination sphere of each terminal dysprosium ion is completed by one chelating $PhCO_2^-$ ligand and two monodentate $PhCO_2H$ ligands. This means that each dysprosium ion in **116** is eight-coordinate (Figure 23). Complex **116** is stated to be an SMM, however even with an applied

field of 3000 Oe, no maxima in the out-of-phase magnetic susceptibility are observed down to 2 K.[84]

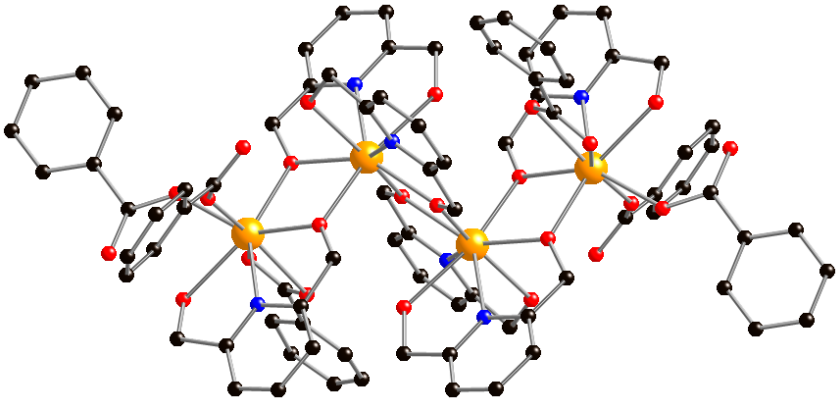

Figure 23. Solid state structure of 116. All hydrogen atoms omitted for clarity. Black = Carbon, Red = Oxygen, Blue = Nitrogen and Orange = Dysprosium

Complex **117** shows no maxima in the out of phase magnetic susceptibility, but a barrier height of U_{eff} = 1.5 cm^{-1} has been calculated. The lack of maxima in the out of phase susceptibility of **117** makes it difficult to unambiguously assign **117** as a true SMM. Complex **117** contains two octadentate $dhampH_3^{2-}$ ligands binding in a 3.1112112 mode and two pentadentate $dhampH_3^{2-}$ ligands binding in a 2.2111 mode. The coordination sphere of the two central dysprosium ions is complete by one η^2-nitrate anion each (Figure 24). Cole-Cole plots reveal that complex **117** has only one relaxation process present within the temperature range of the experiment.[85]

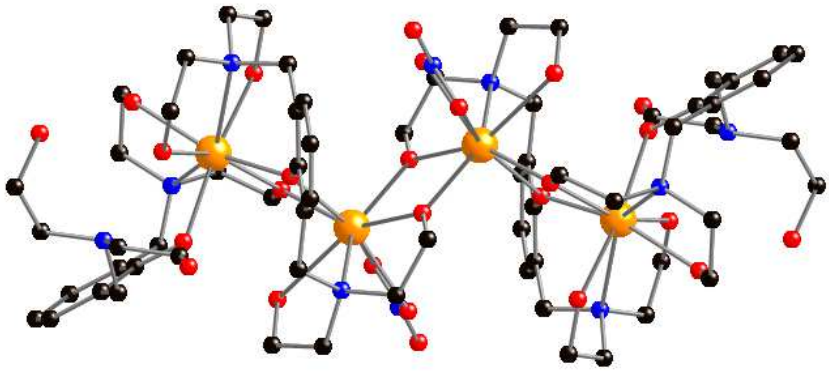

Figure 24. Solid state structure of 117. All hydrogen atoms omitted for clarity. Black = Carbon, Red = Oxygen, Blue = Nitrogen and Orange = Dysprosium

Defect-dicubane structures similar to **103 – 104** have been seen for $Dy_4(\mu_3\text{-}OH)_2(hmmpH)_2(hmmp)_2Cl_4]\cdot 3MeOH\cdot MeCN$ **118**,[86] $[Dy_4(\mu_3\text{-}OH)_2(hmmpH)_2(hmmp)_2(N_3)_4]\cdot 4MeOH$ **119** [86] and $[Dy_4(\mu_3\text{-}OH)_2(L^{23})_2(acac)_6]\cdot 2(H_2L^{23})\cdot 2MeCN$ **120** (H_2L^{23} is shown in Scheme 4).[87] Complexes **118** – **120** all have a central Dy_4 core with two μ_3-OH ligands, one above and one below the Dy_4 plane. Complex **118** contains two $hmmp^{2-}$ ligands binding in a 3.1212 mode and two $hmmpH^-$ ligands binding in a 2.1211 mode. The coordination sphere of two dysprosium ions is then completed by two chloride ligands on each. Complex **119** is essentially isomorphous to **118** with the exception of the chloride anions, which have been replaced with azide anions. Maxima are seen in the out-of-phase susceptibility of **119**, allowing a small energy barrier to be calculated (U_{eff} = 5 cm^{-1}); no peaks are seen for χ_M" for **118**. The difference in magnetic behaviour between **118** and **119** is attributed to the change in crystal field around the Dy(III) caused by replacing chloride anions with azides.[86]

Complex **120** contains the previously mentioned $Dy_4(OH)_2$ core as well as two L^{23} ligands binding in a 3.2112 mode. The two dysprosium ions bound in the "pocket" of each

L^{23} ligand are also coordinated to one chelating acac ligand and one 2.21 acac ligand. The coordination spheres of the remaining two dysprosium ions are completed by one η^2-acac ligand (Figure 25). Complex **120** shows no maxima in the out-of-phase susceptibility in zero applied field. To elucidate the height of the barrier an optimal static field of 1400 Oe was applied during the a.c. susceptibility experiments, which allowed a barrier of U_{eff} = 15 cm^{-1} to be derived.[87]

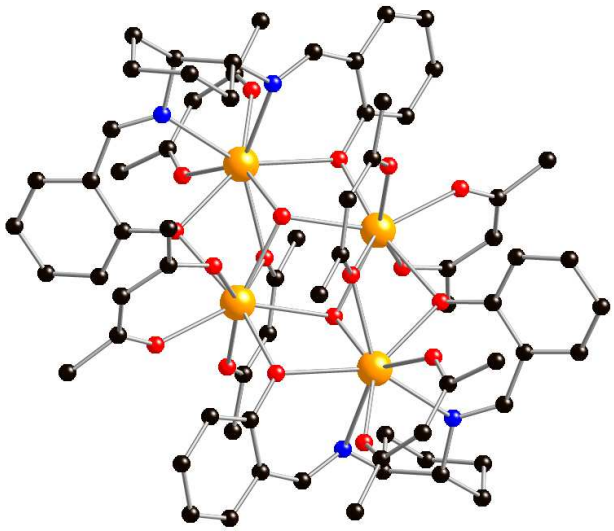

Figure 25. Solid state structure of 120. All hydrogen atoms omitted for clarity. Black = Carbon, Red = Oxygen, Blue = Nitrogen and Orange = Dysprosium

$[Dy_4(L^{24})_2(C_6H_5CO_2)_{12}(MeOH)_4]$ **121** [88] contains a linear Dy_4 chain bridged by six 2.11 benzoate ligands. The two terminal dysprosium ions are bound to one monodentate L^{24} ligand each and two 1.11-$PhCO_2^-$ ligands. The central dysprosium ions are bound to a single chelating benzoate with the coordination sphere of each central dysprosium ion being completed by two methanol ligands (Figure 26). Complex **121** shows SMM behaviour and Cole-Cole plots indicate that multiple relaxation processes are present for **121**. The slowest relaxation process is assigned U_{eff} = 12 cm^{-1}.[88]

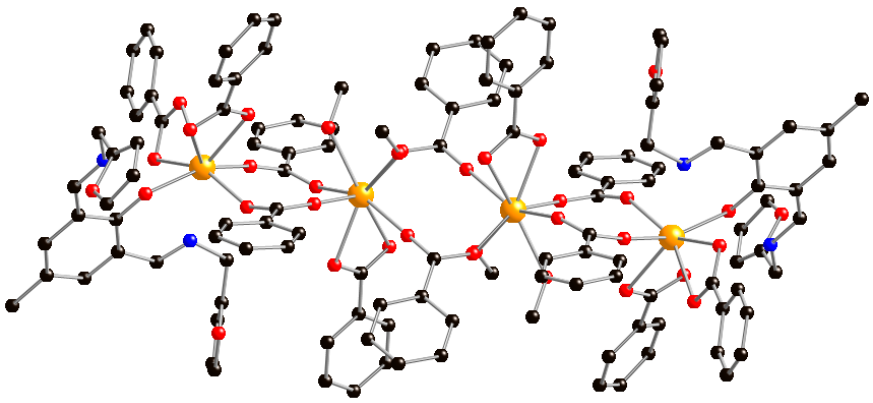

Figure 26. Solid state structure of 121. All hydrogen atoms omitted for clarity. Black = Carbon, Red = Oxygen, Blue = Nitrogen and Orange = Dysprosium

5.4 Other Ligands

Other ligands used to form Ln_4 based SMMs include calixerenes [89,90] and polyoxometallates [91] as well as purely *N*-donor ligands.[92] Both $[Dy_4(OH)_4(L^{15})_2(H_2O)_4(MeOH)_4]\cdot 4H_2O$ **122** [89] and $[Dy_4(\mu_4\text{-}OH)(PTC4A)_2Cl_3(MeOH)_2(H_2O)_3]\cdot 4.7MeOH\cdot 2H_2O$ **123** [90] (see Scheme 4 for ligand structures) contain a Dy_4 unit with one calixarene binding above the unit and one calixarene binding below. Complex **122** contains a disordered Dy_4 cubane in which two phenoxide oxygen atoms from the top calixarene bind to each of the top two dysprosium ions and the same bonding mode is seen for the bottom calixarene with the bottom two dysprosium ions. The coordination sphere of each dysprosium ion is completed with water, methanol and one S-O oxygen atom from the calixarene (Figure 27).[89]

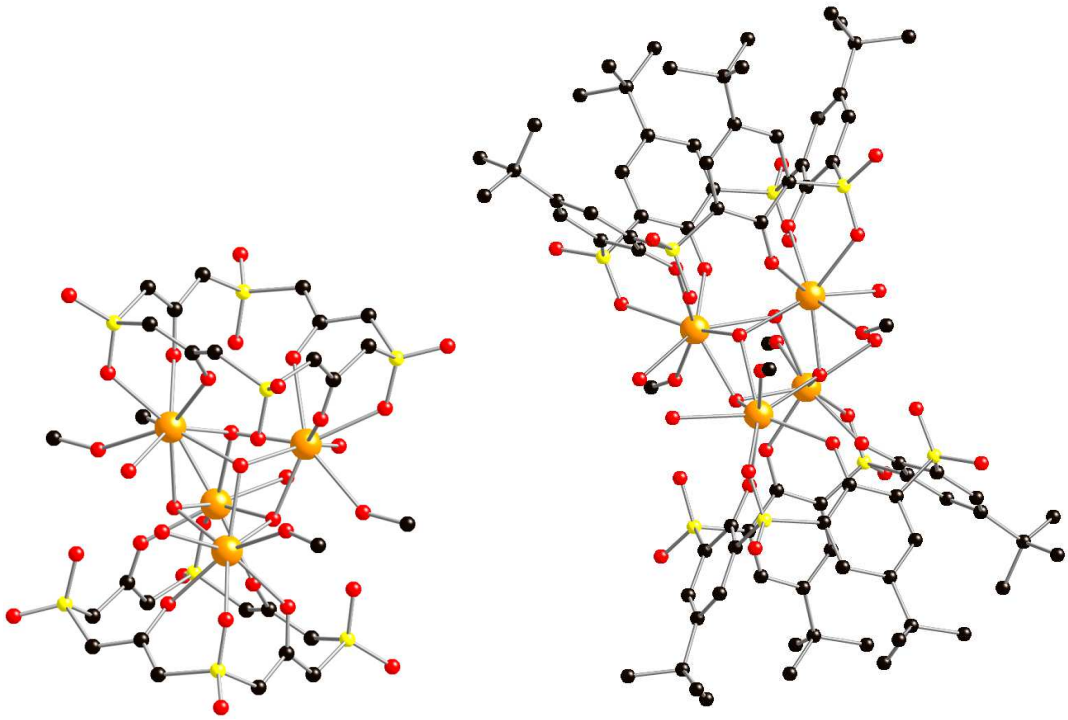

a b

Figure 27. a) Core structure of 122 with peripheral ligand atoms removed b) Solid state structure of 122. All hydrogen atoms omitted for clarity. Black = Carbon, Red = Oxygen, Yellow = Sulfur and Orange = Dysprosium

In contrast complex **122** contains a Dy_4 square in which each edge of the square is bridged by two phenoxide oxygen atoms (one from each calixarene). Each dysprosium ion is also bound by one sulfur atom from each calixarene and the coordination sphere of three dysprosium ions is completed with one water molecule and one chloride anion whilst the other dysprosium ion is coordinated by two water molecule to complete the coordination sphere (Figure 28).[90]

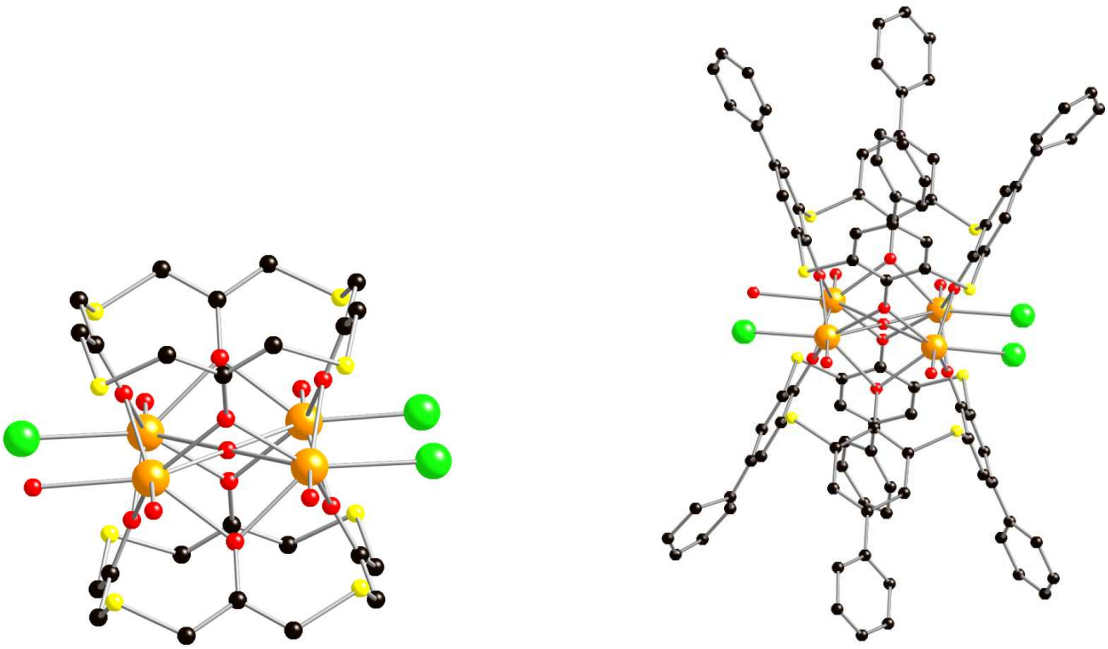

a b

Figure 28. a) Core structure of 123 with all peripheral ligand atoms removed b) Solid state structure of 123. All hydrogen atoms omitted for clarity. Black = Carbon, Red = Oxygen, Yellow = Sulfur, Green = Chlorine and Orange = Dysprosium

Complex **122** has U_{eff} = 16 cm^{-1} whilst the barrier height for **123** shows no peaks in the out-of-phase magnetic susceptibility at temperatures down to 2 K. The differences in magnetic behaviour of **122** and **123**is presumably related to coordination environment and geometry.[90]

An *N*-donor ligand, 3,5-bis(pyridin-2-yl)-1,2,4-triazole (2,2-bptH) has been used to isolate a Dy_4 SMM $[Dy_4(\mu_3\text{-}OH)_2(\mu\text{-}OH)_2(2,2\text{-}bpt)_4(NO_3)_4(EtOH)_2]$**124**.[92] Complex **124** contains four dysprosium ions that lie at the vertices of a parallelogram bridged by two μ_3-OH (above and below the plane of the parallelogram) and two μ_2-OH bridging the short edges of the Dy_4 parallelogram. Two 2,2-bpt ligands chelate to each dysprosium ion on the long edge of the Dy_4 parallelogram meaning **124** contains four 2,2-bpt ligands overall. Two

dysprosium ions are coordinated to one ethanol and one monodentate nitrate anion, whilst the other two dysprosium ions are bound to a single monodentate nitrate to complete its coordination sphere (Figure 29). Complex **124** has U_{eff} = 56 cm^{-1} brought about by the toroidal arrangement of magnetic moments on the dysprosium centers in a similar manner to complexes **89** and **90** (see above). The SMM behaviour of **124** is attributed to the population of a low lying excited state close to the ground state in which the magnetic moments of the dysprosium centers are no longer arranged perpendicular to each other.[92]

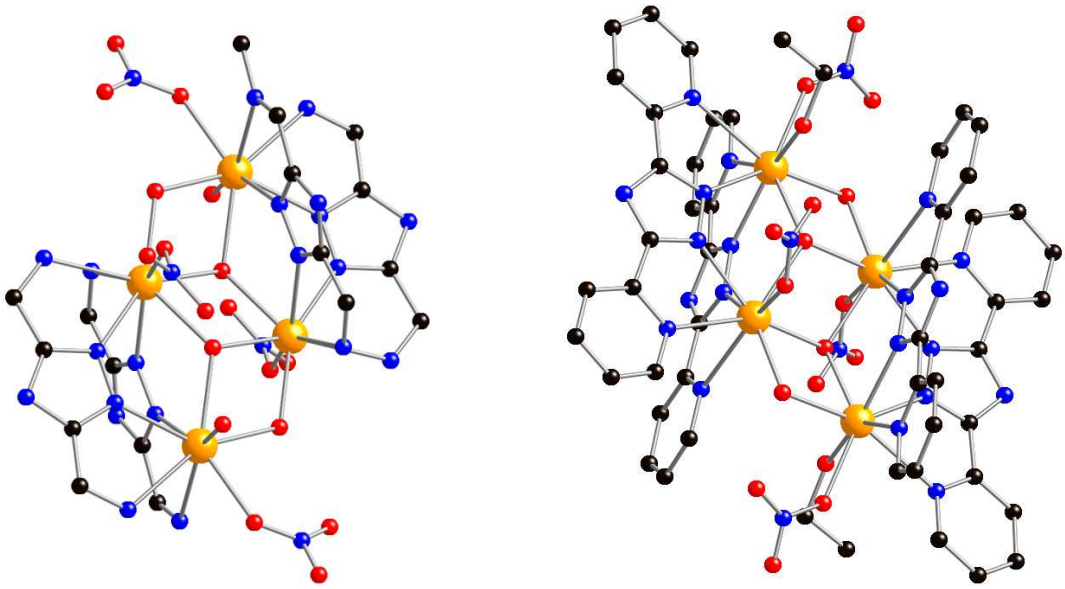

a b

Figure 29. a) Core structure of 124 with all peripheral ligand atoms removed. b) Solid state structure of 124. All hydrogen atoms omitted for clarity. Black = Carbon, Red = Oxygen, Blue = Nitrogen and Orange = Dysprosium

$(HDABCO)_8H_5Li_5[Dy_4As_5W_{40}O_{144}(H_2O)_{10}(gly)_2]\cdot 25H_2O$ **125** [91] (HDABCO = mono-protonated 1,4-diazabicyclooctane, gly = glycine) uses a polyoxometallate to stabilize a Dy_4 core. Complex **125** has U_{eff} = 3 cm^{-1}.[91]

6. Pentametallic and larger 4f-SMMs

Table 5 shows all reported lanthanide SMMs containing five or more lanthanide centers; non-trivial ligands used in these complexes are shown in Scheme 5.

Table 5. Lanthanide SMMs containing five or more lanthanide centers from 2003 to present with the reported values of U_{eff} (cm^{-1})

Compound	Compound Number	U_{eff} (cm^{-1})	Reference
$[Dy_5O(O^iPr)_{13}]$	126	367	93
$[Ho_5O(O^iPr)_{13}]$	127	278	94
$[Dy_5(\mu_4\text{-}OH)(\mu_3\text{-}OH)_4(\mu\text{-}\eta^2\text{-}Ph_2acac)_4(\eta^2\text{-}Ph_2acac)_6]$	128	23	95
$[Dy_5(\mu_3\text{-}OH)_6(Acc)_6(H_2O)_{10}]Cl_9\cdot 24H_2O$	129	1	96
$[Dy_6(teaH)_6(NO_3)_6]\cdot 8MeOH$	130	not measurable	97
$[Dy_6(teaH)_2(teaH_2)_2(CO_3)(NO_3)_2(chp)_7(H_2O)](NO_3)\cdot 4.5MeOH\cdot 1.5H_2O$	131	3	98
$[Tb_6(teaH)_2(teaH_2)_2(CO_3)(NO_3)_2(chp)_7(H_2O)](NO_3)\cdot 4.5MeOH\cdot 1.5H_2O$	132	3	98
$[Dy_6(\mu_3\text{-}OH)_4(L^{17})_4(avn)_4(NO_3)_4(H_2O)_4](NO_3)_2\cdot 3H_2O\cdot 3((CH_3)_2CO)$	133	7	8b
$[Dy_6(\mu_3\text{-}OH)_4(L^{17})_4(L^{25})_2(H_2O)_9Cl]Cl_5\cdot 15H_2O$	134	139	99
$[Dy_6(OAc)_3(\mu_3\text{-}CO_3)_2(L^{26})_5(HL^{26})(MeOH)_2]\cdot 4H_2O\cdot 5MeOH\cdot EtOH$	135	39	100
$[Dy_6(ovph)_4(Hpvph)_2Cl_4(H_2O)_2(CO_3)_2]\cdot MeOH\cdot H_2O\cdot MeCN$	136	53	101
$[Dy_6(\mu_3\text{-}OH)_3(\mu_3\text{-}CO_3)(\mu\text{-}OMe)(Hovph)_6(MeOH)_4(H_2O)_2]\cdot 3MeOH\cdot 2H_2O$	137	26	102
$[Dy_6(L^{27})_4(\mu_3\text{-}OH)_4(MeOH)_2(NO_3)_2]\cdot 6MeCN$	138	2	103

$[Dy_6(\mu_4\text{-}O)_2(C4A)_2(NO_3)_2(HCO_2)_2(MeO)_2(DMF)_4(MeOH)_4]$	139	5	104
$[Dy_7(OH)_6(thmeH_2)_5(thmeH)(tpa)_6(MeCN)_2](NO_3)_2$	140	97	105
$[Dy_8(\mu_3\text{-}OH)_4(L^{17})_2(mvn)_2(p\text{-}NO_2bz)_{14}(MeOH)_2]\cdot 3.09MeCN\cdot 6MeOH\cdot H_2O$	141	not measurable	106
$[Dy_8(HL^{28})_{10}(C_6H_4NH_2CO_2)_2(\mu_3\text{-}OH)_8(OH)_2(NO_3)_2(H_2O)_4]$	142	not measurable	107
$[Dy_8(ovph)_8(CO_3)_4(H_2O)_8]\cdot 12MeCN\cdot 6H_2O$	143	not measurable	108
$[Dy_8(\mu_4\text{-}CO_3)_4(L^{26})_8(H_2O)_8]\cdot 10MeOH\cdot 2H_2O$	144	52	109
$[Dy_7(\mu_3\text{-}OH)_5(MeOsalox)_2(MeOsaloxH)_4(PhCO_2)_7(OH)(H_2O)1.5(MeOH)_{0.5}]\cdot 2.5MeOH\cdot 5.25H_2O$	145	not measurable	110
$[Dy_8(OH)_8(phendox)_6(H_2O)_8]Cl_2\cdot(OH)_2\cdot 18H_2O\cdot 18MeOH$	146	3	111
$[Dy_{30}I(\mu_3\text{-}OH)_{24}(\mu_3\text{-}O)_6(NO_3)_9(IN)_{41}(OH)_3(H_2O)_{38}]$	147	not measurable	112
$[Dy_{12}(L^{29})_6(OH)_4O_2(CO_3)_6][Dy_{12}(L^{36})_6(OH)_4O_4(CO_3)](ClO_4)_4\cdot xH_2O$	148	not measurable	113
$[Dy_9(OH)_{10}(hmp)_8(NO_3)_8(DMF)_8](OH)\cdot 1.6H_2O\cdot 0.6DCM$	149	not measurable	114
$[Dy_{10}(\mu_3\text{-}OH)_4(OAc)_{20}(H_2L^{30})_2(H_3L^{30})_2\{NH_2C(CH_2OH)_3\}_2]$	150	not measurable	115
$[Dy_{11}(OH)_4(phendox)_6(phenda)_3(OAc)_3](OH)\cdot 40H_2O\cdot 7MeOH$	151	1	111
$[\{Dy_{12}(OH)_{16}(phenda)_8(H_2O)_8\}][Cl]_2(OH)_2\cdot 15MeOH\cdot 40H_2O$	152	2	116
$[\{Dy_{12}(OH)_{16}(phenda)_8(H_2O)_8\}][Cl]_2[Dy(phenda)_2]_2$	153	5	116

H_4C4A = *p*-tert-butylcalix[4]arene

$avnH_2$ = aldol-vanillin

$teaH_3$ = triethanolamine

Hchp = 6-chloro-2-hydroxypyridine

$L^{25}H_2$ = 2-hydroxymethyl-6-methoxyphenol

$thmeH_3$ = tris(hydroxymethyl)ethane

tpaH = triphenylacetic acid

hmpH = 2-(hydroxymethyl)pyridine

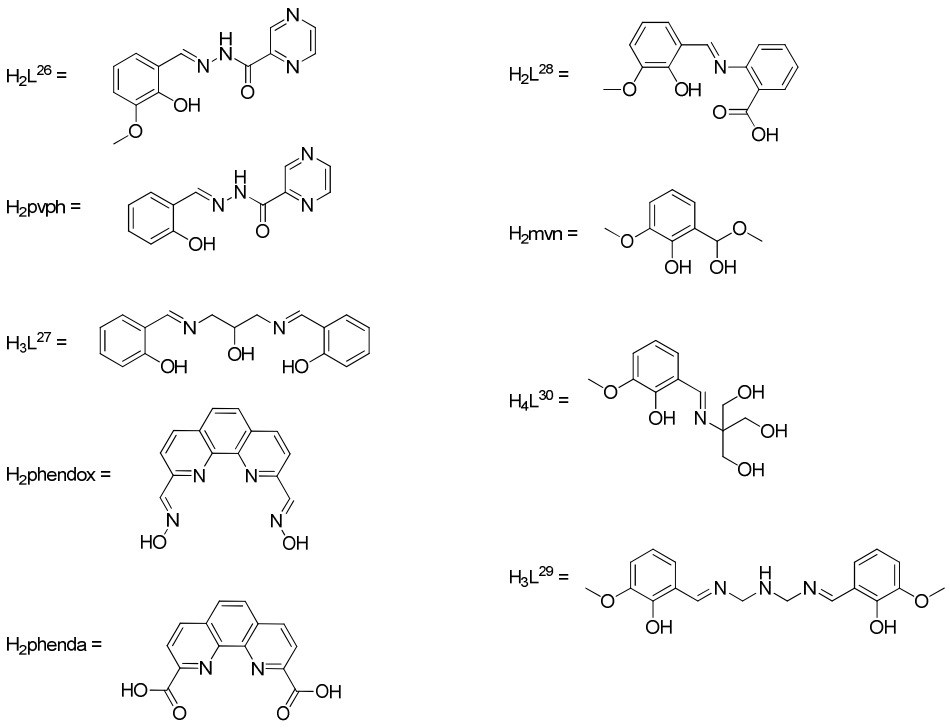

Scheme 5. Chemical structures of non trivial ligands used to produce lanthanide SMMs containing five or more lanthanide centers.

6.1 Ln_5 + Ln_6 SMMs

6.1.1 Alcohols, Ketones and Acids

Alkoxides have been used to create polynuclear lanthanide SMMs including $[Dy_5O(O^iPr)_{13}]$ **126** [93] which holds the record for largest barrier to reversal of magnetization for a

polynuclear lanthanide cluster with U_{eff} = 367cm^{-1} as well as the holmium analogue; [$Ho_5O(O^iPr)_{13}$] **127**.[94] Complexes **126** and **127** are isostructural, and contain a Ln_5 square based pyramid centred around a μ_5-O.Each edge of the Ln_4 square base is bridged by a single μ_2-^{i}PrO$^-$ ligand whilst a μ_3-^{i}PrO$^-$ sits on each vertical face of the Ln_5 pyramid. The coordination sphere of each lanthanide is then completed by one ^{i}PrO$^-$ ligand each (Figure 30). Complex **126** shows frequency dependence of out-of-phase magnetic susceptibility at temperatures up to 56 K and shows evidence of two possible relaxation processes.[93] In contrast complex **127** does not show maxima in the out of phase susceptibility in zero field and as such requires an external static field of 3.5 kG or 5.5 kG to enable elucidation of the barrier height. The external field suppresses quantum tunnelling of magnetization which is aided in **127** by the nuclear spin of holmium. Complex **127** has U_{eff} = 278 cm^{-1}.[94]

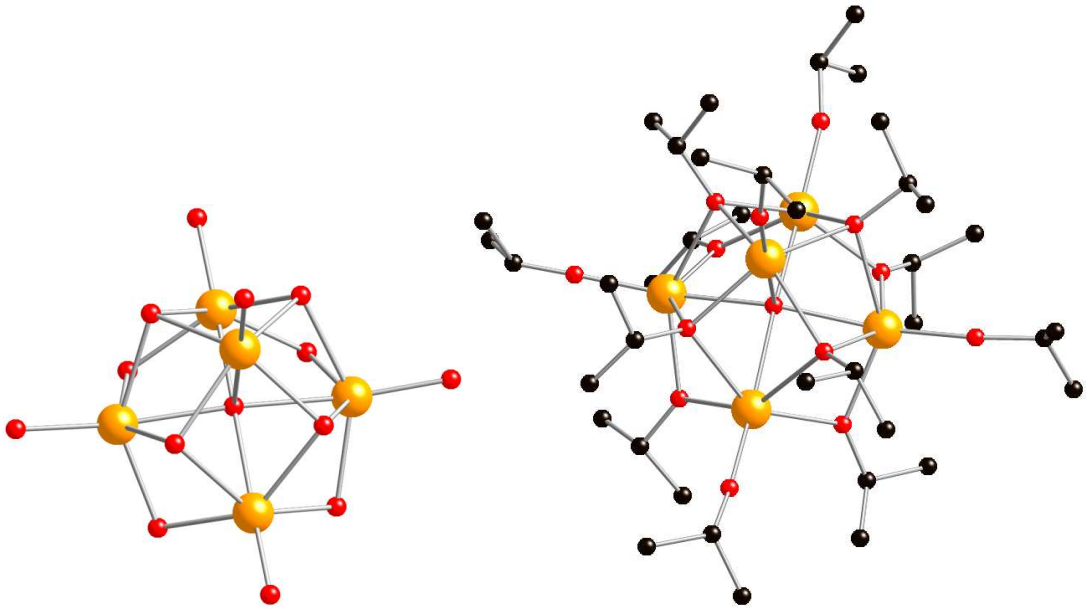

a b

Figure 30. a) Core structure of 126 with all peripheral ligand atoms removed b) Solid state structure of 126. All hydrogen atoms omitted for clarity. Black = Carbon, Red = Oxygen and Orange = Dysprosium

$[Dy_5(\mu_4\text{-}OH)(\mu_3\text{-}OH)_4(Ph_2acac)_4(Ph_2acac)_6]$ **128** [95] has a Dy_5 square based pyramid core, similar to both **126** and **127**, but lacks the central μ_5-oxide and each Dy(III) site is eight-coordinate. Complex **128** has a μ_3-OH on each face of the pyramid as well as the base. Four 2.21 Ph_2acac ligands bridge each edge of the base of the Dy_5 pyramid. The coordination sphere of each dysprosium ion in the Dy_4 plane is completed by one chelating Ph_2acac each whilst the coordination sphere of the final dysprosium ion is completed by two chelating Ph_2acac ligands (Figure 31). Complex **128** shows SMM behaviour and has U_{eff} = 23 cm^{-1}.[95] The differences between the magnetic properties of **126**/**127** and **128** is presumably due to the very different coordination geometries at the lanthanide ions in these complexes.

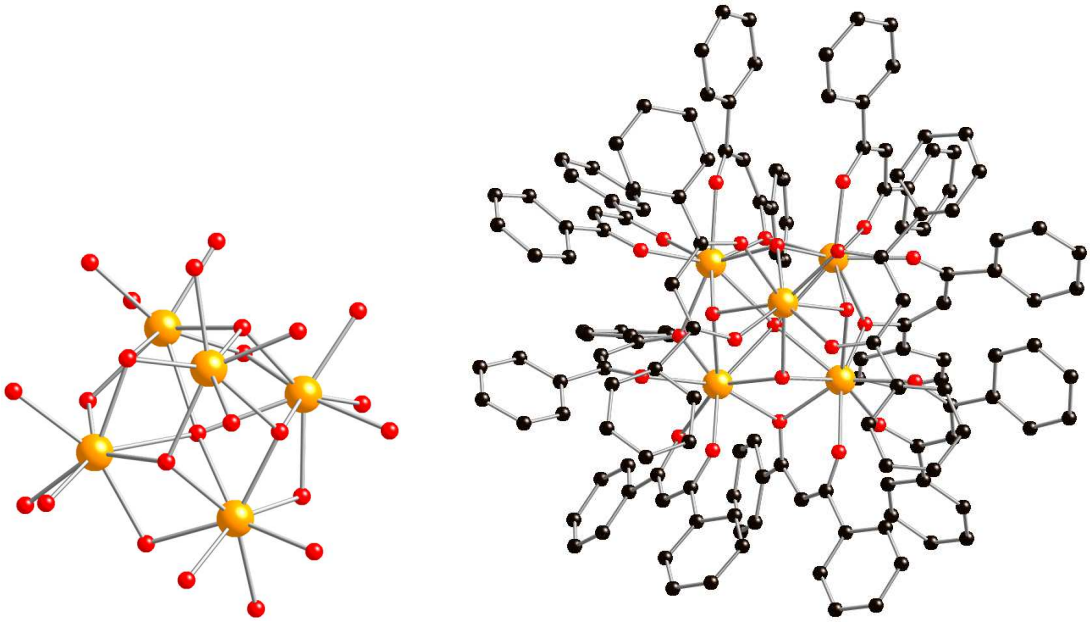

a b

Figure 31. a) Core structure of 128 with all peripheral ligand atoms removed b)Solid state structure of 128. All hydrogen atoms omitted for clarity. Black = Carbon, Red = Oxygen and Orange = Dysprosium

$[Dy_5(\mu_3\text{-}OH)_6(Acc)_6(H_2O)_{10}]Cl_9 \cdot 24H_2O$ **129** [96] contains a trigonal bipyramidal arrangement of dysprosium ions with a μ_3-OH on each face (six on total) and six 2.11 Acc ligands (on bridging each edge of the trigonal bipyramid) (Figure 32). Complex **129** show frequency dependency of out of phase magnetic susceptibility but no maxima. Despite this an energy barrier height of U_{eff} = 1 cm^{-1} has been calculated. The lack of maxima in the out of phase susceptibility of **129** makes the validity of **129** being an SMM questionable.[96]

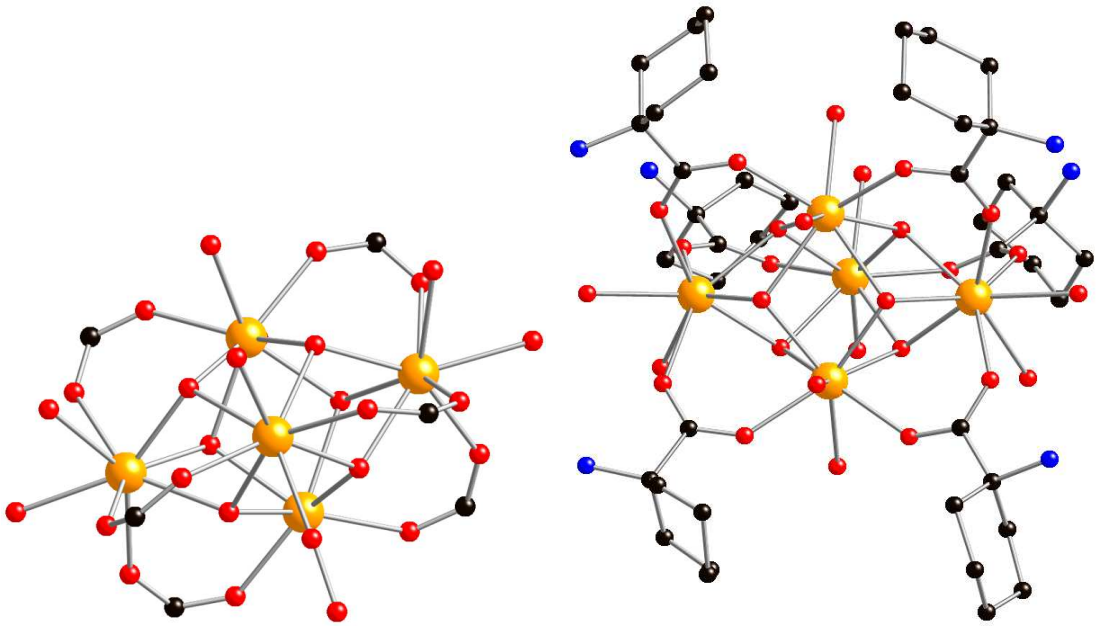

a b

Figure 32. a) Core structure of 129 with all peripheral ligand atoms removed b) Solid state structure of 129. All hydrogen atoms omitted for clarity. Black = Carbon, Red = Oxygen, Blue = Nitrogen and Orange = Dysprosium

As well as simple alcohols, tripodal alcohols in the form of $teaH_3$ (triethanolamine) have been used to create: $[Dy_6(teaH)_6(NO_3)_6] \cdot 8MeOH$ **130**,[97] and $[Ln_6(teaH)_2(teaH_2)_2(CO_3)(NO_3)_2(chp)_7(H_2O)](NO_3) \cdot 4.5MeOH \cdot 1.5H_2O$ (Ln = Dy **131** and Tb **132**, Hchp = 6-

chloro-2-hydroxypyridine).[98] Complex **130** contains a Dy_6 wheel in which six teaH ligands bind in a3.2112mode and the coordination sphere of each dysprosium ion is complete by one η^2-nitrate anion (Figure 33). Complex **130** shows frequency dependency of out of phase susceptibility at temperatures below 7K but no maxima is observed in the measurements.[97]

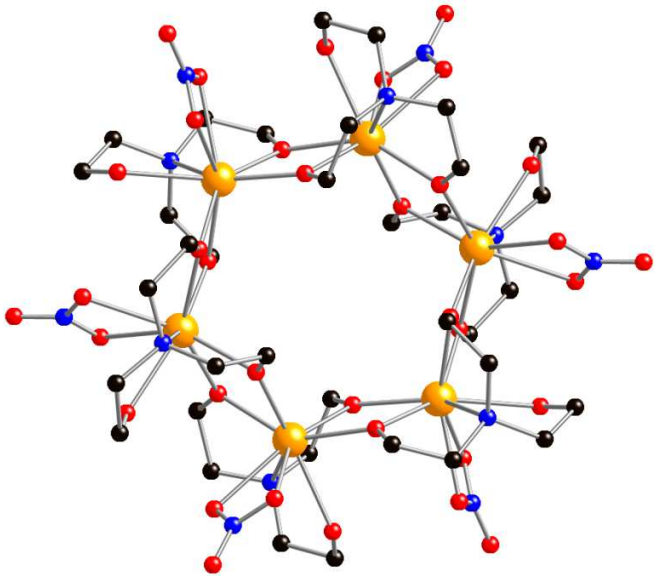

Figure 33. Solid state structure of 130. All hydrogen atoms omitted for clarity. Black = Carbon, Red = Oxygen, Blue = Nitrogen and Orange = Dysprosium

Complexes **131** and **132** are isostructural and contain four coplanar lanthanide ions in a trapezoid motif with one lanthanide ion above the Ln_4 plane and one below. Complexes **131** and **132** contain a central 6.422 CO_3^{2-} anion as well as two 3.2112 teaH ligands and two 2.211 $teaH^2$ ligands. Five chp ligands bind in a 2.21 mode whilst two are monodentate. The coordination spheres of the lanthanide ions above and below the Ln_4 plane are completed by a chelating nitrate anion each (Figure 34). Neither **131** nor **132** shows maxima in the frequency dependency of out of phase susceptibility, even in fields of 5000 Oe.[98]

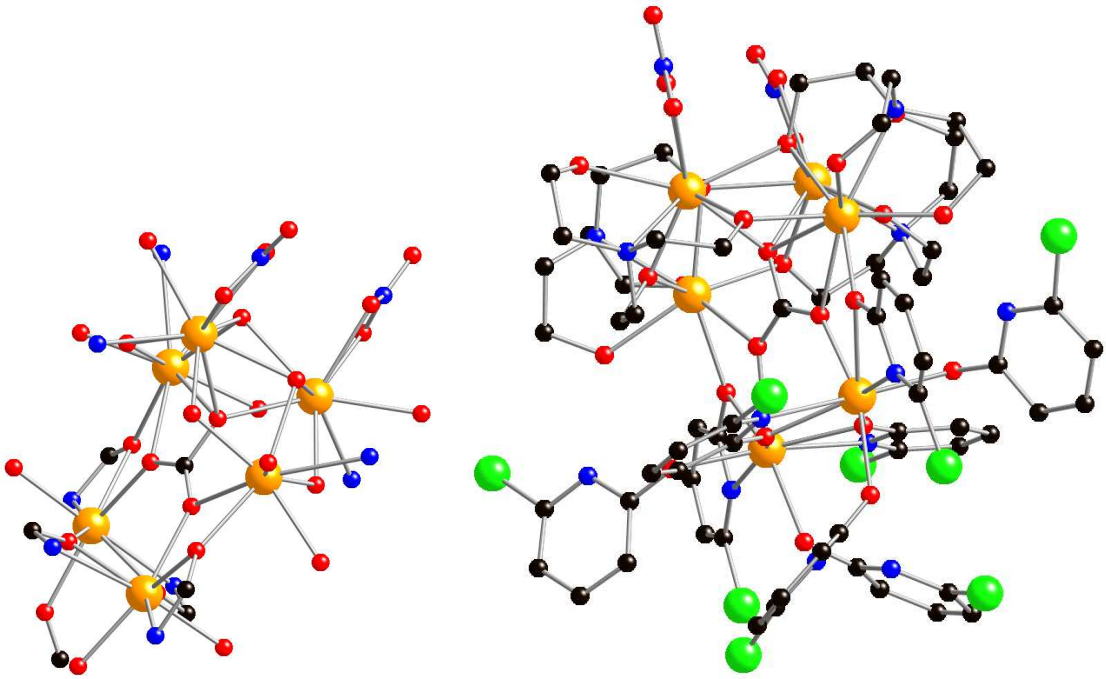

a b

Figure 34. a) Core structure of 131 with all peripheral ligand atoms removed b) Solid state structure of 131. All hydrogen atoms omitted for clarity. Black = Carbon, Red = Oxygen, Blue = Nitrogen, Green = Chlorine and Orange = Dysprosium

$[Dy_6(\mu_3\text{-}OH)_4(L^{17})_4(avn)_4(NO_3)_4(H_2O)_4]\cdot(NO_3)_2\cdot 3H_2O\cdot 3((CH_3)_2CO)$ **133** [8b] and $[Dy_6(\mu_3\text{-}OH)_4(L^{17})_4(L^{25})_2(H_2O)_9Cl]Cl_5\cdot 15H_2O$ **134** [99] ($avnH_2$ = aldol-vanillin and $L^{25}H_2$ = 2-hydroxymethyl-6-methoxyphenol) both contain a pair of linked $Dy_3(\mu_3\text{-}OH)_2$ triangles. Complex **133** contains two 3.2121 avn ligands that bridge between the two Dy_3 triangles. Four L^{17} ligands bind in a 2.121 mode whilst four monodentate nitrate ions and four water molecules complete the coordination spheres of four of the six dysprosium ions (Figure 35).[8b] Complex **133** has U_{eff} = 7cm^{-1} whilst showing evidence of ferromagnetic interactions between dysprosium ions.[8b]

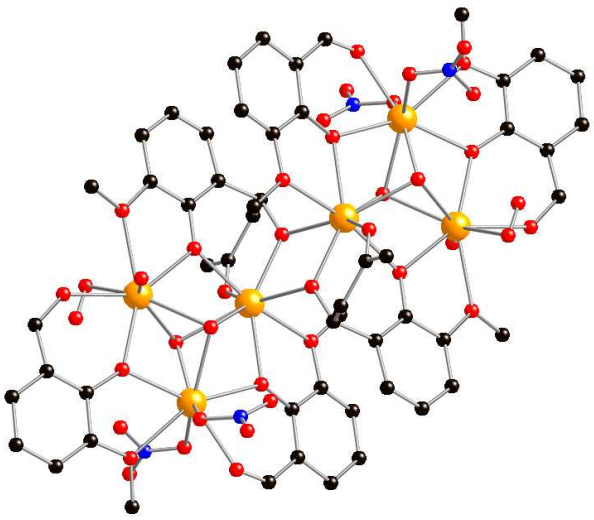

Figure 35. Solid state structure of 133. All hydrogen atoms omitted for clarity. Black = Carbon, Red = Oxygen, Blue = Nitrogen and Orange = Dysprosium

Complex **134** contains two 3.221 L^{25} ligands bridging between the two Dy_3 triangles. Four L^{17} ligands bind in a 3.221 mode and the coordination spheres of two dysprosium ions are completed by two water molecules. The coordination spheres of the two dysprosium ions linking the two Dy_3 triangles are completed by one water molecule whilst the coordination spheres of the remaining two dysprosium ions are completed by one water molecule and one chloride ion each (Figure 36). Complex **134** shows two distinct maxima in the out of phase magnetic susceptibility suggesting the presence of two relaxation processes. The presence of two relaxation processes is attributed to the change in magnetic anisotropy from easy plane (5 K) to easy axis (25 K). The higher temperature relaxation process has U_{eff} = 139 cm^{-1}.[99]

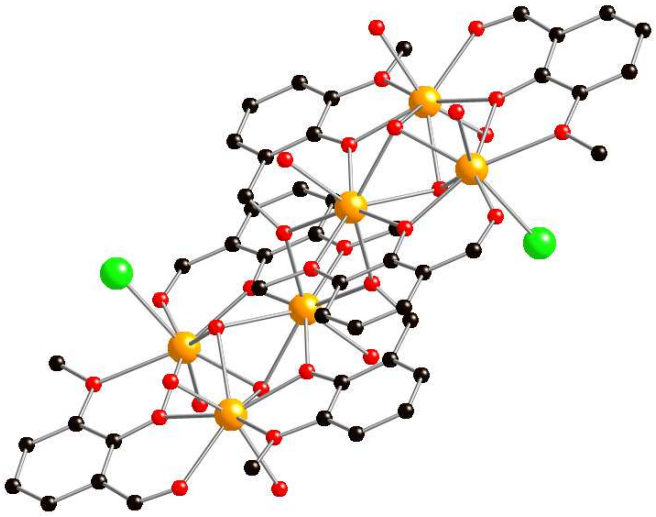

Figure 36. Solid state structure of 134. All hydrogen atoms omitted for clarity. Black = Carbon, Red = Oxygen, Green = Chlorine and Orange = Dysprosium

6.1.2 Schiff Base Ligands

$[Dy_6(OAc)_3(\mu_3\text{-}CO_3)_2(L^{26})_5(HL^{26})(MeOH)_2]\cdot 4H_2O\cdot 5MeOH\cdot EtOH$ **135** [100] and $[Dy_6(ovph)_4(Hpvph)_2Cl_4(H_2O)_2(CO_3)_2]\cdot MeOH\cdot H_2O\cdot MeCN$ **136** [101] ($L^{26}H_2$ and H_2pvph are shown in Scheme 5, H_2ovph = o-vanillin picolinoylhydrazone) both contain Schiff base ligands connecting two Dy_3 triangles to form Dy_6trigonal prism core. Both **135** and **136** contain two Dy_3 triangles each with a central 3.222CO_3^{2-} anion. Complex **135** contains six L^{26} ligands each binding in a 2.1211mode and three OAc^- ligands (one on each edge of the prism) binding in a 2.11 mode. This means each dysprosium ion in **135** is eight coordinate (Figure 37). Complex **135** shows only one relaxation path for magnetization and has U_{eff} = 39 cm^{-1}.[100]

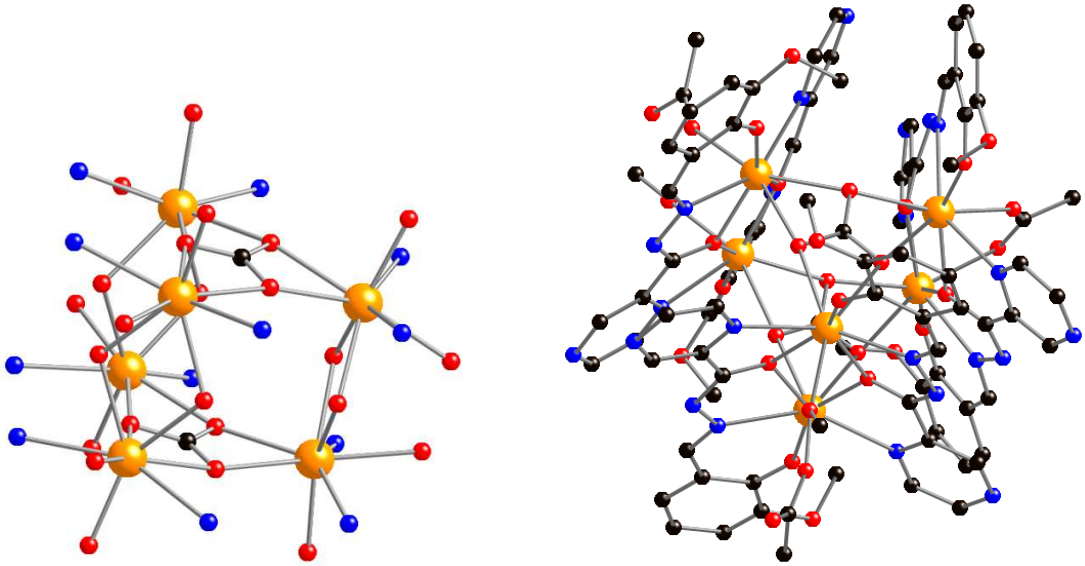

a b

Figure 37. a) Core structure of 135 with all peripheral ligand atoms removed b) Solid state structure of 135. All hydrogen atoms omitted for clarity. Black = Carbon, Red = Oxygen, Blue= Nitrogen and Orange = Dysprosium

Complex **136** contains six ovph/Hovph ligands with each pair binding in a "head to tail" fashion in a 2.1211 mode. The coordination spheres of four dysprosium ions are completed by a single chloride ion each whilst the coordination spheres of the two remaining dysprosium ions are completed by a single water molecule each (Figure 38). Complex **136** shows SMM behaviour and has U_{eff} = 53cm^{-1} whist only showing one relaxation pathway.[101]

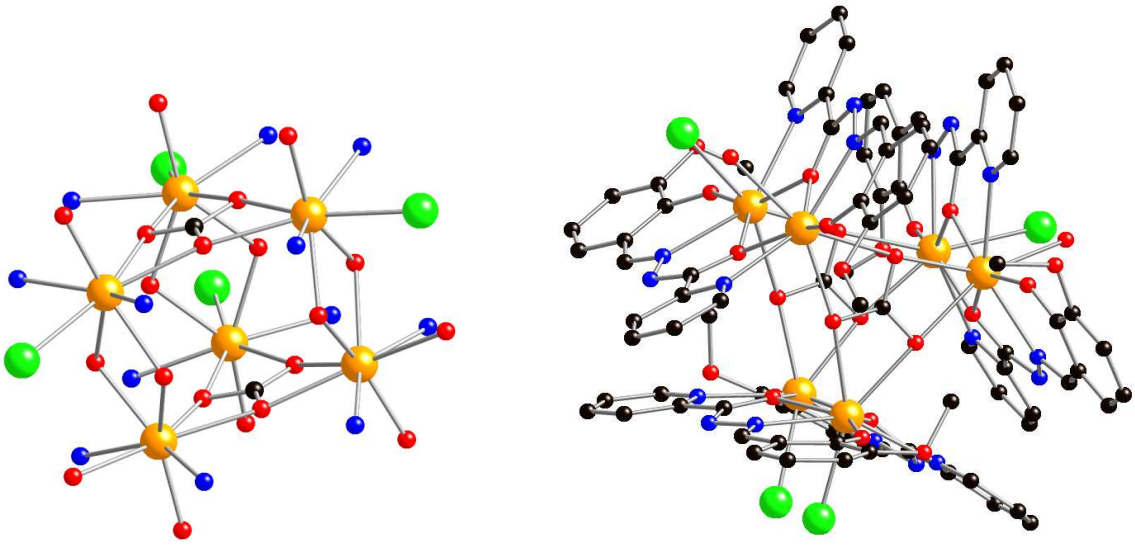

a b

Figure 38. a) Core structure of 136 with all peripheral ligand atoms removed b) Solid state structure of 136. All hydrogen atoms omitted for clarity. Black = Carbon, Red = Oxygen, Blue= Nitrogen and Orange = Dysprosium

$[Dy_6(\mu_3\text{-}OH)_3(\mu_3\text{-}CO_3)(\mu\text{-}OMe)(HL^{30})_6(MeOH)_4(H_2O)_2]\cdot 3MeOH\cdot 2H_2O$ **137** [102] ($L^{30}H_2$ is shown in Scheme 5) has a central Dy_6 core which can be described as a fusion of three capped triangular Dy_3 motifs.[102] Complex **137** contains a total of six HL^{30} ligands binding in a 2.1211 mode. Three μ_3-OH ligands one 3.222 CO_3^{2-} anion and one MeO^- anion bridge between the dysprosium ions. The coordination sphere of one dysprosium ion is completed by two water molecule and one methanol molecule, the coordination spheres of a further three dysprosium ions are completed by one methanol molecule each (Figure 39). Complex **137** shows SMM behaviour below 30K and above 3K shows a thermally activated relaxation process with U_{eff} = 26 cm^{-1} is dominant. At temperatures below 3K a temperature independent relaxation pathway dominates. This is attributed to the quantum tunnelling

relaxation pathway, however measurements in a static field had no effect on the behaviour of **137** at temperatures below 3 K.[102]

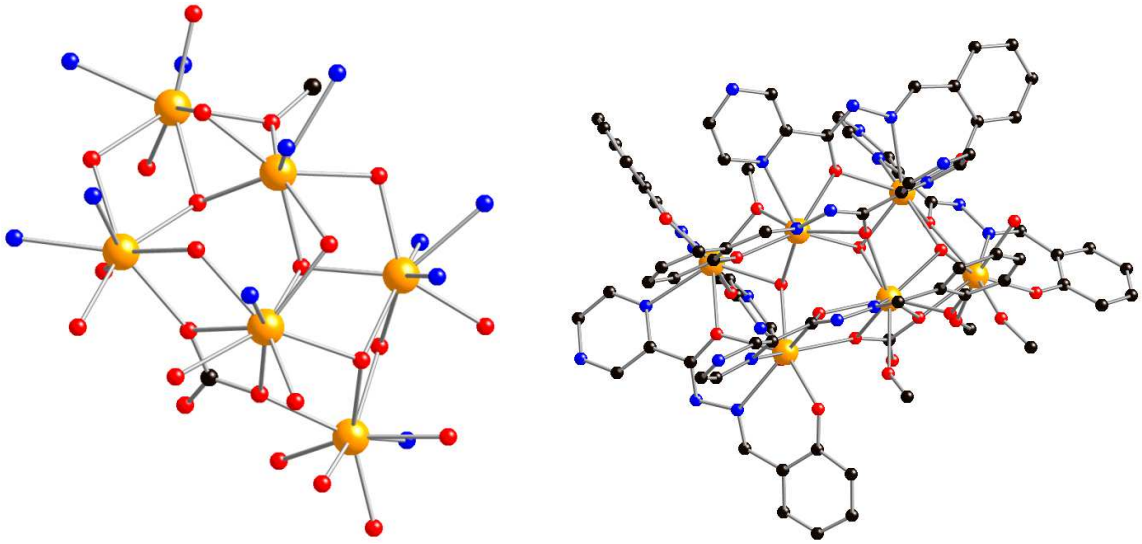

a b

Figure 39. a) Core structure of 137 with all peripheral ligand atoms removed b) Solid state structure of 137. All hydrogen atoms omitted for clarity. Black = Carbon, Red = Oxygen, Blue = Nitrogen, Green = Chlorine and Orange = Dysprosium

$[Dy_6(L^{27})_4(\mu_3\text{-}OH)_4(MeOH)_2(NO_3)_2]\cdot 6MeCN$ **138** [103] ($L^{27}H_3$ is shown in Scheme 5) contains two Dy_3triangular units in an "edge-to-edge" confirmation linked by two μ_3-OH ligands with each Dy_3 triangle containing a central μ_3-OH. Four multidentate L^{27} ligands bind in a 3.11311 mode and the coordination spheres of two dysprosium ions are completed by one methanol molecule each, whilst the coordination spheres of the remaining two dysprosium ions are completed by one η^2-nitrate ion each (Figure 40). Complex **138** does not show any maxima in the out of phase susceptibility measurements.[103]

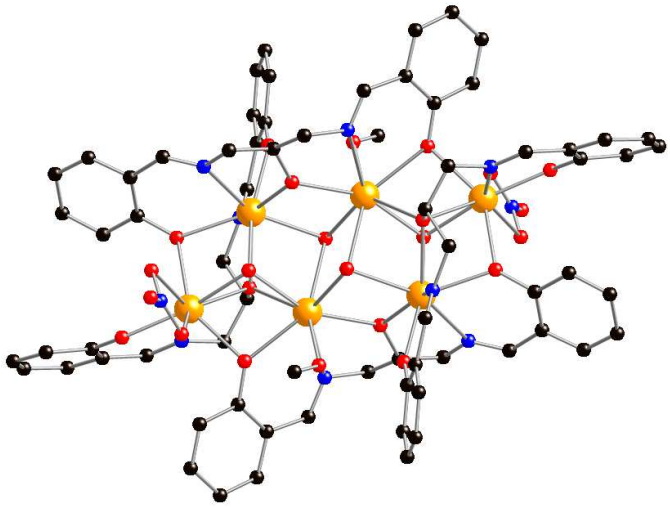

Figure 40. Solid state structure of 138. All hydrogen atoms omitted for clarity. Black = Carbon, Red = Oxygen, Blue = Nitrogen and Orange = Dysprosium

6.1.3 Other Ligands

Again calixerenes have been used to create larger lanthanide cluster SMMS in the form of $[Dy_6(\mu_4\text{-}O)_2(C4A)_2(NO_3)_2(HCOO)_2(MeO)_2(DMF)_4(MeOH)_4]$ **139** [104] (H_4C4A = *p*-tert-butylcalix[4]arene). Complex **139** contains four planar dysprosium ions in a square, one dysprosium above the Dy_4 plane and one below the Dy_4 plane giving a distorted octahedron of dysprosium ions. The dysprosium ions at the top and bottom of the Dy_6 octahedron are seven-coordinate and are bonded by four phenoxo oxygen atoms from one C4A ligand, two μ_4-O, and one methanol. The dysprosium ions in the Dy_4 plane are coordinated to two phenoxo oxygen atoms from two different C4A ligands, one μ_4-O, one μ_2-methanol and one formate oxygen atom. The coordination spheres of two dysprosium ions in the Dy_4 plane are completed by two DMF molecules, whilst the coordination spheres of the two remaining dysprosium ions are completed by one η^2-nitrate ion and one methanol oxygen atom each (Figure 41).[104]

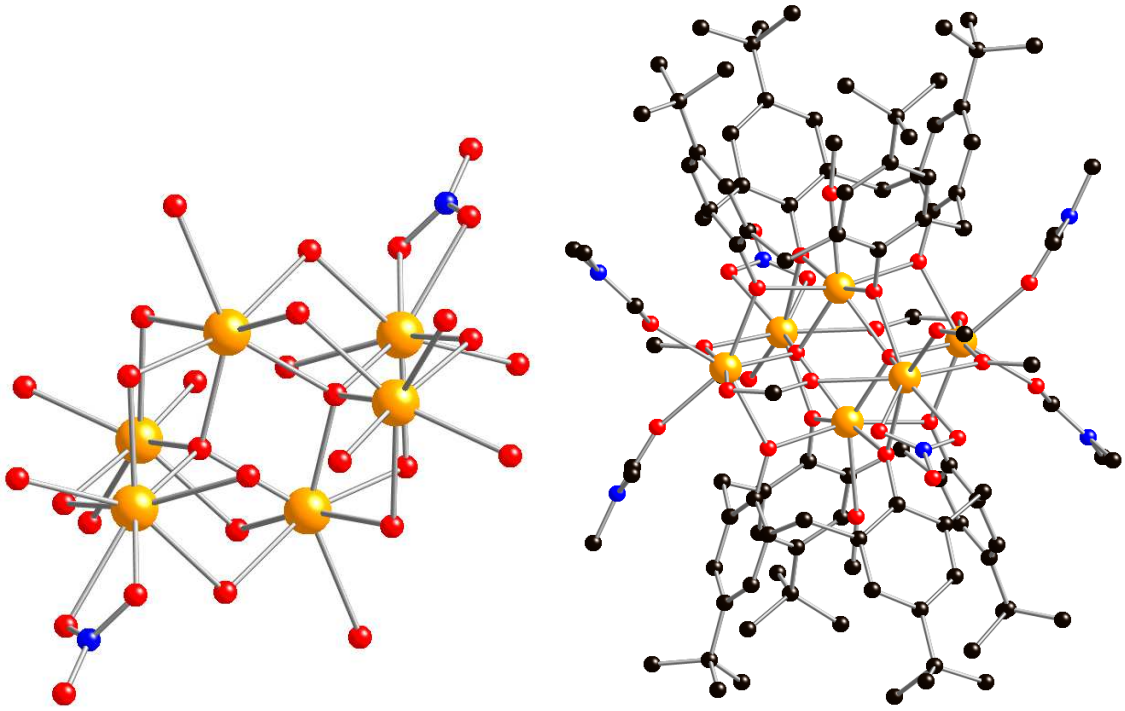

a b

Figure 41. a) Core structure of 139 with all peripheral ligand atoms removed b) Solid state structure of 139. All hydrogen atoms omitted for clarity. Black = Carbon, Red = Oxygen, Blue = Nitrogen and Orange = Dysprosium

Complex **139** shows two maxima in the out of phase susceptibility measurements and these are attributed to two different relaxation processes within **139**. Only one barrier height with U_{eff} = 5cm^{-1} is reported.[104]

6.2. Ln_7 + Ln_8 SMMs

6.2.1 Alcohols, Ketones and Acids

$[Dy_7(OH)_6(thmeH_2)_5(thmeH)(tpa)_6(MeCN)_2](NO_3)_2$ **140** [105] ($thmeH_3$ = tris(hydroxymethyl)ethane and tpaH = triphenylacetic acid) contains a Dy_7 "disc" in which a central dysprosium ion is surrounded by a hexagon of six dysprosium ions. Six μ_3-OH

ligands bridge between the central dysprosium ion and the out dysprosium ions, alternating above and below the plane of the Dy_7 disc. The outer six dysprosium ions are each bridged by a 2.121 thmeH/H_2 ligand and a 2.11 tpa^- ligand. The coordination sphere of the central dysprosium ion is completed by two acetonitrile molecules (one above and one below the plane of the Dy_7 disc) (Figure 42).[105] Complex **140** shows frequency dependency of out of phase susceptibility at temperatures below 28 K with multiple relaxation pathways. The multiple relaxation pathways in **140** are attributed to the different coordination environments of the dysprosium ions which mean the anisotropy axis of each dysprosium ion would not be collinear.[8a,99] Complex **140** has U_{eff} = 97cm^{-1}.[105]

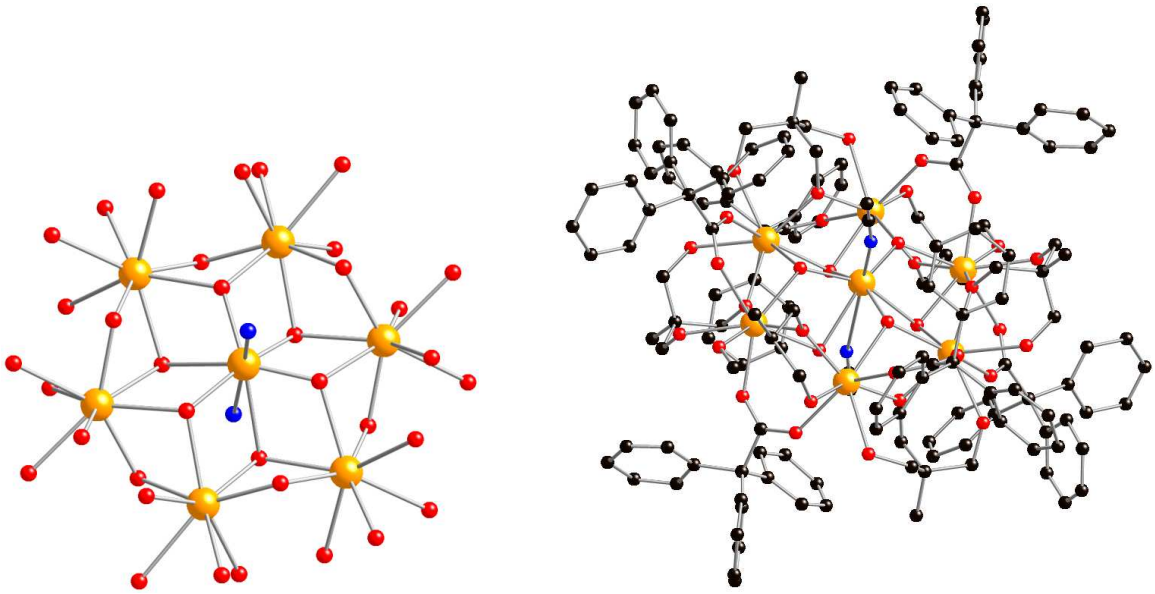

a b

Figure 42. a) Core structure of 140 with all peripheral ligand atoms removed b) Solid state structure of 140. All hydrogen atoms omitted for clarity. Black = Carbon, Red = Oxygen, Blue = Nitrogen and Orange = Dysprosium

$[Dy_8(\mu_3\text{-}OH)_4(L^{17})_2(mvn)_2(p\text{-}NO_2bz)_{14}(MeOH)_2]\cdot 3MeCN\cdot 6MeOH\cdot H_2O$ **141** [106] ($mvnH_2$ = methyl hemiacetal o-vanillin) can be considered as a Dy_8 core consisting of six Dy_3 triangular units sharing vertices. Complex **141** contains four μ_3-OH, twelve 2.11 p-NO_2bz ligands, two η^2 p-NO_2bz ligands, two 2.121 L^{17} ligands and two 4.1321 mvn^{2-} ligands. The coordination spheres of two dysprosium ions are completed by one methanol molecule each (Figure 43). Complex **141** shows no maxima in the out-of-phase susceptibility even under a 3000Oe static field.[106]

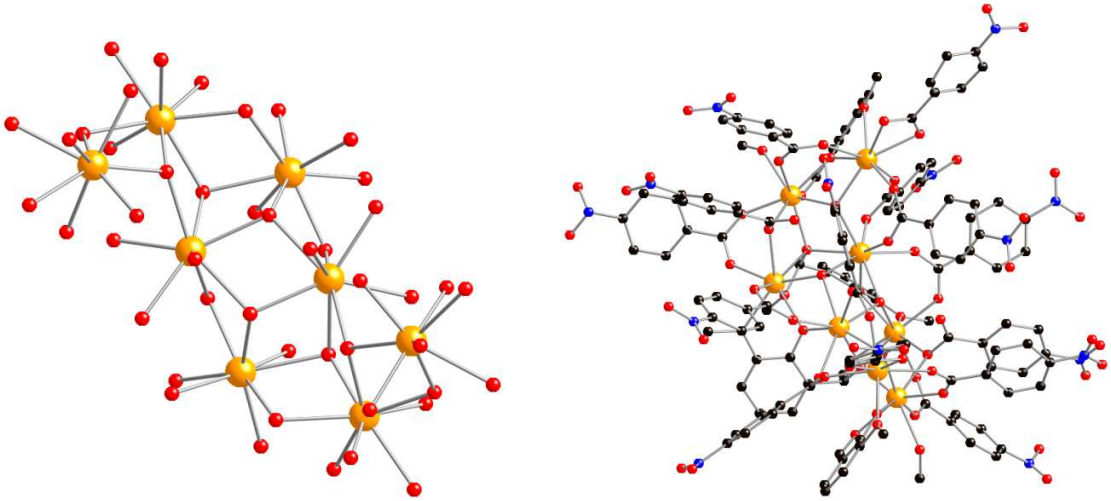

a b

Figure 43. a) Core structure of 141 with all peripheral ligand atoms removed b) Solid state structure of 141. All hydrogen atoms omitted for clarity. Black = Carbon, Red = Oxygen, Blue = Nitrogen and Orange = Dysprosium

6.2.3 Schiff Base Ligands

Schiff base ligands have been used to create Dy_8 SMMS with different core topologies such as $[Dy_8(HL^{28})_{10}(C_6H_4NH_2CO_2)_2(\mu_3\text{-}OH)_8(OH)_2(NO_3)_2(H_2O)_4]$ **142**,[107]

$[Dy_8(ovph)_8(CO_3)_4(H_2O)_8]\cdot 12MeCN\cdot 6H_2O$ **143** [108] and $[Dy_8(\mu_4\text{-}CO_3)_4(L^{26})_8(H_2O)_8]\cdot 10MeOH\cdot 2H_2O$ **144** [109] ($L^{28}H_2$ and $L^{26}H$ are shown in Scheme 5).

Complex **142** contains two $Dy_4(\mu_3\text{-}OH)_4$ tetrahedron linked by two 2.21 HL^{28} ligands. Eight HL^{28} ligands chelate whilst two $C_6H_4NH_2CO_2$ ligands bind in a 2.11 mode. The coordination spheres of two dysprosium ions are completed by one hydroxide on each and the coordination spheres of two other dysprosium ions are completed by a chelating nitrate on each (Figure 44). Complex **142** shows no maxima in the out-of-phase susceptibility.[107]

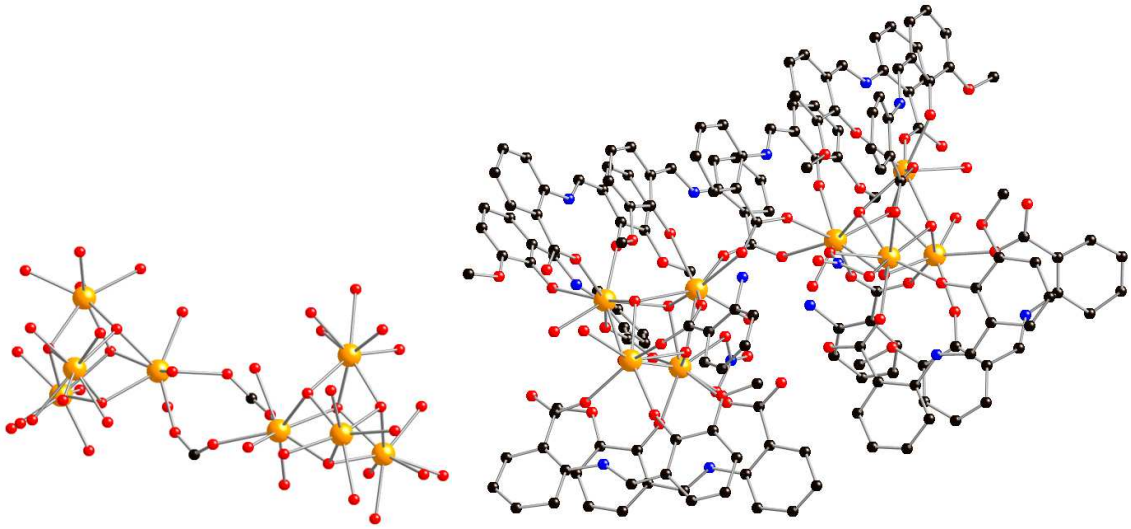

a b

Figure 44. a) Core structure of 142 with all peripheral ligand atoms removed b) Solid state structure of 142. All hydrogen atoms omitted for clarity. Black = Carbon, Red = Oxygen, Blue = Nitrogen and Orange = Dysprosium

Complex **143** contains a $Dy_8(CO_3)_4$ core in which each CO_3^{2-} ligand is binding in a 3.221 mode. Eight ovph ligands bind in a 2.1211 mode and the coordination sphere of each dysprosium ion is completed by one water molecule each (Figure 45). Complex **143** shows no maxima in the out-of-phase susceptibility.[108]

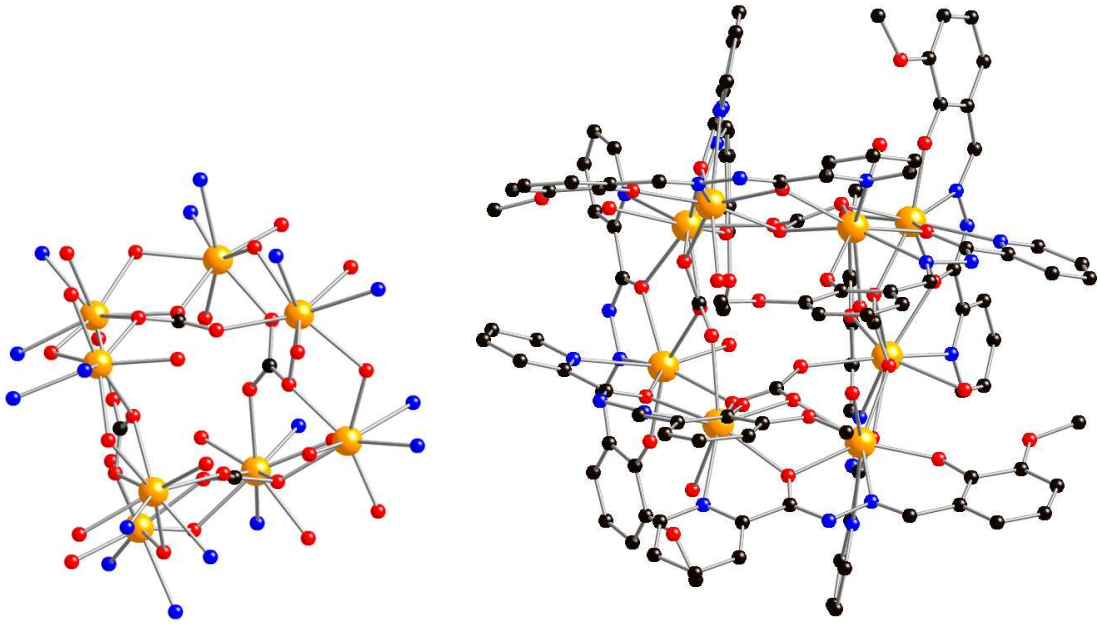

a b

Figure 45. a) Core structure of 143 with all peripheral ligand atoms removed b) Solid state structure of 143. All hydrogen atoms omitted for clarity. Black = Carbon, Red = Oxygen, Blue = Nitrogen and Orange = Dysprosium

Complex **144** contains a Dy_8 square anti-prism in which the dysprosium ions are all connected by four 3.221 CO_3^{2-} ligands. As with complex **143**, eight L^{26} ligands bind in a 2.1211 mode and the coordination sphere of each dysprosium ion is completed by one water molecule each (Figure 46).Complex **144** shows SMM behaviour and has U_{eff} = 52 cm^{-1}.[109] This is the largest 4f-SMM for which a significant U_{eff} has been reported.

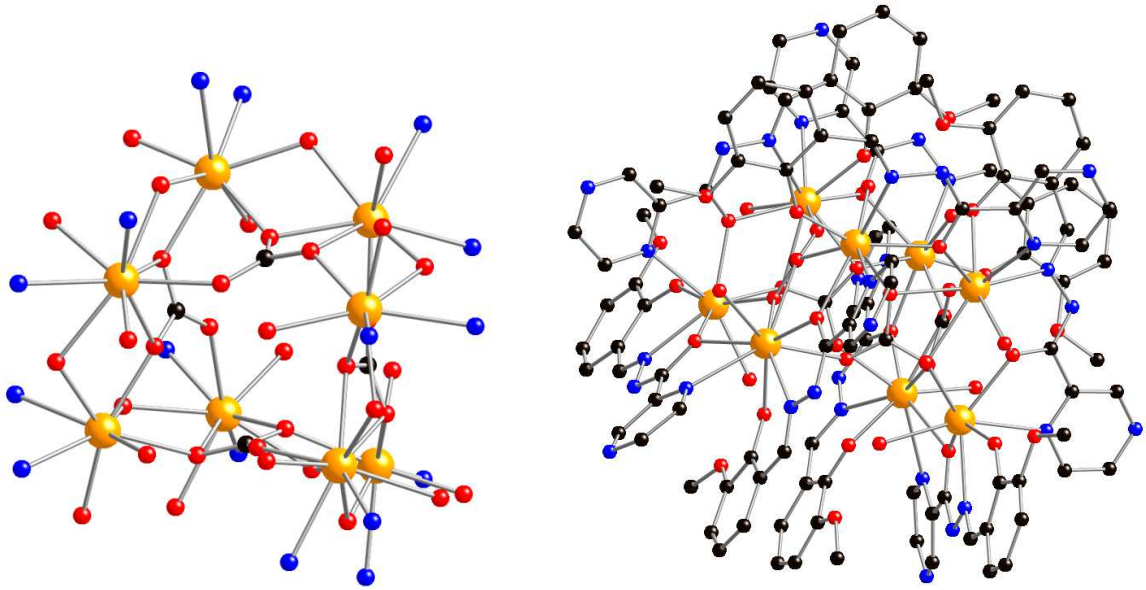

a b

Figure 46. a) Core structure of 144 with all peripheral ligand atoms removed b) Solid state structure of 144. All hydrogen atoms omitted for clarity. Black = Carbon, Red = Oxygen, Blue = Nitrogen and Orange = Dysprosium

6.2.4 Other *N* + *O*-donor Ligands

$[Dy_7(\mu_3\text{-}OH)_5(MeOsalox)_2(MeOsaloxH)_4(PhCO_2)_7(OH)(H_2O)1.5(MeOH)_{0.5}]\cdot 2.5MeOH\cdot 5.25H_2O$ **145** [110] and $[Dy_8(OH)_8(phendox)_6(H_2O)_8]Cl_2\cdot(OH)_2\cdot 18H_2O\cdot 18MeOH$ **146** [111] both contain multidentate *N* + *O*-donor ligands. Complex **145** contains a Dy_7 core that can be described as five edge sharing Dy_3 triangular units (Figure 47). Five μ_3-OH connect all the dysprosium ions, four $PhCO_2^-$ ligands bind in a 2.11 mode, two $PhCO_2^-$ ligands bind in a 2.21, one $PhCO_2^-$ ligand chelates, four MeOsaloxH ligands bind in a 2.121 mode and two MeOsalox ligands bind in a 2.21 mode. Complex **145** shows no maxima in out-of-phase susceptibility measurements.[110]

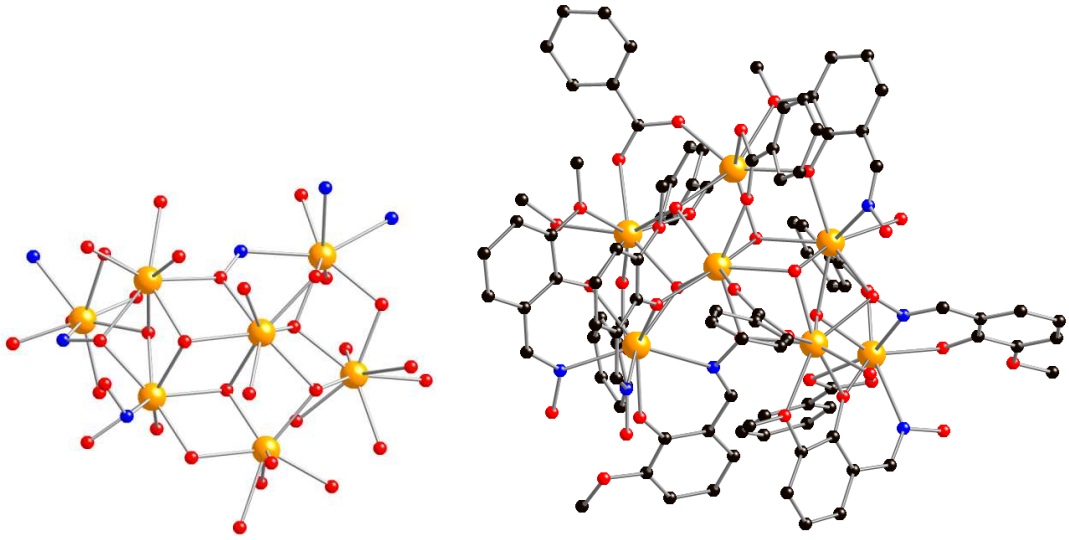

a b

Figure 47. a) Core structure of 145 with all peripheral ligand atoms removed b) Solid state structure of 145. All hydrogen atoms omitted for clarity. Black = Carbon, Red = Oxygen, Blue = Nitrogen and Orange = Dysprosium

Complex **146** contains two $Dy_4(\mu_3\text{-}OH)_4$ tetrahedrons connected by two 4.211111 phendox ligands. Four further phendox ligands bind in a 3.111111 mode and the coordination sphere of each dysprosium ion are completed by one water molecule (Figure 48). Complex **146** shows SMM behaviour and has an estimated barrier height $U_{eff} \approx 3cm^{-1}$.[111]

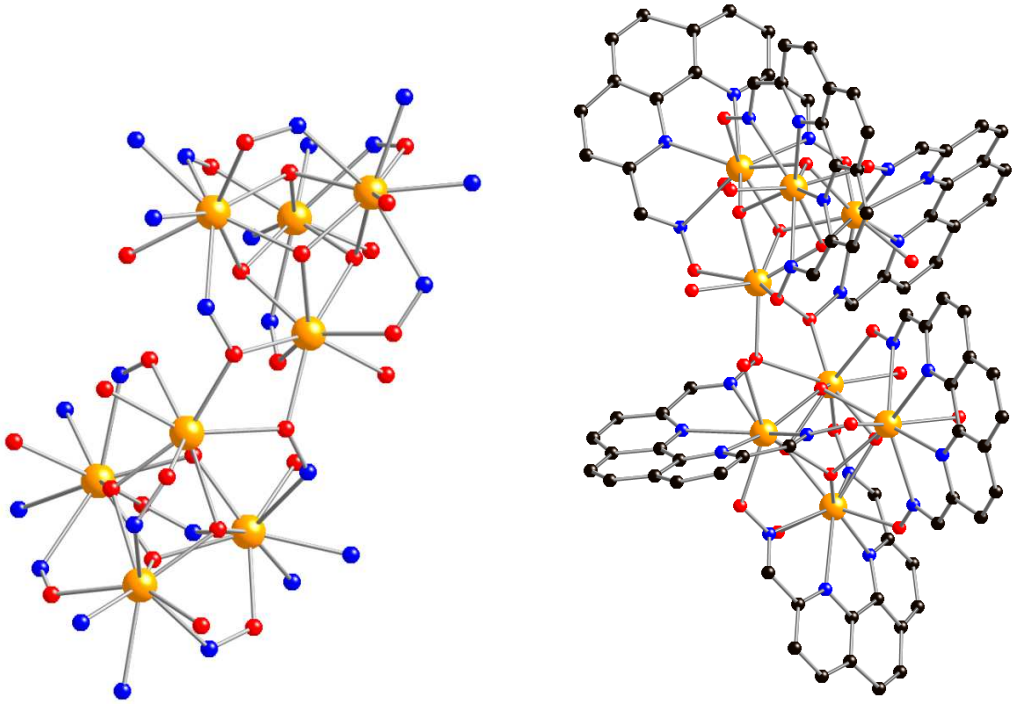

a b

Figure 48. a) Core structure of 146 with all peripheral ligand atoms removed b) Solid state structure of 146. All hydrogen atoms omitted for clarity. Black = Carbon, Red = Oxygen, Blue = Nitrogen and Orange = Dysprosium

6.3. Ln_9 – Ln_{30}SMMs

6.3.1 Alcohols, Ketones and Acids

$[Dy_{30}I(\mu_3\text{-}OH)_{24}(\mu_3\text{-}O)_6(NO_3)_9(IN)_{41}(OH)_3(H_2O)_{38}]$ **147** [112] is the largest polynuclear lanthanide complex that shows any evidence of slow relaxation. Complex **147** contains six $Dy_4(\mu_3\text{-}OH)_4$ tetrahedrons linked to six dysprosium ions *via* nine 3.221 nitrate ions. A total of forty-one IN ligands, thirty-eight water molecules, six μ_3-O and three hydroxides link the dysprosium ions together and complete the coordination spheres of the dysprosium ions. Complex **147** shows frequency dependency of out of phase susceptibility but no maxima.[112]

6.3.2 Schiff Base Ligands

$[Dy_{12}(L^{29})_6(OH)_4O_2(CO_3)_6][Dy_{12}(L^{36})_6(OH)_4O_4(CO_3)](ClO_4)_4 \cdot xH_2O$ **148** [113] contains two Dy_{12} units within one unit cell. Both Dy_{12} units are structurally similar and no covalent bond connects them. The Dy_{12} core of **148** can be considered as a cuboctahedron with a Dy_6 hexagon sandwiched between two Dy_3 triangles in a staggered conformation. Six L^{29} ligands bind in a 3.1211121 mode. Two CO_3^{2-} anions bind in a 2.11 mode in the Dy_6 hexagon, whilst the remaining four CO_3^{2-} ligands bind in a 3.211 mode to link the Dy_3 triangles to the Dy_6 hexagon. Four OH^- ligands and two O^{2-} ligands bridge between various dysprosium ions (Figure 49). Complex **148** shows no frequency dependent peaks in a.c. susceptibility measurements.[113]

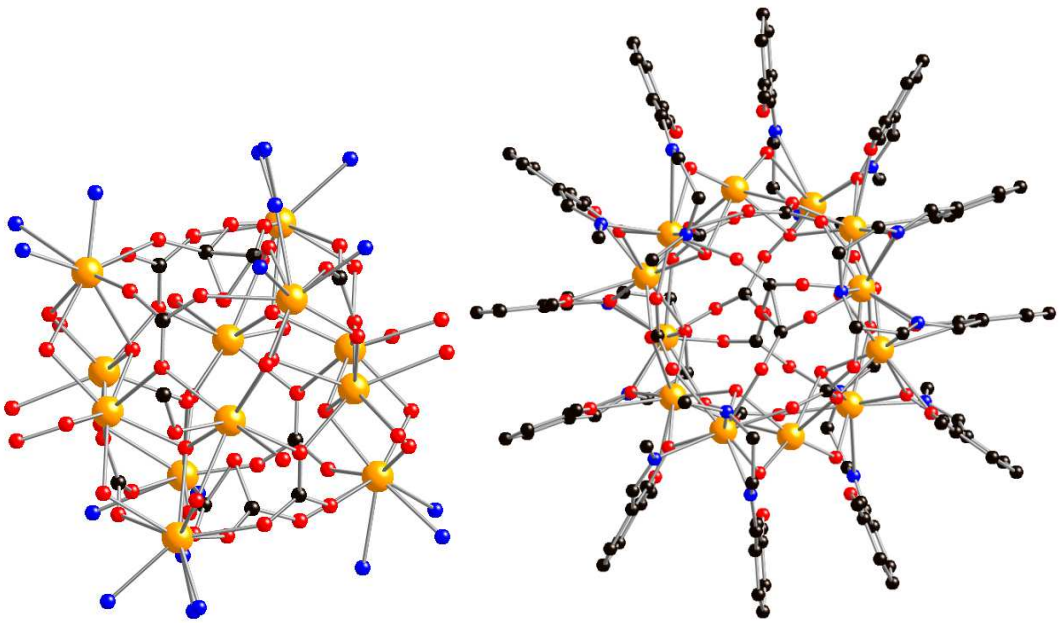

a b

Figure 49. a) Core structure of 148 with all peripheral ligand atoms removed b) Solid state structure of one Dy_{12} unit of 148. All hydrogen atoms omitted for clarity. Black = Carbon, Red = Oxygen, Blue = Nitrogen and Orange = Dysprosium

6.3.3 Other N + O-donor Ligands

$[Dy_9(OH)_{10}(hmp)_8(NO_3)_8(DMF)_8](OH)\cdot 1.6H_2O\cdot 0.6DCM$ **149** [114] (hmpH = 2-(hydroxymethyl)pyridine) contains a Dy_8 square anti-prism with a central dysprosium ion (Figure 53). There are two μ_4-OH centred Dy_4 squares connected to a single central dysprosium ion via eight μ_3-OH ligands. Eight hmp ligands bind in a 2.21 mode on the edges of the Dy_4 squares. The coordination sphere of each dysprosium ion in a square is completed by one DMF molecule and a η^2-nitrate anion (Figure 50. Complex **149** shows no maxima in the out-of-phase susceptibility measurements.[114]

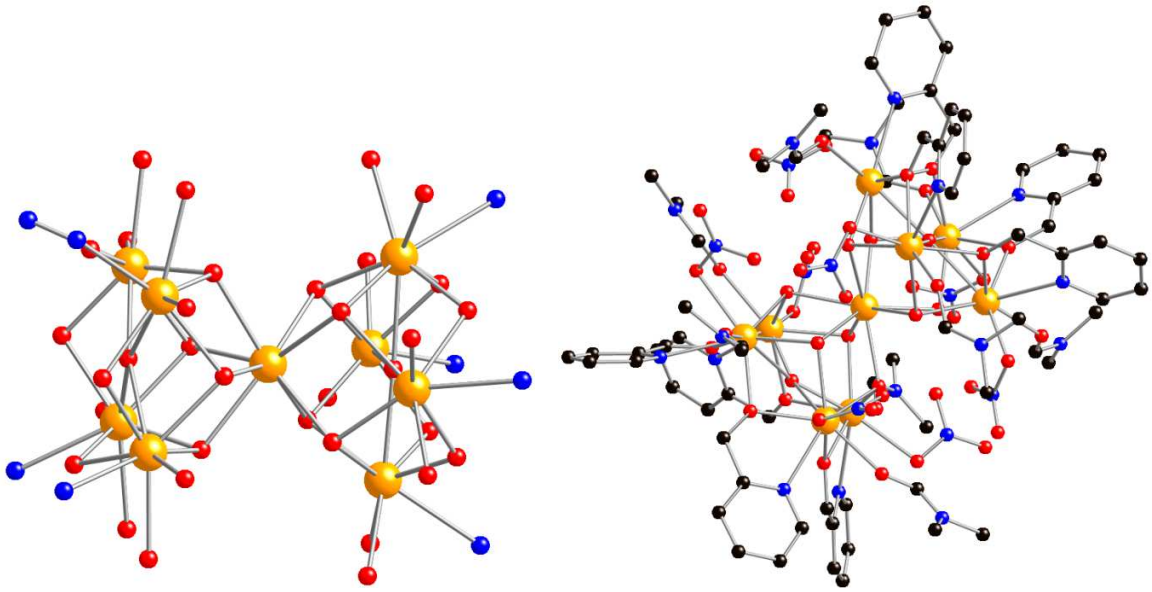

a b

Figure 50. a) Core structure of 149 with all peripheral ligand atoms removed b) Solid state structure of 149. All hydrogen atoms omitted for clarity. Black = Carbon, Red = Oxygen, Blue = Nitrogen and Orange = Dysprosium

$[Dy_{10}(\mu_3\text{-}OH)_4(O_2CMe)_{20}(H_2L^{30})_2(H_3L^{30})_2\{NH_2C(CH_2OH)_3\}_2]$ **150** [115] contains a Dy_{10} core that can be described as two pairs of vertex sharing μ_3-OH bridged Dy_3 triangles (Figure 51).[115] Two acetates bind in a 2.11 mode to connect the two Dy_5 units. Two further acetates

bind in a 2.11 mode, eight in a 2.21 mode, six in a 1.10 mode and two in a 1.11 mode. Two H_2L^{35} ligands bind in a 3.12112 mode and two H_3L^{35} ligands bind in a 2.12111 mode (Figure 51). Complex **150** does not show maxima in the out of phase susceptibility at different frequencies.[115]

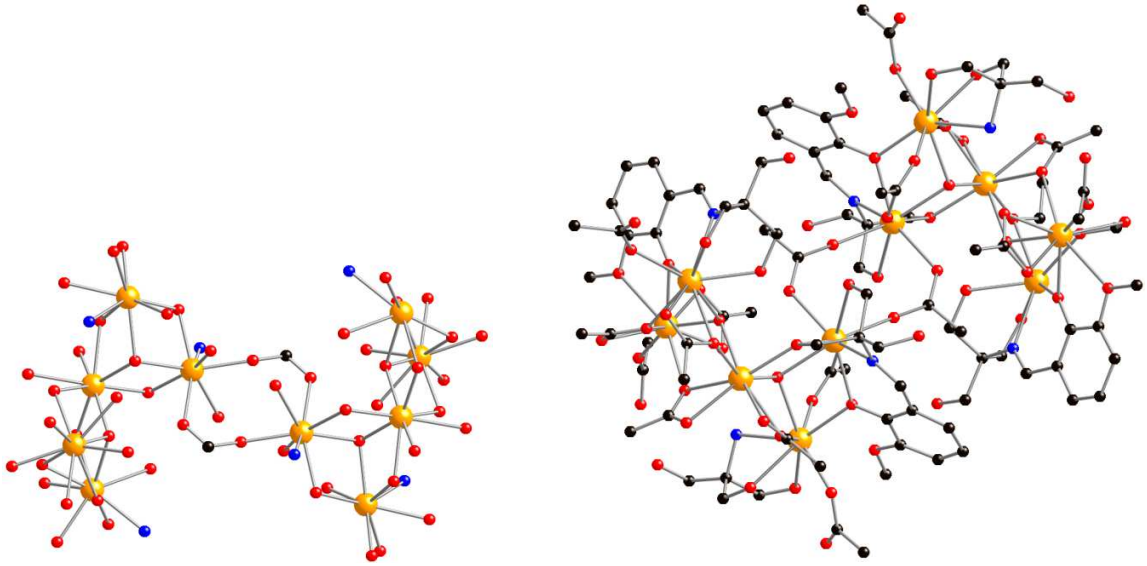

a b

Figure 51. a) Core structure of 150 with all peripheral ligand atoms removed b) Solid state structure of 150. All hydrogen atoms omitted for clarity. Black = Carbon, Red = Oxygen, Blue = Nitrogen and Orange = Dysprosium

$[Dy_{11}(OH)_4(phendox)_6(phenda)_3(OAc)_3](OH)\cdot 40H_2O\cdot 7MeOH$ **151** [111] ($phendaH_2$ = 1,10-phenanthroline-2,9-dicarboxylic acid) contains a Dy_{11} core which can be described as two cubane-like $Dy_4(\mu_3\text{-}OH)_4$motifs and two face-sharing $Dy_4(\mu_3\text{-}OH)_2$defective cubanes.[111] Complex **151** contains four μ_3-OH ligands, three 3.111111 phenda ligands, six 4.211111 phendox ligands and the coordination spheres of three dysprosium ions are completed by one chelating acetate each (Figure 52).Complex **151** shows no maxima in the out-of-phase susceptibility.[111]

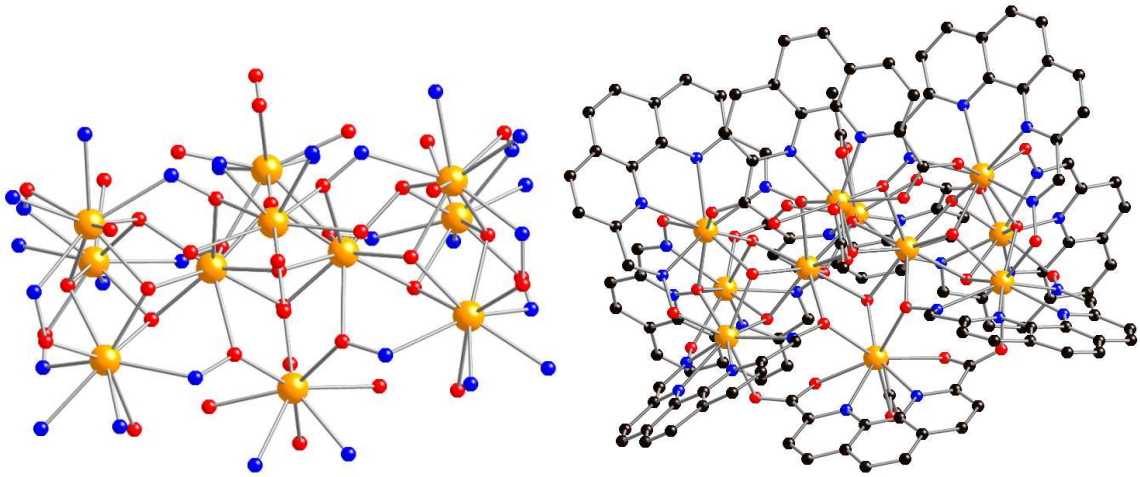

a b

Figure 52. a) Core structure of 151 with all peripheral ligand atoms removed b)Solid state structure of 151. All hydrogen atoms omitted for clarity. Black = Carbon, Red = Oxygen, Blue = Nitrogen and Orange = Dysprosium

Both $[\{Dy_{12}(OH)_{16}(phenda)_8(H_2O)_8\}][Cl]_2(OH)_2\cdot 15MeOH\cdot 40H_2O$ **152** [116] and $[\{Dy_{12}(OH)_{16}(phenda)_8(H_2O)_8\}][Cl]_2[Dy(phenda)_2]_2$ **153** [116] have very similar structures with the only difference being the counter ions present within the crystal structure. As such the structures of **152** and **153** will be described as a whole. The Dy_{12} core of **152/153** can be regarded as four vertex sharing $Dy_4(\mu_3\text{-}OH)_4$ cubanes. Eight phenda ligands bind in a 3.12111 mode and the coordination sphere of each dysprosium ion is completed by one water molecule (Figure 53). Both **152** and **153** shows SMM behaviour below 5K and have U_{eff} = 2 cm^{-1} and 5 cm^{-1} respectively.[116]

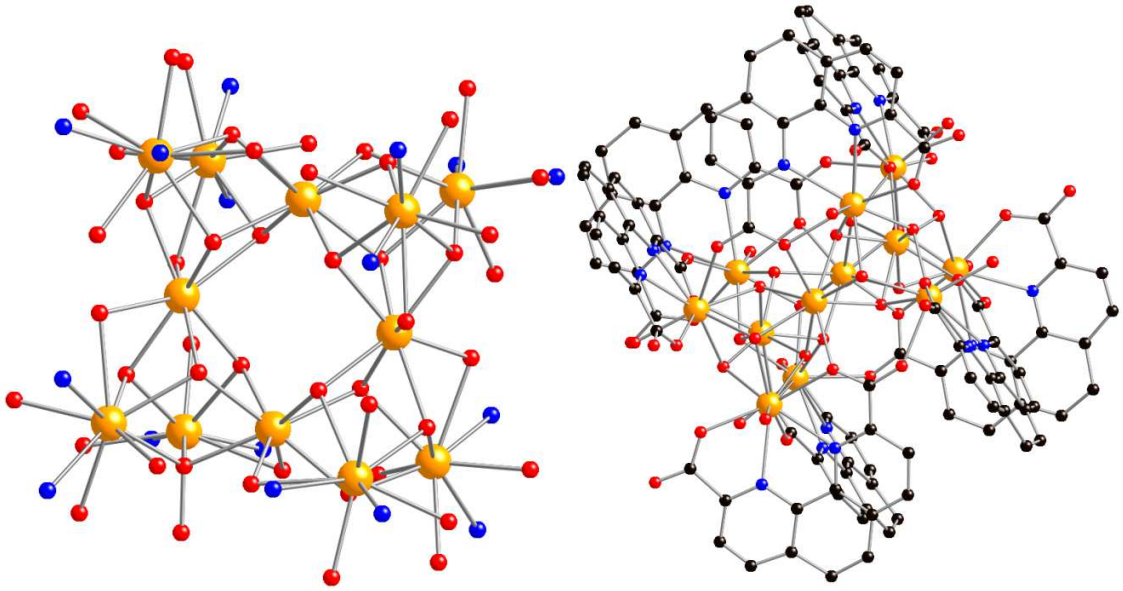

a b

Figure 53. a) Core structure of 152 with all peripheral ligand atoms removed b) Solid state structure of 152. All hydrogen atoms omitted for clarity. Black = Carbon, Red = Oxygen, Blue = Nitrogen and Orange = Dysprosium

7. Conclusions

The field of lanthanide SMMs has grown very rapidly, with a number of research groups consistently publishing in the area. Whilst a wide range of chemistry has been explored to create new SMMs, a large number of research branches still remain unexplored with regards to lanthanide SMMs. We believe this field is only just entering its adolescence and will prove to provide an even larger wealth of knowledge and potential compounds for future applications.

Two points seem worth making as the field progresses. Firstly, for 3d-SMMs it was clear from the mid-1990s what was required to claim an SMM. The two criteria were magnetic hysteresis, which often required very low temperature single crystal

measurements, and/or frequency-dependent peaks in the out-of-phase susceptibility that would allow a energy barrier for thermal relaxation of magnetization. Unfortunately these rules have not been stringently applied to 4f-complexes, and many 4f-SMMs are claimed where there is no evidence beyond a small rise in χ_M" at the lowest temperatures. While we have listed all such claims, for completeness sake, it would seem sensible if the area returned to a stricter definition of an SMM. If there is no peak in χ_M" then the compound should not be claimed as an SMM. The beautiful structural chemistry is still worth reporting, but inaccurate claims concerning the physics of the system are distracting.

The use of small applied external fields is also debatable, but is often justified. Quantum tunnelling of magnetization can be extremely efficient in 4f-SMMs, and use of a small external field to switch off this relaxation path can allow the thermal energy barrier to be measured. This is particularly true for SMMs based on lanthanides with large nuclear spins, e.g. holmium. However energy barriers derived in this way should always be reported as derived in applied external field, and are not absolutely comparable to energy barriers derived in zero applied field.

The second point concerns theoretical understanding of the energy barriers in 4f-SMMs. There is considerable debate at present about the best route to follow. Beautiful work from the Chibotaru group, and more recently from Sessoli and co-workers, has shown that high level calculations using CASSCF approaches are extremely valuable. These are difficult and computationally expensive calculations, and involve much greater informed intervention from the theorist than the conventional DFT calculations. In passing, it is clear that DFT calculations offer little insight in these systems. Whether such an approach will ever become generally used, or whether it will always involve high quality theorists is an

open question. The field of 3d-SMMs became hugely reliant on a very small number of groups able to perform micro-SQUID measurements to low temperature; it would be unfortunate if the area of 4f-SMMs became similarly reliant on a very small number of theorists.

Other groups have proposed a crystal field approach, or more precisely a ligand field approach where the directionality and charge density of ligand donor atoms are accounted for, as well as the geometry produced by the traditional "point negative charges" of crystal field theory. This approach looks much less computationally demanding, but probably has some restrictions, e.g. it may be difficult to allow for the packing of molecules within a crystal. However given its comparative simplicity, and its ability to produce results that can be understood in a simple pictorial way by synthetic chemists, it seems that this ligand field approach should be developed further and it's complementarily with CASSCF calculations explored.

An important contribution to this theoretical understanding is coming from single crystal measurements, which are vital in deciding upon the principle axis of anisotropy in 4f-SMMs. The usefulness of low temperature emission and absorption spectroscopy to measure the splittings within the lowest energy *J*-multiplets also remains to be fully explored. Preliminary results suggest this approach could also be very fruitful.

We have not discussed the use of 4f-SMMs, particularly the [Pc_2Tb] complexes in prototype devices. This is remarkable work, with reports of molecular spin valves and spin transistors arising from controlled deposition of 4f-SMMs on substrates such as carbon nanotubes. This area is already opening up astonishing physics, e.g. the measurement of a single nuclear spin. Applicable technology may arise from this work.

In summary: a huge number of 4f-SMMs have been reported in a little less than a decade. The synthetic chemistry is probably more advanced than either full physical characterization or theoretical understanding, where only a few examples have been subject to detailed investigation using CASSCF methods.

Chapter 3: Aims

The interest in polymetallic complexes with a variety of magnetic properties is constantly growing. The overall aim of this project is to investigate new synthetic routes to polymetallic complexes which have both interesting structural and magnetic properties. Although a number of synthetic routes are available to obtain new magnetically interesting complexes, this research will primarily focus on the use of organometallic/metal-amide precursor materials to deprotonate X-H bond containing pro-ligands in order to form polymetallic cluster complexes.

A second “one pot” synthetic strategy will be employed in which well defined organolithium precursors will be combined with metal halides in order to avoid the deprotonation step and instead use the formation of lithium halide salts as the driving force for complex formation.

All new compounds will be structurally characterized by standard methods, primarily single crystal X-ray diffraction due to their likely air/moisture sensitivity and paramagnetism. Their electronic/magnetic properties will be investigated by multi-frequency EPR spectroscopy and more extensively by SQUID magnetometry. Where possible, series of compounds will be grouped and any trends explored.

Chapter 4: Paper 1

“Single-molecule magnetism in thiolate-bridged terbium and dysprosium squares”

Daniel N. Woodruff, Floriana Tuna, Richard E. P. Winpenny and Richard A. Layfield,

Submitted

Single-molecule magnetism in thiolate-bridged terbium and dysprosium squares

Daniel N. Woodruff,[a] *Floriana Tuna,*[a,b] *Michael Bodensteiner,*[c] *Richard E. P. Winpenny*[a,b] *and Richard A. Layfield**[a]

[a] School of Chemistry, The University of Manchester, Oxford Road, Manchester, M13 9PL, U.K.

[b] EPSRC U.K. National EPR Facility, Photon Science Institute, The University of Manchester, Oxford Road, Manchester, M13 9PL, U.K.

[c] Institute of Inorganic Chemistry, University of Regensburg, Germany, D-93040.

Richard.Layfield@manchester.ac.uk

TOCs graphic

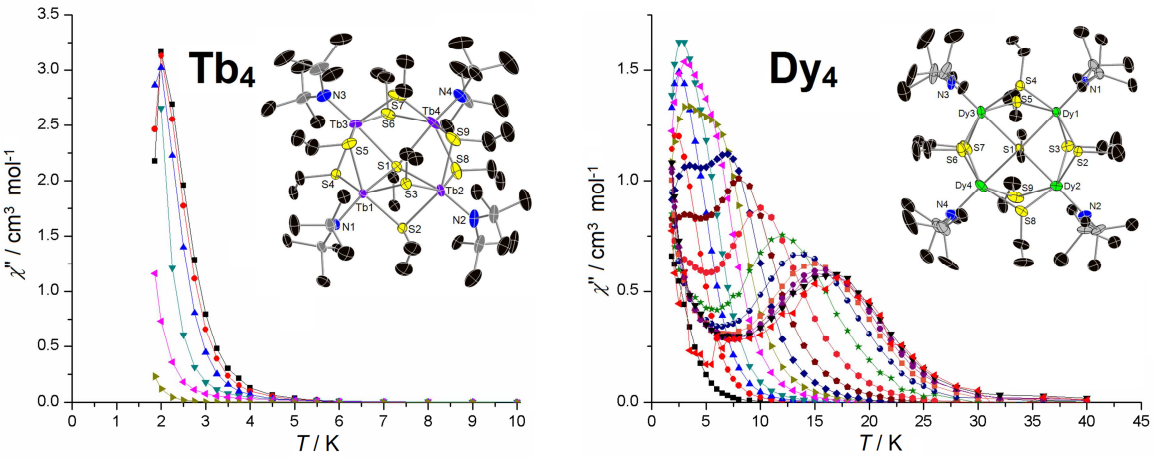

ABSTRACT

Metallation of ethylthiol by [{$(Me_3Si)_2N$}$_3$Ln(μ-Cl)Li(thf)$_3$] (Ln = Gd, Tb or Dy) in thf produces the thiolate-bridged tetra-lanthanide compounds [Li(thf)$_4$][Ln$_4${N$(SiMe_3)_2$}$_4$(μ-SEt)$_8$(μ_4-SEt)], where Ln = Gd is [Li(thf)$_4$][**1**], Ln = Tb is [Li(thf)$_4$][**2**] and Ln = Dy is [Li(thf)$_4$][**3**]. Crystallographic studies reveal that the mono-anions **1**-**3** are essentially isostructural, consisting of Ln$_4$ squares in which the lanthanides are bridged by μ-ethylthiolate ligands, and the individual lanthanide centers occupy distorted six-coordinate {LnNS$_5$} coordination environments. The magnetic susceptibility properties of all three compounds were measured in a static (d.c.) field of 1000 G: the data for the gadolinium anion **1** were reproduced by a model that suggests weak antiferro-magnetic and ferro-magnetic exchange, with coupling constants of J = –0.09 cm^{-1} and +0.04 cm^{-1} (–2J formalism). Magnetic susceptibility measurements in a dynamic (a.c.) field at various frequencies on [Li(thf)$_4$][**2**] and [Li(thf)$_4$][**3**], in zero d.c. field, reveal properties characteristic of a single-molecule magnet. Analysis of the temperature dependence of the out-of-phase magnetic susceptibility for **2** in zero applied field yielded a small anisotropy barrier of U_{eff} = 4.6 cm^{-1}, with a relaxation time of $\tau_0 = 1.5 \times 10^{-5}$ s. A similar analysis on **3** produced U_{eff} = 46 cm^{-1} and $\tau_0 = 4.3 \times 10^{-6}$ s. Compounds [Li(thf)$_4$][**2**] and [Li(thf)$_4$][**3**] are rare examples of sulfur-ligated SMMs.

Introduction

Coordination complexes of terbium(III) and dysprosium(III) have accounted for some of the most significant recent developments in studies of single-molecule magnets (SMMs), i.e. a family of molecules that exhibit magnetic memory effects.[1,2] In an environment of appropriate symmetry, the electronic ground states of terbium(III) and dysprosium(III) ions show strong Ising-type axial anisotropy and have high magnetic moments, and the combinations of these properties can lead to the characteristic slowly relaxing magnetization found in SMMs.[2] Single-ion effects – such as electron-nuclear hyperfine interactions and the symmetry and electrostatic potential of the ligand field – play particularly important roles in influencing the two parameters most often used to characterize an SMM, namely the blocking temperature, T_B, and the effective energy barrier to reversal of magnetization (or anisotropy barrier), U_{eff}.[2,3] The increases in both T_B and U_{eff} that have been enabled through the development of lanthanide SMMs (Ln-SMMs) are unprecedented, and have pushed the field beyond the boundaries that were previously set by transition metal SMMs. For example, whereas the benchmark blocking temperature achieved with a transition metal SMM was T_B = 4.5 K in a hexamanganese(III) {Mn_6} cage,[4] this was recently re-defined by the di-terbium SMM $[Tb_2\{N(SiMe_3)_2\}_4(thf)_2(\mu:\eta^2:\eta^2\text{-}N_2)]^-$, for which a blocking temperature of 14 K was measured.[5] Furthermore, whereas anisotropy barriers in transition metal SMMs usually do not exceed U_{eff} = 60 cm^{-1},[6] anisotropy barriers in excess of 100 cm^{-1} are not uncommon in Ln-SMMs, and the family of *bis*(phthalocyaninate) lanthanide double-decker complexes can even produce anisotropy barriers of several hundred wavenumbers.[3,7,8]

Despite the step-changes that have undoubtedly occurred with the development of Ln-SMMs, important challenges remain. Firstly, a comprehensive understanding of the complex magnetic behavior of Ln-SMMs is still a work in progress. Secondly, and closely linked to the

first challenge, is the need to develop Ln-SMMs for applications in areas such as molecular spintronics and information storage/processing,[9] which inevitably requires systems to function as SMMs at higher temperatures. We and others have attempted to address the challenges within the SMM field by developing systems based on organometallic ligand environments.[10,11] Most SMMs are synthesized using 'classical' Werner-type coordination chemistry, meaning that the ligands tend to be based on hard *O*-donors,[1] with notable exceptions being the use of *N*-donor phthalocyanine ligands and other, related ligands.[12] Our simple hypothesis was that organometallic chemistry might be able to provide alternative chemical environments with which to explore the magnetism of the lanthanides, potentially resulting in new fundamental insight and improved SMM properties. Our efforts have focused on a series of heteroatom-bridged *bis*(cyclopentadienide) SMMs of the type $[(\eta^5\text{-Cp})_2\text{Dy}(\mu\text{-X})]_2$, where X = benzotriazolate, chloride or triphenylsilylthiolate.[10] An *ab initio* computational study of the $[(\eta^5\text{-Cp})_2\text{Dy}(\mu\text{-X})]_2$ SMMs revealed that mechanistic aspects of the relaxation of magnetization can be very complicated. However, the thermally assisted relaxation in the thiolate-bridged SMM $[(\eta^5\text{-Cp})_2\text{Dy}(\mu\text{-SSiPh}_3)]_2$ resulted in a large anisotropy barrier of U_{eff} = 133 cm^{-1},[10a] and this observation motivated us to extend our studies of polymetallic thiolate-bridged Ln-SMMs.

We now describe the synthesis, structure and magnetic properties of the tetrametallic thiolate-bridged cage compounds $[\text{Li(thf)}_4][\text{Ln}_4\{\text{N(SiMe}_3)_2\}_4(\mu\text{-SEt})_8(\mu_4\text{-SEt})]$, where Ln = Gd is $[\text{Li(thf)}_4][\mathbf{1}]$, Ln = Tb is $[\text{Li(thf)}_4][\mathbf{2}]$ and Ln = Dy is $[\text{Li(thf)}_4][\mathbf{3}]$. Compounds $[\text{Li(thf)}_4][\mathbf{2}]$ and $[\text{Li(thf)}_4][\mathbf{3}]$ are only the second and third examples of thiolate-bridged SMMs.

Results and discussion

Synthetic and structural studies. Compounds $[Li(thf)_4][\mathbf{1}]$, $[Li(thf)_4][\mathbf{2}]$ and $[Li(thf)_4][\mathbf{3}]$ were synthesized by adapting the method reported by Lang *et al*. for the praseodymium and samarium congeners.[13] A thf solution of ethylthiol was added to an equimolar amount of $[\{(Me_3Si)_2N\}_3Ln(\mu\text{-}Cl)Li(thf)_3]$ (Ln = Gd, Tb or Dy) in thf at room temperature (Scheme 1). After stirring for four hours, the thf solvent was evaporated, the residue was extracted into toluene, and the concentrated filtrate stored at +4°C for two days. $[Li(thf)_4][\mathbf{1}]$, $[Li(thf)_4][\mathbf{2}]\cdot thf$ and $[Li(thf)_4][\mathbf{3}]\cdot thf$ subsequently crystallized as large blocks suitable for X-ray crystallography (see below and Supporting Information). The nascent solvent was removed by syringe, and the crystals were washed with a small amount of pentane: drying in vacuo resulted in removal of the lattice solvent, hence $[Li(thf)_4][\mathbf{1}]$, $[Li(thf)_4][\mathbf{2}]$ and $[Li(thf)_4][\mathbf{3}]$ were typically isolated in yields greater than 90%.

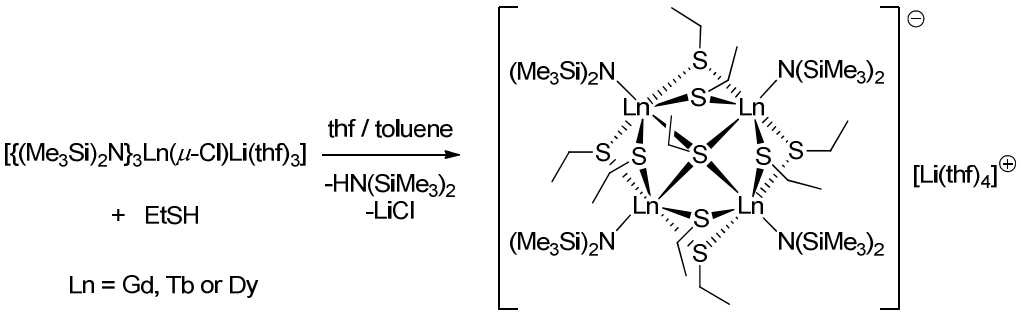

Scheme 1. Synthesis of $[Li(thf)_4][\mathbf{1}]$, $[Li(thf)_4][\mathbf{2}]$ and $[Li(thf)_4][\mathbf{3}]$

The crystal and molecular structures of $[Li(thf)_4][\mathbf{1}]$, $[Li(thf)_4][\mathbf{2}]\cdot thf$ and $[Li(thf)_4][\mathbf{3}]\cdot thf$ are very similar (Table S1). The $[Li(thf)_4]^+$ cations are unremarkable, hence only the structure of the terbium-containing anion **2** will be described in detail (Figure 1), whereas the structures of **1** and

3 are shown in the ESI (Figures S1 and S2). Selected bond lengths and angles for the anions **1**-**3** are collated in Table 2. The structure of **2** features four crystallographically unique but chemically similar, co-planar terbium ions. Each terbium resides in a very distorted octahedral coordination geometry, and is complexed by four μ-SEt ligands, with Tb–S distances in the range 2.766(2)-2.838(2) Å, one μ_4-SEt ligand that produces Tb–S distances in the range 2.944(2)-3.050(2) Å, and terminal $N(SiMe_3)_2$ ligands that result in Tb–N distances of 2.250(9)-2.267(7) Å. The sulfur donor atom of the μ_4-SEt ligand resides approximately 0.95 Å out of the plane of the four terbiums. The distorted nature of the terbium coordination environments in **2** is further reflected in the range of S-Ln-N and S-Ln-S bond angles: for Tb(1), these angles are 97.8(2)-165.9(2)° and 67.1(6)-149.6(9)°, respectively, with similar values being observed for the other terbiums (Table 1). The local symmetry at each Tb site is therefore very low, with no well-defined C_n axes.

As expected based on the relative values of the ionic radii of gadolinium, terbium and dysprosium trications, the Gd–S and Gd–N distances in **1** are slightly longer than those in **2**,

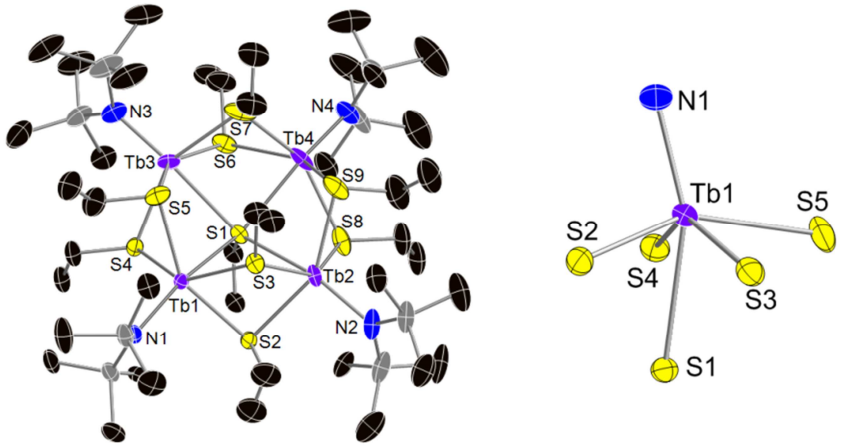

Figure 1. Structure of the $[Tb_4\{N(SiMe_3)_2\}_4(\mu\text{-SEt})_8(\mu_4\text{-SEt})]^-$ anion **2** (left) and an expansion of the Tb(1) coordination environment (right). Thermal ellipsoids set at 30% probability. All hydrogen atoms omitted for clarity. Unlabeled atoms are carbon (black) and silicon (grey).

whereas the analogous distances in **3** are slightly shorter than those in **2**. The N/S-Ln-S bond angles in **1** and **3** are distributed in a similar manner to those in **2**.

Magnetic susceptibility measurements

Static field (d.c.) measurements. Magnetic susceptibility measurements were conducted on polycrystalline samples of [Li(thf)$_4$][**1**], [Li(thf)$_4$][**2**] and [Li(thf)$_4$][**3**], using an applied field of H_{dc} = 1000 G in the temperature range 2-300 K. For each sample, the value of $\chi_M T$ at 300 K is close to that expected for four non-interacting gadolinium, terbium or dysprosium ions, with ground terms of $^8S_{7/2}$ (g = 2), $^7F_6$ (g = 3/2) and $^6H_{15/2}$ (g = 4/3), respectively. At 300 K, for [Li(thf)$_4$][**1**] the value of $\chi_M T$ = 31.52 cm^3 K mol^{-1}, for [Li(thf)$_4$][**2**] $\chi_M T$ = 47.80 cm^3 K mol^{-1}, and for [Li(thf)$_4$][**3**] $\chi_M T$ = 56.66 cm^3 K mol^{-1} (Figure 2). The temperature dependence of $\chi_M T$ in the three compounds follow similar patterns, with the value decreasing only slightly down to about 25 K, followed by much more rapid decreases at lower temperatures. In [Li(thf)$_4$][**1**], $\chi_M T$ = 10.63 cm^3 K mol^{-1} at 2 K, whereas the analogous values for [Li(thf)$_4$][**2**] and [Li(thf)$_4$][**3**] are 33.24 and 25.72 cm^3 K mol^{-1}, respectively.

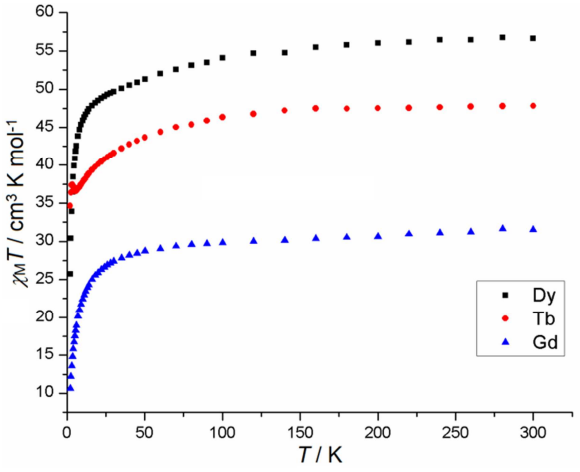

Figure 2. Temperature dependence of $\chi_M T$ for [Li(thf)$_4$][**1**], [Li(thf)$_4$][**2**] and [Li(thf)$_4$][**3**] in an applied field of 1000 G.

Table 2. Selected bond lengths and angles in the $[Ln_4\{N(SiMe_3)_2\}_4(\mu\text{-}SEt)_8(\mu_4\text{-}SEt)]^-$ anions **1**-**3**

	Bond lengths [Å]				Bond angles [°]		
	1 (Ln = Gd)	**2** (Ln = Tb)	**3** (Ln = Dy)		**1** (Ln = Gd)	**2** (Ln = Tb)	**3** (Ln = Dy)
Ln(1)–N(1)	2.262(7)	2.250(9)	2.222(5)	S(1)-Ln(1)-S(2)	69.65(6)	69.77(7)	66.33(4)
Ln(1)–S(1)	3.082(2)	3.050(2)	2.9406(15)	S(1)-Ln(1)-S(3)	82.36(7)	82.63(9)	85.89(5)
Ln(1)–S(2)	2.793(2)	2.777(3)	2.8226(17)	S(1)-Ln(1)-S(4)	65.09(5)	65.71(6)	73.32(5)
Ln(1)–S(3)	2.793(3)	2.776(4)	2.7815(18)	S(1)-Ln(1)-S(5)	85.05(5)	85.05(7)	79.87(5)
Ln(1)–S(4)	2.821(2)	2.804(2)	2.7613(17)	S(1)-Ln(1)-N(1)	166.44(18)	165.9(2)	158.40(14)
Ln(1)–S(5)	2.780(2)	2.773(3)	2.7599(17)	S(2)-Ln(1)-S(3)	71.05(8)	71.25(9)	78.32(5)
Ln(2)–N(2)	2.284(8)	2.256(9)	2.233(6)	S(2)-Ln(1)-S(4)	105.09(6)	104.01(7)	113.17(5)
Ln(2)–S(1)	2.973(2)	2.947(2)	3.0147(16)	S(2)-Ln(1)-S(5)	149.28(7)	149.58(9)	141.59(5)
Ln(2)–S(2)	2.820(2)	2.814(3)	2.7917(16)	S(2)-Ln(1)-N(1)	101.8(2)	101.0(2)	103.14(14)
Ln(2)–S(3)	2.794(3)	2.775(4)	2.7555(18)	S(3)-Ln(1)-S(4)	146.06(7)	147.04(9)	148.11(5)
Ln(2)–S(8)	2.795(3)	2.776(3)	2.7678(19)	S(3)-Ln(1)-S(5)	89.03(8)	89.32(9)	81.70(5)
Ln(2)–S(9)	2.828(3)	2.809(4)	2.760(2)	S(3)-Ln(1)-N(1)	105.22(19)	104.9(2)	111.19(14)
Ln(3)–N(3)	2.292(7)	2.258(9)	2.245(6)	S(4)-Ln(1)-S(5)	79.27(6)	79.48(8)	71.19(5)
Ln(3)–S(1)	3.968(2)	2.944(2)	2.9294(16)	S(4)-Ln(1)-N(1)	108.61(19)	108.0(2)	95.53(13)
Ln(3)–S(4)	2.803(2)	2.782(3)	2.7546(17)	S(5)-Ln(1)-N(1)	106.01(19)	106.6(2)	114.63(14)
Ln(3)–S(5)	2.820(2)	2.798(3)	2.7531(17)				
Ln(3)–S(6)	2.800(2)	2.781(3)	2.7863(18)				
Ln(3)–S(7)	2.784(2)	2.767(2)	2.758(2)				
Ln(4)–N(4)	2.246(6)	2.267(7)	2.228(6)				
Ln(4)–S(1)	2.993(2)	2.968(2)	2.9346(15)				
Ln(4)–S(6)	2.791(2)	2.777(2)	2.795(2)				
Ln(4)–S(7)	2.846(2)	2.838(2)	2.738(2)				
Ln(4)–S(8)	2.815(2)	2.799(3)	2.790(2)				
Ln(4)–S(9)	2.785(2)	2.766(2)	2.747(2)				

The temperature dependence of $\chi_M T$ in [Li(thf)$_4$][**1**] most likely indicates weak antiferromagnetic exchange between the Gd(III) ions, although zero-field splitting may also contribute to the decrease in $\chi_M T$. The plot of magnetization versus field for [Li(thf)$_4$][**1**] at 2 K shows that the magnetization reaches a saturation value of M = 27.2 $N\mu_B$ under the maximum applied field of 7 Tesla (Figure S1), which agrees well with the 28 unpaired electrons expected for four uncoupled Gd(III) ions. The exchange between mutually '*trans*' gadolinium ions in **1**, i.e. Gd(1) with Gd(4), and Gd(2) with Gd(3), can be represented by the exchange coupling constant J_1; the exchange between mutually '*cis*' gadolinium ions, i.e. Gd(1) with Gd(2) and Gd(3), etc., is represented by J_2. Modeling the χ_MT data for [Li(thf)$_4$][**1**] using the spin Hamiltonian $H = -2J_1(S_1S_2 + S_1S_4 + S_2S_3 + S_3S_4) - 2J_2(S_1S_3 + S_2S_4)$ allowed the exchange coupling constants to be determined as $J_1 = -0.15$ cm^{-1} and $J_2 = +0.04$ cm^{-1} (Figure S4). Thus, the exchange coupling is weak and antiferromagnetic between *cis* gadoliniums, which is consistent with the exchange in the thiolate bridged dimer [(η^5-Cp)$_2$Gd(μ-SSiPh$_3$)]$_2$,[10a] and our model produces very weak *trans* ferromagnetic coupling.

The temperature dependence of $\chi_M T$ in [Li(thf)$_4$][**3**] is similar to that observed in other tetrametallic Dy$_4$ cage compounds,[14] and is likely to indicate a gradual depopulation of the excited m_J sub-levels (or so-called Stark sub-levels) within the electronic ground state as the temperature is lowered or, by analogy to [Li(thf)$_4$][**1**], to weak antiferromagnetic exchange. A similar interpretation can be applied to the $\chi_M T(T)$ plot for [Li(thf)$_4$][**2**] (Figure 2). The low-temperature isothermal magnetization versus field data for [Li(thf)$_4$][**2**] and [Li(thf)$_4$][**3**] do not reach saturation in fields ranging from 0-7 T (Figures S5 and S6). At H_{dc} = 7 T, the magnetization reaches values of 24.6 $N\mu_B$ and 21.2 $N\mu_B$ in [Li(thf)$_4$][**2**] and [Li(thf)$_4$][**3**],

respectively, which indicate the presence of significant magnetic anisotropy or low-lying excited states.

Dynamic field (a.c.) measurements. $[Li(thf)_4][\mathbf{2}]$ and $[Li(thf)_4][\mathbf{3}]$ provide an opportunity to explore the dynamic magnetic susceptibility of terbium(III) and dysprosium(III) ions in soft-donor, low-symmetry environments. Using a small dynamic field of H_{ac} = 1.55 G, the out-of-phase magnetic susceptibility (χ'') in $[Li(thf)_4][\mathbf{2}]$, measured at several a.c. frequencies in the range ν = 1-1200 Hz, is temperature dependent below about 4 K (Figure 3). Maxima in the $\chi''(T)$ curves are only observed at frequencies greater than 498 Hz, however these features are characteristic of a single-molecule magnet. A Cole-Cole plot of χ'' versus χ' produced parabolic curves that imply that the magnetization in the anion **2** relaxes via a single mechanism (Figure S7). Using the $\chi''(T)$ data, a plot of the magnetization relaxation time (τ) versus reciprocal temperature (Figure 4) allowed the value of the anisotropy barrier to be determined using the Arrhenius relationship $\tau = \tau_0 \exp(U_{eff}/k_BT)$. For $[Li(thf)_4][\mathbf{2}]$, U_{eff} = 4.6 cm^{-1}, with a pre-exponential factor of $\tau_0 = 1.5 \times 10^{-5}$ s.

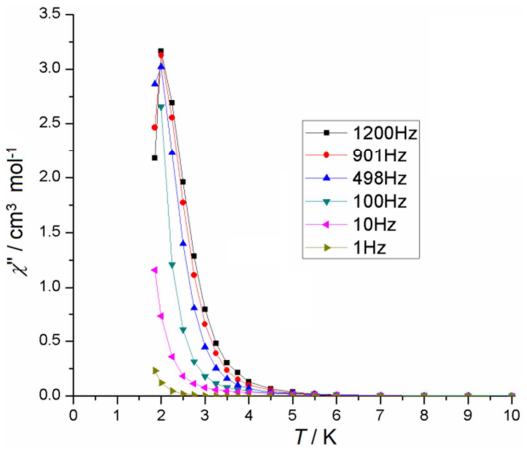

Figure 3. Temperature dependence of χ'' in $[Li(thf)_4][\mathbf{2}]$ at various frequencies in zero applied d.c. field and an a.c. field of H_{ac} = 1.55 G.

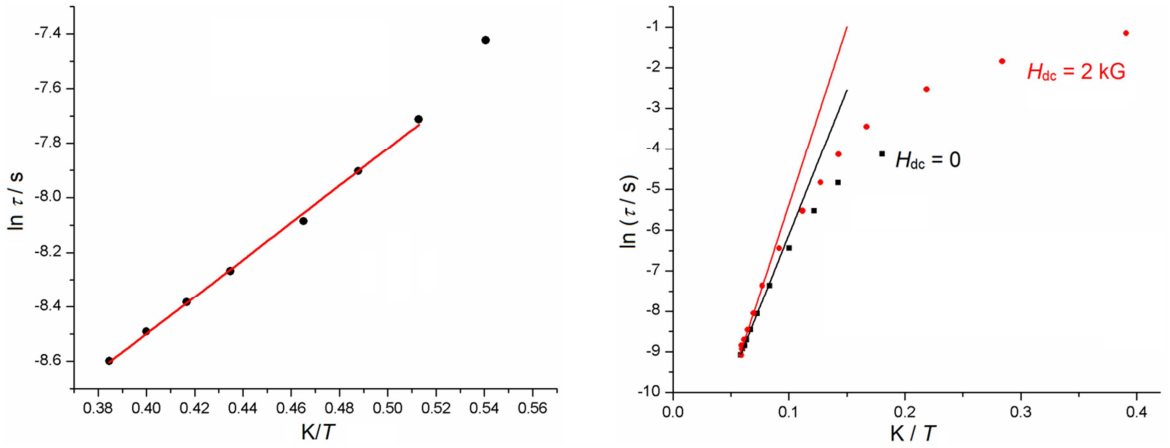

Figure 4. Left: Arrhenius plot of ln τ versus (1/ T) for [Li(thf)$_4$][**2**] in zero d.c. field. Right: Plot of ln τ vs. (1/ T) for [Li(thf)$_4$][**3**] in H_{dc} = 0 (black squares) and in H_{dc} = 2000 G (red circles).The solid lines are the best fit of the data in the thermally activated regimes.

For the dysprosium(III)-containing cage [Li(thf)$_4$][**3**], the SMM properties are much more pronounced, with χ'' displaying a strong temperature dependence below about 28 K, and, furthermore, two relaxation processes are apparent (Figures 5, 6 and S10). In zero applied dc field, a series of $\chi''(T)$ peaks can be seen in the higher-temperature region, with the peak maximum shifting to a lower temperature as the frequency is decreased: this indicates a thermally activated relaxation process, most likely via the first excited Kramers' doublet (Figure 5a). With H_{dc} = 0, in the lower-temperature region a sharp increase in χ'' was observed, which can be interpreted as relaxation occurring via quantum tunneling of the magnetization (QTM) directly from the ground state. The occurrence of two relaxation processes within dysprosium SMMs is not without precedent,[1c] and in the case of the anion **2** most likely corresponds to the magnetization within the four dysprosiums relaxing via the same pathway, rather than via different mechanisms for each crystallographically unique (but chemically identical) dysprosium.

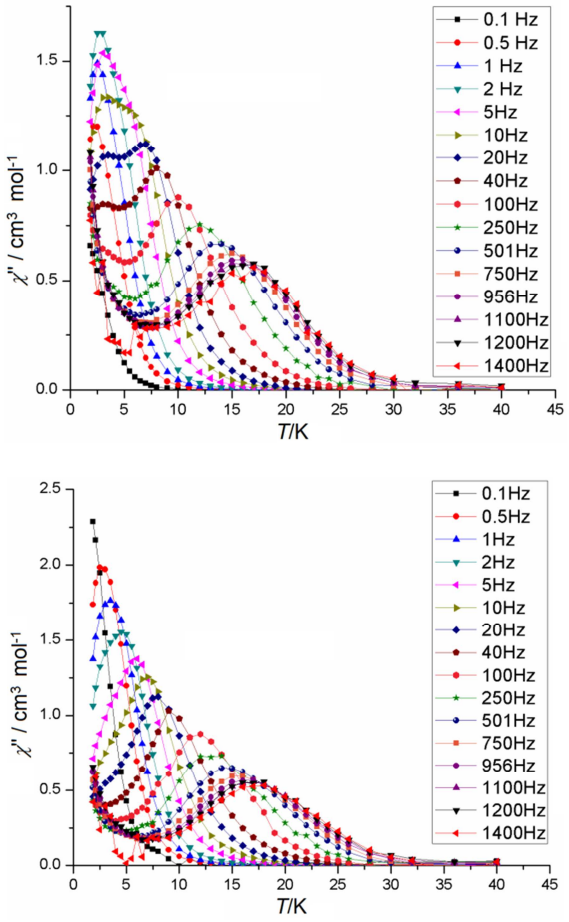

Figure 5. Temperature dependence of χ'' in [Li(thf)$_4$][**3**] at various frequencies and an a.c. field of H_{ac} = 1.55 G. Upper: zero applied d.c. field. Lower: applied d.c. field of H_{dc} = 2000 G.

The Cole-Cole plots for [Li(thf)$_4$][**3**] support the occurrence of two relaxation processes, with the lower-temperature $\chi''(\chi')$ curves displaying a distinct asymmetry (Figure 6).

Relaxation via QTM in Ln-SMMs can be suppressed by the application of a static magnetic field.[15] In the case of [Li(thf)$_4$][**3**], an optimum applied field of H_{dc} = 2000 G was found to reduce the QTM rate at a.c. frequencies greater than 0.5 Hz (Figure 5b), with the corresponding Cole-Cole plots developing a more symmetrical appearance (Figure S10). The plot of ln τ versus 1/T for [Li(thf)$_4$][**3**] in zero applied field revealed that the thermally activated process is followed down to temperatures of about 10 K, and at lower temperatures the negative

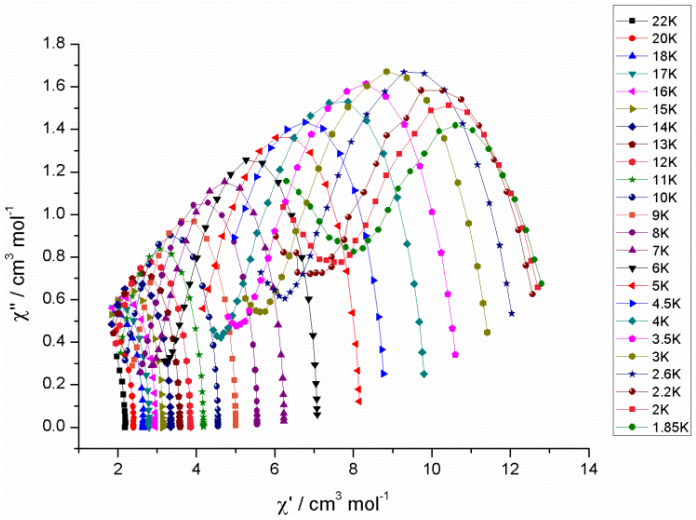

Figure 6. Cole-Cole plot of χ'' vs. χ' for [Li(thf)$_4$][**3**] in zero applied field. The solid lines connecting the data points are a guide for the eye.

curvature of the data indicates that thermally activated relaxation is gradually supplanted by a QTM process (Figure 4). Arrhenius analysis of the zero-field a.c. data on [Li(thf)$_4$][**3**] yielded U_{eff} = 46 cm^{-1}, and $\tau_0 = 4.30 \times 10^{-6}$ s. The same analysis in an applied field of 2000 G gave U_{eff} = 49 cm^{-1}, with a pre-exponential factor of $\tau_0 = 2.01 \times 10^{-6}$ s.

Although both [Li(thf)$_4$][**2**] and [Li(thf)$_4$][**3**] are SMMs, the much larger anisotropy barrier arising from the dysprosium(III) ions in the anion **3** is noteworthy. Terbium(III) and dysprosium(III) are particularly good candidates for SMM applications because of the high magnetic moment and the significant anisotropy of their respective electronic ground states. However, because dysprosium(III) is a Kramers' ion, the bistable ground state necessary for SMM behavior is assured irrespective of the symmetry of the coordination environment.[2] In contrast, terbium(III) is a non-Kramers' ion, and so well-defined axial symmetry is required for a bistable ground state. The low symmetry of the terbium coordination environments in **2**

described above (Figure 1 and Table 1) suggests that the formal requirement for a bistable ground state is not met, and this is likely to be responsible for the weak SMM behavior in $[Li(thf)_4][\mathbf{2}]$. However, despite its small anisotropy barrier, $[Li(thf)_4][\mathbf{2}]$ is still the first sulfur-ligated terbium SMM, and it is also the first $\{Tb_4\}$ SMM. Several examples of $\{Dy_4\}$ SMMs are known, but to the best of our knowledge only four examples have zero-field anisotropy barriers greater than that measured in $[Li(thf)_4][\mathbf{3}]$.[13]

Conclusion

The gadolinium, terbium and dysprosium tetrametallic, thiolate-bridged cage compounds $[Li(thf)_4][\mathbf{1}]$, $[Li(thf)_4][\mathbf{2}]$ and $[Li(thf)_4][\mathbf{3}]$ were synthesized and their structures were determined by X-ray crystallography. The lanthanides within the anions **1**-**3** reside in highly distorted six-coordinate environments, and analysis of the relevant metric parameters revealed that no local symmetry axes coincide with the metal positions. The variable-temperature magnetic susceptibility of $[Li(thf)_4][\mathbf{1}]$ was modeled using two exchange coupling constants, which revealed that the Gd(III) ions are weakly coupled. The dynamics of the magnetization in $[Li(thf)_4][\mathbf{2}]$ and $[Li(thf)_4][\mathbf{3}]$ were investigated in zero applied d.c. field, and SMM behavior was observed in both cases. For the terbium version $[Li(thf)_4][\mathbf{2}]$, an anisotropy barrier of U_{eff} = 4.6 cm^{-1} was determined, with a relaxation time of $\tau = 1.5 \times 10^{-5}$ s, and the small value of U_{eff} is likely to be a consequence of the very low-symmetry environments in which the Tb(III) ions reside. A larger U_{eff} value of 46 cm^{-1}, with a relaxation time of $\tau = 2.1 \times 10^{-6}$ s, was determined for $[Li(thf)_4][\mathbf{3}]$, and the plot of the out-of-phase susceptibility against temperature revealed the occurrence of two relaxation processes, one being thermally activated and the other being due to quantum tunneling of the magnetization at very low temperatures.

The SMMs [Li(thf)$_4$][**3**] and [Li(thf)$_4$][**3**] expand the small but growing family of polymetallic SMMs based on non-oxygen donor ligands. The interesting dynamic magnetic properties of these two compounds suggest that there is merit in using soft-donor ligands that are 'unconventional' in the context of SMM studies.

ASSOCIATED CONTENT

Supporting Information. Synthetic details for [Li(thf)$_4$][**1**], [Li(thf)$_4$][**2**] and [Li(thf)$_4$][**3**]. X-ray crystallographic data in CIF format. Additional magnetism graphs for [Li(thf)$_4$][**1**], [Li(thf)$_4$][**2**] and [Li(thf)$_4$][**3**]. This material is available free of charge via the Internet at http://pubs.acs.org.

AUTHOR INFORMATION

Corresponding Author

Richard.Layfield@manchester.ac.uk

Author Contributions

The manuscript was written through contributions of all authors. All authors have given approval to the final version of the manuscript.

ACKNOWLEDGMENT

RAL thanks the Alexander von Humboldt Foundation for the award of a Fellowship for Experienced Researchers. REPW thanks the Royal Society for a Wolfson Merit Award. The authors acknowledge the support of the EPSRC (U.K.).

References

1. (a) Luzon, J.; Sessoli, R, *Dalton Trans*. **2012**, *41*, 13556. (b) Sorace, L.; Benelli, C.; Gatteschi, D. *Chem. Soc. Rev*. **2011**, *40*, 3092. (c) Guo, Y. –N.; Xu, G. –F.; Guo, Y.; Tang, J. *Dalton Trans*. **2011**, *40*, 9953. (d) Sessoli, R.; Powell, A. K.; *Coord. Chem. Rev*. **2009**, *253*, 2328.

2. Rinehart, J. D.; Long, J. R.; *Chem. Sci.* **2011**, *3*, 2078.

3. (a) Ishikawa, N.; Sugita, M.; Ishikawa, T.; Koshihara, S.; Kaizu, Y. *J. Am. Chem. Soc.* **2003**, *125*, 8694. (b) Ishikawa, N. *Polyhedron* **2007**, *26*, 2147.

4. Milios, C. J.; Vinslava, A.; Wernsdorfer, W.; Moggach, S.; Parsons, S.; Perlepes, S. P.; Christou, G.; Brechin E. K. *J. Am. Chem. Soc*. **2007**, *129*, 2754.

5. (a) Rinehart, J. D.; Fang, M.; Evans, W. J.; Long, J. R.; *Nature Chem.* **2011**, *3*, 538. (b) Rinehart, J. D.; Fang, M.; Evans, W. J.; Long, J. R.; *J. Am. Chem. Soc.* **2011**, *133*, 14236.

6. Aromí, G.; Brechin, E. K. *Struct. Bonding* **2006**, *122*, 1.

7. Gonidec, M.; Biagi, R.; Corradini, V.; Moro, F.; De Renzi, V.; del Pennino, U.; Summa, D.; Muccioli, L.; Zannoni, C.; Amabilino, D. B.; Veciana, J. *J. Am. Chem. Soc*. **2011**, *133*, 6603.

8. (a) Katoh, K.; Kajiwara, T.; Nakano, M.; Nakazawa, Y.; Wernsdorfer, W.; Ishikawa, N.; Breedlove, B. K.; Yamashita, M. *Chem. Eur. J.* **2011**, *17*, 117. (b) Guo, Y.; Xu, G.; Wernsdorfer, W.; Ungur, L.; Guo, Y.; Tang, J.; Zhang, H.; Chibotaru, L. F.; Powell, A. K. *J. Am. Chem. Soc.* **2011**, *133*, 11948. (c) Blagg, R. J.; Muryn, C. A.; McInnes, E. J. L.; Tuna, F.; Winpenny, R. E. P. *Angew. Chem. Int. Ed.* **2011**, *50*, 6530. (d) Blagg, R. J.; Tuna, F.;

McInnes, E. J. L.; Winpenny, R. E. P. *Chem. Commun.* **2011**, *47*, 10587. (e) Hewitt, I. J.; Tang, J.; Madhu, N. T.; Anson, C. E.; Lan, Y.; Luzon, J.; Etienne, M.; Sessoli, R.; Powell, A. K. *Angew. Chem. Int. Ed.* **2010**, *49*, 6352. (f) Gonidec, M.; Luis, F.; Vilchez, A.; Esquena, J.; Amabilino, D. B.; Veciana, J. *Angew. Chem. Int. Ed.* **2010**, *49*, 1623. (g) Takamatsu, S.; Ishikawa, T.; Koshihara, S.; Ishikawa, N. *Inorg. Chem.* **2007**, *46*, 7250. (h) Ishikawa, N.; Sugita, M.; Tanaka, N.; Ishikawa, T.; Koshihara, S.; Kaizu, Y. *Inorg. Chem.* **2004**, *43*, 5498.

9. (a) Vincent, R.; Klyatskaya, S.; Ruben, M.; Wernsdorfer, W.; Balestro, F. *Nature*, **2012**, *488*, 357. (b) Urdampilleta, M.; Cleuziou, J.-P.; Klyatskaya, S.; Ruben, M; Wernsdorfer, W. *Nature Mater*. **2011**, *10*, 502. (c) Mannini, M.; Pineider, F.; Sainctavit, P.; Danieli, C.; Otero, E.; Sciancalepore, C.; Talarico, A. M.; Arrio, M. –A.; Cornia, A.; Gatteschi, D.; Sessoli, R. *Nature Mater*. **2009**, ***8***, 194. (d) Bogani, L.; Wernsdorfer, W. *Nature Mater*. **2008**, *7*, 179. (e) Leuenberger, M. N.; Loss, D. *Nature* **2001**, *410*, 789.

10. (a) Tuna, F.; Smith, C. A.; Bodensteiner, M.; Ungur, L.; Chibotaru, L. F.; McInnes, E. J. L.; Winpenny, R. E. P.; Collison, D.; Layfield, R. A. *Angew. Chem. Int. Ed.* **2012**, *51*, 6976. (b) Sulway, S. A.; Layfield, R. A.; Tuna, F.; Wernsdorfer, W.; Winpenny, R. E. P. *Chem. Commun.* **2012**, *48*, 1508. (c) Layfield, R. A.; McDouall, J. J. W.; Sulway, S. A.; Tuna, F.; Collison, D.; Winpenny, R. E. P. *Chem. Eur. J.* **2010**, *16*, 4442.

11. (a) Magnani, N.; Apostolidis, C.; Morgenstern, A.; Colineau, E.; Griveau, J. –P.; Bolvin, H.; Walter, O.; Caciuffo, R. *Angew. Chem. Int. Ed.* **2011**, *50*, 1696. (b) Jeletic, M.; Lin, P. –H.; Le Roy, J. J.; Korobkov, I.; Gorelsky, S. I.; Murugesu, M. *J. Am. Chem. Soc*. **2011**, *133*, 19286. (c) Jiang, S. –D.; Wang, B. –W.; Sun, H. L.; Wang, Z. M.; Gao, S. *J. Am. Chem. Soc.*

2011, *133*, 4730. (d) Jiang, S. –D.; Liu, S. S.; Zhou, L. –N.; Wang, B. –W.; Gao, S. *Inorg. Chem.* **2012**, *51*, 3079.

12. (a) Cucinotta, G.; Perfetti, M.; Luzon, J.; Etienne, M.; Car, P.-E.; Caneschi, A.; Calvez, G.; Bernot, K.; Sessoli, R.; *Angew. Chem. Int. Ed*. **2012**, *51*, 1606. (b) Williams, U. J.; Mahoney, B. D.; DeGregorio, P. T.; Carroll, P. J.; Nakamura-Ogiso, E.; J. M. Kikkawa, Schelter, E. J. *Chem. Commun*. **2012**, *48*, 5593. (c) Wang, H.; Wang, K.; Tao, J.; Jiang, J. *Chem. Commun*. **2012**, *48*, 2973.

13. Cheng, M.; Li, H.; Zhang, W.; Ren, Z.; Zhang, Y.; Lang, J. *Eur. J. Inorg. Chem.* **2007**, 1889.

14. (a) Xue, S.; Zhao, L.; Chen, X. –H.; Tang, J. *Chem. Commun*. **2012**, *48*, 7031. (b) Guo, P. H.; Liu, J. –L.; Zhang, Z. –M.; Ungur, L.; Chibotaru, L. F.; Leng, J. –D.; Guo, F. –S.; Tong, M. –L. *Inorg. Chem*. **2012**, *51*, 1233. (c) Lin, P.; Burchell, T. J.; Ungur, L.; Chibotaru, L. F.; Wernsdorfer, W.; Murugesu, M.; *Angew. Chem. Int. Ed.* **2009**, *48*, 9489. (d) Guo, Y. N.; Xu G. –F.; Gamez, P.; Zhao. L.; Lin, S. –Y.; Deng, R.; Tang, J.; Zhang, H. –J. *J. Am. Chem. Soc*. **2010**, *132*, 8538.

15. Thomas, L.; Lionti, F.; Ballou, R.; Gatteschi, D.; Sessoli, R.; Barbara, B. *Nature* **1996**, *383*, 145.

Supporting information for:

Single-molecule magnetism in thiolate-bridged terbium and dysprosium squares

Daniel N. Woodruff,[a] Floriana Tuna,[a,b] Michael Bodensteiner,[c] Richard E. P. Winpenny[a,b] and Richard A. Layfield[a]*

[a] School of Chemistry, The University of Manchester, Oxford Road, Manchester, M13 9PL, U.K.

[b] EPSRC U.K. National EPR Facility, Photon Science Institute, The University of Manchester, Oxford Road, Manchester, M13 9PL, U.K.

[c] Institute of Inorganic Chemistry, University of Regensburg, Germany, D-93040.

Experimental section

General considerations. All syntheses were carried out using standard Schlenk techniques, using an inert atmosphere of dinitrogen. THF solvent was pre-dried over sodium wire before being refluxed over sodium-potassium alloy. Toluene was dried using an Innovative Technology Inc. Solvent Purification System, and was then stored over activated 4 Å molecular sieves. X-ray diffraction data for $[Li(thf)_4][\mathbf{1}]$, $[Li(thf)_4][\mathbf{2}]$ and $[Li(thf)_4][\mathbf{3}]$ were collected on an Oxford Instruments XCalibur2 X-ray diffractometer, using MoKα radiation. The precursor material

[{$(Me_3Si)_2N$}$_3$Ln(μ-Cl)Li(thf)$_3$] (Ln = Gd, Tb or Dy) was synthesized according to a literature procedure.[1] Ethylthiol was purchased from Aldrich, and was used as supplied.

Synthesis of [Li(thf)$_4$][1]. A solution of EtSH (0.13 mL, 1.7 mmol) in THF (5 mL) was added drop-wise to a solution of [{$(Me_3Si)_2N$}$_3$Gd(μ-Cl)Li(thf)$_3$] (1.51 g, 1.7 mmol) in THF (20 mL) at room temperature. After stirring for four hours, the THF was removed in vacuo. Toluene (20 mL) was then added and the mixture brought to reflux, before being filtered to give a colourless solution. Colourless crystals of [Li(thf)$_4$][**1**] were obtained after storing the solution at 4°C for two days. Removing the nascent solvent, washing the crystals with a small amount of pentane followed by drying in vacuo resulted in [Li(thf)$_4$][**1**] being isolated as a colourless polycrystalline material (0.38 g, 91%). Elemental analysis calculated for $C_{58}H_{149}N_4Gd_4S_9Si_8O_4$: C 33.03, H 7.12, N 2.66; found: C 33.28, H 7.04, N 2.57.

Synthesis of [Li(thf)$_4$][2]. Compound [Li(thf)$_4$][**2**] was synthesized in an identical manner to [Li(thf)$_4$][**1**], using [{$(Me_3Si)_2N$}$_3$Tb(μ-Cl)Li(thf)$_3$] (1.51 g, 1.7 mmol) and EtSH (0.13 mL, 1.7 mmol). Diffraction-quality, colourless crystals of [Li(thf)$_4$][**2**]·thf were obtained after storing the solution at 4°C for two days. Elemental analysis revealed that the lattice thf is removed on drying the crystalline material in vacuo for ca. one hour (0.37 g, 90%). Calculated for $C_{58}H_{149}N_4Tb_4S_9Si_8O_4$: C 32.93, H 7.10, N 2.65; found: C 33.14, H 7.06, N 2.53.

Synthesis of [Li(thf)$_4$][3]. Compound [Li(thf)$_4$][**3**] was synthesized in an identical manner to [Li(thf)$_4$][**1**], using [{$(Me_3Si)_2N$}$_3$Dy(μ-Cl)Li(thf)$_3$] (1.52 g, 1.7 mmol) and EtSH (0.13 mL, 1.7 mmol). Diffraction-quality, colourless crystalline blocks of [Li(thf)$_4$][**3**]·toluene were obtained after storing the solution at 4°C for two days. [Li(thf)$_4$][**3**] was isolated as a colourless polycrystalline material (0.40 g, 95%). Elemental analysis calculated for $C_{58}H_{149}N_4Dy_4S_9Si_8O_4$: C 32.70, H 7.05, N 2.63; found: C 32.98, H 7.09, N 2.48.

Table S1. Crystal data and structure refinement for $[Li(thf)_4][\mathbf{1}]$, $[Li(thf)_4][\mathbf{2}]$ and $[Li(thf)_4][\mathbf{3}]$

	$[Li(thf)_4][\mathbf{1}]$	$[Li(thf)_4][\mathbf{2}]\cdot thf$	$[Li(thf)_4][\mathbf{3}]\cdot thf$
Formula	$Gd_4S_9Si_8O_4N_4LiC_{58}H_{149}$	$Tb_4S_9Si_8O_5N_4LiC_{62}H_{157}$	$Dy_4S_9Si_8O_5N_4LiC_{60.5}H_{154}$
FW	2188.12	2194.80	2188.08
Crystal system	monoclinic	monoclinic	monoclinic
Space group	$P2_1/c$	$P2_1/c$	$P2_1/c$
a/Å	14.8584(5)	14.8431(9)	14.8218(5)
b/Å	25.4645(8)	25.4673(12)	25.4429(7)
c/Å	26.6088(10)	26.4317(15)	26.2217(8)
α/°	90	90	90
β/°	91.664(3)	91.784(5)	91.779(3)
γ/°	90	90	90
V/Å^3	10063.5(6)	9986.7(10)	9883.3(5)
Z	4	4	4
Crystal size/mm^3	$0.45 \times 0.43 \times 0.34$	$0.26 \times 0.22 \times 0.05$	$0.64 \times 0.26 \times 0.14$
θ range/°	2.98-28.65	2.86-28.52	2.99-28.52
Reflections collected	71405	73484	70504
Independent reflections, R(int)	23018, 0.0613	22713, 0.0973	22417, 0.0685
Completeness/%	99.7%	99.8%	99.8%
Data/restraints/parameters	23018 / 288 / 749	22713 / 289 / 749	22417 / 565 / 903
Goodness-of-fit on F^2	1.111	0.993	0.916
Final R indices [$I>2\sigma(I)$]	$R_1 = 0.0696$ $wR_2 = 0.1830$	$R_1 = 0.0823$ $wR_2 = 0.1883$	$R_1 = 0.0568$ $wR_2 = 0.1362$
R indices (all data)	$R_1 = 0.1430$ $wR_2 = 0.2021$	$R_1 = 0.1791$ $wR_2 = 0.2312$	$R_1 = 0.1244$ $wR_2 = 0.1472$

Structures were solved and refined with SHELX and SHELXL was used for the refinement.[2] The lattice solvent was treated with the SQUEEZE function of the PLATON software.[3]

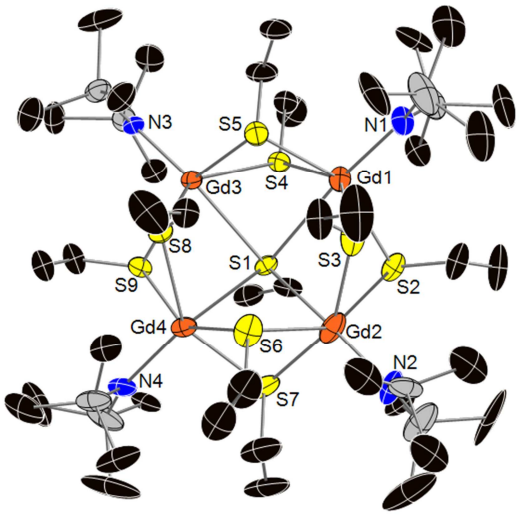

Figure S1. Structure of the $[Gd_4\{N(SiMe_3)_2\}_4(\mu\text{-}SEt)_8(\mu_4\text{-}SEt)]^-$ anion **1**. Thermal ellipsoids set at 30% probability. All hydrogen atoms omitted for clarity. Unlabeled atoms are carbon (black) and silicon (grey).

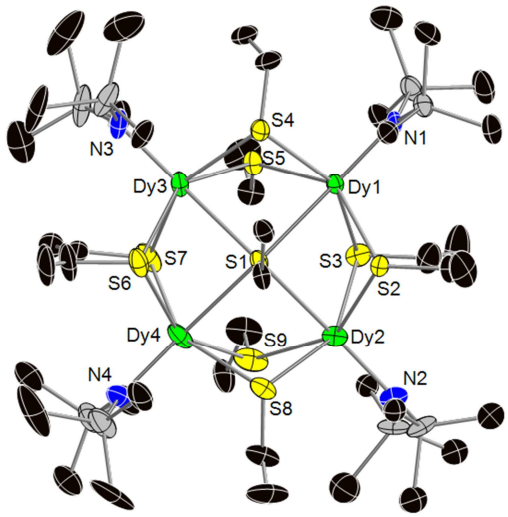

Figure S2. Structure of the $[Dy_4\{N(SiMe_3)_2\}_4(\mu\text{-}SEt)_8(\mu_4\text{-}SEt)]^-$ anion **1**. Thermal ellipsoids set at 30% probability. All hydrogen atoms omitted for clarity. Unlabeled atoms are carbon (black) and silicon (grey).

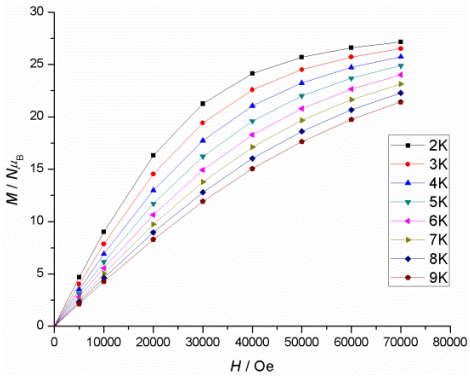

Figure S3. Plot of magnetization vs. field at various temperatures for [Li(thf)$_4$][**1**].

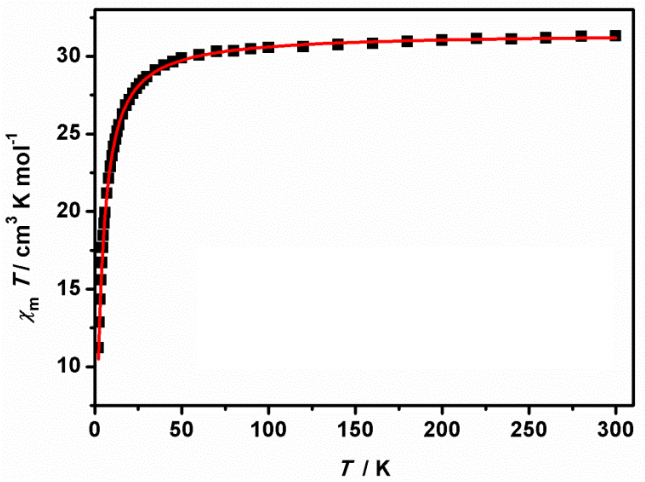

Figure S4. Plot of $\chi_M T$ vs. T for [Li(thf)$_4$][**1**] in an applied field of H_{dc} = 1000 G. The solid line is the theoretical fit of the data according to the spin Hamiltonian and parameters stated in the manuscript text.

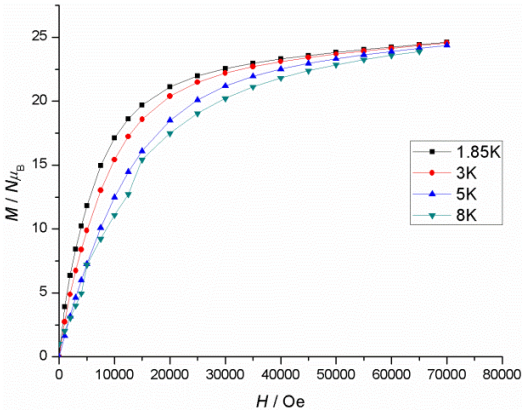

Figure S5. Plot of magnetization vs. field at various temperatures for $[Li(thf)_4][\mathbf{2}]$.

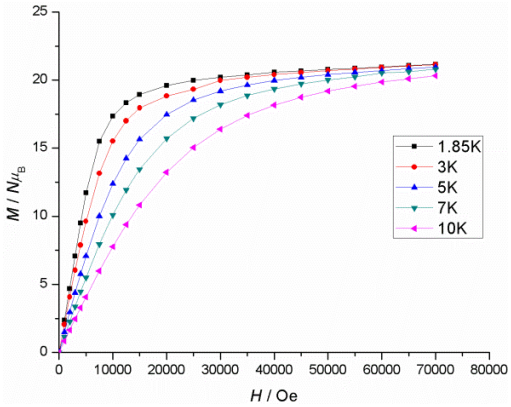

Figure S6. Plot of magnetization vs. field at various temperatures for $[Li(thf)_4][\mathbf{3}]$.

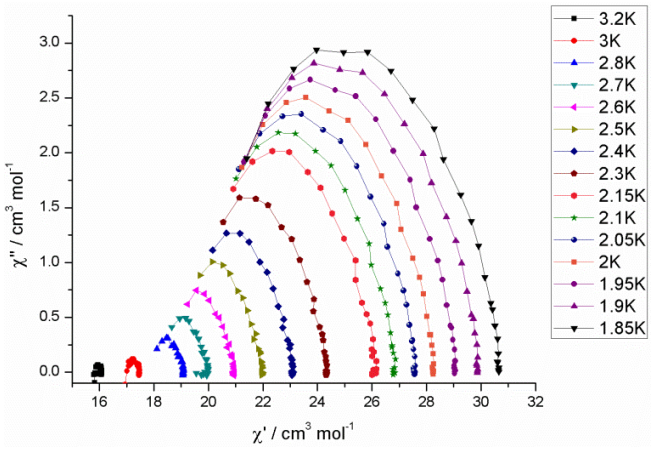

Figure S7. Cole-Cole plot of χ'' vs. χ' for $[Li(thf)_4][\mathbf{2}]$ in zero applied field. The solid lines connecting the data points are a guide for the eye.

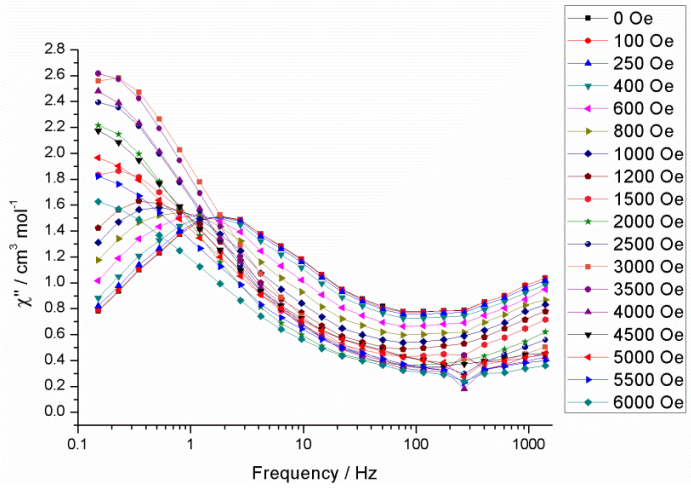

Figure S8. χ'' vs. ac frequency at various applied dc field for $[Li(thf)_4][\mathbf{3}]$ at 2 K.

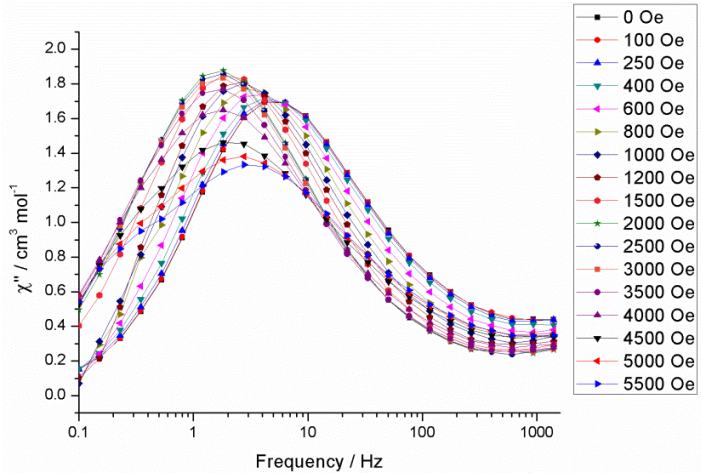

Figure S9. χ'' vs. ac frequency at various applied dc field for $[Li(thf)_4][\mathbf{3}]$ at 5 K.

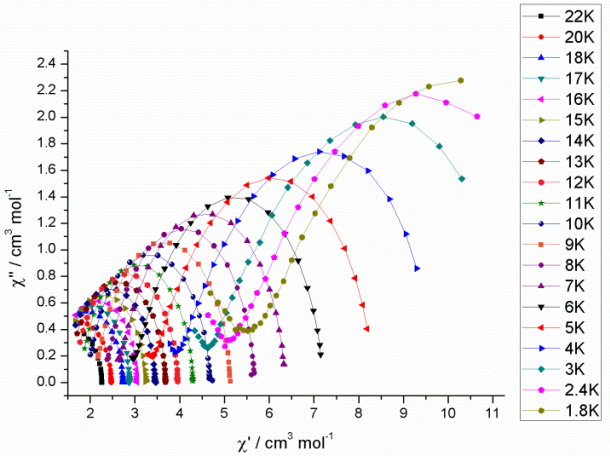

Figure S10. Cole-Cole plot of χ'' vs. χ' for $[Li(thf)_4][\mathbf{2}]$ in an applied field of H_{dc} = 2000 G. The solid lines connecting the data points are a guide for the eye.

References

1. Cheng, M.; Li, H.; Zhang, W.; Ren, Z.; Zhang, Y.; Lang, J. *Eur. J. Inorg. Chem.* **2007**, 1889.
2. Sheldrick, G. M. *Acta Cryst.* **2008**, *A64*, 112.
3. Sluis, P.; Spek A. L. *Acta Cryst.* **1990**, *A46*, 194.

Chapter 5: Paper 2

“Single Molecule Magnets (SMMs) from ether cleavage: A Dy(III) dimer SMM formed from *in situ* solvent cleavage”

Daniel N. Woodruff, Richard E. P. Winpenny, Floriana Tuna and Richard A, Layfield,

Submitted

Journal Name

Dynamic Article Links ►

Cite this: DOI: 10.1039/c0xx00000x

www.rsc.org/xxxxxx

ARTICLE TYPE

Single Molecule Magnets (SMMs) from ether cleavage: A Dy(III) dimer SMM formed from *in situ* solvent cleavage

Daniel N. Woodruff,[a] Richard E. P. Winpenny,[b] Floriana Tuna [b] and Richard A, Layfield* [a]

Received (in XXX, XXX) Xth XXXXXXXXX 20XX, Accepted Xth XXXXXXXXX 20XX

DOI: 10.1039/b000000x

The reactions of LiTMP (TMP- = anion of 2,2,6,6-tetramethylpiperidine) with $DyCl_3$ and $YbCl_3$ in Et_2O result in the formation of $[Ln(TMP)_2(\mu\text{-OEt})]_2$ (Ln = Dy (**1**), Yb (**2**)) which contains two ethoxide ligands generated from *in situ* ether cleavage. The Dy analogue shows SMM behaviour in zero field at temperatures below 15K but requires an external field of 7000 Oe to allow a barrier to reversal of magnetisation U_{eff} = 23.6 cm^{-1} and relaxation time $\tau_0 = 6.5 \times 10^{-7}$ s to be determined.

Introduction

The magnetic properties of low-coordinate lanthanide-containing complexes have remained largely unexplored until recently, due to the challenges presented in synthesizing low coordinate lanthanide containing complexes and the greater interest in their catalytic properties.[1,2] To date the only low coordinate lanthanide containing SMMs are the dysprosium and terbium dimers reported by Long *et al.*,[3,4] in which each lanthanide center is formally four-coordinate, and the chloride and sulfur bridged dysprosium dimers reported by Layfield et al.,[5,6] where the Ln centers are also formally four-coordinate in some cases.

Despite this small number of low-coordinate lanthanide SMMs, a large number of low coordinate lanthanide containing complexes have been reported with a variety of different ligands and synthetic strategies.[7] Of particular interest here is the synthetic strategy used by Lappert and co-workers, in which reactions of YCl_3 or $CeCl_3$ in Et_2O with LiTMP (TMP = 2,2,6,6-tetramethylpypiridine) give $[Y(TMP)_2(\mu\text{-OEt})]_2$ and $[Ce(TMP)_2(\mu\text{-OEt})]_2$ respectively *via in situ* formation of ethoxide anions.[8] The *in situ* formation of ethoxide ligands via ether cleavage has a wide precedent in the literature [9] and with this synthetic strategy in mind we have extended the method used by Lappert *et al*, to produce the dysprosium and ytterbium analogues; $[Dy(TMP)_2(\mu\text{-OEt})]_2$ (**1**) and $[Yb(TMP)_2(\mu\text{-OEt})]_2$ (**2**), with the dysprosium analogue (**1**) showing SMM behaviour.

Structural Studies

The crystal data for **1** and **2** are shown in Table 1. Complex **1** crystallizes as pale yellow blocks in the monoclinic space group $P2_1/c$ (Figure 1). Complex **1** contains a crystallographic inversion centre at the centre of **1** and as such the asymmetric unit of **1** contains one dysprosium centre, one μ_2-OEt and two TMP^- ligands. As complex **1** is symmetry generated there is only one Dy – O bond distance of 2.634(18) Å and a Dy – O – Dy angle of 107.12(7) °. Each TMP ligand is monodentate with Dy – N bond distances are in the range of 2.225(2) – 2.238(2) Å. The dysprosium centers in 1 have a distorted tetrahedral coordination environment with an O – Dy – O bond angle of72.88(7) °, N-Dy-N bond angle of 118.77(8) ° and O-Dy-N bond angles in the range 105.42(7) ° – 123.08(7) ° (average: 114.39 °).

Table 1. Crystal data for **1** and **2**

	1	2
Formula	$Dy_2O_2N_4C_{40}H_{82}$	$Yb_2O_2N_4C_{40}H_{82}$
Formula weight	976.122	997.202
Crystal system	monoclinic	monoclinic
Space group	$P2_1/c$	$C2/c$
a/Å	13.3295(4)	26.2052(14)
b/Å	11.3302(3)	11.2400(5)
c/Å	14.6243(4)	14.8714(7)
α/°	90	90
β/°	105.319(3)	105.454(5)
γ/°	90	90
V/Å^3	2130.17(10)	4221.9(4)
Z	2	1
Crystal size/mm^3	0.50× 0.50× 0.40	0.50 × 0.40× 0.40
θ range/°	3.01-27.50	3.02-28.69
Reflections collected	4763	5345
Independent reflections,	3145	5147
R(int)	0.0276	0.0378
Completeness/%	97.3%	98.1%
Data/restraints/parameters	4763 / 0 / 217	5345 / 0 / 217
Goodness-of-fit on F^2	1.076	1.045
Final R indices [$I>2\sigma(I)$]	R_1 = 0.0192	R_1 = 0.0428
	wR_2 = 0.0448	wR_2 = 0.1112
R indices (all data)	R_1 = 0.0348	R_1 = 0.0520
	wR_2 = 0.0469	wR_2 = 0.1153

Complex **2** crystallizes as red blocks in the monoclinic space group *C*2/*c* and has a structure very similar to that of **1**. Both **1** and **2** are formed as a result of cleavage of the reaction solvent. The reactions forming **1** and **2** could not be followed by NMR, due to their paramagnetic nature, but the mechanisms by which **1** and **2** form have been previously investigated for both Ce and Y.

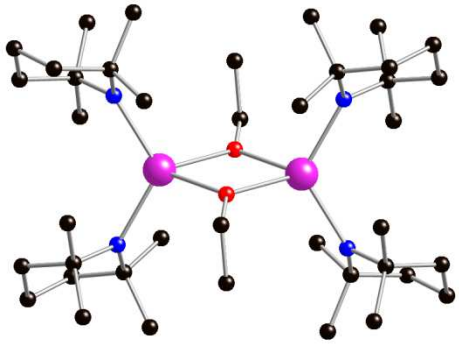

Figure 1. Solid state structure of **1**. Thermal ellipsoids shown at 50% probability. All hydrogen atoms omitted for clarity. Black = Carbon, Blue = Nitrogen, Red = Oxygen and Purple = Dysprosium.

DC Magnetic Properties of 1 and 2

In order to investigate the magnetic properties of **1** and **2** magnetic susceptibility measurements were performed on polycrystalline samples of **1** and **2**. The plots of χ_MT vs T, where χ_M is the molar susceptibility and *M* vs *H*/*T* for **1** are shown in Figure 2. The observed χ_MT value for **1** at 300K is 28.35 cm^3 K mol^{-1} which is in good agreement with the value of 28.34 cm^3 K mol^{-1}expected for two uncoupled Dy(III) ions ($^6H_{15/2}$, g = 4/3). Upon reducing temperature the χ_MT value of **1** decreases to 9.72 cm^3 K mol^{-1} at 1.85K. This behavior can be attributed to the progressive depopulation of Stark sub-levels of **1** and may also hint at anti-ferromagnetic coupling between the two dysprosium centers in **1**.[10] Magnetization measurements on **1** (Figure 2b) do not fully saturate, with a value at 7T of 10.57 $N\mu_B$ (less than the 20Nμ_B expected for two non interacting Dy(III) ions); this is most likely due to the large anisotropy associated with the dysprosium ions present in **1**.[11]

a)

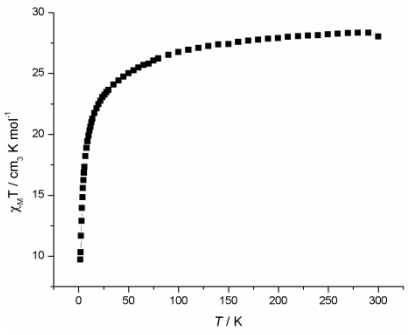

b)

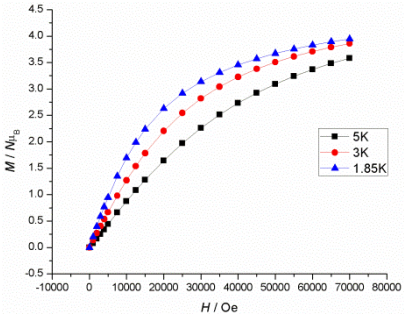

Figure 2. Plots for **1** of: **a)** χ_MT vs T and **b)** *M* vs *H*

Similar magnetic studies were performed on **2** with both χ_MT vs T and *M* vs *H* plots being shown in Figure 3. At 300K the χ_MT value for 2 is 5.79 cm^3 K mol^{-1} which is larger than expected value of 5.08 cm^3 K mol^{-1} for two uncoupled Yb(III) ions ($^2F_{7/2}$, g = 8/7). The decrease observed in χ_MT upon reducing temperature in 2 is again attributed to the depopulation of Stark sub-levels. The magnetization of 2 does not saturate to 7 T, with a value of 3.97 $N\mu_B$ at the highest field measured. This value is in good agreement with other ytterbium containing complexes.[12]

a)

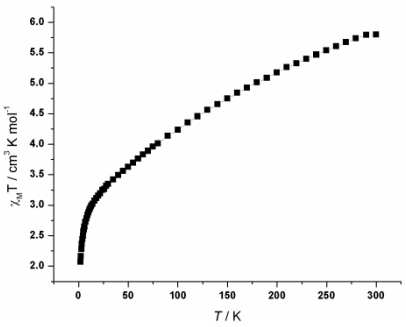

b)

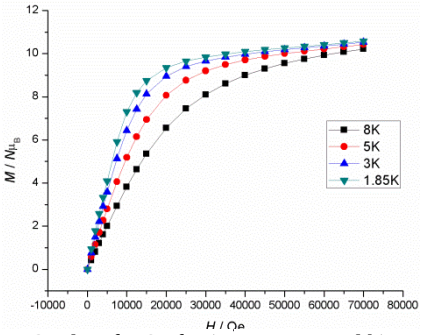

Figure 3. Plots for **2** of: a) χMT vs T and b) M vs H

AC Magnetic Properties of 2

To further investigate the magnetic properties of **1** and **2**, alternating current (AC) susceptibility measurements were carried out on both. Whilst **2** showed no frequency dependency of either in or out of phase susceptibility (Figure S1), **1** showed a shoulder in both χ' vs T and χ'' vs T plots at low temperatures (below 15K) (Figure 4) suggesting frequency dependency of both in and out of phase magnetic susceptibility and potential SMM

behaviour.

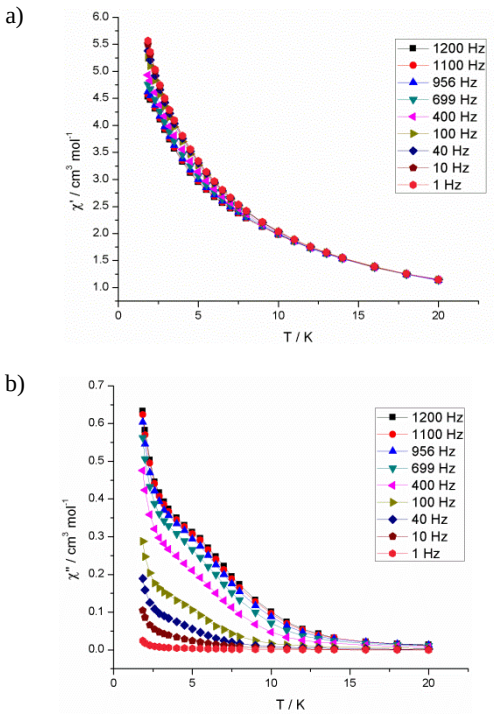

Figure 4. In phase (a) and out of phase (b) magnetic susceptibility vs temperature plots for **1** in zero field

The relaxation process for **1** in the absence of a magnetic field is fast, as evidenced by the absence of a maximum in the out of phase magnetic susceptibility. This is most likely due to quantum tunnelling. This effect can be switched off by the application of an external magnetic field. The in- and out-of-phase susceptibilities of **1** were measured with various applied fields (see Figure S2 in supplementary material) and the optimum field of 7000 Oe was found. AC susceptibility measurements were performed under a 7000 Oe static field (Figure 5) and allowed a maximum to be observed in both the in and out of phase magnetic susceptibility of **1**.

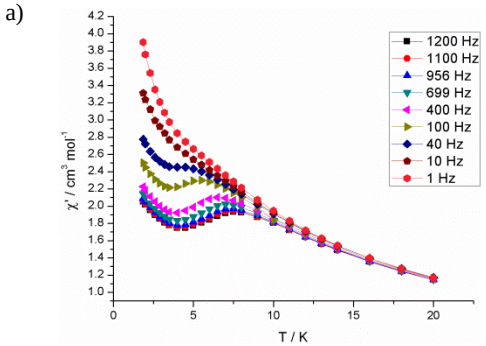

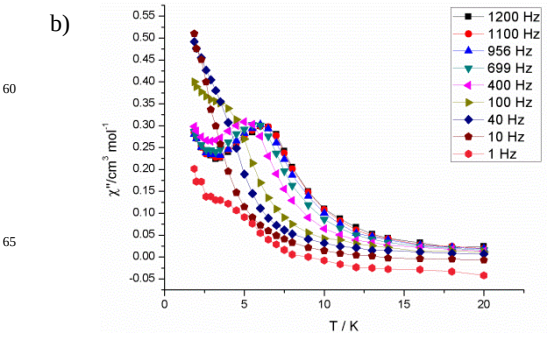

Figure 5. In phase (a) and out of phase (b) magnetic susceptibility vs temperature plots for **2** in a 7000 Oe field

Analysis of the slow dynamics of magnetization via a Cole-Cole diagram (Figure 6) shows that two relaxation processes are present in **1** even under a large applied field of 7000 Oe. The relaxation time and energy barrier of the first process can be estimated using the Arrhenius law as $\tau_0 = 6.5 \times 10^{-7}$ s and U_{eff} = 23.6 cm^{-1} (Figure S3). The presence of two relaxation processes can be attributed to contributions from higher excited states which can be populated due to the large static field applied to the sample**.**

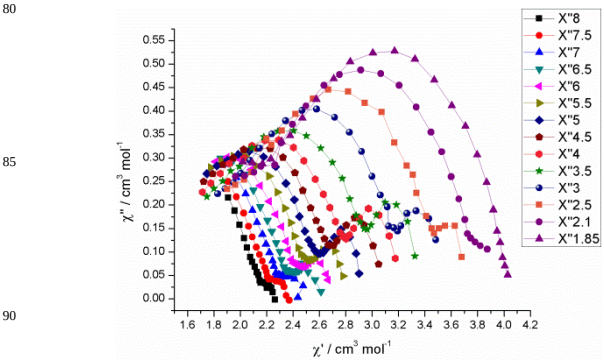

Figure 6. Cole-Cole plot for **2** in a 7000 Oe applied field

Conclusions

The use of solvent cleavage as an *in situ* source of ethoxide ligands has lead to the isolation of two ethoxide bridged dimmers with general formula $[Ln(TMP)_2(\mu\text{-}OEt)]_2$ with the dysprosium analogue showing SMM behavior in a 7000 Oe field at temperatures below 15K. This synthetic route provides an interesting and relatively unexplored strategy to lanthanide SMM formation which could allow tuning of ligand properties by selection of an appropriate solvent.

Experimental

All syntheses were carried out using standard Schlenk techniques using an inert atmosphere of dinitrogen. Et_2O was pre-dried over sodium wire before being dried by refluxing over molten sodium. Toluene was dried using an Innovative Technology Solvent Purification System, and then stored over activated 4 Å molecular sieves. Single crystal data for **1** and **2** were collected on an Oxford XCalibur 2 X-ray diffractometer with a MoKα X-ray source. SQUID data were collected on a Quantum Design MPMS

XL SQUID magnetometer. LiTMP was synthesized by addition of ^{n}BuLi to an hexane solution of 2,2,6,6-tetramethylpipyridine at -78°C. The resulting white powder was collected on a frit, washed with hexane and isolated before use. All other reagents were used as supplied.

Synthesis of 1. $DyCl_3$ (0.269, 1mmol) and LiTMP (0.442g, 3mmol) were solvated in Et_2O (30ml) at room temperature. The resulting pale yellow mixture was left to stir for 18 hours after which the Et_2O was removed *in vaccuo*. Toluene (20ml) was added and the yellow mixture brought to reflux before being filtered. The resulting pale yellow solution was reduced down to ~5ml. After storage of the solution for 3 days at room temperature pale yellow crystals of **1** formed (0.195g, 0.2mmol, 40% (based on dysprosium)). Elemental analysis calculated for $Dy_2O_2N_4C_{40}H_{82}$: C 49.20, H 8.47, N 5.74; found C 49.15, H 8.39, N 5.79.

Synthesis of 2. $YbCl_3$ (0.279g, 1mmol) and LiTMP (0.442g, 3mmol) were solvated in Et_2O (30ml) at room temperature. The resulting pale red mixture was left to stir for 18 hours after which a dark red mixture had formed and the Et_2O was removed *in vaccuo*. Toluene (20ml) was added and the red mixture brought to reflux before being filtered. The resulting red solution was reduced down to ~5ml. After storage of the solution for 3 days at -10°C, dark red crystals of **2** formed (0.224g, 0.23mmol, 45%). Elemental analysis calculated for $Yb_2O_2N_4C_{40}H_{82}$: C 48.16, H 8.29, N 5.62; found C 48.21, H 8.30, N 5.60.

Notes and references

[a] *School of Chemistry, University of Manchester, Oxford Road, Manchester, M13 9PL, UK. Tel:*
[b] *Photon Science Institute, University of Manchester, Oxford Road, Manchester, M13 9PL, UK. Tel:*

† Electronic Supplementary Information (ESI) available: Ac susceptibility plots of **2** and Argand plots of **1** are available in the supplementery material. See DOI: 10.1039/b000000x/

1. a) Z. Hou and Y. Wakatsuki, *Coord. Chem. Rev*., 2002, **231**, 1 b) W. E. Piers and D. J. H. Emslie, *Coord. Chem. Rev*., 2002, **231**, 131
2. P. A. Arnold and S. T. Liddle, *Chem. Commun*.,2006, **42**, 3959
3. J. D. Rinehart, M. Fang, W. J. Evans and J. R. Long, *Nat. Chem.*, 2011, **3**, 538
4. J. D. Rinehart, M. Fang, W. J. Evans and J. R. Long, *J. Am. Chem. Soc*., 2011, **133**, 14236
5. S. A. Sulway,R. A. Layfield, F. Tuna, W. Wernsdorfer and R. E. P. Winpenny, *Chem. Commun.*,2012, **48**, 1508
6. F. Tuna, C. A. Smith, M. Bodensteiner, L. Ungur, L. F. Chibotaru, E. J. L. McInnes, R. E. P. Winpenny, D. Collison, and R. A. Layfield, *Angew. Chem. Int. Ed.*, 2012, **51**, 6976 – 6980
7. D. C. Bradley, J. S. Ghotra and F. A. Hart, *J. Chem. Soc. Dalton Trans.*, 1973, **10**, 1021
8. P. Hitchcock, Q. Huang, M. Lappert and X. Wei, *J. Mater. Chem.*, 2004, **14**, 3266
9. A. Maercker, *Angew. Chem.*, 1987, **99**, 1002
10. M. L. Kahn, R. Ballou, P. Porcher, O. Kahn, and J. P. Sutter, *Chem. Eur. J*., 2002, **8**, 525
11. J. Tang, I. Hewitt, N. T. Madhu, G. Chastanet,W. Wernsdorfer, C. E. Anson, C. Benelli, R. Sessoli and A. K. Powell, *Angew. Chem. Int. Ed.*, 2006, **45**, 1729
12. M. Menelaou, F. Ouharrou, L. Rodreguez, O. Roubeau, S. J. Teat and N. Aliaga-Alcalde, *Chem. Eur. J*., DOI: 10.1002/chem.201200955

Supplementary Information

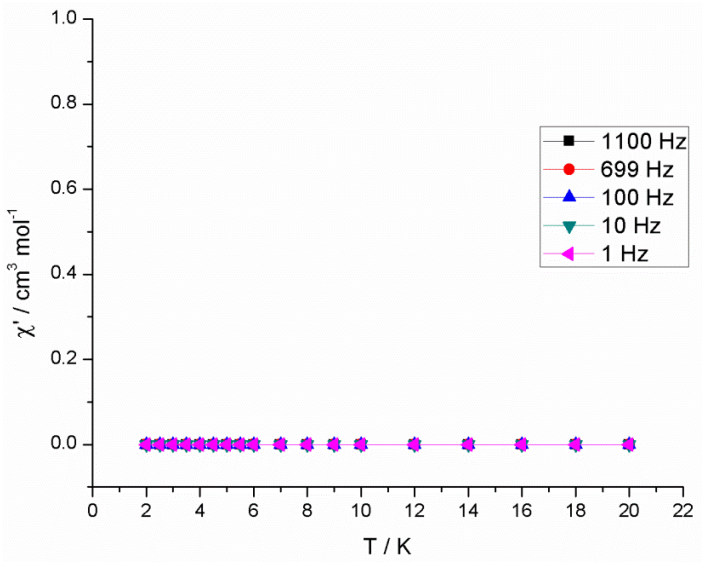

Figure S1a. χ' vs T plot for **2** in 1000 Oe static field

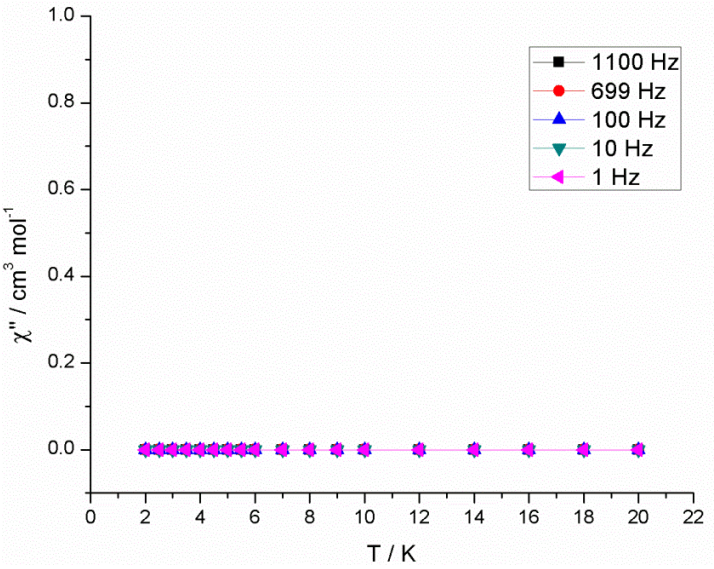

Figure S1b. χ'' vs T plot for **2** in 1000 Oe static field

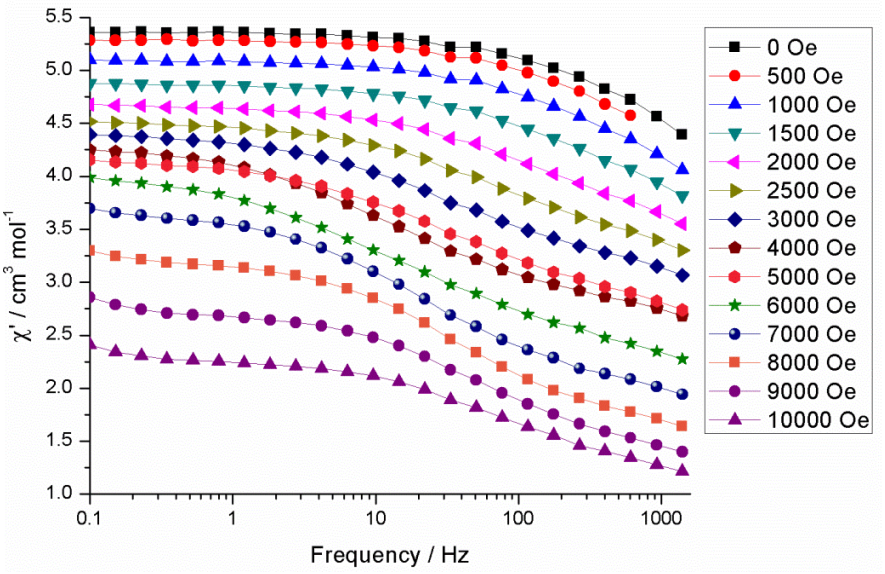

Figure S2a. Plot of χ' vs Frequency for **1** in various applied fields

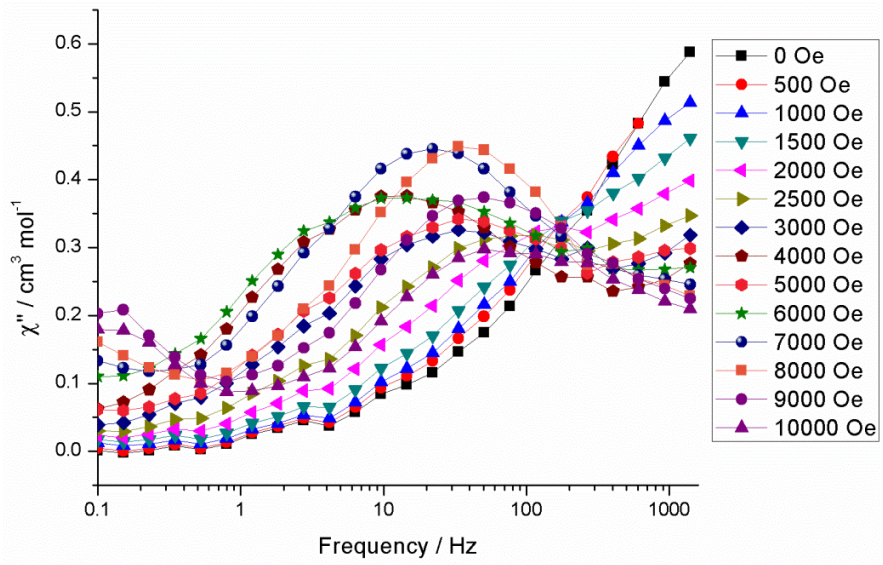

Figure S2b. Plot of χ'' vs Frequency for **1** in various applied fields

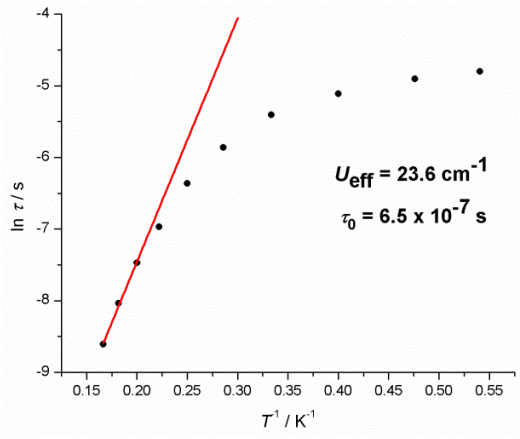

Figure S3. Arrhenius plot of ln (τ) vs T^{-1} for **1**

Chapter 6: Paper 3

"Synthesis, Structure, and Paramagnetism of Manganese(II) Iminophosphate Complexes"

Daniel N. Woodruff, Eric J. L. McInnes, Daniel O. Sells, Richard E. P. Winpenny and Richard A. Layfield, *Inorg. Chem.*, **2012**, *51*, 9104 – 9109

Inorganic Chemistry

Article

pubs.acs.org/IC

Synthesis, Structure, and Paramagnetism of Manganese(II) Iminophosphate Complexes

Daniel N. Woodruff,[†] Eric J. L. McInnes,[†,‡] Daniel O. Sells,[†,‡] Richard E. P. Winpenny,[†,‡] and Richard A. Layfield*[,†]

[†]School of Chemistry, The University of Manchester, Oxford Road, Manchester, M13 9PL, United Kingdom

[‡]EPSRC U.K. National EPR Facility, Photon Science Institute, The University of Manchester, Oxford Road, Manchester, M13 9PL, United Kingdom

Supporting Information

ABSTRACT: The coordination chemistry of the bidentate bis(imino)bis(amino)phosphate ligands $[Me_3SiN{=}P\{NR\}\{N(H)R\}_2]^-$, where R = *n*-propyl is $[L^1H_2]^-$, R = cyclohexyl is $[L^2H_2]^-$, and R = *tert*-butyl is $[L^3H_2]^-$, with manganese(II), is described. The bis(imino)bis(amino)phosphate-manganese(II) complexes $[(\eta^5\text{-Cp})Mn(\mu\text{-}L^1H_2)]_2$ (**1**), $[Mn(L^2H_2)_2]\cdot THF$ (**2**·THF), and $[(\eta^5\text{-Cp})Mn(L^3H_2)]$ (**3**) were synthesized by monodeprotonation of the respective pro-ligands by manganocene, Cp_2Mn. The molecular structures of **1**−**3** reveal that the steric demands of the ligand N-substituents play a dominant role in determining the aggregation state and overall composition of the manganese(II) complexes. The coordination geometries of the Mn(II) centers are six-coordinate pseudotetrahedral in **1**, four-coordinate distorted tetrahedral in **2**, and five-coordinate in **3**, resulting in formal valence electron counts of 17, 13, and 15, respectively. EPR studies of **1**−**3** at Q-band reveal high-spin manganese(II) ($S = {}^5/_2$) in each case. In the EPR spectrum of **1**, no evidence of intramolecular magnetic exchange was found. The relative magnitudes of the axial zero-field splitting parameter, *D*, in **2** and **3** are consistent with the symmetry of the manganese environment, which are D_{2d} in **2** and C_{2v} in **3**.

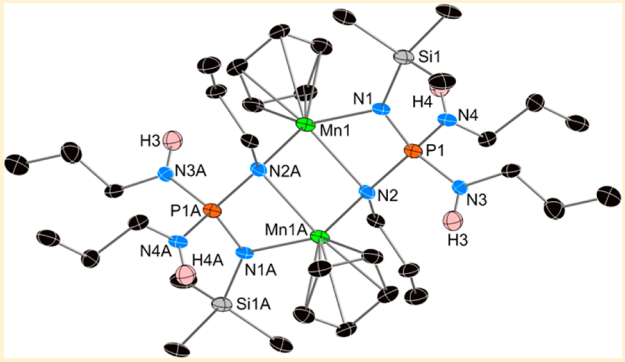

Oxygen-donor ligands centered on phosphorus(V), such as phosphate and phosphonates, display extremely rich coordination chemistry.[1,2] Organophosphonate ligands of the type $[RPO_3]^{2-}$ have been widely applied in transition metal and main group metal chemistry to develop, for example, porous metal−organic frameworks (MOFs).[3] The diverse range of phosphonate coordination modes has also enabled the synthesis of an array of polymetallic phosphonate-bridged cage compounds of 3d transition metals, some of which possess interesting magnetic properties, such as the ability to act as magnetic coolants.[4] Imino analogues of phosphate and phosphonate ligands, in which up to four oxygen atoms are notionally replaced by isoelectronic imino (NR) groups, have also attracted considerable interest owing to the potential changes in chemical and physical properties that these ligands can introduce relative to related compounds with simple phosphonate ligands.[5] The family of phosphorus(V)-imino ligands include tris(imino)phosphates, and their thio and seleno versions, and the tetrakis(imino)phosphates,[6,7] all of which are known in mono-, di-, and trianionic forms represented by $[E{=}P\{N(H)R\}_{3-n}\{NR\}_n]^{n-}$ (n = 1−3; E = $NSiMe_3$, O, S, Se; R = alkyl or aryl).

The development of phosphorus(V)-imino ligands was pioneered by Chivers and co-workers.[5,6] Detailed studies of phosphorus(V)-imino complexes of s-block metals, zinc, and aluminum have established the fundamental properties of these ligands, and revealed that the structures and reactivity of their complexes depend on a range of factors. Notably, the imino N-substituents strongly influence the extent to which the ligand precursor can be deprotonated, and it was also found that the spatial demands of the N-substituents play an important role in determining cage nuclearity in the solid state.[5−7] In contrast to their coordination chemistry with main group metals, transition metal complexes of phosphorus(V)-imino ligands are very rare. Indeed, only one phosphorus(V)-imino ligand has been used in transition metal chemistry, namely, the monoanionic (imino)-thiophosphate $[S{=}P\{N(H)R\}_2\{NR\}]^-$ (**L**), for which complexes of molybdenum(VI), rhodium(I), and nickel(II) are known, although no studies on the paramagnetism of the distorted tetrahedral nickel(II) complex $[Ni(\mathbf{L})_2]$ were reported.[8]

The paucity of transition metal complexes of phosphorus(V)-imino ligands, particularly of paramagnetic ions, has prompted us to develop the coordination chemistry of ligands derived from the tris(amino)phosphoranes $[Me_3SiN{=}P\{N(H)R\}_3]$, where R = *n*-propyl (L^1H_3), cyclohexyl (L^2H_3), or *tert*-butyl (L^3H_3). Our choice of transition metal ion was

Received: June 29, 2012
Published: August 9, 2012

   dx.doi.org/10.1021/ic3014046 | *Inorg. Chem.* 2012, 51, 9104−9109

determined by our previous studies on manganese(II) amido/imido cage compounds, which can be synthesized conveniently by direct deprotonation (manganation) of simple aromatic amines by bis(cyclopentadienyl)manganese(II) (manganocene, Cp_2Mn).[9,10] The primary, secondary, and tertiary alkyl substituents on the amino nitrogens in L^nH_3 were chosen to allow the effects of increasing steric bulk to be investigated. Thus, we now report the synthesis, structures, and EPR spectroscopic properties of the manganese(II) complexes $[(\eta^5\text{-Cp})Mn(\mu\text{-}L^1H_2)]_2$ (**1**), $[Mn(L^2H_2)_2]\cdot THF$ (**2**·THF), and $[(\eta^5\text{-Cp})Mn(L^3H_2)]$ (**3**).

RESULTS AND DISCUSSION

Synthetic and Structural Studies. The syntheses of ligands L^2H_3 and L^3H_3 have been reported previously,[6b] whereas we have developed L^1H_3 for our current study. Complexes **1**−**3** were synthesized by direct manganation of the corresponding pro-ligand L^nH_3 in toluene or THF solvent, according to Scheme 1. Single crystals of **1**−**3** were obtained by

Scheme 1. Synthesis of 1−3

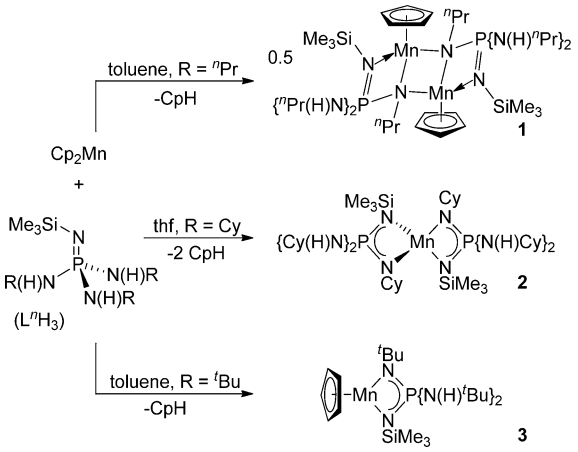

slow cooling of saturated solutions of each compound in its reaction solvent, and their structures were determined by X-ray diffraction. Solutions of **1**−**3** in their respective reaction solvents are stable for the duration of the synthesis, although heating the solutions to reflux even for brief periods results in decomposition to insoluble brown material. Crystalline samples of **1**−**3** are stable at room temperature in a glovebox for two weeks, before gradual decomposition becomes apparent.

The dimer $[(\eta^5\text{-Cp})Mn(\mu\text{-}L^1H_2)]_2$ (**1**) crystallized as extremely air-sensitive green blocks, in an isolated yield of 60%. Molecules of **1** are located about a crystallographic inversion center, which coincides with the midpoint of the Mn(1)···Mn(1A) axis (Figure 1). The molecular structure of the dimer consists of two manganese centers μ-bridged by the amido nitrogen atoms formally deprotonated in the synthesis of **1**, resulting in Mn(1)−N(2) and Mn(1)−N(2A) bond lengths of 2.316(4) and 2.167(4) Å, respectively. The resulting N(2)−Mn(1)−N(2A) and Mn(1)−N(2)−Mn(1A) angles are 94.85(14)° and 85.14(14)°, respectively. The trimethylsilyl-imino nitrogen N(1) bonds in a terminal manner to Mn(1), giving an Mn(1)−N(1) bond length of 2.183(4) Å and N(1)−Mn(1)−N(2) and N(1)−Mn(1)−N(2A) angles of 63.38(14)° and 104.69(15)°, respectively. The P(1)−N(1) distance in **1** is 1.588(4) Å whereas the P(1)−N(2) distance is 1.637(4) Å, indicating that the formal negative charge in the $[L^1H_2]^-$

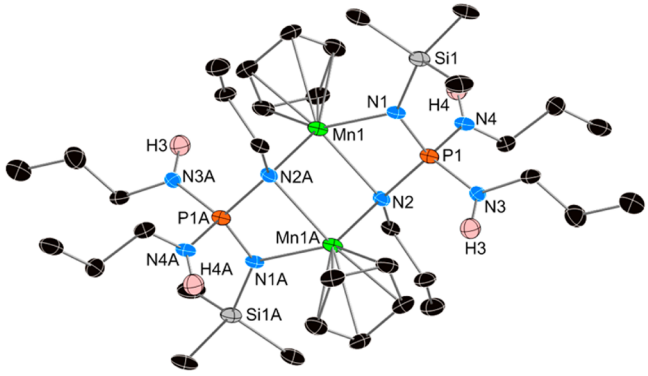

Figure 1. Thermal ellipsoid representation (50% probability) of the molecular structure of $[(\eta^5\text{-Cp})Mn(\mu\text{-}L^1H_2)]_2$ (**1**). Unlabeled atoms are carbon (black). For clarity, hydrogen atoms, except those bonded to nitrogen, are omitted.

ligand is localized on N(2) in order to allow more effective μ-bridging between the manganese centers. The coordination environment of each manganese in **1** is completed by an η^5-cyclopentadienyl ligand, with the Mn−C bond lengths of 2.469(5)−2.600(5) Å implying a high-spin $S = {}^5/_2$ configuration at Mn(II) (see EPR Spectroscopy section, below). The manganese centers in **1** occupy a pseudotetrahedral or "piano-stool" coordination geometry, and they have a formal valence electron count of 17.

The reaction of manganocene and L^2H_3 produced the same outcome irrespective of the relative amounts of Cp_2Mn and pro-ligand in the reaction mixture, producing $[Mn(L^2H_2)_2]\cdot THF$ (**2**·THF) as pale-brown needles. Placing samples of **2**·THF under vacuum for about 30 min removed the THF of crystallization, allowing **2** to be isolated in a yield of 56%. In the crystal structure of **2**·THF, equivalent atoms are related by a crystallographic 2-fold rotation axis that passes through Mn(1) and runs parallel to the *b*-axis. The molecular structure of **2** reveals that the manganese center resides in a very distorted tetrahedral environment, formed by four nitrogen donors from two $[L^2H_2]^-$ ligands (Figure 2), which produces a valence electron count of 13. The $[L^2H_2]^-$ ligands in **2** are κ^2-coordinated to Mn(1) through one nitrogen bearing a cyclohexyl substituent and another bearing a trimethylsilyl

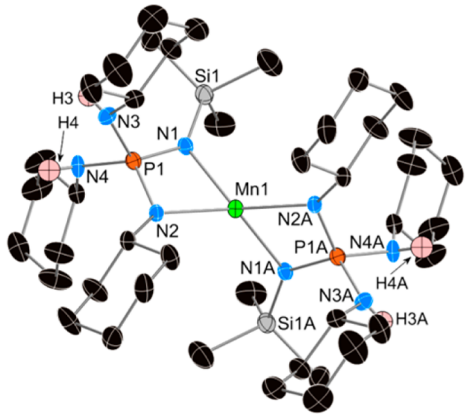

Figure 2. Thermal ellipsoid representation (50% probability) of the molecular structure of $[Mn(L^2H_2)_2]\cdot THF$ (**2**·THF), viewed along the crystallographic *b*-axis. Unlabeled atoms are carbon (black). For clarity, hydrogen atoms, except those bonded to nitrogen, are omitted.

dx.doi.org/10.1021/ic3014046 | Inorg. Chem. 2012, 51, 9104−9109

substituent, which produces Mn(1)−N(1) and Mn(1)−N(2) bond distances of 2.085(3) and 2.149(3) Å, respectively. The distorted nature of the tetrahedral Mn(1) environment is clearly revealed by the N−Mn(1)−N angles, which are in the range 71.2(1)−135.0(2)° (average 116.6°). The dihedral angle between the N(1)−Mn(1)−N(2) and N(1A)−Mn(1)−N(2A) planes in **2** is 87.9(2)°. The P(1)−N(1) and P(1)−N(2) distances of 1.596(8) and 1.601(6) Å are essentially the same (within crystallographic uncertainty), suggesting that the formal negative charge of the ligand is delocalized equally onto both nitrogen donor atoms, and that the different lengths of the Mn−N bonds in **2** are probably due to steric interactions between the substituents.

The 1:1 stoichiometric reaction of Cp_2Mn and L^3H_3 produced $[(\eta^5\text{-Cp})Mn(L^3H_2)]$ (**3**) as amber crystals, in a yield of 35%. In the half-sandwich complex **3** (Figure 3), a pseudo-three-coordinate manganese(II) center is complexed by a κ^2-$[L^3H_2]^-$ ligand and an η^5-Cp ligand, which produces a valence electron count of 15.

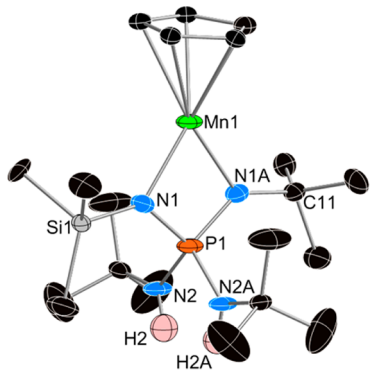

Figure 3. Thermal ellipsoid representation (30% probability) of the molecular structure of $[(\eta^5\text{-Cp})Mn(L^3H_2)]$ (**3**). Unlabeled atoms are carbon (black). For clarity, hydrogen atoms, except those bonded to nitrogen, are omitted.

Compound **3** crystallizes in the space group *Pmmn*. The crystallographic mirror plane running parallel to the *c*-axis, in which Mn(1), N(2), and N(2A) lie, results in the $NSiMe_3$ group and the N^{t}Bu group containing N(1) being disordered over equivalent sites, with equal occupancies, meaning that they cannot be distinguished from each other in the crystal structure. The second mirror plane, parallel to the crystallographic *a*-axis, passes through Mn(1), Si(1), and C(11): the two mirror planes also coincide at the center of the η^5-Cp ligand; hence, each of these carbon atoms is disordered over four sites. The Mn−N(1) distance in **3** is 2.073(5) Å, which as expected is similar to the analogous distances in **2**, but is considerably shorter than the Mn−N distances in **1**. The P(1)−N(2) distance of 1.669(5) Å in **3** is approximately 0.07 Å longer than the P(1)−N(1) distance of 1.601(5) Å, and indicates that the formal negative charge on the $[(L^3H_2)]^-$ ligand is delocalized across an N(1)−P(1)−N(1A) π-system, as observed in **2**. The range of Mn−C distances in **3** is 2.393(17)−2.415(17) Å, suggesting high-spin manganese(II).

Compounds **1**−**3** are the first transition metal complexes of an imino-phosphorane ligand, and they are very rare examples of d-block complexes of imino-analogues of phosphate and organophosphonate ligands. The synthesis of **1**−**3** highlights that manganocene is indeed capable of singly deprotonating the L^nH_3 pro-ligands; however, multiple deprotonations of one pro-ligand by manganocene are apparently not possible under the conditions used. The reasons for the selective monodeprotonations may be due in part to the fact that we have employed aliphatic N-substituents, which would result in the N−H bonds in L^nH_3 having lower thermodynamic acidity relative to analogues of these ligands with aryl substituents. This idea is broadly consistent with a study of the reactions of Cp_2Mn with N-aryl primary amines and with *N*,*N*′-dibenzylethylenediamine, which resulted in deprotonation in the former instance and simple complexation by the diamine in the second instance.[10b]

The most notable contrast in the synthesis and structures of **1**−**3** is that the outcome seemingly depends on the steric demands of the N-alkyl substituent: as the alkyl substituent changes from primary to secondary and then to tertiary in **1**, **2**, and **3**, respectively, the coordination number of manganese changes from six to four to five. In the absence of sterically demanding substituents, mono(cyclopentadienyl)manganese(II) complexes typically adopt pseudotetrahedral, piano-stool geometries, resulting in 17-electron complexes of the type $[(\eta^5\text{-Cp})MnX(L)_2]$ (X = anionic ligand, L = neutral two-electron donor).[9−12] The typical piano-stool geometry is achieved in the dimer **1** via the μ-bridging amido group within the $[L^1H_2]^-$ ligand, which carries sterically nondemanding *n*-propyl substituents. In contrast, the *t*-butyl group in **3** precludes dimerization on steric grounds. Comparing the structures of **1** and **3** with that of **2** must be done cautiously because **2** was synthesized in THF solvent, as opposed to toluene for **1** and **3**. Indeed, the effects of using THF are potentially significant because polar aprotic solvents coordinate to the manganese(II) center in Cp_2Mn and lengthen the Mn−C bonds,[13] which conceivably labilize the Cp ligands toward metalation of N−H acidic substrates. This analysis can explain why both Cp ligands were cleaved in the reaction of Cp_2Mn with L^2H_3, whereas in toluene only one Cp ligand was cleaved in the reactions of Cp_2Mn with L^1H_3 and with L^2H_3.

EPR Spectroscopy. Q-band EPR spectra of polycrystalline samples of **1**−**3** were recorded in order to investigate the electronic structure of the manganese(II) centers. In each case, the spectra at low temperature are rich, and they exhibit extensive fine structure (Figure 4), which can be modeled accurately on the basis of isolated $S = {}^5/_2$ centers, hence confirming the high-spin nature of the Mn(II) ions. This gave the following axial (D) and rhombic (E) zero-field splitting (ZFS) parameters: $D = +0.11$ and $E = 0.005$ cm^{-1} for **1**; $D = -0.12$ and $E = 0.005$ cm^{-1} for **2**; $D = +0.49$ and $E = 0.078$ cm^{-1} for **3**. In each case an isotropic *g*-value of 2.00 was used, and because the relative intensities of the features in EPR spectra are sensitive to the sign of D, the values were determined by comparing simulations with negative and positive D.

Compared to **1** and **2**, there are two notable features in the EPR data for complex **3**: the ZFS (D) of the $S = {}^5/_2$ ion in **3** is much greater, as is the rhombicity parameter $|E/D|$ [which can take values between 0 (axial) and ${}^1/_3$ (the rhombic limit) in the usual definition]. The relative magnitudes of $|D|$ in the monometallic complexes **3** and **2** are consistent with the local coordination geometries, which is distorted tetrahedral (D_{2d}) $\{MnN_4\}$ in **2**, and formally five-coordinate, pseudo-three-coordinate (C_{2v}) $\{CpMnN_2\}$ in **3**. Furthermore, if, as expected, the local ligand field in **3** is dominated by the Mn−Cp(centroid) axis (defining a local *z*-direction), then the two in-plane (x, y) directions (in and perpendicular to the $\{MnN_2\}$ plane) are very different, hence giving a large $|E/D|$. The EPR spectra for dimer **1** are very similar to those of monometallic **2**.

dx.doi.org/10.1021/ic3014046 | *Inorg. Chem.* 2012, 51, 9104−9109

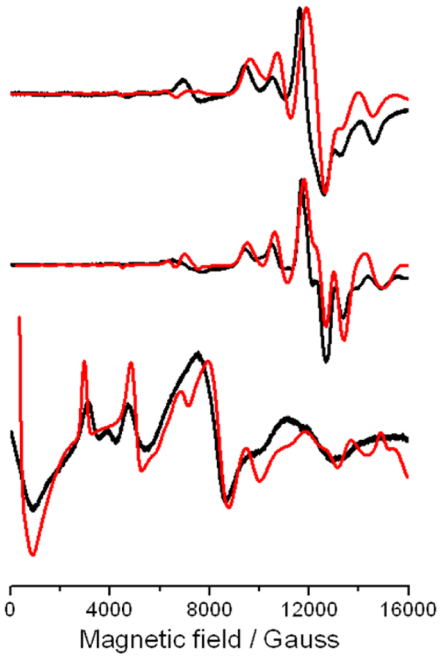

Figure 4. Q-band (ca. 34 GHz) EPR spectra of polycrystalline samples of **1** (top), **2** (middle), and **3** (bottom) at T = 5 K: experimental (black) and calculated (red), with the parameters in the text.

The fact that there is no evidence of a Mn···Mn interaction in the EPR spectrum of **1** means that the exchange coupling must be extremely weak. Several attempts were made to support the conclusion of very weak magnetic exchange in **1** by variable-temperature SQUID magnetometry experiments; however, the extreme air-sensitivity of **1** meant that it was not possible to obtain reliable data. Given that the $\{CpMnN_3\}$ coordination environment in **1** is much more closely related to the $\{CpMnN_2\}$ environment in **3** than to the $\{MnN_4\}$ environment in **2**, the similarity of $|D|$ for **1** and **2** is surprising. The near axiality of **1** is easier to explain: in contrast to the pseudo-C_{2v} $\{CpMnN_2\}$ environment in **3**, the six-coordinate pseudotetrahedral $\{CpMnN_3\}$ environment in **1** makes it nearer to trigonal (although the distortion of the three N-donors from C_{3v} is substantial).

CONCLUSION

The bis(imino)bis(amino)phosphate-manganese(II) complexes $[(\eta^5\text{-Cp})Mn(\mu\text{-}L^1H_2)]_2$ (**1**), $[Mn(L^2H_2)_2]\cdot$THF (**2**·THF), and $[(\eta^5\text{-Cp})Mn(L^3H_2)]$ (**3**) were synthesized by monodeprotonation of (L^nH_3) by manganocene in toluene (**1** and **3**) or THF (**2**). Complexes **1** and **3**, which adopt the general formula $[(\eta^5\text{-Cp})Mn(\mu\text{-}L^nH_2)]_x$, with x = 1 (**1**) or 2 (**3**), reveal that the steric bulk of the N-substituents on the ligands plays an important role in determining aggregation state. The bulky *t*-butyl group in **3** precludes dimerization on steric grounds, whereas the *n*-propyl group in **1** has sufficiently low steric demands that dimerization is possible, which results in a higher valence electron count of 17. The intermediate steric demands of the cyclohexyl groups in **2** enable two of these ligands to coordinate to the same manganese(II) center, although the effects of using THF as the solvent may also influence the outcome of the reaction that results in **2**. The Q-band EPR spectra of **1**−**3** were recorded at 5 K, and were simulated on the basis of isolated high-spin manganese(II) centers ($S = {}^5/_2$) with g = 2.00. The values of the ZFS parameter D are typical of high-spin manganese(II); however, the magnitude of D in **3** was found to be much greater than the D values of **1** and **2**. Although antiferromagnetic exchange in polymetallic manganese(II) amides has been observed previously,[10,11] the EPR spectrum of the dimer **1** did not show any evidence of exchange, which suggests that such interactions must be extremely weak.

With only three examples, the diverse coordination behavior of imino-phosphate ligands toward manganese(II) is apparent. The use of imino analogues of oxygen-containing phosphorus(V) ligands more widely in transition metal chemistry is an underdeveloped area, and our ongoing research will pursue this topic.

EXPERIMENTAL SECTION

All syntheses were carried out using standard Schlenk techniques using an inert atmosphere of dinitrogen. THF was predried over sodium wire before being dried by refluxing over molten potassium. Toluene was dried using an Innovative Technology solvent purification system, and then stored over activated 4 Å molecular sieves. Cp_2Mn,[14] $Me_3SiN{=}PCl_3$,[15] and $Me_3SiN{=}P(NHR)_3$ (R = Cy, ^{t}Bu) were synthesized using literature procedures,[6b] and all other reagents were purchased and used as supplied. NMR spectra were recorded on a Bruker Avance III 400 MHz spectrometer operating at a temperature of 298 K and frequencies of 400.13 (^{1}H), 100.61 (^{13}C), and 161.97 MHz (^{31}P). Q-band EPR spectra were measured on a Bruker EMX spectrometer.

Synthesis of $Me_3SiN{=}P(NH^nPr)_3$ (L^1H_3). The method used to synthesize $Me_3SiN{=}P(NH^nPr)_3$ is essentially identical to that developed by Chivers for the cyclohexyl and *tert*-butyl analogues: $Me_3SiN{=}PCl_3$ (3.93 g, 17.5 mmol) was added dropwise to a stirred suspension of $LiNH^nPr$ (3.90 g, 60.0 mmol) in Et_2O (70 mL) at 0 °C. After 30 min, the reaction mixture was slowly warmed to room temperature and stirred for a further 18 h. A white precipitate formed, which was removed via filtration (Celite, P3), and the solvent was removed from the filtrate *in vacuo* to give a white powder. The white powder was recrystallized from pentane (20 mL), resulting in the formation of $Me_3SiN{=}P(NH^nPr)_3$ as colorless crystals (1.83 g, 6.3 mmol, 36%). ^{1}H NMR ($CDCl_3$, δ/ppm, J/Hz): 2.76, broad triplet, 6H, $CH_2CH_2CH_3$ ^3J = 8.0; 2.01, broad singlet, 3H, NH; 1.44, sextet, 6H, $CH_2CH_2CH_3$ ^3J = 8.0; 0.89, t, 9H $CH_2CH_2CH_3$ ^3J = 8.0; −0.04, s, 9H, $SiMe_3$. ^{13}C NMR ($CDCl_3$, δ/ppm, J/Hz): 43.24, $CH_2CH_2CH_3$; 25.54, $CH_2CH_2CH_3$; 11.55, $CH_2CH_2CH_3$; 3.81, $SiMe_3$. ^{31}P NMR ($CDCl_3$, δ/ppm, J/Hz): 7.78. Anal. Calcd for $C_{12}H_{33}N_4PSi$: C 49.28, H 11.37, N 19.16. Found: C 49.41, H 10.98, N 19.09.

Synthesis of 1. A solution of Cp_2Mn (0.06 g, 0.3 mmol) in toluene (10 mL) was added to a stirred solution of $Me_3SiN{=}P(NH^nPr)_3$ (0.10 g, 0.3 mmol) in toluene (10 mL) at −78 °C. The dark brown solution was stirred for 30 min and then slowly warmed to room temperature, producing a green solution. The reaction was stirred for two hours and filtered (Celite, P3). Storage of the solution for six days at +2 °C produced green crystals of **1** (0.072 g, 60% based on manganese). Anal. Calcd for $C_{34}H_{74}Mn_2N_8P_2Si_2$: C 49.62, H 9.06, N 13.62. Found: C 49.78, H 9.43, N 13.35. ^{1}H NMR (C_6D_6, δ/ppm): very broad resonance extending from approximately +46 to −14 ppm, maximum at 17.1 ppm, overlaps with all other observed resonances, C_5H_5; 14.97, broad singlet, $SiMe_3$; resonances due to *n*-propyl groups observed at 14.29, 10.49, 9.91, 9.13, 8.14; NH protons not observed.

Synthesis of 2. A solution of Cp_2Mn (0.05 g, 0.2 mmol) in THF (10 mL) was added to a stirred solution of $Me_3SiN{=}P(NHCy)_3$ (0.20 g, 0.5 mmol) in THF (10 mL) at −78 °C. The dark brown solution was stirred for 30 min and then slowly warmed to room temperature upon which the solution turned orange-brown in color. The reaction was stirred for a further 18 h and then filtered (Celite, P3). The filtrate was reduced in volume until solid material began to be deposited on the walls of the Schlenk tune, and the solution was then stored at −5 °C. Pale brown crystals of **2** formed after five days (0.12 g, 56%). Anal. Calcd for $C_{42}H_{88}MnN_8P_2Si_2$: C 57.44, H 10.10, N 12.76. Found: C

dx.doi.org/10.1021/ic3014046 | Inorg. Chem. 2012, 51, 9104−9109

Table 1. Crystal Data and Structure Refinement for 1−3

	1	2	3
formula	$C_{34}H_{70}Mn_2N_8P_2Si_2$	$C_{42}H_{88}MnN_8P_2Si_2$	$C_{20}H_{43}MnN_4PSi$
fw	818.98	878.28	453.58
cryst syst	triclinic	monoclinic	orthorhombic
space group	$P\bar{1}$	$C2/c$	$Pmmn$
a/Å	10.4186(12)	24.6619(11)	11.366(2)
b/Å	10.8372(12)	10.9942(4)	11.833(3)
c/Å	10.9199(12)	21.8157(9)	9.4828(13)
α/deg	91.861(9)	90	90
β/deg	98.026(9)	90.494(4)	90
γ/deg	115.271(11)	90	90
V/Å^3	1098.2(2)	5914.8(4)	1275.4(4)
Z	2	1	2
cryst size/mm^3	0.21 × 0.15 × 0.10	0.33 × 0.30 × 0.15	0.30 × 0.20 × 0.20
θ range/deg	2.95−28.51	3.09−27.50	3.29−25.02
reflns collected	4717	6611	2986
indep reflns	2079	4680	1252
R(int)	0.2308	0.0559	0.0585
completeness/%	98.5	97.2	99.7
data/restraints/params	4717/0/223	6611/0/289	1252/184/121
GOF on F^2	0.777	1.033	1.054
final R indices [$I > 2\sigma(I)$]	R1 = 0.0548	R1 = 0.0669	R1 = 0.0640
	wR2 = 0.1099	wR2 = 0.1679	wR2 = 0.1561
R indices (all data)	R1 = 0.1343	R1 = 0.0904	R1 = 0.0928
	wR2 = 0.1365	wR2 = 0.1747	wR2 = 0.1776

57.34, H 9.96, N 12.72. ^{1}H NMR: 31.0, broad shoulder overlapping with adjacent resonances; 19.57, broad, overlapping with adjacent resonances; 14.14, broad, overlapping with adjacent resonances.

Synthesis of 3. A solution of Cp_2Mn (0.06 g, 0.3 mmol) in toluene (10 mL) was added to a stirred solution of $Me_3SiN{=}P(NH^tBu)_3$ (0.10 g, 0.3 mmol) in toluene (10 mL) at −78 °C. After 30 min, the dark brown solution was slowly warmed to room temperature, resulting in an amber solution. The solution was stirred for two hours, gently heated, and filtered while hot (Celite, P3). The resultant solution was reduced in volume and stored at −5 °C for seven days, giving amber crystals of **3** (0.047 g, 35%). Anal. Calcd for $C_{20}H_{43}Mn_1N_4PSi$: C 52.96, H 9.56, N 12.35. Found: C 52.82, H 9.46, N 12.24. ^{1}H NMR (C_6D_6, δ/ppm): 33.78, v broad, C_5H_5; 14.10, ^{t}Bu; 13.36, ^{t}Bu; 8.86 ^{t}Bu; 8.23, $SiMe_3$; NH protons not observed.

X-ray Crystallography. Crystallographic studies were carried out using an Oxford Diffraction XCalibur2 instrument. Data were collected at 100(2) K, and molybdenum radiation (λ = 0.710 73 Å) was used in each case. Full-matrix least-squares on F^2 was used to refine all structures. CCDC deposition numbers 884430−884432.

■ ASSOCIATED CONTENT

Ⓢ Supporting Information

X-ray crystallographic data on **1**−**3** in CIF format. This material is available free of charge via the Internet at http://pubs.acs.org.

■ AUTHOR INFORMATION

Corresponding Author

*E-mail: Richard.Layfield@manchester.ac.uk.

Author Contributions

The manuscript was written through contributions of all authors. All authors have given approval to the final version of the manuscript.

Notes

The authors declare no competing financial interest.

■ ACKNOWLEDGMENTS

R.A.L. thanks the Alexander von Humboldt Foundation for the award of a Fellowship for Experienced Researchers. The authors acknowledge the support of the EPSRC (U.K.). Dr. Madeleine Helliwell is acknowledged for assistance in refining the crystal structure of **3**.

■ REFERENCES

(1) (a) *Metal Phosphonate Chemistry: From Synthesis to Applications*; Clearfield, A., Demadis, K., Eds.; Royal Society of Chemistry Publishing: Cambridge, U.K., 2012. (b) Clearfield, A. *Dalton Trans.* **2008**, 6089.

(2) Chandrasekhar, V.; Senapati, T.; Dey, A.; Hossain, S. *Dalton Trans.* **2011**, *40*, 5394.

(3) (a) Iremonger, S. S.; Liang, J.; Vaidhyanathan, R.; Shimizu, G. K. H. *Chem. Commun.* **2011**, *47*, 4430. (b) Taylor, J. M.; Mah, R. K.; Moudrakovski, I. L.; Ratcliffe, C. I. *J. Am. Chem. Soc.* **2010**, *132*, 14055.

(4) (a) See, for example: Zheng, Y. Z.; Pineda, E. M.; Helliwell, M.; Winpenny, R. E. P. *Chem.—Eur. J.* **2012**, *18*, 4161. (b) Zheng, Y. Z.; Evangelisti, M.; Tuna, F.; Winpenny, R. E. P. *J. Am. Chem. Soc.* **2012**, *134*, 1057. (c) Zheng, Y. Z.; Evangelisti, M.; Winpenny, R. E. P. *Angew. Chem., Int. Ed.* **2011**, *50*, 3692. (d) Khanra, S.; Kloth, M.; Mansaray, H.; Muryn, C. A.; Tuna, F.; Sanudo, E. C.; Helliwell, M.; McInnes, E. J. L.; Winpenny, R. E. P. *Angew. Chem., Int. Ed.* **2007**, *46*, 5568.

(5) (a) Chivers, T.; Brask, J. K. *Angew. Chem., Int. Ed.* **2001**, *40*, 3960. (b) Aspinall, G. M.; Copsey, M. C.; Leddham, A. P.; Russell, C. A. *Coord. Chem. Rev.* **2002**, *227*, 217. (c) Steiner, A.; Zacchini, S.; Richards, P. *Coord. Chem. Rev.* **2002**, *227*, 193.

(6) (a) Chivers, T.; Krahn, M.; Parvez, M.; Schatte, G. *Chem. Commun.* **2001**, 1922. (b) Armstrong, A.; Chivers, T.; Krahn, M.; Parvez, M.; Schatte, G. *Chem. Commun.* **2002**, 2332. (c) Chivers, T.; Krahn, M.; Schatte, G.; Parvez, M. *Inorg. Chem.* **2002**, *42*, 3994. (d) Armstrong, A.; Chivers, T.; Krahn, M.; Parvez, M.; Schatte, G.; Boeré, R. T. *Inorg. Chem.* **2004**, *43*, 3453. (e) Armstrong, A.; Chivers, T.; Parvez, M.; Boeré, R. T. *Angew. Chem., Int. Ed.* **2004**, *43*, 502. (f) Armstrong, A.; Chivers, T.; Krahn, M.; Parvez, M. *Can. J. Chem.* **2005**, *83*, 1768.

(7) (a) Bickley, J. F.; Copsey, M. C.; Jeffrey, J. C.; Leedham, A. P.; Russell, C. A.; Stalke, D.; Steiner, A.; Stey, T.; Zacchini, T. *Dalton Trans.* **2004**, 989. (b) Raithby, P. R.; Russell, C. A.; Steiner, A.; Wright, D. S. *Angew. Chem., Int. Ed.* **1997**, *36*, 649.
(8) (a) Rufanov, K. A.; Ziemer, B.; Meisel, M. *Dalton Trans.* **2004**, 3808. (b) Scherer, O.; Kerth, J.; Sheldrick, W. S. *Angew. Chem., Int. Ed.* **1984**, *23*, 156.
(9) Layfield, R. A. *Chem. Soc. Rev.* **2008**, *37*, 1098.
(10) (a) Alvarez, C. S.; Boss, S. R.; Burley, J. C.; Humphrey, S. M.; Layfield, R. A.; Kowenicki, R. A.; McPartlin, M.; Rawson, J. M.; Wheatley, A. E. H.; Wood, P. T.; Wright, D. S. *Dalton Trans.* **2004**, 3481. (b) Alvarez, C. S.; Bond, A. D.; Harron, E. A.; Layfield, R. A.; Mosquera, M. E. G.; McPartlin, M.; Rawson, J. M.; Wright, D. S. *Dalton Trans.* **2003**, 3002. (c) Alvarez, C. S.; Bond, A. D.; Cave, D.; Mosquera, M. E. G.; Harron, E. A.; Layfield, R. A.; McPartlin, M.; Rawson, J. M.; Wood, P. T.; Wright, D. S. *Chem. Commun.* **2002**, 2980. (d) Alvarez, C. S.; Bond, A. D.; Harron, E. A.; Layfield, R. A.; McAllister, J. A.; Pask, C. M.; Rawson, J. M.; Wright, D. S. *Organometallics* **2001**, *20*, 4135.
(11) (a) Köhler, F. H.; Hebendanz, N.; Müller, G.; Thewalt, U. *Organometallics* **1987**, *6*, 115. (b) Köhler, F. H.; Hebendanz, N.; Thewalt, U.; Kanellakopulos, B.; Klenze, R. *Angew. Chem., Int. Ed.* **1984**, *23*, 721.
(12) (a) Stokes, F. A.; Less, R. J.; Haywood, J.; Melen, R. L.; Thompson, R. I.; Wheatley, A. E. H.; Wright, D. S. *Organometallics* **2012**, *31*, 23. (b) Krinsky, J. L.; Stavis, M. N.; Walter, M. D. *Acta Crystallogr.* **2003**, *E59*, m497. (c) Bashall, A.; Beswick, M. A.; Ehlenberg, H.; Kidd, S. J.; McPartlin, M.; Palmer, J.; Raithby, P. R.; Rawson, J. M.; Wright, D. S. *Chem. Commun.* **2000**, 749. (d) Heck, J.; Massa, W.; Weinig, P. *Angew. Chem., Int. Ed.* **1984**, *23*, 722. (e) Scheuermayer, S.; Tuna, F.; Bodensteiner, M.; Scheer, M.; Layfield, R. A. *Chem. Commun.* **2012**, *48*, 8087.
(13) Howard, C. G.; Girolami, G. S.; Wilkinson, G.; Thornton-Pett, M.; Hursthouse, M. B. *J. Am. Chem. Soc.* **1984**, *106*, 2033.
(14) Wilkinson, G.; Cotton, F. A.; Birmingham, J. M. *J. Inorg. Nucl. Chem.* **1956**, *2*, 95.
(15) Wang, B.; Rivard, E.; Manners, I. *Inorg. Chem.* **2002**, *41*, 1690.

dx.doi.org/10.1021/ic3014046 | *Inorg. Chem.* 2012, 51, 9104−9109

Chapter 7: Paper 4

"Synthesis and structure of cationic guanidinate-bridged bimetallic {Li_7M} cubes (M = Mn, Co, Zn) with inverse crown counter anions"

Daniel Woodruff, Michael Bodensteiner, Daniel O. Sells, Richard. E. P. Winpenny and Richard A. Layfield, *Dalton Trans.*, **2011**, *40*, 10918 – 10923

Dalton Transactions

Cite this: *Dalton Trans.*, 2011, **40**, 10918

www.rsc.org/dalton

PAPER

Synthesis and structure of cationic guanidinate-bridged bimetallic $\{Li_7M\}$ cubes (M = Mn, Co, Zn) with inverse crown counter anions†

Daniel Woodruff,[a] Michael Bodensteiner,[b] Daniel O. Sells,[a] Richard. E. P. Winpenny[a,c] and Richard A. Layfield*[a,b]

Received 27th May 2011, Accepted 27th July 2011
DOI: 10.1039/c1dt10999e

The reactions of the heteroleptic lithium amide $[Li_3(\mu\text{-hmds})_2(\mu,\mu\text{-hpp})]$ (**1**), where $[hmds]^-$ = hexamethyldisilazide and $[hpp]^-$ = hexahydropyrimidopyrimidide, with $MnCl_2$, $CoCl_2$ or $ZnBr_2$ result in the formation of the separated ion-pairs $[MLi_7(\mu_8\text{-O})(\mu,\mu\text{-hpp})_6]^+[A]^-$, which each consist of a $\{MLi_7\}$ oxo-centred cube structural motif (M = Mn **2**, Co **4**, Zn **5**), with each face of the cube being bridged by an $[hpp]^-$ ligand. In the case of M = Mn and Co, the counter ion, $[A]^-$, is the pentagonal anionic inverse crown $[\{Li(\mu\text{-hmds})\}_5(\mu_5\text{-Cl})]^-$ (**3**), whereas the reaction with M = Zn produces the known tris-amido zincate $[Zn(hmds)_3]^-$ counter anion.

Introduction

Serendipitous assembly is a successful method for the synthesis of polymetallic cage compounds.[1] With this method, a pro-ligand with molecular symmetry and structure likely to encourage cage formation is combined with a simple metal-containing precursor, such as a metal halide, in an appropriate solvent. The reaction between the various components then proceeds such that specific outcomes are not targeted. Rather, the chemical and physical conditions of the reaction result in the product self assembling to give a stable arrangement of ligands and metal atoms. The strategy has been put to particularly effective use in the synthesis of transition metal cages, based predominantly on μ-(*O*-donor) ligands.[2] Not only are the structures of the self-assembled compounds intrinsically interesting, the reliability and scope of the synthetic method, most notably in the case of transition metals, has allowed such cage compounds to be developed as single molecule magnets and as magnetic refridgerants.[3,4]

The importance of the serendipitous assembly method for the synthesis of oxygen-bridged transition metal cages has prompted us to combine our interests in this area with our interests in the structures of alkali metal complexes of functionalized amido ligands.[5] Here, our aim is to select N–H acidic nitrogen-containing heterocyclic ligands whose structures should encourage metal cage formation, and then to metallate these heterocycles with alkali metals. Subsequently, the alkali-metallated heterocycles can be used as ligand sources in salt metathesis reactions with transition metal halides, allowing access to nitrogen-bridged polymetallic transition metal cages. In addition to the new structural chemistry of transition metal amides that could be developed, this method also potentially allows access to a range of cage compounds with magnetic properties that are influenced by μ-amido ligands rather than by μ-(*O*-donor) ligands.

Results and discussion

We now report the synthesis and structure of the heteroleptic trilithium complex $[Li_3(\mu\text{-hmds})_2(\mu_4\text{-hpp})]$ (**1**) ($[hmds]^-$ = hexamethyldisilazide, $[hpp]^-$ = hexahydropyrimidopyrimidide), and its reaction with d-block metal(II) halides, namely manganese(II) chloride, cobalt(II) chloride and zinc bromide. The reactions of **1** with $MnCl_2$ or with $CoCl_2$ result in the formation of separated ion-pairs consisting of the guanidinate-bridged, oxo-centred cationic metal cubes $[MLi_7(\mu_8\text{-O})(\mu,\mu'\text{-hpp})_6]^+$ (M = Mn **2**, M = Co **4**), which in the case of each transition metal is accompanied by formation of the new anionic inverse crown $[\{Li(\mu\text{-hmds})\}_5(\mu_5\text{-Cl})]^-$ (**3**). The reaction of **1** with $ZnBr_2$ produces a separated ion pair consisting of the cage complex $[ZnLi_7(\mu_8\text{-O})(\mu\text{-hpp})_6]^+$ (**5**), which is isostructural to **2** and **4**, and the known tris(amido) zincate counter anion $[Zn(hmds)_3]^-$.

Compound **1** was synthesized by adding three equivalents of [Li(hmds)] to one of hppH in toluene. A standard work-up of the reaction followed by storage of a concentrated toluene solution at −4°C produced pale yellow crystals of **1** (Scheme 1). X-ray diffraction revealed that two independent molecules of **1**, **1a** and **1b**, are found in the unit cell. The structures of **1a** (Fig. 1) and **1b** are essentially identical, and that of **1b** is shown in Fig. S1.† The pyramidal coordination environments of Li(1/1A) in **1a** consist of one $[hmds]^-$ nitrogen and both nitrogens of the $[hpp]^-$ ligand,

[a]*School of Chemistry, The University of Manchester, Oxford Road, Manchester, U.K., M13 9PL. E-mail: Richard.Layfield@manchester.ac.uk*
[b]*Universität Regensburg, Institut für Anorganische Chemie, 93040 Regensburg, Germany*
[c]*The Photon Science Institute, The University of Manchester, Alan Turing Building, Oxford Road, Manchester, U.K., M13 9PL*

† Electronic supplementary information (ESI) available: NMR and EPR spectroscopy data, structure of **1b**. CCDC reference numbers 815987, 827193, 815986 and 827194. For ESI and crystallographic data in CIF or other electronic format see DOI: 10.1039/c1dt10999e

Table 1 Metal–ligand bond distances [Å] for **1a** and for the cations **2**, **4**, and **5**

	1a	2	4	5
Li/M–O	—	2.072(10)–2.192(7)	2.0371(14), 2.0298(15)	1.983(5)—2.072(7)
Li/M–N	—	1.999(8)–2.192(7)	1.990(3)–2.092(3)	1.970(7)–2.169(7)
Li–O	—	—	2.001(3), 2.065(3)	—
Li–N	1.959(17)–2.091(13)	—	2.054(4)–2.082(2)	—

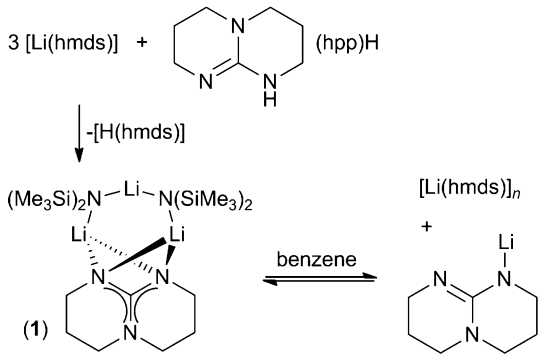

Scheme 1

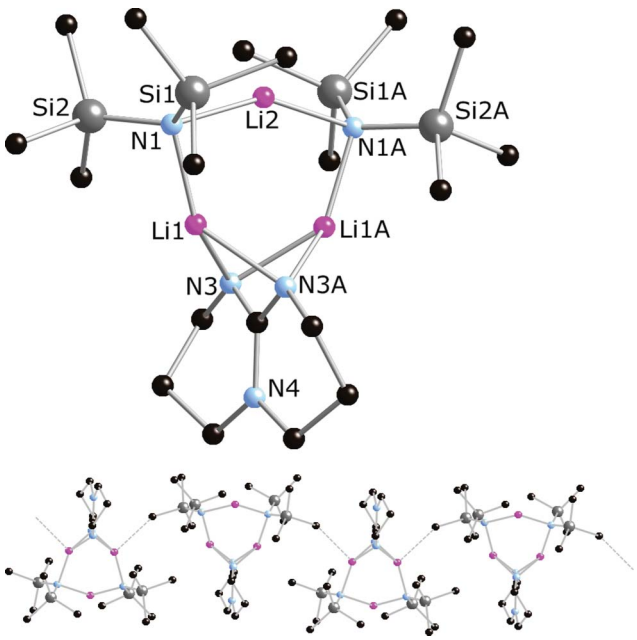

Fig. 1 Molecular structure of **1a** (upper), and the interactions between **1a** and **1b** (lower). Li = pink, N = blue, Si = grey.

resulting in Li(1)–N(1) and Li(1)–N(3) bond distances of 1.959(17) and 2.091(13) Å, respectively (Table 1). The bent, two-coordinate environment of Li(2) consists of two $[hmds]^-$ ligands, with the Li(2)–N(1) distance being 1.998(8) Å, and the N(1)-Li(2)-N(1A) angle 148.9(12)°. The molecular structure of **1a** (and of **1b**) can be regarded as being formed by substitution of an $[hmds]^-$ ligand in the unsolvated cyclic trimeric rings of $[Li(hmds)]_3$[6] with an $[hpp]^-$ ligand from the guanidine-solvated dimer $[Li(hpp)\{hpp(H)\}]_2$.[7] In the extended structure of **1** (Fig. 1), molecules of **1a** and **1b** interact *via* CH···Li pseudo-agostic interactions involving the $SiMe_3$ substituents. This type of interaction has precedent in the structure of methyllithium itself[13] and in the structures of trimethylsilyl-containing organolithiums.[9]

The room-temperature ^{1}H NMR spectrum of **1** in benzene-d_6 consists of broad, overlapping resonances in the range $\delta(^1H)$ = 1.38–3.35 ppm, and a broad singlet at 0.22 ppm (Fig. S2–S4†). Although these resonances can be assigned to the ^{1}H environments in **1**, it is clear that a dynamic process is occurring. A variable-temperature ^{1}H NMR spectroscopic study revealed that the dynamic process can be suppressed on cooling toluene solutions to −40 °C, such that the solid-state molecular structure of **1** is observed intact. On warming to +70 °C, the resonances coalesce and sharpen, implying a dynamic equilibrium, probably involving dissociation of **1** into [Li(hpp)] and [Li(hmds)] (Scheme 1, Fig. S5†).

The ease with which **1** can be synthesized, combined with the known ability of the $[hpp]^-$ ligand to encourage cage formation,[10,11] make this ligand a promising candidate for use in the synthesis of transition metal cages. To test this hypothesis, the reactions of **1** with anhydrous manganese(II) chloride, cobalt(II) chloride and zinc bromide were carried out. Addition of **1** to $MnCl_2$ produced an amber-coloured solution after stirring, and following hot filtration of the reaction mixture and then storage of the solution, amber crystals of $[MnLi_7(\mu_8\text{-}O)(\mu,\mu'\text{-}hpp)_6][\{Li(\mu\text{-}hmds)\}_5(\mu_5\text{-}Cl)]\cdot$(2 toluene), **[2][3]**·(2 toluene), formed. The same method using either $CoCl_2$ or $ZnBr_2$ produced large blue crystals of $[CoLi_7(\mu_8\text{-}O)(\mu,\mu'\text{-}hpp)_6][\{Li(\mu\text{-}hmds)\}_5(\mu_5\text{-}Cl)]\cdot$(2 toluene), **[4][3]**·(2 toluene), or yellow crystals of $[ZnLi_7(\mu_8\text{-}O)(\mu,\mu'\text{-}hpp)_6][Zn(hmds)_3]$, **[5]**$[Zn\{N(SiMe_3)_2\}_3]$, respectively (Scheme 2).

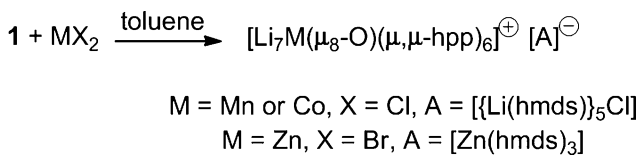

Scheme 2

The structures of the $[MLi_7(\mu_8\text{-}O)(\mu,\mu'\text{-}hpp)_6]^+$ cations (M = Mn, Co, Zn) are essentially identical, hence only **4** will be discussed in detail. Key bond lengths for **2**, **4** and **5** are shown for comparison in Table 1, and the structures of **2** and **5** are shown in Fig. S6 and S7.† The structure of **4** (Fig. 2) consists of a μ_8-oxo-centred $\{CoLi_7\}$ cube, and each face of the cube is bridged by two nitrogens of an $[hpp]^-$ ligand. Four of the eight metal positions in **4** are mixed positions of cobalt and lithium, *i.e.* Co(1)/Li(1) and Co(2)/Li(2), both in a ratio of one quarter to three quarters. Each metal atom in **4** resides in a distorted tetrahedral environment that consists of the oxo ligand and three $[hpp]^-$ nitrogens. The mixed position Li(1)/Co(1)–O(1) bond lengths are 2.0371(14) and 2.0298(15) Å, and the Co/Li–N bond lengths are in the range 1.990(3)–2.092(3) Å (average 2.042 Å).

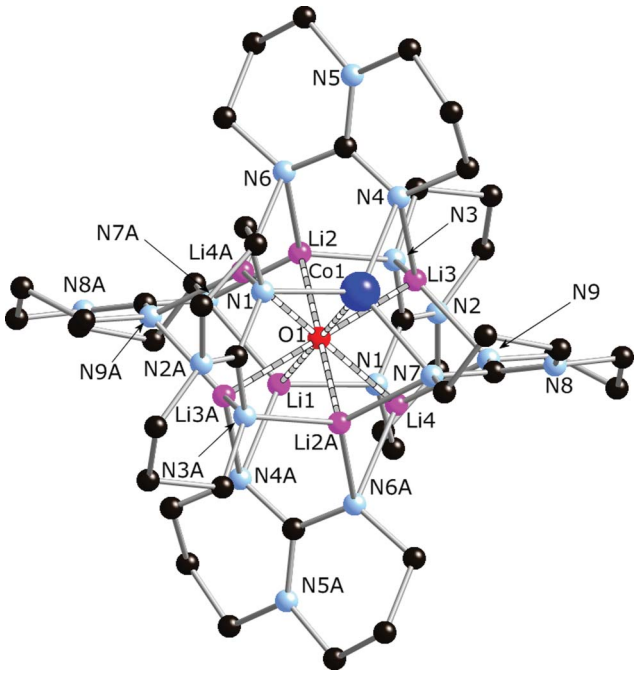

Fig. 2 Molecular structure of the cation **4**. Co = dark blue.

For the fully occupied lithium positions, the Li–O bond lengths are 2.001(3) and 2.065(3) Å, and the range of Li–N bond lengths is 2.054(4)–2.082(4) Å (average 2.065 Å). A thermal ellipsoid plot of **4** is shown in Fig. S11.†

The manganese atom in the cation **2** is disordered over the four sites of the asymmetric unit, i.e all eight metal positions of the $\{MnLi_7\}$ cube, with occupancies of 22, 16, 9 and 3 per cent. The zinc atom in **5** is disordered over all eight of the metal positions in the $\{ZnLi_7\}$ cube, with occupancies of 31, 5, 25, 11, 14, 7, 1 and 6 per cent.

The anion **3** in [**4**][**3**] (Fig. 3) consists of a pentagonal arrangement of lithium cations bridged by a μ_5-chloro ligand, with each pair of adjacent lithiums being bridged by a μ-[hmds]$^-$ ligand. The Li(5)–Cl(1) bond coincides with a mirror plane. The range of Li–Cl distances in **3** is 2.445(4)–2.458(7) (average 2.449 Å), and the Li–N

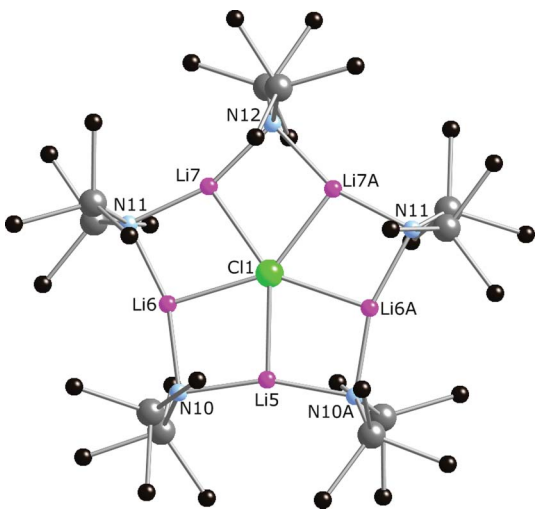

Fig. 3 Structure of the anion **3**. Chloride = green.

distances are in the range 2.050(5)–2.064(5) Å (average 2.058 Å). The chloride ion in **3** is co-planar with the lithium cations. The anion **3** in [**2**][**3**] is essentially isostructural with that in [**4**][**3**] (Fig. S7†).

In contrast to the reactions of **1** with $MnCl_2$ and $CoCl_2$, the reactions of **1** with $ZnBr_2$ produce a cation-anion pair in which the anion is the trigonal planar tris(amido) zincate $[Zn(hmds)_3]^-$ (Fig. S18†), the structure of which has been reported previously by others.[12] In terms of the counter anion, we attribute the different outcome in the case of [**5**][$Zn(hmds)_3$] to the greater radius of the bromide anion, which presumably is too great to enable it to act as a template in the formation of a crown based on [Li(hmds)] units.

Analytically pure samples of [**2**][**3**], [**4**][**3**] and [**5**][$Zn(hmds)_3$] were obtained by placing the crystalline materials under vacuum. In the case of [**2**][**3**] and [**4**][**3**] the lattice toluene was evaporated. The Q-band EPR spectrum of [**2**][**3**] (Fig. S10†) recorded at 5 K features a broad resonance centred on 11963 G (g = 2.001). The resonance is a six-line multiplet with a separation of 80 G between the components of the multiplet. The EPR spectrum is consistent with high-spin manganese(II). The X- and Q-band EPR spectra of [**4**][**3**] at 5 K show resonances at 1062 G (full width at half-maximum = 89 ± 1.5 G) and 3650 G (full width at half-maximum = 228 ± 4 G), respectively, consistent with g' = 6.518 ± 0.058, and there is an inflection in the X-band spectrum at 12040 G (g' = 0.588) (Fig. S15 and S16). These g-values fall within a typical range for low-symmetry Co(II) coordination environments.[13]

The paramagnetism of [**2**][**3**] resulted in the ^{1}H NMR spectrum of this compound consisting of a series of broad, overlapping resonances approximately in the region $\delta(^1H)$ = 0.9–3.6 ppm (Fig. S8†). These resonances are likely due to be due to the [hpp]$^-$ protons, and the two sharp singlets at $\delta(^1H)$ = 0.29 and 0.10 ppm can be assigned to the $SiMe_3$ substituents (Fig. S9†). The ^{7}Li NMR spectrum of [**2**][**3**] consists of three sharp resonances at $\delta(^7Li)$ = 1.52, 1.92 and 2.39 ppm, and a broad resonance approximately in the range $\delta(^7Li)$ = –0.5–3.5 ppm, centred on 1.71 ppm (Fig. S9†). Structural assignments based on the paramagnetic NMR spectra of [**2**][**3**] cannot be completely free from ambiguity, however the ^{7}Li NMR spectrum may indicate that the compound exists as two components in benzene: one type that contains manganese(II) and one that does not, although there is no evidence to suggest that the solid-state structure of [**2**][**3**] is preserved in solution. Similarly, the paramagnetism of [**4**][**3**] resulted in the ^{1}H NMR spectrum of this compound consisting of a series of broad, low-intensity resonances in the region $\delta(^1H)$ = 0.79–4.45 ppm assignable to the hpp protons, two sharp singlets at $\delta(^1H)$ = 0.62 and 0.01 ppm assignable to the $SiMe_3$ substituents, and seven resonances at lower field with $\delta(^1H)$ = 15.14–44.72 ppm (Fig. S13†). The ^{7}Li NMR spectrum of [**4**][**3**] consists of four sharp resonances in the region $\delta(^7Li)$ = 2.33–2.86 ppm, and six broad, overlapping resonances in the region $\delta(^7Li)$ = –0.06–2.17 ppm (Fig. S14†). As with [**2**][**3**], the NMR spectroscopic data may again indicate that [**4**][**3**] exists as a cobalt(II)-containing component and a lithium-only component.

The ^{1}H and ^{13}C NMR spectra of [**5**][$Zn(hmds)_3$] in benzene show environments characteristic of the [hpp]$^-$ and [hmds]$^-$ ligands (Fig. S19 and S20†). Thus the ^{1}H NMR spectrum consists of group of mutually coupled resonances in the region $\delta(^1H)$ = 3.43–1.54 ppm corresponding to the [hpp]$^-$ environments and sharp singlets at 0.81 and 0.10 ppm corresponding to the $SiMe_3$ substituents. The ^{13}C NMR spectrum has the [hpp]$^-$ environments at $\delta(^{13}C)$ = 25.42,

45.46, 49.66 and 162.11 ppm and a trimethylsilyl resonance at $\delta(^{13}C) = 2.62$ ppm.

The structures of the cationic cubes **2**, **4** and **5** are similar to that of μ_8-hydride-containing cation $[Li_8(\mu_8\text{-}H)(hpp)_6]^+$, which has been reported with several different counter anions, including $[Zn^tBu_3]^-$.[14] The observation of μ_8-oxo ligands in molecular compounds is rare. A search of the Cambridge Structural Database reveals that the few previously reported μ_8-oxo compounds are based entirely on alkali metals,[11] meaning that the cations **2**, **4** and **5** are the first d-block metal complexes of μ_8-oxo ligands. The oxygen-scavenging ability of alkali metal oragnometallics is well known.[15] Indeed, several examples of oxo-containing lithium organozincates are known in which μ_n-oxo ligands ($n = 3$–6) derive either from molecular oxygen or from adventitious water from the reaction solvent.[16] A lithium-manganese(II) amido inverse crown ether has also been shown to be able to accommodate a μ_4-oxo ligand.[17] The oxygen scavenging ability of bimetallic alkali metal organometallics is seen consistently with the synthesis of [**2**][**3**], [**4**][**3**] and [**5**][Zn(hmds)$_3$]. Molecular oxygen is unlikely to be the source of the oxo ligands in the three $\{MLi_7\}$ cubes because performing the syntheses using rigorous anaerobic conditions either with a Schlenk line or in an efficient glove box (dioxygen levels less than 0.5 ppm) does not affect the outcome. The μ_8-oxo ligand in the structure of the cation **2** therefore most likely derives from the presence of adventitious water in the toluene solvent. To test this hypothesis, a small amount of degassed water was added to rigorously dried toluene (approximately 50 μL in 15 mL) and stirred vigorously for 30 min, and the mixture then subsequently added to MX_2. A dry toluene solution of **1** was then added to the suspension of MX_2, and following the same reaction time and workup conditions as in the case of the serendipitous formation of the oxo-centred cubes, formation of crystalline [**2**][**3**], [**4**][**3**] and [**5**][Zn(hmds)$_3$] was again observed, but in slightly higher yields.

The structural chemistry of lithium amido zincates[16,18,19] and, to a lesser extent, lithium amido manganates[9,17,20,21] has been investigated in some detail. In recent years, interest in both types of amido metallate has increased substantially owing to their applications as superbasic metallating reagents.[19,21,22] Somewhat surprisingly, the cation **4** in [**4**][**3**] provides the first crystallographically characterized example of a lithium amido cobaltate.

Lithium amide/halide co-complexes are widely used to enhance the efficiency of key organic syntheses, such as the aldol reaction,[23] however crystallographically characterized examples such as **3** are rare. The anion **3** is also a new member of the s-block metal inverse crown family, a term describing complexes consisting of a macrocyclic arrangement of metal amide units that host an anionic guest within the crown.[24] The majority of inverse crowns are heterobimetallic combinations of an alkali metal with a less polar divalent metal, so it is notable that the inverse crown in **3** is a cyclic pentamer of [Li(hmds)].[25] The solid-state structure of lithium hexamethyldisilazide is the cyclic trimer [Li(hmds)]$_3$, however in hydrocarbon solution a tetramer-dimer equilibrium has been observed.[26] To account for the formation of **3**, an aggregation process involving [Li(hmds)]$_n$ units with n = 1, 2, 3 or 4 templating around the nascent chloride ion can be envisaged, although proof for this cannot be obtained by NMR spectroscopy owing to the paramagnetism of [**2**][**3**] and [**4**][**3**]. A mechanism qualitatively similar to that which we propose for **3** is thought to account for the formation of the anionic phospha(V)zane cyclic pentamer $[\{P(\mu\text{-}N^tBu)_2(\mu\text{-}NH)\}_5(HCl)]$, in which the chloride ion templates the formation of the macrocycle *via* a series of hydrogen bonds.[27] A pentameric structural motif related to **3** was also observed in the mercury-based inverse crown $[\{(F_3C)_2CHg\}_5(\mu_5\text{-}Cl)_2]$, although in this instance the macrocycle was pre-synthesized and the chloride guest added subsequently.[28]

Conclusions

In summary, the heteroleptic lithium amide **1** has been used as a precursor for the synthesis of the ion-separated compounds [**2**][**3**], [**4**][**3**] and [**5**][Zn(hmds)$_3$]. The heterobimetallic cations **2**, **4** and **5** contain (μ_8-oxo)-centred $\{MLi_7\}$ cubes (M = Mn, Co, Zn), with each face of the cube capped by a μ,μ′-[hpp]$^-$ ligand. An additional serendipitous outcome was the formation of the anionic inverse crown **3**. The apparent ability of d-block metals to replace lithium in a structural type more commonly found in s-block chemistry may enable more extensive investigations of the less common coordination environment for the transition metals, such as tetrahedral cobalt(II), which would add to the considerable current interest in cage compounds of octahedral cobalt(II).[29] Our ongoing research in this area will also extend the synthetic method described for [**2**][**3**], [**2**][**3**] and [**5**][Zn(hmds)$_3$] to other N–H acidic organic heterocycles.

Experimental

Synthesis of 1

A solution of $LiN(SiMe_3)_2$ (0.50 g, 3.0 mmol) in toluene (15 mL) was added to hppH (0.14 g, 1.0 mmol) at −78 °C and stirred for 30 min. The reaction was warmed to room temperature and stirred for 1 h, producing a colourless precipitate. Gentle heating of the reaction mixture produced a pale yellow solution, which was filtered and stored overnight at −4 °C, resulting in the formation of **1** as pale yellow crystals (0.32 g, 66%). Elemental analysis calculated for $C_{19}H_{48}N_5Si_4Li_3$: C 47.56, H 10.08, N 14.60; found: C 47.42, H 9.93, N 14.51. Crystal data for **1**: $C_{19}H_{48}N_5Si_4Li_3$, M = 479.80, tetragonal, $P4_2bc$, a = 16.4053(3), c = 21.4837(10) Å, V = 5781.99(31) Å^3, T = 100(2) K, Z = 8, 12200 reflections collected, 4177 independent reflections (R_{int} = 0.0397), 89.6% completeness to θ = 28.66° (λ = 0.71073 Å), final R indices [$I > 2\sigma(I)$] R_1 = 0.0393 and wR_2 = 0.0989, R indices (all data) R_1 = 0.0551, wR_2 = 0.1060.

Synthesis of [2][3]

A solution of **1** (0.48 g, 1.0 mmol) in toluene (10 mL) was added to a stirred suspension of $MnCl_2$ (0.06 g, 0.5 mmol) in toluene (15 mL) at room temperature. The pale pink reaction mixture was stirred overnight, resulting in a pale amber solution and a precipitate. Filtration of the hot reaction mixture (Celite, porosity 3) produced an amber solution, which was reduced in volume to approximately 5 mL and stored at −4 °C. After two days, amber crystals of [**2**][**3**] formed. For spectroscopic and analytical studies, the nascent solvent was removed by syringe and the crystalline material then washed with hexane (2 × 5 mL), before being dried in vacuo, which resulted in evaporation of the lattice toluene to give [**2**][**3**] (0.05 g, 30% isolated yield). An alternative synthesis of [**2**][**3**], using the same amounts of each reagent but with the suspension of $MnCl_2$ in toluene containing 50 μL of

degassed water, was also accomplished (0.06 g, 36% isolated yield). Elemental analysis for $C_{72}H_{162}N_{23}OSi_{10}ClLi_7Mn$: calculated C 48.42; H 9.14, N 18.04; found C 48.11, H 8.99, N 17.67. Crystal data for **1**: $C_{86}H_{178}N_{23}OSi_{10}ClLi_7Mn$, M = 1988.96, monoclinic, $C2/c$, a = 20.1096(12), b = 24.4769(15), c = 24.9736(17) Å, β = 105.769(6)°, V = 11829.9(13) Å^3, T = 100(1) K, Z = 4, 21119 reflections collected, 7584 independent reflections (R_{int} = 0.0906), 99.7% completeness to θ = 21.00° (λ = 0.71073 Å), final R indices [$I > 2\sigma(I)$] R_1 = 0.0857 and wR_2 = 0.1979, R indices (all data) R_1 = 0.1783, wR_2 = 0.2215.

Synthesis of [4][3]

This compound was synthesized in an identical manner to **[2][3]** using a suspension of anhydrous $CoCl_2$ (0.11 g, 0.5 mmol) in toluene (10 mL) and a solution of **1** (0.24 g, 0.5 mmol) in toluene (10 mL). The resulting blue solution was stored overnight at room-temperature to result in blue crystals of **[4][3]**·(2 toluene). Drying the crystals *in vacuo* resulted in evaporation of the lattice toluene to give **[2][3]** (0.42 g, 24% isolated yield; with water 0.49 g, 28%). Elemental analysis calculated for $C_{72}H_{162}N_{23}OSi_{10}ClCoLi_7$: C 48.31; H 9.12, N 18.00; found C 47.82, H 8.98, N 17.51. Crystal data for **1**: the SQUEEZE function of PLATON was applied to two independent toluene molecules, which could not be refined owing to severe disorder at special positions,[30] $C_{86}H_{178}N_{23}OSi_{10}ClLi_7Co$, M = 2009.07, monoclinic, $C2/c$, a = 20.1006(4), b = 24.5598(4), c = 24.9957(5) Å, β = 105.786(2)°, V = 11874.2(4) Å^3, T = 123(1) K, Z = 4, 43649 reflections collected, 12325 independent reflections (R_{int} = 0.0275), 98.8% completeness to θ = 76.56° (λ = 1.54178 Å), final R indices [$I > 2\sigma(I)$] R_1 = 0.0629 and wR_2 = 0.1746, R indices (all data) R_1 = 0.0653, wR_2 = 0.1763.

Synthesis of [5][3]

This compound was synthesized in an identical manner to **[2][3]** using anhydrous $ZnBr_2$ (0.11 g, 0.5 mmol) and **1** (0.24 g, 0.5 mmol). The resulting yellow solution stored overnight at room-temperature to result in yellow crystals of **[5][3]** (0.04 g, 32% isolated yield; with water 0.06 g, 48%). Elemental analysis calculated for $C_{60}H_{126}N_{21}OSi_6Li_7Zn_2$: C 47.93; H 8.31, N 19.56; found C 47.78, H 8.19, N 19.59. Crystal data for **[5][3]**: $C_{60}H_{126}N_{21}OSi_6Li_7Zn_2$, M = 1505.70, orthorhombic, $Pba2$, a = 27.7860(13), b = 24.4230(11), c = 12.1310(7) Å, V = 8232.3(7) Å^3, T = 100(2) K, Z = 4, 33772 reflections collected, 10107 independent reflections (R_{int} = 0.1008), 94.5% completeness to θ = 23.25° (λ = 0.71073 Å), final R indices [$I > 2\sigma(I)$] R_1 = 0.0481 and wR_2 = 0.1150, R indices (all data) R_1 = 0.1317, wR_2 = 0.1268.

Acknowledgements

The authors acknowledge the EPSRC, The EPSRC UK National Electron Paramagnetic Resonance Facility at The University of Manchester, the Alexander von Humboldt Foundation (Fellowship for Experienced Researchers awarded to RAL) and the Royal Society (Wolfson Merit Award to REPW). We thank Prof. D. Collison (Manchester) for helpful discussions.

References

1 R. E. P. Winpenny, *J. Chem. Soc., Dalton Trans.*, 2002, 1.
2 V. Chandrasekhar, T. Senapati, A. Dey and S. Hossain, *Dalton Trans.*, 2011, **40**, 5394.
3 (*a*) R. Sessoli, D. Gatteschi, A. Caneschi and M. A. Novak, *Nature*, 1993, **365**, 141; (*b*) D. Gatteschi, R. Sessoli and J. Villain, *Molecular Nanomagnets*, Oxford University Press Inc., New York, 2006.
4 (*a*) G. Aromí and E. K. Brechin, *Struct. Bonding*, 2006, **122**, 1; (*b*) A. J. Tasiopoulos and S. P. Perlepes, *Dalton Trans.*, 2008, 5538; (*c*) R. Bagai and G. Christou, *Chem. Soc. Rev.*, 2009, **38**, 1011.
5 S. A. Sulway, D. Collison, J. J. W. McDouall, F. Tuna and R. A. Layfield, *Inorg. Chem.*, 2011, **50**, 2521.
6 D. Mootz, A. Zinnius and D. Böttcher, *Angew. Chem.*, 1969, **81**, 398.
7 M. P. Coles and P. B. Hitchcock, *Chem. Commun.*, 2005, 3165.
8 E. Weiss and E. A. C. Lucken, *J. Organomet. Chem.*, 1964, **2**, 197.
9 (*a*) D. Scheschkewitz, M. Menzel, M. Hofmann, P. von Ragué Schleyer, W. Massa, K. Harms and A. Berndt, *Angew. Chem., Int. Ed.*, 1999, **38**, 2936; (*b*) W. Uhl, E. Er and M. Matar, *Z. Anorg. Allg. Chem.*, 2006, **632**, 1011.
10 C. Brinkmann, F. García, J. V. Morey, M. McPartlin, S. Singh, A. E. H. Wheatley and D. S. Wright, *Dalton Trans.*, 2007, 1570.
11 (*a*) S. Beaini, G. B. Deacon, A. P. Erven, P. C. Junk and D. R. Turner, *Chem.–Asian J.*, 2007, **2**, 539; (*b*) E. Iravani and B. Neumüller, *Organometallics*, 2005, **24**, 842; (*c*) P. C. Andrews, J. G. MacLellan, R. E. Mulvey and P. J. Nichols, *J. Chem. Soc., Dalton Trans.*, 2002, 1651; (*d*) F. A. Cotton, L. M. Daniels, C. A. Murillo and H. C. Zhou, *C. R. Acad. Paris*, 1999, 579; (*e*) F. M. Mackenzie, R. E. Mulvey, W. Clegg and L. Horsburgh, *Polyhedron*, 1998, **17**, 993; (*f*) W. J. Evans, M. S. Sollberger and J. W. Ziller, *J. Am. Chem. Soc.*, 1993, **115**, 4120.
12 (*a*) G. C. Forbes, A. R. Kennedy, R. E. Mulvey, B. A. Roberts and R. B. Rowlings, *Organometallics*, 2002, **21**, 5115; (*b*) G. C. Forbes, A. R. Kennedy, R. E. Mulvey and P. J. A. Rodger, *Chem. Commun.*, 2001, 1400; (*c*) M. A. Putzer, B. Neumüller and K. Dehnicke, *Z. Anorg. Allg. Chem.*, 1997, **623**, 539.
13 (*a*) A. Bencini, I. Bertini, G. Canti, D. Gatteschi and C. Luchinat, *J. Inorg. Biochem.*, 1981, **14**, 81; (*b*) W. W. De Horrocks and D. A. Burlone, *Inorg. Chim. Acta*, 1979, **35**, 165.
14 (*a*) W. Clegg, R. P. Davies, S. T. Liddle, D. J. Linton, P. R. Raithby, R. Snaith and A. E. H. Wheatley, *Angew. Chem., Int. Ed.*, 1999, **38**, 3367; (*b*) S. R. Boss, M. P. Coles, V. Eyre-Brook, F. García, R. Haigh, P. B. Hitchcock, J. V. Morey, H. Naka, P. R. Raithby, H. A. Sparkes, C. W. Tate and A. E. H. Wheatley, *Dalton Trans.*, 2006, 5574.
15 A. E. H. Wheatley, *Chem. Soc. Rev.*, 2001, **30**, 265.
16 (*a*) C. K. Williams and A. J. P. White, *J. Organomet. Chem.*, 2007, **692**, 912; (*b*) S. R. Boss, R. Haigh, D. J. Linton and A. E. H. Wheatley, *J. Chem. Soc., Dalton Trans.*, 2002, 3129; (*c*) R. P. Davies, D. J. Linton, P. Schooler, R. Snaith and A. E. H. Wheatley, *Chem.–Eur. J.*, 2001, **7**, 3696; (*d*) A. D. Bond, D. J. Linton, P. Schooler and A. E. H. Wheatley, *J. Chem. Soc., Dalton Trans.*, 2001, 3173; (*e*) R. P. Davies, D. J. Linton, R. Snaith and A. E. H. Wheatley, *Chem. Commun.*, 2000, 1819; (*f*) M. A. Malik, P. O'Brien, M. Motavelli and A. C. Jones, *Inorg. Chem.*, 1997, **36**, 5076.
17 A. R. Kennedy, J. Klett, R. E. Mulvey, S. Newton and D. S. Wright, *Chem. Commun.*, 2008, 308.
18 (*a*) W. Clegg, D. V. Graham, E. Herd, E. Hevia, A. R. Kennedy, M. D. McCall and L. Russo, *Inorg. Chem.*, 2009, **48**, 5320; (*b*) P. B. Hitchcock, M. F. Lappert and X.-H. Wei, *Dalton Trans.*, 2006, 1181.
19 (*a*) R. Campbell, P. García-Álvarez, A. R. Kennedy and R. E. Mulvey, *Chem.–Eur. J.*, 2010, **16**, 9964; (*b*) R. Campbell, B. Conway, G. S. Fairweather, P. García-Álvarez, A. R. Kennedy, J. Klett, R. E. Mulvey, C. T. O'Hara and G. M. Robertson, *Dalton Trans.*, 2010, **39**, 511; (*c*) E. Hevia, A. R. Kennedy, J. Klett and M. D. McCall, *Chem. Commun.*, 2009, 3240; (*d*) F. García, M. McPartlin, J. V. Morey, D. Nobotu, Y. Kondo, H. Naka, M. Uchiyama and A. E. H. Wheatley, *Eur. J. Org. Chem.*, 2008, 644; (*e*) D. R. Armstrong, E. Herd, D. V. Graham, E. Hevia, A. R. Kennedy, W. Clegg and L. Russo, *Dalton Trans.*, 2008, 1323; (*f*) D. R. Armstrong, C. Dougan, D. V. Graham, E. Hevia and A. R. Kennedy, *Organometallics*, 2008, **27**, 6063; (*g*) Y. Kondo, J. V. Morey, J. C. Morgan, H. Naka, D. Nobuto, P. R. Raithby, M. Uchiyama and A. E. H. Wheatley, *J. Am. Chem. Soc.*, 2007, **129**, 12734; (*h*) W. Clegg, S. H. Dale, A. M. Drummond, E. Hevia, G. W. Honeyman and R. E. Mulvey, *J. Am. Chem. Soc.*, 2006, **128**, 7434; (*i*) D. V. Graham, E. Hevia, A. R. Kennedy and R. E. Mulvey, *Organometallics*, 2006, **25**, 3297; (*j*) W. Clegg, S. H. Dale, E. Hevia, G. W. Honeyman and R. E. Mulvey, *Angew. Chem., Int. Ed.*, 2006, **45**, 2370; (*k*) H. R. L. Barley, W. Clegg, S. H. Dale, E. Hevia, G. W. Honeyman, A. R. Kennedy and R. E. Mulvey, *Angew. Chem., Int. Ed.*, 2005, **44**, 6018.
20 (*a*) A. J. Blake, N. L. Gillibrand, G. J. Moxey and D. L. Kays, *Inorg. Chem.*, 2009, **48**, 10837; (*b*) R. A. Layfield, *Chem. Soc. Rev.*, 2008, **37**,

1098; (*c*) A. A. Danopoulos, G. Wilkinson, T. K. N. Sweet and M. B. Hursthouse, *J. Chem. Soc., Dalton Trans.*, 1994, 1037; (*d*) A. Belforte, F. Calderazzo, U. Englert and J. Strähle, *J. Chem. Soc., Chem. Commun.*, 1989, 801; (*e*) B. D. Murray and P. P. Power, *Inorg. Chem.*, 1984, **23**, 4584.

21 (*a*) R. E. Mulvey, V. L. Blair, W. Clegg, A. R. Kennedy, J. Klett and L. Russo, *Nat. Chem.*, 2010, **2**, 588; (*b*) V. L. Blair, W. Clegg, R. E. Mulvey and L. Russo, *Inorg. Chem.*, 2009, **48**, 8863; (*c*) V. L. Blair, L. M. Carrella, W. Clegg, J. Klett and R. E. Mulvey, *Chem.–Eur. J.*, 2009, **15**, 856; (*d*) V. L. Blair, L. M. Carrella, W. Clegg, B. Conway, R. W. Harrington, L. M. Hogg, J. Klett and R. E. Mulvey, *Angew. Chem., Int. Ed.*, 2008, **47**, 6208; (*e*) V. L. Blair, W. Clegg, B. Conway, E. Hevia, A. Kennedy, J. Klett, R. E. Mulvey and L. Russo, *Chem.–Eur. J.*, 2008, **14**, 65; (*f*) L. M. Carrella, W. Clegg, D. V. Graham, L. M. Hogg, A. R. Kennedy, J. Klett and R. E. Mulvey, *Angew. Chem., Int. Ed.*, 2007, **46**, 4662; (*g*) J. García-Álvarez, A. R. Kennedy, J. Klett and R. E. Mulvey, *Angew. Chem., Int. Ed.*, 2007, **46**, 1105.

22 (*a*) S. H. Wunderlich, T. Bresser, C. Dunst, G. Monzon and P. Knochel, *Synthesis*, 2010, **15**, 2670; (*b*) S. H. Wunderlich, M. Kienle and P. Knochel, *Angew. Chem., Int. Ed.*, 2009, **48**, 7256.

23 (*a*) K. W. Henderson, A. E. Dorigo, Q.-Y. Liu, P. G. Williard, P. von R. Schleyer and P. R. Bernstein, *J. Am. Chem. Soc.*, 1996, **118**, 1339; (*b*) E. Hevia and R. E. Mulvey, *Angew. Chem., Int. Ed.*, 2011, **50**, 6448.

24 (*a*) R. E. Mulvey, *Acc. Chem. Res.*, 2009, **42**, 743; (*b*) R. E. Mulvey, *Chem. Commun.*, 2001, 1049.

25 The structure of a sodium-only inverse crown has also been reported, see: N. M. Clark, P. García-Álvarez, A. R. Kennedy, C. T. O'Hara and G. M. Robertson, *Chem. Commun.*, 2009, 5835.

26 B. L. Lucht and D. B. Collum, *Acc. Chem. Res.*, 1999, **32**, 1035.

27 A. Bashall, A. D. Bond, E. L. Doyle, F. García, S. Kidd, G. T. Lawson, M. C. Parry, M. McPartlin, A. D. Woods and D. S. Wright, *Chem.–Eur. J.*, 2002, **8**, 3377.

28 V. B. Shur, I. A. Tikhonova, F. M. Dolgushin, A. I. Yanovsky, Y. T. Struchkov, A. Y. Volkonsky, E. V. Solodova, S. Y. Panov, P. V. Petrovskii and M. E. Vol'pin, *J. Organomet. Chem.*, 1993, **443**, C19.

29 (*a*) M. Murrie, *Chem. Soc. Rev.*, 2010, **39**, 1986; (*b*) S. Langley, M. Helliwell, R. Sessoli, S. J. Teat and R. E. P. Winpenny, *Inorg. Chem.*, 2008, **47**, 49; (*c*) A. B. Boeer, A.-L. Barra, L. F. Chibotaru, D. Collison, E. J. L. McInnes, R. A. Mole, G. G. Simeoni, G. A. Timco, L. Ungur, T. Unruh and R. E. P. Winpenny, *Angew. Chem., Int. Ed.*, 2011, **50**, 4007.

30 P. Sluis and A. L. Spek, *Acta Crystallogr., Sect. A: Found. Crystallogr.*, 1990, **A46**, 194.

Dalton Transactions

Electronic Supplementary Information for:

Synthesis and structure of cationic guanidinate-bridged bimetallic {Li_7M} cubes with inverse crown counter anions

Daniel Woodruff, Michael Bodensteiner, Daniel O. Sells, Richard. E. P. Winpenny and Richard A. Layfield*

General considerations

Synthesis. All reactions were carried out using conventional Schlenk techniques. Reagents were obtained from commerical sources and used as supplied. Toluene was either dried using an Innovative Technologies Solvent Purification System, or by refluxing over sodium-potassium alloy. Solvents for NMR spectroscopy were distilled under nitrogen off sodium-potassium alloy or molten potassium, and were stored over activated 4 Å molecular sieves.

X-ray crystallography. Data on **1** were collected using an Oxford Diffraction Xcalibur2 diffractometer using an enhance molybdenum X-ray source with graphite monochromator (λ = 0.71073 Å) and a CCD detector. Data on [**2**][**3**] were collected using an Oxford Diffraction SuperNova diffractometer using a copper microfocus X-ray source with mirror optics (λ = 1.54178 Å) and a CCD area detector.

NMR spectroscopy. NMR spectra were acquired using a Bruker Avance III spectrometer operating at 400.13 MHz (^{1}H), 100.61 MHz (^{13}C) and 155.51 MHz (^{7}Li).

EPR spectroscopy. The X-band EPR spectrum of [**2**][**3**] was recorded on a Bruker EMX spectrometer using a dielectric X-band resonator. The Q-band EPR spectrum of [**2**][**3**] was recorded on a Bruker Elexsys spectrometer using a dielectric Q-band resonator. An Oxford Instruments continuous flow He-cryostat was used with both resonators. Field corrections were carried out using a Bruker E0361200 teslameter. This is only sensitive to fields between 1500-15000 G, so for the X-band measurement, a calibration plot of these fields *vs*. the Hall probe was made, and extrapolated to 0 G so as to obtain a correction for the peak at 1065 G. Samples were prepared and sealed in a glove box, ensuring the exclusion of atmospheric oxygen.

Elemental analysis. Elemental analyses on **1** and [**2**][**3**] were carried out at the Elemental Analysis Service of London Metropolitan University.

[Li_3(μ-hmds)$_2$(μ-hpp)] (1)

X-ray crystallography. A semi-empirical absorption correction from equivalents was applied.[1] The structure was solved by charge-flipping methods using Superflip,[2] and full-matrix least-square refinements on F^2 in SHELXL-97 were performed with anisotropic displacements for all non-hydrogen atoms.[3] Data were erroneously collected in the centric crystal class, resulting in lowered data completeness. During the least-square-refinement three ISOR restraints were applied to model reasonable displacement parameters for atoms at special positions (Li2, C13 and C17).

Table S1. Crystal data and structure refinement for compound **1**.

Empirical formula	$C_{19}H_{48}Li_3N_5Si_4$
Formula weight	479.80
Temperature	100(2) K
Crystal system	tetragonal
Space group	$P4_2bc$
Unit cell dimensions	a = 16.4053(3) Å α = 90°
	b = 16.4053(3) Å β = 90°
	c = 21.4837(10) Å γ = 90°
Volume	5781.99(31) Å^3
Z	8
Density (calculated)	1.102 Mg/m^3
Absorption coefficient	0.220 mm^{-1}
F(000)	2096
Crystal size	0.18 × 0.23 × 0.24 mm^3
Theta range for data collection	3.12 to 28.66°.
Index ranges	$-18 < h < 21$, $-16 < k < 21$, $-28 < l < 10$
Reflections collected	12200
Independent reflections	4177 [R(int) = 0.0397]
Completeness to full theta	0.896
Max. and min. transmission	1.000, 0.892
Data / restraints / parameters	4177 / 19 / 297
Goodness-of-fit on F^2	0.995
Final R indices [$I>2\sigma(I)$]	R_1 = 0.0393, wR_2 = 0.0989
R indices (all data)	R_1 = 0.0551, wR_2 = 0.1060
Flack parameter	0.3(3)
Largest diff. hole and peak	–0.221, 0.539 eÅ^{-3}

1. SCALE3 ABSPACK, CrysAlisPro, Oxford Diffraction Ltd., Version 1.171.33.52, 2009

2. L. Palatinus and G. Chapuis, *J. Appl. Cryst*., 2007, **40**, 786.

3. G. M. Sheldrick, *Acta Cryst*., 2008, **A64**, 112.

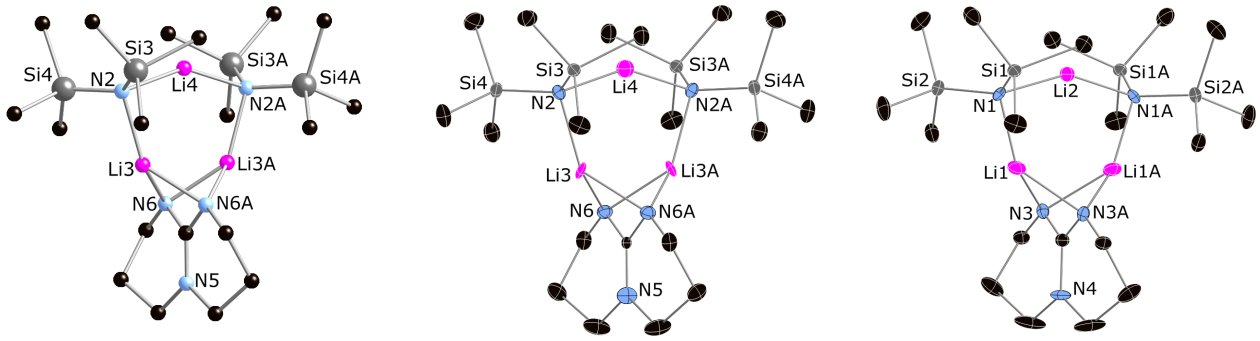

Figure S1. Molecular structure of **1b** (left), thermal ellipsoid plot of **1b** (50% probability, centre) and thermal ellipsoid plot of **1a** (50% probability, right), Selected bond lengths [Å] and angles [°] for **1b**: N(2)–Li(3) 2.060(17), N(2)–Li(4) 1.987(9), N(6)–Li(3) 2.051(13), N(2)-Li(3)-N(6) 132.4(6), N(2)-Li(4)-N(2A) 146.7(14).

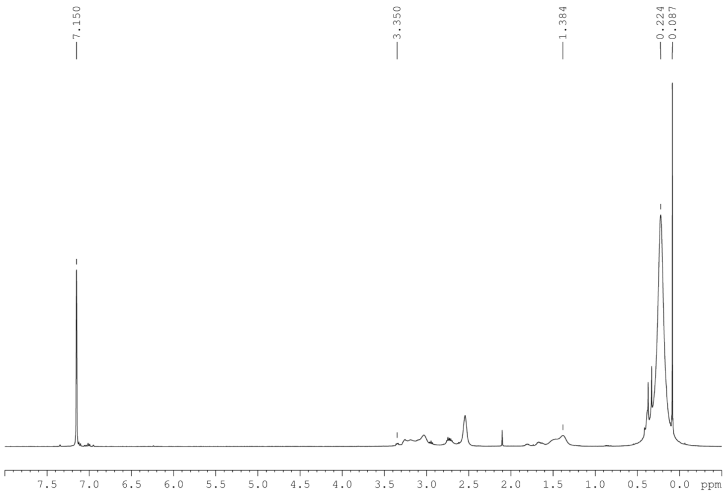

Figure S2. ^{1}H NMR spectrum of **1** recorded in benzene-d_6 at 298 K. The broad resonances in the region $\delta(^{1}H)$ = 1.38-3.35 ppm correspond to the [hpp] proton environments, and the broad resonance at $\delta(^{1}H)$ = 0.22 ppm is due to the $SiMe_3$ substituents. The sharp resonance at $\delta(^{1}H)$ = 0.09 ppm is due to small amount of hydrolysis, which was found to be unavoidable even if the solvent was distilled from sodium-potassium alloy and stored over activated 4 Å molecular sieves.

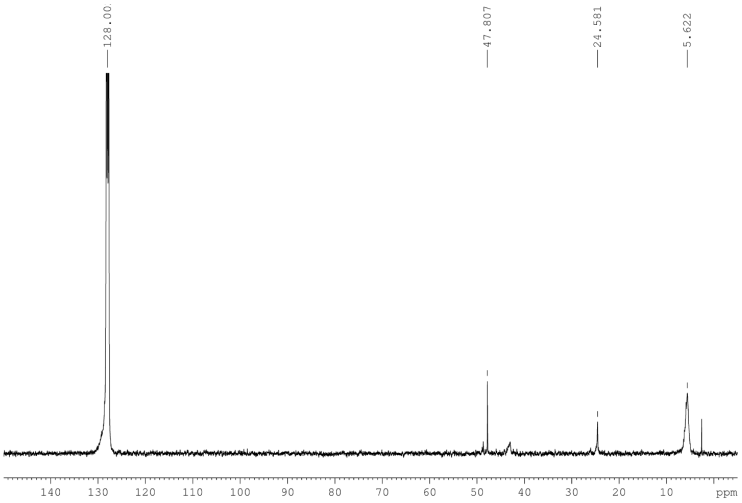

Figure S3. ^{13}C NMR spectrum of **1** recorded in benzene-d_6 at 298 K. The resonances at $\delta(^{13}C)$ = 47.81 and 24.58 ppm correspond to hpp ^{13}C NMR environments, and the resonance at $\delta(^{13}C)$ = 5.62 ppm ($\omega_{1/2}$ = 69.8 Hz) is due to the trimethylsilyl substituents. The low intensity of the signals is due to the fluxional behaviour of the compound.

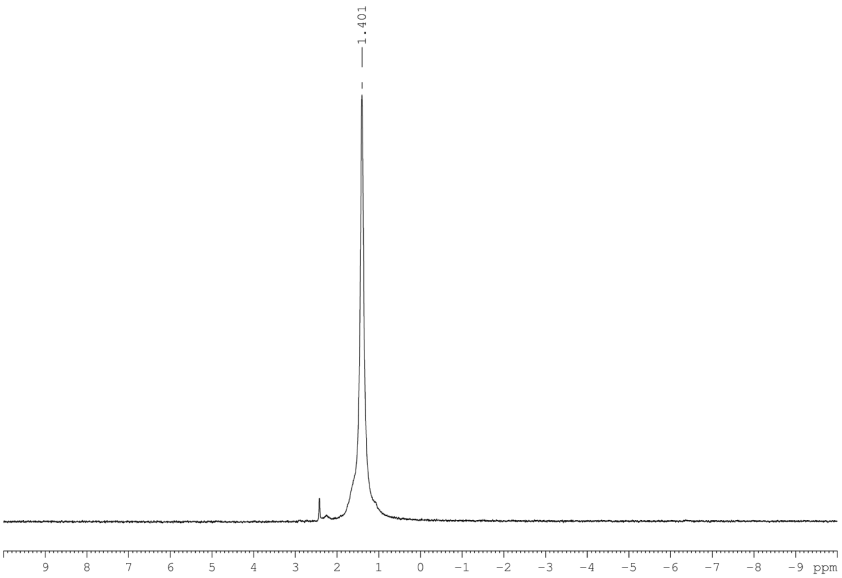

Figure S4. ^{7}Li NMR spectrum of **1** recorded in benzene-d_6 at 298 K.

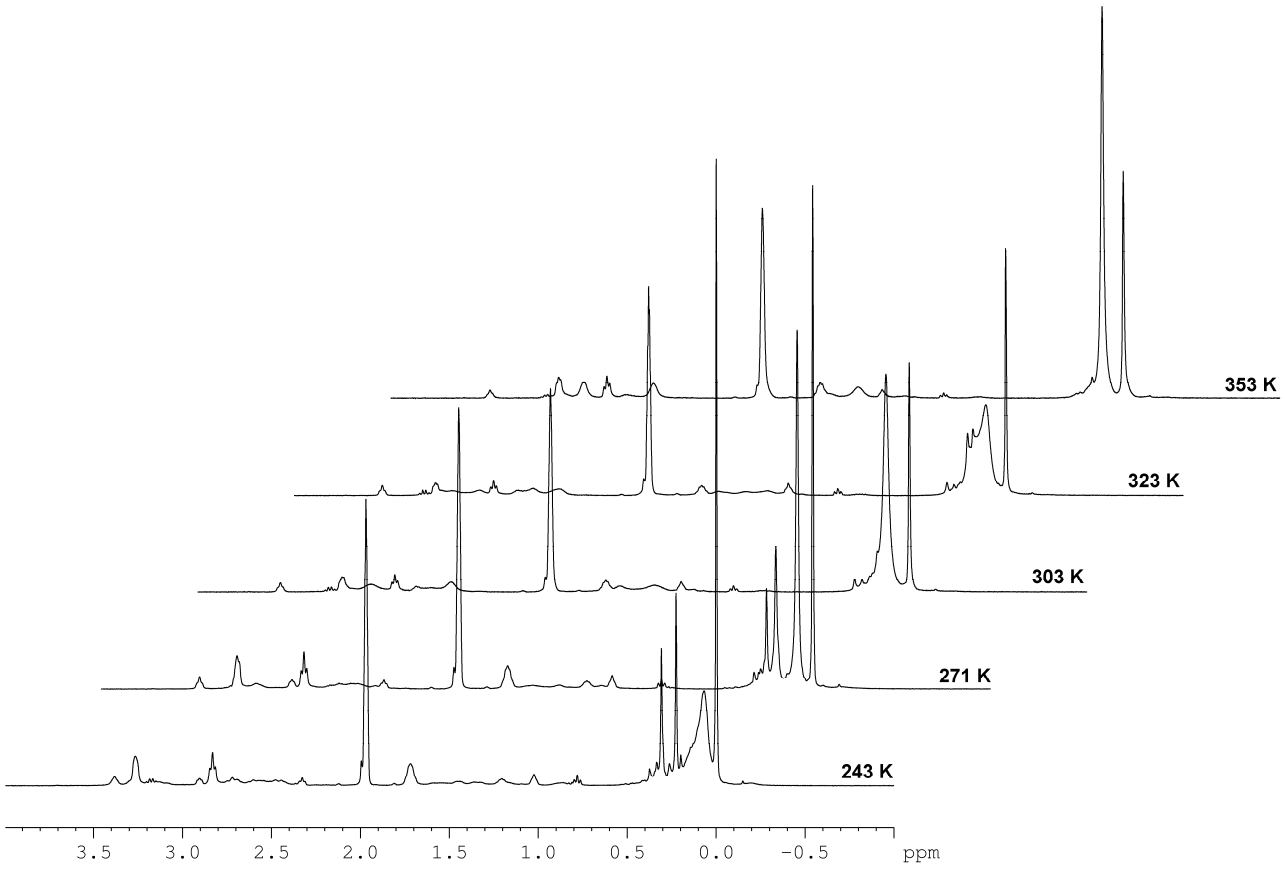

Figure S5. Variable-temperature ^{1}H NMR spectrum of **1** recorded in toluene-d_8. The temperature-non-dependent singlet at 0.08 ppm is due to hydrolysis.

$[MnLi_7(\mu_8\text{-}O)(\mu,\mu'\text{-}hpp)_6][\{Li(\mu\text{-}hmds)\}_5(\mu_5\text{-}Cl)]$ [2][3]

X-ray crystallography. A semi-empirical absorption correction from equivalents was applied.[1] The crystal was only poorly diffracting and no better crystal could be found. Repeated experiments also resulted only weakly scattering crystals. The structure was solved by direct methods (SHELXS-97) and refined by full-matrix anisotropic least squares (SHELXL97).[2] The H-atoms were calculated geometrically and a riding model was used during refinement process.

Table S2. Crystal data and structure refinement for [**2**][**3**]

Empirical formula	$C_{86}H_{178}ClLi_{12}MnN_{23}OSi_{10}$	
Formula weight	1988.96	
Temperature	100(1) K	
Wavelength	0.71073 Å	
Crystal system	monoclinic	
Space group	*C*2/*c*	
Unit cell dimensions	*a* = 20.1096(12) Å	α = 90°.
	b = 24.4769(15) Å	β = 105.769(6)°.
	c = 24.9736(17) Å	γ = 90°.
Volume	11829.9(13) Å^3	
Z	4	
Density (calculated)	1.117 Mg/m^3	
Absorption coefficient	0.284 mm^{-1}	
F(000)	4260	
Crystal size	0.200 × 0.100 × 0.100 mm^3	
Theta range for data collection	2.92 to 24.04°.	
Index ranges	-22<=*h*<=21, -26<=*k*<=27, -25<=*l*<=18	
Reflections collected	21119	
Independent reflections	7584 [*R*(int) = 0.0906]	
Completeness to theta = 21.00°	99.7%	
Max. and min. transmission	1.00000 and 0.66492	
Data / restraints / parameters	7584 / 0 / 617	
Goodness-of-fit on F^2	1.040	
Final *R* indices [$I>2\sigma(I)$]	*R*1 = 0.0857, *wR*2 = 0.1979	
R indices (all data)	*R*1 = 0.1783, *wR*2 = 0.2215	
Largest diff. peak and hole	0.491 and -0.273 e.Å^3	

1. SCALE3 ABSPACK, CrysAlisPro, Oxford Diffraction Ltd., Version 1.171.33.52, 2009

2. G. M. Sheldrick, *Acta Cryst.*, 2008, **A64**, 112.

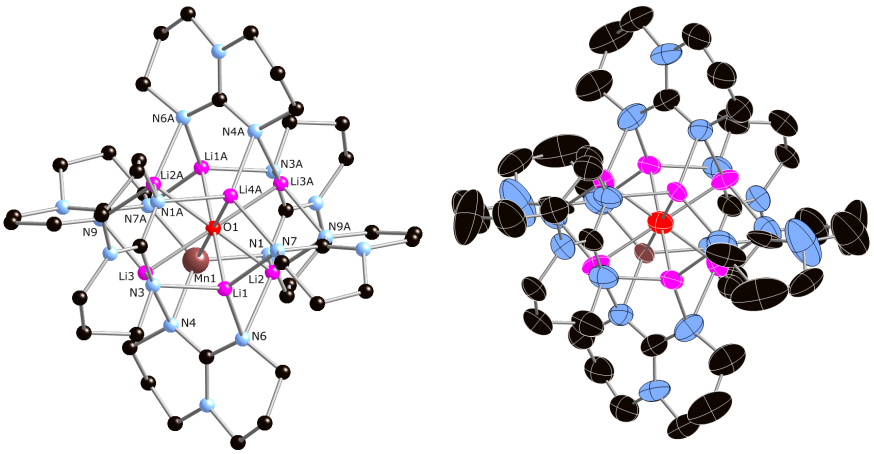

Figure S6. Molecular structure of the cation **2** in [**2**][**3**]: ball and stick model (left) and thermal ellipsoid plot (50% probability, right).

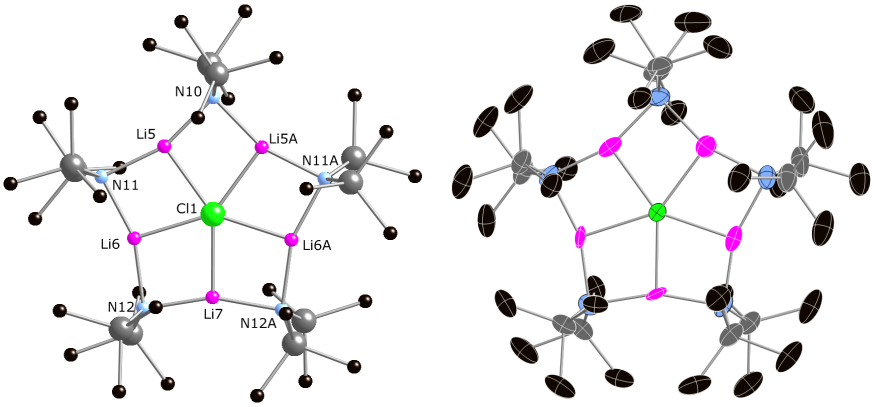

Figure S7. Molecular structure of the anion **3** in [**2**][**3**]: ball and stick model (left) and thermal ellipsoid plot (50% probability, right).

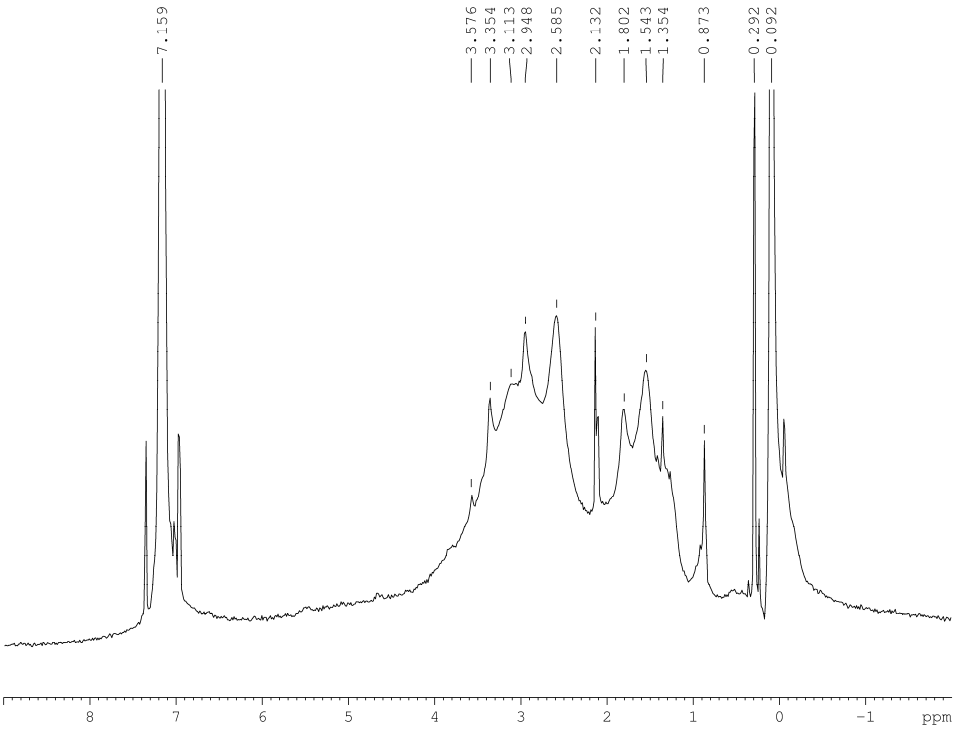

Figure S8. ^{1}H NMR spectrum of [**2**][**3**] recorded in benzene-d_6 at 298 K. The resonances of the $[hpp]^-$ ^{1}H environments are in the region $\delta(^{1}H)$ = 0.87-3.58 ppm, and the $SiMe_3$ substituents have $\delta(^{1}H)$ = 0.29, 0.09 ppm.

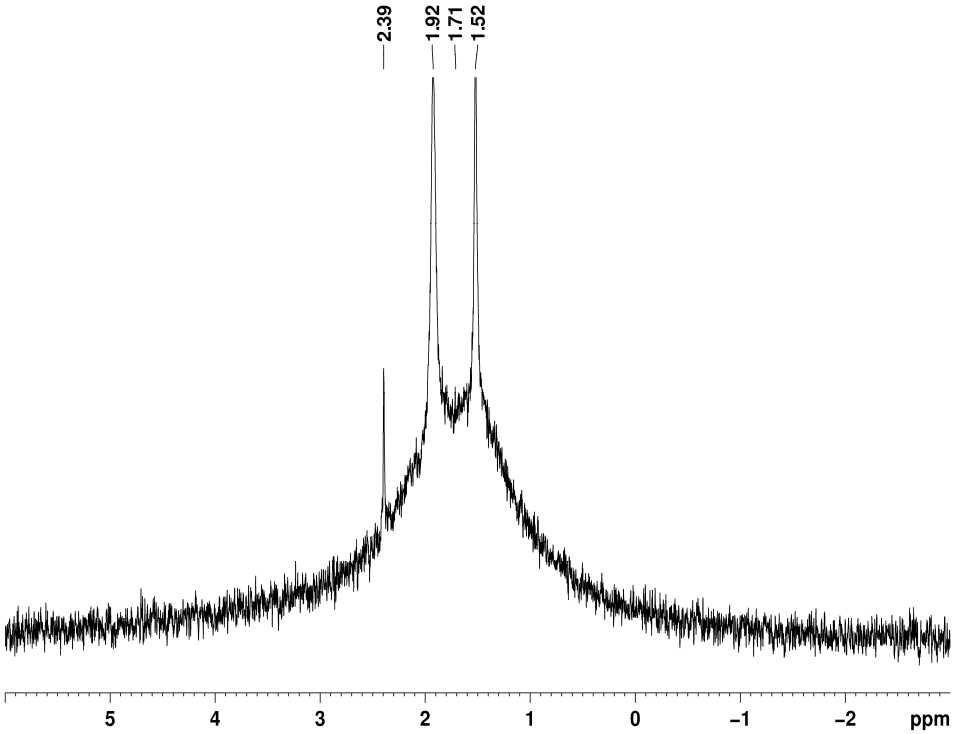

Figure S9. ^{7}Li NMR spectrum of [**2**][**3**] recorded in benzene-d_6 at 298 K.

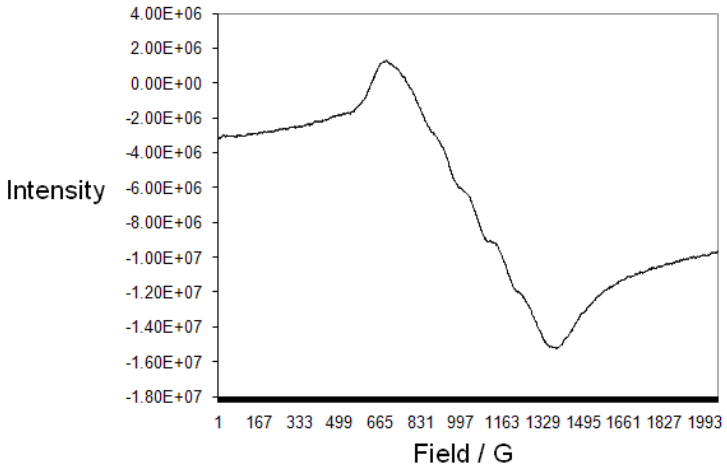

Figure S10. Q-band EPR spectrum of a polycrystalline sample of [**2**][**3**] recorded at $T = 5$ K.

$[CoLi_7(\mu_8\text{-}O)(\mu\text{-}hpp)_6][\{Li(\mu\text{-}hmds)\}_5(\mu_5\text{-}Cl)]$ [4][3]

X-ray crystallography. An analytical absorption correction from crystal faces was carried out.[4] EXYZ and EADP constraints were applied to the Co/Li mixed positions. The SQUEEZE function of PLATON was applied to two independent toluene molecules, which could not be refined due to severe disorder at special positions.[5]

Table S3. Crystal data and structure refinement for [**4**][**3**]

Empirical formula	$C_{86}H_{178}ClCoLi_{12}N_{23}OSi_{10}$
Formula weight	1824.81
Temperature	123(1) K
Crystal system	monolinic
Space group	*C*2/*c*
Unit cell dimensions	a = 20.1006(4) Å α = 90°
	b = 24.5598(4) Å β = 105.786(2)°
	c = 24.9957(5) Å γ = 90°
Volume	11874.2(4) Å^3
Z	2
Density (calculated)	1.021 Mg/m^3
Absorption coefficient	2.679 mm^{-1}
F(000)	3932
Crystal size	0.44 x 0.22 x 0.14 mm^3
Theta range for data collection	3.09 to 76.56 °.
Index ranges	$-24 < h < 24$, $-30 < k < 29$, $-31 < l < 29$
Reflections collected	43649
Independent reflections	12325 [R(int) = 0.0293]
Completeness to full theta	0.988
Max. and min. transmission	0.414, 0.783
Data / restraints / parameters	12325 / 0 / 604
Goodness-of-fit on F^2	1.091
Final R indices [$I>2\sigma(I)$]	R_1 = 0.0629, wR_2 = 0.1746
R indices (all data)	R_1 = 0.0653, wR_2 = 0.1763
Largest diff hole and peak	–0.481, 0.639 eÅ^{-3}

4. R. C. Clark and J. S. Reid, *Acta Cryst*., 1995, **A51**, 887.

5. P. Sluis and A. L. Spek, *Acta Cryst*., 1990, **A46**, 194.

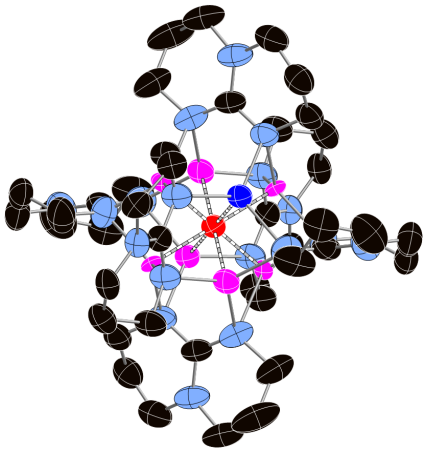

Figure S11. Molecular structure of the cation **4** in [**4**][**3**]: thermal ellipsoid plot (50% probability). Nitrogen = light blue, oxygen = red, lithium = pink, cobalt = dark blue.

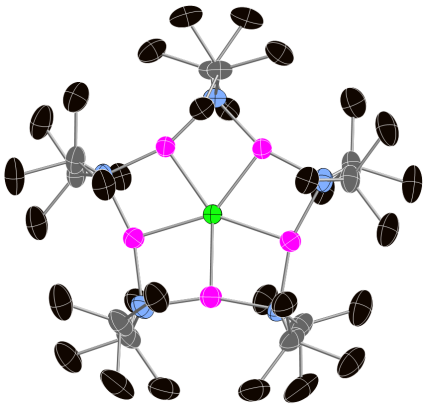

Figure S12. Molecular structure of the cation **3** in [**4**][**3**]: thermal ellipsoid plot (50% probability, right). Silicon = grey, chlorine = green.

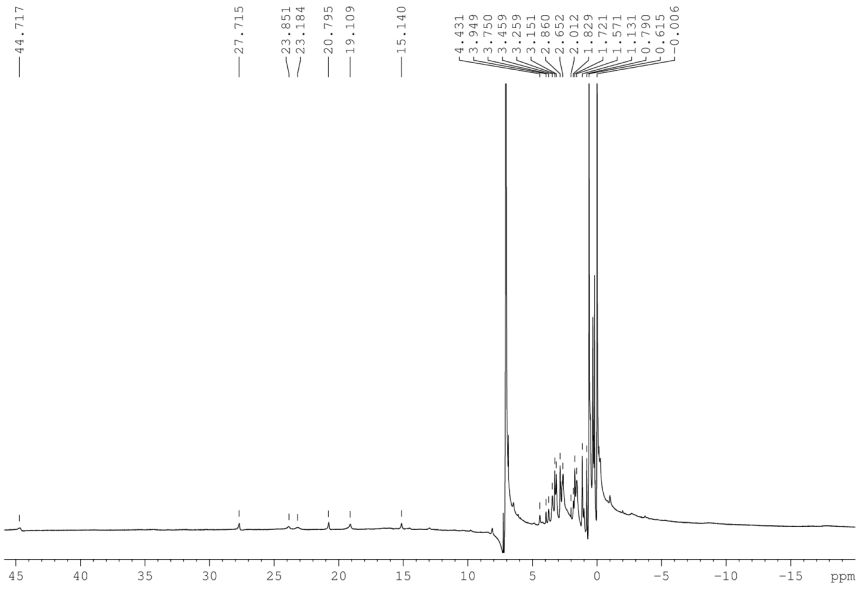

Figure S13. ^{1}H NMR spectrum of [**4**][**3**] recorded in benzene-d_6 at 298 K.

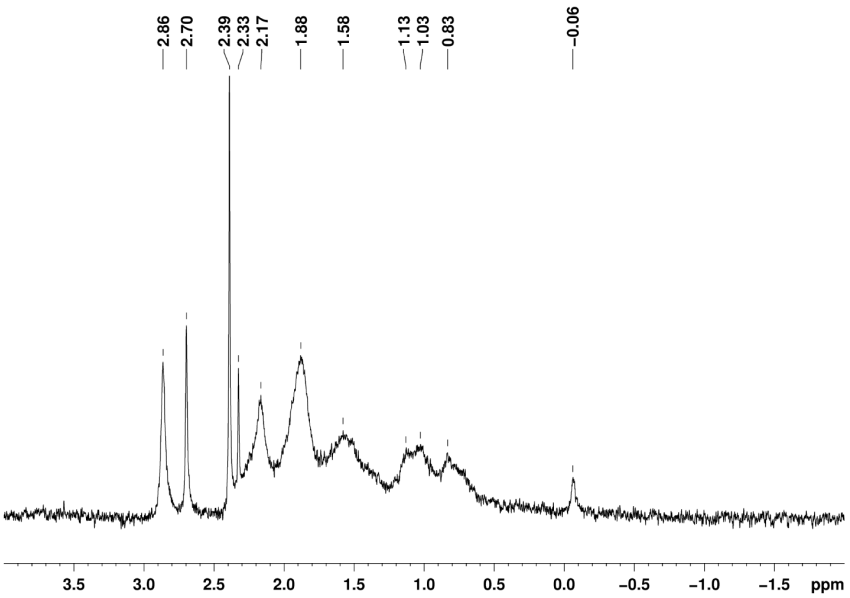

Figure S14. ^{7}Li NMR spectrum of [**4**][**3**] recorded in benzene-d_6 at 298 K.

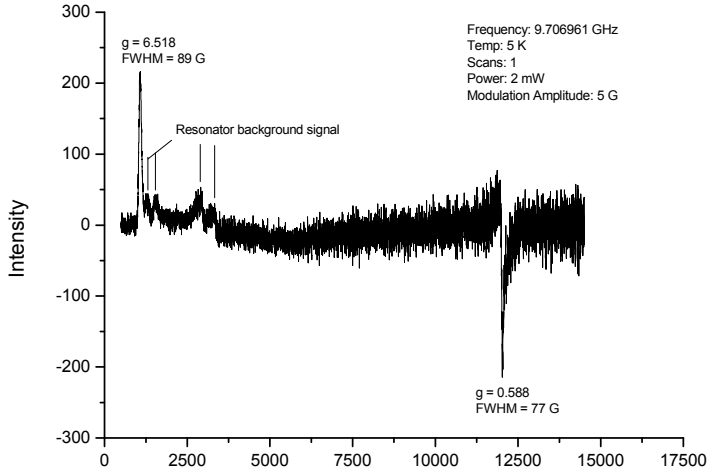

Figure S15. X-band EPR spectrum of a polycrystalline sample of [**4**][**3**]. The resonance at 1062 G has full width at half-maximum = 89 ± 1.5 G.

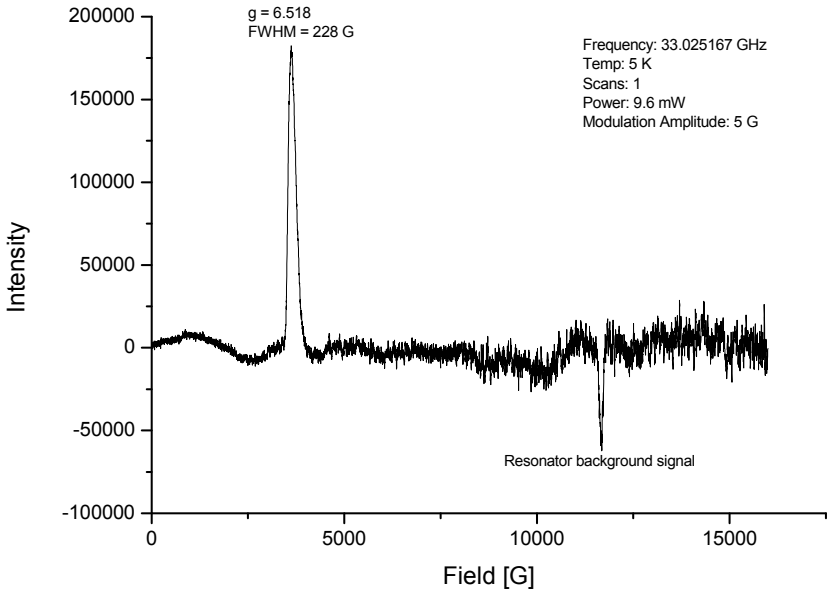

Figure S16. Q-band EPR spectrum of a polycrystalline sample of [**4**][**3**]. The resonance at 3650 G has full width at half-maximum = 228 ± 4 G.

$[ZnLi_7(\mu_8\text{-}O)(\mu\text{-}hpp)_6][Zn(hmds)_3]$ [5][$Zn(hmds)_3$]

A semi-empirical absorption correction from equivalents was applied.1 The crystals were only weakly diffracting. EXYZ and EADP constraints were applied to the Zn/Li mixed positions. Several restraints (DFIX, SIMU, DELU, ISOR) were used to refine the disordered hmds ligands.

Table S4. Crystal data and structure refinement for [**5**][$Zn(hmds)_3$]

Empirical formula	$C_{60}H_{126}Li_7N_{21}OSi_6Zn_2$	
Formula weight	1505.70	
Temperature	100(2) K	
Wavelength	0.71073 Å	
Crystal system	orthorhombic	
Space group	*Pba*2	
Unit cell dimensions	a = 27.7860(13) Å	α = 90°.
	b = 24.4230(11) Å	β = 90°.
	c = 12.1310(7) Å	γ = 90°.
Volume	8232.3(7) Å^3	
Z	4	
Density (calculated)	1.155 Mg/m^3	
Absorption coefficient	0.720 mm^{-1}	
F(000)	3224	
Crystal size	0.1 × 0.1 × 0.05 mm^3	
Theta range for data collection	2.89 to 23.25°.	
Index ranges	-30<=h<=22, -25<=k<=25, -12<=l<=13	
Reflections collected	33772	
Independent reflections	10107 [R(int) = 0.1008]	
Completeness to theta = 23.25°	94.5 %	
Max. and min. transmission	1.000 and 0.785	
Data / restraints / parameters	10107 / 199 / 937	
Goodness-of-fit on F^2	0.876	
Final R indices [I>2σ(I)]	R1 = 0.0481, wR2 = 0.1150	
R indices (all data)	R1 = 0.1317, wR2 = 0.1268	
Absolute structure parameter	0.013(19)	
Largest diff. peak and hole	0.380 and -0.232 e.Å^{-3}	

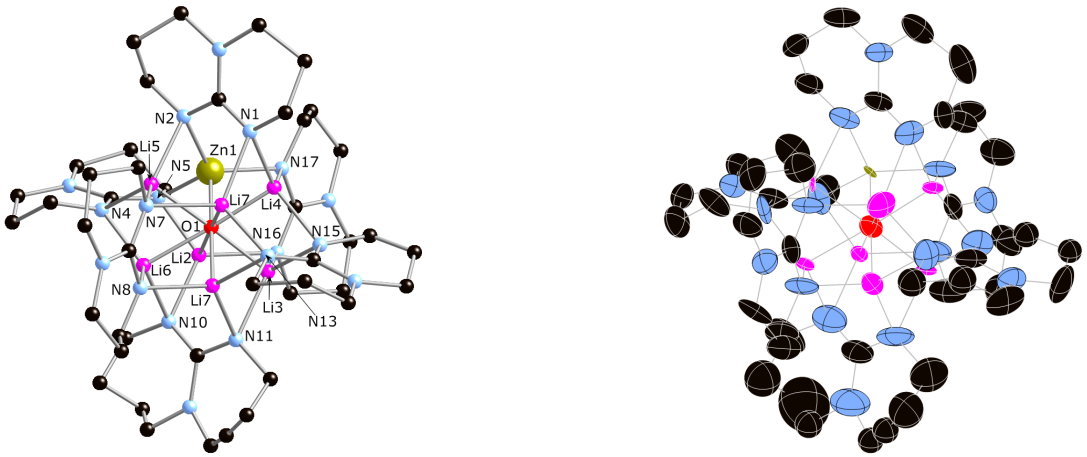

Figure S17. Molecular structure of the cation **5** in [**5**][Zn(hmds)$_3$]: ball and stick model (left) and thermal ellipsoid plot (50% probability, right).

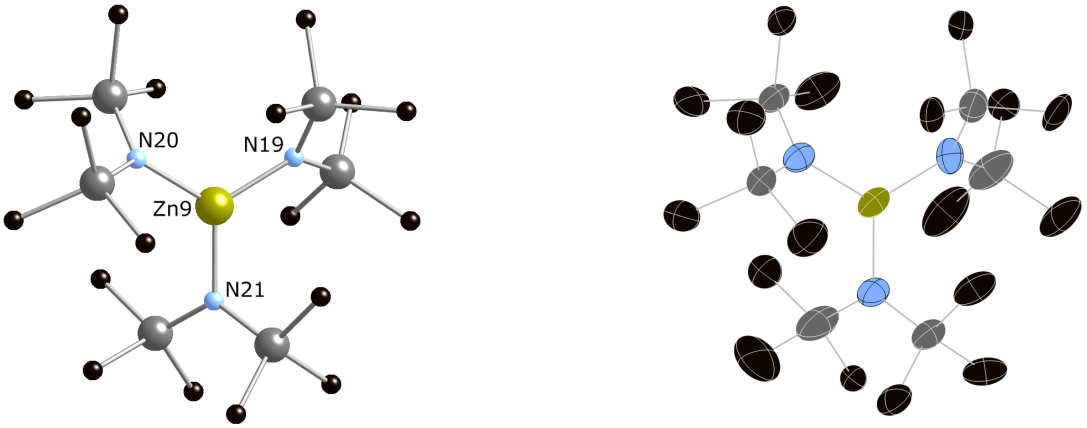

Figure S18. Molecular structure of the [Zn(hmds)$_3$]$^-$ in [**5**][Zn(hmds)$_3$]: ball and stick model (left) and thermal ellipsoid plot (50% probability, right).

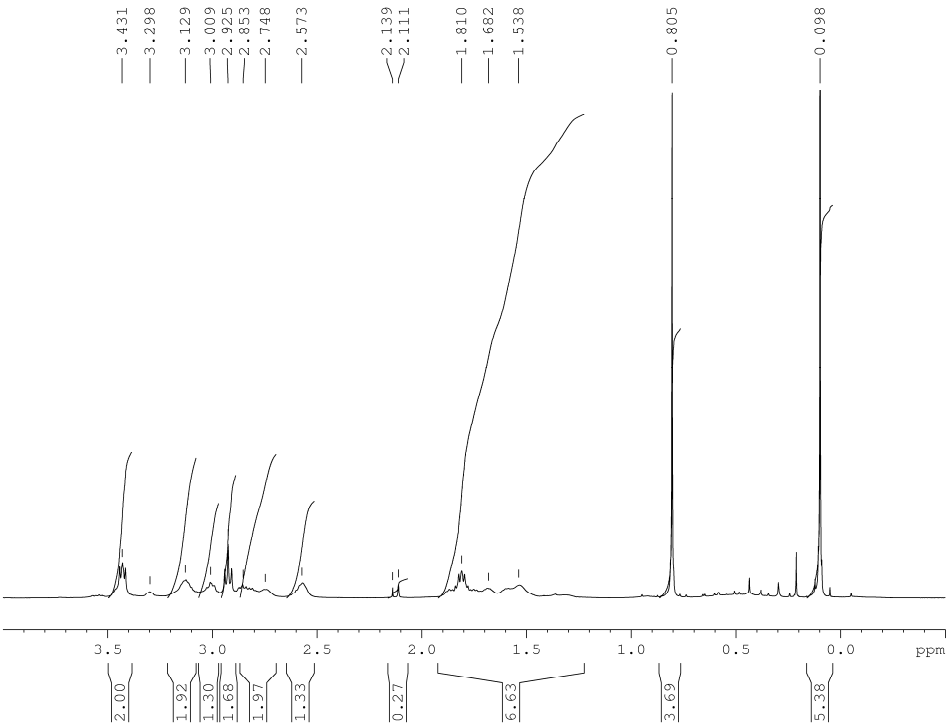

Figure S19. ^{1}H NMR spectrum of [**5**][Zn(hmds)$_3$] in the region 4.0 to -1.0 ppm, recorded in benzene-d$_6$ at 298 K. No resonances observed at lower field (except solvent).

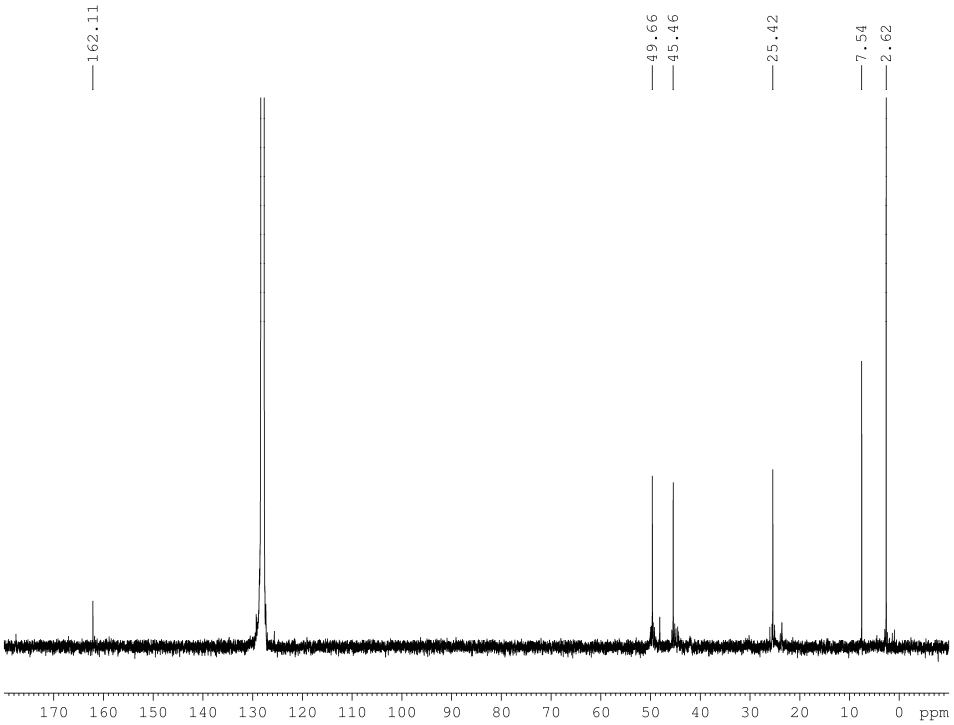

Figure S20. ^{13}C NMR spectrum of [**5**][Zn(hmds)$_3$] recorded in benzene-d$_6$ at 298 K.

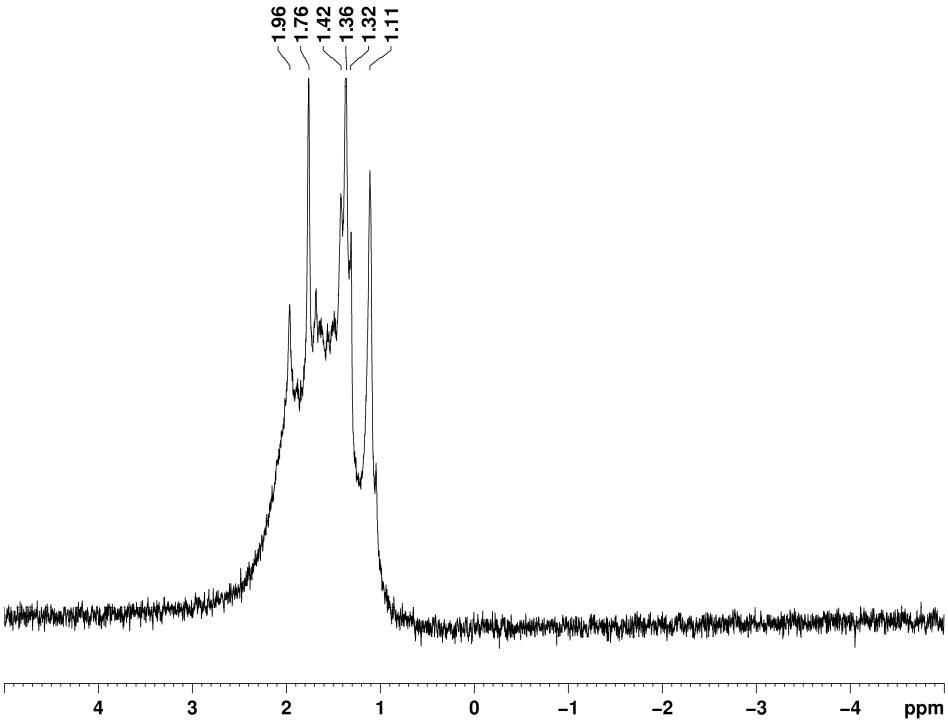

Figure S21. ^{7}Li NMR spectrum of [**5**][Zn(hmds)$_3$] recorded in benzene-d$_6$ at 298 K.

Chapter 8: Conclusions and Future Work

A number of different transition metal and lanthanide cluster complexes have been synthesised via a number of different methods. Chapter 4 shows the simple synthetic route of combining a lanthanide amide with a thiol in order to create a series of $[\{Ln(N(SiMe_3)_2)(\mu_2\text{-}SEt)_2\}_4(\mu_3\text{-}SEt)][Li(THF)_4]$ "Ln_4" squares (Ln = Gd , Tb and Dy) with the Tb and Dy analogues being the second and third examples of sulphur bridged lanthanide SMMs. Both analogues are SMMs in zero field however, the Dy analogue shows quantum tunnelling of magnetisation in zero field and requires a 2000 Oe applied field in order to "switch off" the quantum tunnelling. Chapter 4 shows a clear gap in the Ln SMMs research field in which lanthanide-amides/organometallics can be combined with simple ligands to create larger Ln clusters showing SMM behaviour.

Chapter 5 highlights an unusual synthetic route to lanthanide SMMs in which solvent cleavage provides the bridging ligands between lanthanide centres in $[Ln(TMP)_2(\mu\text{-}OEt)]_2$ (Ln = Dy and Yb). The one pot synthesis allows the isolation of potentially unstable lanthanide-amide compounds to be avoided. The Dy analogue shows field induced SMM behaviour and requires a field of 7000 Oe to show SMM behaviour.

Chapter 6 focuses on the use $MnCp_2$ to deprotonate imino phosphonates to create a series of Mn(II) imino phosphonate compounds. Altering the R group attached to the *N*-donor "arms" of the ligand affects the aggregation state of each compound and in turn alters the electronic properties of the Mn(II) centre in each compound. EPR spectroscopy confirms the oxidation state of the Mn(II) centre and also the local crystal field symmetry around the Mn(II) centre in each complex. The complexes isolated in Chapter 6 are the first three examples of paramagnetic transition metal imino phosphonate complexes and highlight the

large potential these ligands offer in synthesis of cluster complexes with interesting electronic and magnetic properties.

Chapter 7 shows the interesting chemistry that can take place when trace amounts of water are present in a reaction mixture. A new, well defined organolithium precursor [$Li_3(\mu$-$N(SiMe_3)_2)_2(\mu$-hpp)] can be combined with MX_2 salts (M = Co, Mn, Zn; X = Cl or Br) to create a series of oxo cantered MLi7 cubes. EPR studies on the Co and Mn analogues confirm that both metal centers are in the +2 oxidation state. Both the Co and Mn analogues contain an "inverse crown" [{Liμ-$N(SiMe_3)_2$}$_5$(μ_5-Cl)] counter ion, formed by the encapsulation of a Cl^- ion by "free" $LiN(SiMe_3)_2$.

Overall the use of organometallic and metal amide precursors are reagents in the synthesis of new magnetically interesting compounds has proved successful. Unusual ligands such as thiols and imino phosphonates have yielded new and interesting complexes with two new SMMs being isolated. Future work would extend to the use of lanthanide-amides and organometallics to deprotonate imino phosphonates and others thiols (e.g. dithiols) in the hope of synthesizing larger cluster complexes with interesting electronic and magnetic properties. Further investigation into other potential one pot synthetic methodologies are likely to yield interesting results, with the potential to eliminate the need to isolate potentially unstable organometallic and metal-amide precursors.

Chapter 9: Experimental

Synthesis

Syntheses of all compounds reported in this thesis were carried out under inert dinitrogen atmospheres using standard Schlenk line techniques. All manipulations were carried out on a double manifold line or where appropriate in a MBRAUN LabStar glovebox containing a dinitrogen atmosphere. THF, Hexane, Benzene and Diethyl ether were pre-dried over sodium wire before being refluxed over molten potassium for a minimum of 2 days and were stored over activated 4Å molecular sieves before use. Toluene and Pentane were collected from an Innovative Technology Solvent Purification System and stored over activated 4Å molecular sieves for 5 days before use. All commercially purchased chemicals were used as received with the exception of PCl_3 and SO_2Cl_2 which were both distilled under dinitrogen before use.

Elemental Analysis

All CHN elemental analyses were performed by Stephen Boyer at the London Metropolitan University.

NMR

Benzene-d_6 was refluxed over molten potassium and stored over activated 4Å molecular sieves for 5 days before use. All NMR spectra were recorded on a Bruker Avance III 400MHz spectrometer operating at a temperature of 298 K (unless otherwise stated) and frequencies of 400.13 MHz (^{1}H), 100.61 MHz (^{13}C), 161.97 MHz (^{31}P) and 155.51MHz

(^{7}Li). Paramagnetic NMR spectra were recorded over a -200 to + 200ppm sweep range in order to obtain the full spectrum for each compound.

EPR

All Q-band EPR spectra were measured on a Bruker EMX spectrometer. The resulting spectra were simulated using SIM EPR software [117] with the parameters reported.

SQUID

Magnetic measurements were performed on a Quantum Design MPMS XL SQUID magnetometer on polycrystalline samples

Single Crystal X-ray Crystallography

All crystallographic studies were carried out using an Oxford Diffraction XCalibur2 instrument with the exception of $[CoLi_7(\mu_8\text{-}O)(\mu\text{-}hpp)_6]^+$ $[\{Li\mu\text{-}N(SiMe_3)_2\}_5(\mu_5\text{-}Cl)]^-$ which was collected on a Bruker APEX2 instrument. Data were collected at 100(2) K, and molybdenum radiation (λ = 0.71073 Å) was used in each case except for $[CoLi_7(\mu_8\text{-}O)(\mu\text{-}hpp)_6]^+$ $[\{Li\mu\text{-}N(SiMe_3)_2\}_5(\mu_5\text{-}Cl)]^-$, for which copper radiation (λ = 1.53740 Å) was used. Full-matrix least-squares on $F^2$was used to refine all structures. All refinements were processed in SHELX [118] software with some initial solutions being produced by using the superflip [119] program before being further processed in SHELX.

Crystal data for [{Gd(N(SiMe$_3$)$_2$)(μ_2-SEt)$_2$}$_4$(μ_3-SEt)][Li(THF)$_4$]·C$_6$H$_5$CH$_3$

Empirical formula	$Gd_4S_9Si_8O_4N_4LiC_{65}H_{157}$	
Formula weight	2208.218	
Temperature	100K	
Wavelength	0.71073 Å	
Crystal system	monoclinic	
Space group	$P2_{1/c}$	
Unit cell dimensions	a = 14.8693(5)Å	alpha = 90°
	b = 25.4713(8)Å	beta = 91.684(3)°
	c = 26.6193(10) Å	gamma = 90°
Volume	10077.5(6) Å^3	
Z	1	
Density (calculated)	1.455 Mg/m^3	
Absorption coefficient	2.918 mm^{-1}	
F(000)	4488	
Crystal size	0.40 × 0.40 × 0.30 mm	
Range for data collection	2.86-27.82°	
Limiting indices	–14 < h < 14, –25 < k < 22, –26 < l < 26	
Reflections collected	22657	
Independent reflections	11862 (Rint = 0.0491)	
Completeness to full theta	99.7 %	
Data / restraints / parameters	10523 / 961 / 826	
Goodness-of-fit on F^2	1.020	
Final R indices [I>2σ(I)]	R_1 = 0.1066, wR_2 = 0.2400	
R indices (all data)	R_1 = 0.1321, wR_2 = 0.2683	
Largest diff. peak and hole	2.743 and –2.039 Å^3	

Crystal data for [{Tb(N(SiMe$_3$)$_2$)(μ_2-SEt)$_2$}$_4$(μ_3-SEt)][Li(THF)$_4$]·C$_6$H$_5$CH$_3$

Empirical formula	$Tb_4S_9Si_8O_4N_4LiC_{65}H_{157}$	
Formula weight	2214.918	
Temperature	100K	
Wavelength	0.71073 Å	
Crystal system	monoclinic	
Space group	$P2_{1/c}$	
Unit cell dimensions	a = 14.8088(8) Å	alpha = 90°
	b = 25.4578(11) Å	beta = 91.718(4)°
	c = 26.2490(13) Å	gamma = 90°
Volume	9959.2(8) Å^3	
Z	1	
Density (calculated)	1.477 Mg/m^3	
Absorption coefficient	3.130 mm^{-1}	
F(000)	4504	
Crystal size	0.50 × 0.40 × 0.40 mm	
Range for data collection	2.86 to 26.37°	
Limiting indices	–18 < h < 18, –31 < k < 31, –32 < l < 32	
Reflections collected	20352	
Independent reflections	10647 (Rint = 0.2392)	
Completeness to full theta	99.9 %	
Data / restraints / parameters	20352 / 949 / 841	
Goodness-of-fit on F^2	0.797	
Final R indices [I>2σ(I)]	R_1 = 0.0638, wR_2 = 0.1477	
R indices (all data)	R_1 = 0.1848, wR_2 = 0.1778	
Largest diff. peak and hole	1.675 and –1.581 Å^3	

Crystal data for [{Dy(N(SiMe$_3$)$_2$)(μ_2-SEt)$_2$}$_4$(μ_3-SEt)][Li(THF)$_4$]·C$_6$H$_5$CH$_3$

Empirical formula	$Dy_4S_9Si_8O_4N_4LiC_{65}H_{157}$	
Formula weight	2229.218	
Temperature	100K	
Wavelength	0.71073 Å	
Crystal system	monoclinic	
Space group	$P2_{1/c}$	
Unit cell dimensions	a = 14.8449(5) Å	alpha = 90°
	b = 25.4878(7) Å	beta = 91.760(3)°
	c = 26.2581(9) Å	gamma = 90°
Volume	9930.4(5) Å^3	
Z	1	
Density (calculated)	1.491 Mg/m^3	
Absorption coefficient	3.300 mm^{-1}	
F(000)	4520	
Crystal size	0.50 × 0.40 × 0.35 mm	
Range for data collection	2.99 to 26.37°	
Limiting indices	–18 < h < 9, –31 < k < 31, –29 < l < 32	
Reflections collected	20281	
Independent reflections	12697 (Rint = 0.1012)	
Completeness to full theta	99.8 %	
Data / restraints / parameters	20281 / 1131 / 844	
Goodness-of-fit on F^2	1.056	
Final R indices [I>2σ(I)]	R_1 = 0.0864, wR_2 = 0.1937	
R indices (all data)	R_1 = 0.1468, wR_2 = 0.2346	
Largest diff. peak and hole	2.516 and –2.188 Å^3	

Crystal data for $[Dy(TMP)_2(\mu\text{-}OEt)]_2$

Empirical formula	$Dy_2O_2N_4C_{40}H_{82}$	
Formula weight	976.122	
Temperature	100K	
Wavelength	0.71073 Å	
Crystal system	monoclinic	
Space group	$P2_1/c$	
Unit cell dimensions	a = 13.3295(4) Å	alpha = 90°
	b = 11.3302(3) Å	beta = 105.319(3)°
	c = 14.6243(4) Å	gamma = 90°
Volume	2130.17(10)Å^3	
Z	2	
Density (calculated)	1.522 Mg/m^3	
Absorption coefficient	3.517 mm^{-1}	
F(000)	996	
Crystal size	0.50 × 0.50 × 0.40 mm	
Range for data collection	3.01 to 27.50°	
Limiting indices	–16 < h < 14, –14 < k < 14, –18 < l < 18	
Reflections collected	4763	
Independent reflections	3145 (Rint = 0.0276)	
Completeness to full theta	97.3 %	
Data / restraints / parameters	4763 / 0 / 217	
Goodness-of-fit on F^2	1.076	
Final R indices [I>2σ(I)]	R_1 = 0.0192, wR_2 = 0.0448	
R indices (all data)	R_1 = 0.0348, wR_2 = 0.0469	
Largest diff. peak and hole	1.228 and –0.667 Å^3	

Crystal data for $[Yb(TMP)_2(\mu\text{-}OEt)]_2$

Empirical formula	$Yb_2O_2N_4C_{40}H_{82}$	
Formula weight	997.202	
Temperature	100K	
Wavelength	0.71073 Å	
Crystal system	monoclinic	
Space group	*C2/c*	
Unit cell dimensions	a = 26.2052(14)Å	alpha = 90°
	b = 11.2400(5) Å	beta = 105.454(5)°
	c = 14.8714(7) Å	gamma = 90°
Volume	4221.9(4) $Å^3$	
Z	1	
Density (calculated)	1.559 Mg/m^3	
Absorption coefficient	4.439 mm^{-1}	
F(000)	2000	
Crystal size	0.50 × 0.40 × 0.40 mm	
Range for data collection	3.02 to 28.69°	
Limiting indices	–33 < h < 24, –14 < k < 13, –19 < l < 18	
Reflections collected	5345	
Independent reflections	5147 (Rint =0.0378)	
Completeness to full theta	98.1%	
Data / restraints / parameters	5345 / 0 / 217	
Goodness-of-fit on F^2	1.045	
Final R indices [I>2σ(I)]	R_1 = 0.0428, wR_2 = 0.1112	
R indices (all data)	R_1 = 0.0520, wR_2 = 0.1153	
Largest diff. peak and hole	5.182 and –1.965 $Å^3$	

Crystal data for [(η^5-Cp)Mn(μ-L^1H_2)]$_2$

Empirical formula	$C_{34}H_{70}Mn_2N_8P_2Si_2$	
Formula weight	818.98	
Temperature	100K	
Wavelength	0.71073 Å	
Crystal system	triclinic	
Space group	*P*–1	
Unit cell dimensions	a = 10.4186(12) Å	alpha = 91.861(9)°
	b = 10.8372(12) Å	beta = 98.026(9)°
	c = 10.9199(12) Å	gamma = 115.271(11)°
Volume	1098.2(2) Å^3	
Z	2	
Density (calculated)	1.238 Mg/m^3	
Absorption coefficient	0.735 mm^{-1}	
F(000)	438	
Crystal size	0.21 × 0.15 × 0.10 mm	
Range for data collection	2.95 to 28.51°	
Limiting indices	–8 < h < 13, –13 < k < 13, –12 < l < 13	
Reflections collected	4717	
Independent reflections	2079 (Rint = 0.2308)	
Completeness to full theta	98.5 %	
Data / restraints / parameters	4717 / 0 / 223	
Goodness-of-fit on F^2	0.777	
Final R indices [I>2σ(I)]	R_1 = 0.0548, wR_2 = 0.1099	
R indices (all data)	R_1 = 0.1343, wR_2 = 0.1365	
Largest diff. peak and hole	0.593 and –0.448 Å^3	

Crystal data for $[Mn(L^2H_2)_2]\cdot thf$

Empirical formula	$C_{42}H_{88}MnN_8P_2Si_2$	
Formula weight	878.28	
Temperature	100K	
Wavelength	0.71073 Å	
Crystal system	monoclinic	
Space group	*C*2/*c*	
Unit cell dimensions	a = 24.6619(11) Å	alpha = 90°
	b = 10.9942(4) Å	beta = 90.494(4)°
	c = 21.8157(9) Å	gamma = 90°
Volume	5914.8(4)Å^3	
Z	1	
Density (calculated)	1.130Mg/m^3	
Absorption coefficient	0.359 mm^{-1}	
F(000)	2172	
Crystal size	0.33 × 0.30 × 0.15 mm	
Range for data collection	3.09 to 27.50°	
Limiting indices	–30 < h < 32, –14 < k < 12, –28 < l < 27	
Reflections collected	6611	
Independent reflections	4680 (Rint = 0.0559)	
Completeness to full theta	97.2 %	
Data / restraints / parameters	6611 / 0 / 289	
Goodness-of-fit on F^2	1.033	
Final R indices [I>2σ(I)]	R_1 = 0.0669, wR_2 = 0.1679	
R indices (all data)	R_1 = 0.0904, wR_2 = 0.1747	
Largest diff. peak and hole	1.108 and –0.580 Å^3	

Crystal data for [(η^5-Cp)Mn(L^3H_2)]

Empirical formula	$C_{20}H_{43}MnN_4PSi$
Formula weight	453.58
Temperature	100K
Wavelength	0.71073 Å
Crystal system	orthorhombic
Space group	*Pmmn*
Unit cell dimensions	a = 11.366(2) Å alpha = 90°
	b = 11.833(3) Å beta = 90°
	c = 9.4828(13) Å gamma = 90°
Volume	1275.4(4) $Å^3$
Z	2
Density (calculated)	1.181 Mg/m^3
Absorption coefficient	0.639 mm^{-1}
F(000)	490
Crystal size	0.30 × 0.20 × 0.20 mm
Range for data collection	3.29 to 25.02°
Limiting indices	–13 < h < 12, –10 < k < 14, –7 < l < 11
Reflections collected	2986
Independent reflections	1252 (Rint = 0.0585)
Completeness to full theta	99.7%
Data / restraints / parameters	1252 / 184 / 121
Goodness-of-fit on F^2	1.054
Final R indices [I>2σ(I)]	R_1 = 0.0640, wR_2 = 0.1561
R indices (all data)	R_1 = 0.0928, wR_2 = 0.1776
Largest diff. peak and hole	0.469 and –0.546 $Å^3$

Crystal data for [Li_3(μ-N($SiMe_3$)$_2$)$_2$(μ-hpp)]

Empirical formula	$C_{19}H_{48}Li_3N_5Si_4$	
Formula weight	479.80	
Temperature	100K	
Wavelength	0.71073 Å	
Crystal system	tetragonal	
Space group	$P4_2bc$	
Unit cell dimensions	a = 16.4053(3) Å	alpha = 90°
	b = 16.4053(3) Å	beta = 90°
	c = 21.4837(10) Å	gamma = 90°
Volume	5781.99(31) $Å^3$	
Z	8	
Density (calculated)	1.102 Mg/m^3	
Absorption coefficient	0.220 mm^{-1}	
F(000)	2096	
Crystal size	0.18 x 0.23 x 0.24 mm^3	
Range for data collection	3.12 to 28.66°	
Limiting indices	–18 < h < 21, –16 < k < 21, –28 < l < 10	
Reflections collected	12200	
Independent reflections	4177 (Rint = 0.0397)	
Completeness to full theta	89.6 %	
Data / restraints / parameters	4177 / 12 / 297	
Goodness-of-fit on F^2	0.995	
Final R indices [I>2σ(I)]	R_1 = 0.0393, wR_2 = 0.0989	
R indices (all data)	R_1 = 0.0551, wR_2 = 0.1060	
Largest diff. peak and hole	0.539 and –0.221 $eÅ^3$	

Crystal data for [$CoLi_7(\mu_8$-O)(μ-hpp)$_6$][{Liμ-N($SiMe_3$)$_2$}$_5$(μ_5-Cl)]

Empirical formula	$C_{86}H_{178}ClLi_{12}CoN_{23}OSi_{10}$	
Formula weight	1824.81	
Temperature	100K	
Wavelength	1.53740 Å	
Crystal system	monoclinic	
Space group	*C*2/*c*	
Unit cell dimensions	a = 20.1006(4) Å	alpha = 90°
	b = 24.5598(4) Å	beta = 105.786(2)°
	c = 24.9957(5) Å	gamma = 90°
Volume	11874.2(4) $Å^3$	
Z	2	
Density (calculated)	1.021 Mg/m^3	
Absorption coefficient	2.679 mm^{-1}	
F(000)	3932	
Crystal size	0.44 x 0.22 x 0.14 mm	
Range for data collection	3.09 to76.56°	
Limiting indices	–24 < h < 24, –30 < k < 29, –31 < l < 29	
Reflections collected	43649	
Independent reflections	12325 (Rint = 0.0293)	
Completeness to full theta	99.8%	
Data / restraints / parameters	12.325 / 0 / 604	
Goodness-of-fit on F^2	1.091	
Final R indices [I>2σ(I)]	R_1 = 0.0629, wR_2 = 0.1746	
R indices (all data)	R_1 = 0.0653, wR_2 = 0.1763	
Largest diff. peak and hole	0.639 and –0.481 $eÅ^3$	

Crystal data for $[MnLi_7(\mu_8\text{-}O)(\mu\text{-}hpp)_6][\{Li\mu\text{-}N(SiMe_3)_2\}_5(\mu_5\text{-}Cl)]$

Empirical formula	$C_{86}H_{178}ClLi_{12}MnN_{23}OSi_{10}$	
Formula weight	1988.96	
Temperature	100K	
Wavelength	0.71073 Å	
Crystal system	monoclinic	
Space group	*C*2/*c*	
Unit cell dimensions	a = 20.1096(12) Å	alpha = 90°
	b = 24.4769(15) Å	beta =105.769(6)°
	c = 24.9736(17) Å	gamma = 90°
Volume	11829.9(13) $Å^3$	
Z	4	
Density (calculated)	1.117 Mg/m^3	
Absorption coefficient	0.284 mm^{-1}	
F(000)	4260	
Crystal size	0.20 x 0.10 x 0.10 mm	
Range for data collection	2.92 to 24.04°	
Limiting indices	–22 < h < 21, –26 < k < 27, –25 < l < 18	
Reflections collected	21119	
Independent reflections	7548 (Rint = 0.0906)	
Completeness to theta = 21°	99.7 %	
Data / restraints / parameters	5784 / 0 / 617	
Goodness-of-fit on F^2	1.040	
Final R indices [I>2σ(I)]	R_1 = 0.0857, wR_2 = 0.1979	
R indices (all data)	R_1 = 0.1783, wR_2 = 0.2215	
Largest diff. peak and hole	0.491 and –0.273 $eÅ^3$	

Crystal data for $[ZnLi_7(\mu_8\text{-}O)(\mu\text{-}hpp)_6][Zn\{N(SiMe_3)_2\}_3]$

Empirical formula	$C_{60}H_{126}Li_7N_{21}OSi_6Zn_2$	
Formula weight	1505.70	
Temperature	100K	
Wavelength	0.71073 Å	
Crystal system	orthorhombic	
Space group	*Pba*2	
Unit cell dimensions	a = 27.7860(13) Å	alpha = 90°
	b = 24.4230(11) Å	beta = 90°
	c = 12.1310(7) Å	gamma = 90°
Volume	8232.3(7) $Å^3$	
Z	4	
Density (calculated)	1.155 Mg/m^3	
Absorption coefficient	0.720 mm^{-1}	
F(000)	3224	
Crystal size	0.10 x 0.10 x 0.05 mm	
Range for data collection	2.89 to 23.25°	
Limiting indices	$-30 < h < 22$, $-25 < k < 25$, $-12 < l < 13$	
Reflections collected	33772	
Independent reflections	10107 (Rint = 0.1008)	
Completeness to theta = 23.25°	94.5 %	
Data / restraints / parameters	10107 / 199 / 937	
Goodness-of-fit on F^2	0.876	
Final R indices [I>2σ(I)]	$R_1 = 0.0481$, $wR_2 = 0.1150$	
R indices (all data)	$R_1 = 0.1317$, $wR_2 = 0.1268$	
Largest diff. peak and hole	0.380 and –0.232 $eÅ^3$	

Chapter 10: References

1. a) Ishikawa, N.; Sugita, M.; Ishikawa, T.; Koshihara, S.; Kaizu, Y.; Lanthanide Double-Decker Complexes Functioning as Magnets at the Single-Molecular Level. *J. Am. Chem. Soc.*, **2003**, *125*, 8694 – 8695 b) Ishikawa, N.; Sugita, M.; Ishikawa, T.; Koshihara, S.; Kaizu, Y.; Mononuclear Lanthanide Complexes with a Long Magnetization Relaxation Time at High Temperatures: A New Category of Magnets at the Single-Molecular Level. *J. Phys. Chem. B,***2004**, *108*, 11265 – 11271 c) Branzoli, F.; Carretta, P.; Filibian, M.; Zoppellaro, G.; Graf, M. J.; Galan-Mascaros, J. R.; Fuhr, O.; Brink, S.; Ruben. M.; Spin Dynamics in the Negatively Charged Terbium (III) Bis-phthalocyaninato Complex. *J. Am. Chem. Soc.*, **2009**, *131*, 4387 – 4396

2. Takamatsu, S.; Ishikawa, T.; Koshihara, S.; Ishikawa, N.; Significant Increase of the Barrier Energy for Magnetization Reversal of a Single-4f-Ionic Single-Molecule Magnet by a Longitudinal Contraction of the Coordination Space. *Inorg. Chem.*, **2007**, *46*, 7250 – 7252

3. Rinehart, J. D.; Fang, M.; Evans, W. J.; Long, J. R.; A N_2^{3-} Radical-Bridged Terbium Complex Exhibiting Magnetic Hysteresis at 14 K. *J. Am. Chem. Soc.*, **2011**, *133*, 14236 – 14239

4. Kajiwara, T.; Hasegawa, M.; Ishii, A.; Katagiri, K.; Baatar, M.; Takaishi, S.; Iki, N.; Yamashita, M.; Highly Luminescent Superparamagnetic Diterbium(III) Complex Based on the Bifunctionality of *p-tert*-Butylsulfonylcalix[4]arene. *Eur. J. Inorg. Chem.*, **2008**, 5565 – 5568

5. a) AlDamen, M. A.; Cardona-Serra, S.; Clemente-Juan, J. M.; Coronado, E.; Gaita-Arino, A.; Martı-Gastaldo, C.; Luis, F.; Montero, O.; Mononuclear Lanthanide Single Molecule Magnets Based on the Polyoxometalates b) AlDamen, M. A.; Clemente-Juan, J. M.;

Coronado, E.; Martı´-Gastaldo, C.; Gaita-Arin˜o, A.; Mononuclear Lanthanide Single-Molecule Magnets Based on Polyoxometalates. *J. Am. Chem. Soc.*, **2008**, *130*, 8874 – 8875 $[Ln(W_5O_{18})_2]^{9-}$ and $[Ln(\beta_2\text{-}SiW_{11}O_{39})_2]^{13-}$ (Ln^{III}) Tb, Dy, Ho, Er, Tm, and Yb). *Inorg. Chem.*, **2009**, *48*, 3467 – 3479

6. a) Waters, M.; Moro, F.; Krivokapic, I.; McMastera, J.; van Slageren, J.; Synthesis, characterisation and magnetic study of a cyano-substituted dysprosium double decker single-molecule magnet. *Dalton Trans.*, **2012**, *41*, 1128 – 1130 b) Katoh, K.; Umetsu, K.; Breedlove, B. K.; Yamashita, M.; Magnetic relaxation behavior of a spatially closed dysprosium(III) phthalocyaninato double-decker complex. *Sci. China Chem.*, **2012**, *55*, 918 – 925 c) Gonidec, M.; Luis, F.; Vilchez, A.; Esquena, J.; Amabilino, D. B.; Veciana, J.; A Liquid-Crystalline Single-Molecule Magnet with Variable Magnetic Properties. *Angew. Chem. Int. Ed.*, **2010**, *49*, 1623 – 1626 b) Ishikawa, N.; Mizuno, Y.; Takamatsu, S.; Ishikawa, T.; Koshihara, S.; Effects of Chemically Induced Contraction of a Coordination Polyhedron on the Dynamical Magnetism of Bis(phthalocyaninato)disprosium, a Single-4f-Ionic Single-Molecule Magnet with a Kramers Ground State. *Inorg. Chem.*, **2008**, *47*, 10217 – 10219

7. a) Anwar, M. U.; Thompson, L. K.; Dawe, L. N.; Habibb, F.; Murugesub, M.; Predictable self-assembled [2×2] $Ln(III)_4$ square grids (Ln = Dy, Tb) – SMM behavior in a new lanthanide cluster motif. *Chem. Commun.*, **2012**, *48*, 4576 – 4578 b) Long, J.; Habib, F.; Lin, P.; Korobkov, I.; Enright, G.; Ungur, L.; Wernsdorfer, W.; Chibotaru, L. F.; Murugesu, M.; Single-Molecule Magnet Behavior for an Antiferromagnetically Superexchange-Coupled Dinuclear Dysprosium(III) Complex. *J. Am. Chem. Soc.*, **2011**, *133*, 5319 – 5328

8. a) Lin, P.; Burchell, T. J.; Ungur, L.; Chibotaru, L. F.; Wernsdorfer, W.; Murugesu, M.; A Polynuclear Lanthanide Single-Molecule Magnet with a Record Anistropic Barrier. *Angew. Chem. Int. Ed.*, **2009**, *48*, 9489 – 9492 b) Hussain, B.; Savard, D.; Burchell, T. J.; Wernsdorfer. W.; Murugesu, M.; Linking high anisotropy Dy_3 triangles to create a Dy6 single-molecule magnet. *Chem. Commun.*, **2009**, *45*, 1100 – 1102

9. Tuna, F.; Smith, C. A.; Bodensteiner, M.; Ungur, L.; Chibotaru, L. F.; McInnes, E. J. L.; Winpenny, R. E. P.; Collison, D.; Layfield, R. A.; A High Anisotropy Barrier in a Sulfur-Bridged OrganodysprosiumSingle-Molecule Magnet. *Angew. Chem. Int. Ed.*, **2012**, *51*, 6976 – 6980

10. Rinehart, J. D.; Fang, M.; Evans, W. J.; Long, J. R.; Strong exchange and magnetic blocking in N_2^{3-}-radical-bridged lanthanide complexes. *Nat. Chem.*, **2011**, *3*, 538 – 542

11. a) Milios, C. J. Inglis, R.; Vinslava, A.; Bagai, R.; Wernsdorfer, W.; Parsons, S.; Perlepes, S. P.; Christou, G.; Brechin, E. K.; Toward a Magnetostructural Correlation for a Family of Mn_6 SMMs. *J. Am. Chem. Soc.*, **2007**, *129*, 12505 – 12511 b) Milios, C. J.; Vinslava, A.; Wernsdorfer, W.; Moggach, S.; Parsons, S.; Perlepes, S. P.; Christou, G.; Brechin, E. K.; A Record Anisotropy Barrier for a Single-Molecule Magnet. *J. Am. Chem. Soc.*, **2007**, *129*, 2754 – 2755

12. Rinehart, J. D.; Long, J. R.; Exploiting single-ion anisotropy in the design of f-element single-molecule magnets. *Chem. Sci.*, **2011**, *2*, 2078 – 2085

13. Bencini, A.; Benelli, C.; Caneschi, A.; Carlin, R. L.; Dei, A.; Gatteschi, D.; Crystal and molecular structure of and magnetic coupling in two complexes containing gadolinium(III) and copper(II) ions. *J. Am. Chem. Soc.*, 1985, *107*, 8128–8136

14. a) Guillou, O.; Bergerat, P.; Kahn, O.; Bakalbassis, E.; Boubekeur, K.; Batail, P.; Guillot, M.; Ferromagnetically coupled gadolinium(III)copper(II) molecular material. *Inorg. Chem.*, 1992, *31*, 110 –114 b) Thomas, L.; Lionti, F.; Ballou, R.; Gatteschi, D.; Sessoli, R.; Barbara, B.; Macroscopicquantum tunneling of magnetization in a single crystal of nanomagnets. *Nature*, **1996**, *383*,145 – 147

15. Benelli, C.; Caneschi, A.; Gatteschi, D.; Sessoli, R.; Magnetic ordering in a molecular material containing dysprosium(III) and a nitronyl nitroxide.*Adv. Mater.*, **1992**, *4*, 504–505.

16. a) Katoha, K.; Isshiki, H.; Komedab, T.; Yamashitaa, M.; Multiple-decker phthalocyaninato Tb(III) single-molecule magnets and Y(III) complexes for next generation devices. *Coord. Chem. Rev.*, **2011**, *255*, 2124 – 2148 b) Sessoli, R.; Powell, A. K.; Stratergies towards single molecule magnets based on lanthanide ions. *Coord. Chem. Rev.*, **2009**, *253*, 2328 – 2341 c) Sorace, L.; Benellib, C.; Gatteschi, D.; Lanthanides in molecular magnetism: old tools in a new field. *Chem. Soc. Rev.*, **2011**, *40*, 3092 – 3104 d) Nakano, M.; Oshio, H.; Magnetic anisotropies in paramagnetic polynuclear metal complexes. *Chem. Soc. Rev.*, **2011**, *40*, 3239 – 3248 e) Aromi, G.; Aguila, D.; Gamez, P.; Luis, F.; Roubeau, O.; Design of magnetic coordination complexes for quantum computing. *Chem. Soc. Rev.*, **2012**, *41*, 537 – 546

17. Ishikawa, N.; Sugita, M.; Tanaka, N.; Ishikawa, T.; Koshihara, S.; Kaizu, Y.; Upward Temperature Shift of the Intrinsic Phase Lag of the Magnetization of Bis(phthalocyaninato)terbium by Ligand Oxidation Creating an S = ½ Spin. *Inorg. Chem.*, **2004**, *43*, 5498 – 5500

18. Wang, H.; Wang, K.; Tao, J.; Jiang, J.; Twist angle perturbation on mixed (phthalocyaninato)(porphyrinato) dysprosium(III) double-decker SMMs. *Chem. Commun.*, **2012**, *24*, 2973 – 2975

19. a) Ishikawa, N.; Sugita, M.; Okubo, T.; Tanaka, N.; Iino, T.; Kaizu, Y.; Determination of Ligand-Field Parameters and f-Electronic Structures of Double-Decker Bis(phthalocyaninato)lanthanide Complexes. *Inorg. Chem.*, **2003**, *42*, 2440 – 2446 b) Ishikawa, N.; Determination of Ligand-Field Parameters and f-Electronic Structures of Hetero-Dinuclear Phthalocyanine Complexes with a Diamagnetic Yttrium(III) and a Paramagnetic Trivalent Lanthanide Ion. *J. Phys. Chem. A*, **2002**, *106*, 9543 – 9550 c) Ishikawa, N.; Iino, T.; Kaizu, Y.; Interaction between f-Electronic Systems in Dinuclear Lanthanide Complexes with Phthalocyanines.*J. Am. Chem. Soc.*, **2002**, *124*, 11440 – 11447

20. a) Ishikawa, N.; Ohno, O.; Kaizu, Y.; Kobayashi, H.; Localized orbital study on the electronic structure of phthalocyanine dimers. *J. Phys. Chem.*,**1992**, *96*, 8832 – 8839 b) Ishikawa, N.; Ohno, O.; Kaizu, Y.; Electronic states of bis(phthalocyaninato)lutetium radical and its related compounds: the application of localized orbital basis set to open-shell phthalocyanine dimers. *J. Phys. Chem.*,**1993**, *97*, 1004 – 1010

21. Williams, U. J.; Mahoney, B. D.; DeGregorio, P. T.; Carroll, P. J.; Nakamaru-Ogiso, E.; Kikkawac, J. M.; Schelter, E. J.; A comparison of the effects of symmetry and magnetoanisotropy on paramagnetic relaxation in related dysprosium single ion magnets. *Chem. Commun.*, **2012**, *48*, 5593 – 5595

22. Jiang, S.; Wang, B.; Su, G.; Wang, Z. Gao, S.; A Mononuclear Dysprosium Complex Featuring Single-Molecule-Magnet Behaviour., *Angew Chem. Int. Ed.*, **2010**, *49*, 7448 – 7451

23. Bi, Y.; Guo, Y.; Zhao, L.; Guo, Y.; Lin, S.; Jiang, S.; Tang, J.; Wang, B.; Gao, S.; Capping Ligand Perturbed Slow Magnetic Relaxation in Dysprosium Single-Ion Magnets. *Chem. Eur. J.*, **2011**, *17*, 12476 – 12481

24. Chen, G.; Gao, C.; Tian, J.; Tang, J.; Gu, W.; Liu, X.; Yan, S.; Liao, D.; Cheng, P.; Coordination-perturbed single-molecule magnet behaviour of mononuclear dysprosium complexes. *Dalton Trans.*, **2011**, *40*, 5579 – 5583

25. Li, D.; Zhang, X.; Wang, T.; Ma, B.; Li, C.; Li, Y.; You, X.; Distinct magnetic dynamic behavior for two polymorphs of the same Dy(III) complex. *Chem. Commun.*, **2011**, *47*, 6867 – 6869

26. Li, D.; Wang, T.; Li, C.; Liu, D.; Li, Y.; You, X.; Single-ion magnets based on mononuclear lanthanide complexes with chiral Schiff base ligands [Ln(FTA)$_3$L} (Ln = Sm, Eu, Gd, Tb and Dy). *Chem. Commun.*, **2010**, *46*, 2929 – 2931

27. Wang, Y.; Li, X.; Wang, T.; Song, Y.; You, X.; Slow Relaxation Processes and Single-Ion Magnetic Behaviors in Dysprosium-Containing Complexes. *Inorg. Chem.*, **2010**, *49*, 969 – 976

28. Sugita, M.; Ishikawa, N.; Ishikawa, T.; Koshihara, S.; Kaizu, Y.; Static Magnetic-Field-Induced Phase Lag in the Magnetization Response of Tris(dipicolinato)lanthanides. *Inorg. Chem.*, **2006**, *45*, 1299 – 1304

29. a) Car, P.; Perfetti, M.; Mannini, M.; Favre, A.; Caneschi, A.; Sessoli, R.; Giant field dependence of the low temperature relaxation of the magnetization in a dysprosium(III)-DOTA complex. *Chem. Commun.*, **2011**, *47*, 3751 – 3753 b) Cucinotta, G.; Perfetti, M.;

Luzon, J.; Etienne, M.; Car, P.; Caneschi, A.; Calvez, G.; Bernot, K.; Sessoli, R.; Magnetic Anisotropy in a Dysprosium/DOTA Single-Molecule Magnet: Beyond Simple Magneto-Structural Correlations. *Angew. Chem. Int. Ed.*, **2012**, *51*, 1606 – 1611

30. Bhunia, A.; Gamer, M. T.; Ungur, L.; Chibotaru, L. F.; Powell, A. K.; Lan, Y.; Roesky, P. W.; Menges, F.; Riehn, C.; Niedner-Schatteburg, G.; From a Dy(III) Single Molecule Magnet (SMM) to a Ferromagnetic [Mn(II)Dy(III)Mn(II)] Trinuclear Complex. Inorg. Chem., 2012, 51, Article ASAP

31. Jeletic, M.; Lin, P.; Le Roy, J. J.; Korobkov, I.; Gorelsky, S. I.; Murugesu, M.; An Organometallic Sandwich Lanthanide Single-Ion Magnet with an Unusual Multiple Relaxation Mechanism. *J. Am. Chem. Soc.*, **2011**, *133*, 19286 – 19289

32. a) Jiang, S.; Liu, S.; Zhou, L.; Wang, B.; Wang, Z.; Gao, S.; Series of Lanthanide Organometallic Single-Ion Magnets. *Inorg. Chem.*, **2012**, *51*, 3079 – 3087 b) Jiang, S.; Wang, B.; Sun, H.; Wang, Z.; Gao, S.; An Organometallic Single-Ion Magnet. J. Am. Chem. Soc., 2011, 133, 4730 – 4733

33. a) Zhou, N.; Ma, Y.; Wang, C.; Xu, G. F.; Tang, J.; Xu, J.; Yan, S.; Cheng, P.; Li, L.; Liao, D.; A monometallic tri-spin single-molecule magnet based on rare earth radicals. *Dalton Trans.*, **2009**, *38*, 8489 – 8492 b) Wang, X.; Bao, X.; Xu, P.; Li, L.; From Discrete Molecule to One-Dimension Chain: Two New Nitronyl Nitroxide–Lanthanide Complexes Exhibiting Slow Magnetic Relaxation. *Eur. J. Inorg. Chem.*, **2011**, 3586 – 3591 c) Wang, X.; Li, L.; Liao, D.; Slow Magnetic Relaxation in Lanthanide Complexes with Chelating Nitronyl Nitroxide Radical. *Inorg. Chem.*, **2010**, *49*, 4735 – 4737 d) Coronado, E.; Gimenez-Saiz, C.; Recuenco, A.; Tarazon, A.; Romero, F. M.; Camon, A.; Luis, F.; Single-Molecule

Magnetic Behavior in a Neutral Terbium(III) Complex of a Picolinate-Based Nitronyl Nitroxide Free Radical. *Inorg. Chem.*, **2011**, *50*, 7370 – 7372 e) Mei, X.; Ma, Y.; Li, L.; Liao, D.; Ligand field-tuned single-molecule magnet behaviour of 2p–4f complexes. *Dalton Trans.*, **2012**, *41*, 505 – 511

34. Lopez, N.; Prosvirin, A. V.; Zhao, H.; Wernsdorfer, W.; Dunbar, K. R.; Heterospin Single-Molecule Magnets Based on Terbium Ions and TCNQF4 Radicals: Interplay between Single-Molecule Magnet and Phonon Bottleneck Phenomena Investigated by Dilution Studies. *Chem. Eur. J.*, **2009**, *15*, 11390 – 11400

35. Wang, X.; Tian, H.; Ma, Y.; Yang, P.; Li, L.; Liao, D.; Slow magnetic relaxation in lanthanide complexes with chelating imino nitroxide radicals. *Inorg. Chem. Comm.*, **2011**, *14*, 1728 – 1731

36. Katoh, K.; Kajiwara, T.; Nakano, M.; Nakazawa, Y.; Wernsdorfer, W.; Ishikawa, N.; Breedlove, B. K.; Yamashita, M.; Magnetic Relaxation of Single-Molecule Magnets in an External Magnetic Field: An Ising Dimer of a Terbium(III)-Phthalocyaninate Triple-Decker Complex. *Chem. Eur. J.*, **2011**, *17*, 117 – 122

37. Sakaue, S.; Fuyuhiro, A.; Fukuda, T.; Ishikawa, N.; Dinuclear single-molecule magnets with porphyrin–phthalocyanine mixed triple-decker ligand systems giving SAP and SP coordination polyhedral. *Chem. Commun.*, **2012**, *48*, 5337 – 5339

38. Ishikawa, N.; Otsuka, S.; Kaizu, Y.; The Effect of the f-f Interaction on the Dynamic Magnetism of a Coupled $4f^8$ System in a Dinuclear Terbium Complex with Phthalocyanines. *Angew. Chem. Int. Ed.*, **2005**, *44*, 731 – 733

39. Guo, Y.; Xu, G.; Wernsdorfer, W.; Ungur, L.; Guo, Y.; Tang, J.; Zhang, H.; Chibotaru, L. F.; Powell, A. K.; Strong Axiality and Ising Exchange Interaction Suppress Zero-Field Tunneling of Magnetization of an Asymmetric Dy_2 Single-Molecule Magnet. *J. Am. Chem. Soc.*, **2011**, *133*, 11948 – 11951

40. Guo, Y.; Chen, X.; Xue, S.; Tang, J.; Modulating Magnetic Dynamics of Three Dy_2 Complexes through Keto-Enol Tautomerism of the o-Vanillin Picolinoylhydrazone Ligand. *Inorg. Chem.*, **2011**, *50*, 9705 – 9713

41. Habib, F.; Long, J.; Lin, P.; Korobkov, I.; Ungur, L.; Wernsdorfer, W.; Chibotaruc, L. F.; Murugesu, M.; Supramolecular architectures for controlling slow magnetic relaxation in field-induced single-molecule magnets. *Chem. Sci.*, **2012**, *3*, 2158 – 2164

42. Zou, L.; Zhao, L.; Chen, P.; Guo, Y.; Guo, Y.; Lib, Y.; Tang, J.; Phenoxido and alkoxido-bridged dinuclear dysprosium complexes showing single-molecule magnet behavior. *Dalton Trans.*, **2012**, *41*, 2966 – 2971

43. Harris notation describes the binding mode as [X.Y1Y2Y3…Y*n*], whereX is the overall number of metals bound by the whole ligand, and eachvalue of Y refers to the number of metal atoms attached to the differentdonor atoms. See R. A. Coxall, S. G. Harris, D. K. Henderson, S.Parsons, P. A. Tasker and R. E. P. Winpenny, *Dalton Trans.*, 2000,2349–2356.

44. Lin, P.; Burchell, T. J.; Clerac, R.; Murugesu, M.; Dinuclear Dysprosium(III) Single-Molecule Magnets with a Largen Anisotrpic Barrier. *Angew. Chem. Int. Ed.*, **2008**, *47*, 8848 – 8851

45. Lin, S.; Xu, G.; Zhao, L.; Guo, Y.; Guo, Y.; Tang, J.; Observation of slow magnetic relaxation in triple-stranded lanthanide helicates. *Dalton Trans.*, **2011**, *40*, 8213 – 8217

46. Luis, F.; Bartolome, J.; Fernandez, J. F.; Tejada, J.; Hernandez, J. M.; Zhang, X. X.; Ziolo, R.; Thermally activated and field-tuned tunneling in Mn12Ac studied by ac magnetic susceptibility. *Phys. Rev. B.*, **1997**, *55*, 11448

47. Lin, P.; Sun, W.; Yu, M.; Li, G.; Yan, P.; Murugesu, M.; An unsymmetrical coordination environment leading to two slow relaxation modes in a Dy_2 single-molecule magnet. *Chem. Commun.*, **2011**, *47*, 10993 – 10995

48. Peng, J.; Ren, Y.; Kong, X.; Long, L.; Huang, R.; Zheng, L.; A series of di-, tri- and tetranuclear lanthanide clusters with slow magnetic relaxation for Dy_2 and Dy_4. *Cryst. Eng. Comm.*, **2011**, *13*, 2084 – 2090

49. Liang, L., a Peng, G.; Li, G.; Lan, Y.; Powell, A. K.; Deng, H.; In situ hydrothermal synthesis of dysprosium(III) single-molecule magnet with lanthanide salt as catalyst. *Dalton Trans.*, **2012**, *41*, 5816 – 5823

50. Joarder, B.; Chaudhari, A. K.; Rogez G.; Ghosh, S. K.; A carboxylate-based dinuclear dysprosium(III) cluster exhibiting slow magnetic relaxation behavior. *Dalton Trans.*, **2012**, *41*, 7695 – 7699

51. Liu, B.; Wang, B.; Wang, Z.; Gao, S.; Static field induced magnetic relaxations in dinuclear lanthanide compounds of $[phen_2Ln_2(HCOO)_4(HCOO)_{2-2x}(NO_3)_{2x}]$ (1, Ln = Gd and x = 0.52; 2, Ln = Er and x = 0.90; phen = 1,10-phenanthroline). *Sci. China Chem.*, **2012**, *55*, 926 – 933

52. Song, Y.; Luo, F.; Luo, M.; Liao, Z.; Sun, G.; Tian, X.; Zhu, Y.; Yuan, Z.; Liu, S.; Xu, W.; Feng, X.; The application of single-crystal-to-single-crystal transformation towards adjustable SMM properties. *Chem. Commun.*, **2012**, *48*, 1006 – 1008

53. Pointillart, F.; Klementieva, S.; Kuropatov, V.; Le Gal, Y.; Golhen, S.; Cador, O.; Cherkasov, V.; Ouahab, L.; A single molecule magnet behavior in a D_{3h} symmetry Dy(III) complex involving a quinone-tatrathiafulvalene-quinone bridge. *Chem. Commun.*, **2012**, *48*, 714 – 716

54. Xu, G.; Wang, Q.; Gamez, P.; Ma, Y.; Clerac, R.; Tang, J.; Yan, S.; Cheng, P.; Liao, D.; A promising new route towards single-molecule magnets based on the oxalate ligand. *Chem. Commun.*, **2010**, *46*, 1506 – 1508

55. Sulway, S. A.; Layfield, R. A.; Tuna, F.; Wernsdorfer, W.; Winpenny, R. E. P.; Single-molecule magnetism in cyclopentadienyl-dysprosium chlorides. *Chem. Commun.*, **2012**, *48*, 1508 – 1510

56. Layfield, R. A.; McDouall, J. J. W.; Sulway, S. A.; Tuna, F.; Collison, D.; Winpenny, R. E. P.; Influence of the N-Bridging Ligand on Magnetic Relaxation in an Organometallic Dysprosium Single-Molecule Magnet. *Chem. Eur. J.*, **2010**, *16*, 4442 – 4446

57. Mei, X.; Liu, R.; Wang, C.; Yang, P.; Li, L.; Liaoa, D.; Modulating spin dynamics of cyclic Ln^{III}-radical complexes (Ln^{III} = Tb, Dy) by using phenyltrifluoroacetylacetonate coligand. *Dalton Trans.*, **2012**, *41*, 2904 – 2909

58. a) Poneti, G.; Bernot, K.; Bogani, L.; Caneschi, A.; Sessoli, R.; Wernsdorfer, W.; Gatteschi, D.; A rational approach to the modulation of the dynamics of the magnetisation in

a dysprosium–nitronyl-nitroxide radical complex. *Chem. Commun.*, **2007**, *18*, 1807 – 1809

b) Xu, J. X.; Ma, Y.; Liao, D. Z.; Xu, G. F.; Tang, J. K.; Wang, C.; Zhou, N.; Yan, S. P.; Cheng, P.; Li, L. C.; Four new lanthanide-nitronyl nitroxide (Ln(III) = Pr(III), Sm(III), Eu(III), Tm(III)) complexes and a Tb(III) complex exhibiting single-molecule magnet behavior. *Inorg. Chem.*, **2009**, 48, 8890 – 8896

59. Bernot, K.; Pointillart, F.; Rosa, P.; Etienne, M.; Sessoli, R.; Gatteschia, D.; Single molecule magnet behavior in robust dysprosium-biradical complexes. *Chem. Commun.*, **2010**, *46*, 6458 – 6460

60. Tian, H.; Liu, R.; Wang, X.; Yang, P.; Li, Z.; Li, L.; Liao, D.; Magnetic Slow Relaxation in Cyclic Tb^{III}-Nitronyl Nitroxide Radical Complexes. *Eur. J. Inorg. Chem.*, **2009**, 4498 – 4502

61. Xu, J.; Ma, Y.; Liao, D.; Xu, G.; Tang, J.; Wang, C.; Zhou, N.; Yan, S.; Cheng, P.; Li, L.; Four New Lanthanide-Nitronyl Nitroxide (Ln^{III}=Pr^{III}, Sm^{III}, Eu^{III}, Tm^{III}) Complexes and a Tb^{III} Complex Exhibiting Single-Molecule Magnet Behavior. *Inorg. Chem.*, **2009**, *48*, 8890 – 8896

62. Ma, Y.; Xu, G.; Yang, X.; Li, L. Tang, J.; Yan, S.; Chenga, P.; Liao, D.; Pyrazine-bridged Dy_2 single-molecule magnet with a large anisotropic barrier. *Chem. Commun.*, **2010**, *46*, 8264 – 8266

63. Pointillart, F.; Le Gal, Y.; Golhen, S.; Cador, O.; Ouahab, L.; Single-Molecule Magnet Behaviour in a Tetrathiafulvalene-Based Electroactice Antiferromagnetically Coupled Dinculear Dysprosium(III) Complex. *Chem. Eur. J.*, **2011**, *17*, 10397 – 10404

64. a) Tang, J.; Hewitt, I.; Madhu, N. T.; Chastanet, G.; Wernsdorfer, W.; Anson, C. E.; Benelli, C.; Sessoli, R.; Powell, A. K.; Dysprosium Triangles Showing Single-Molecule Magnet Behaviour of Thermally Excited Spin States. *Angew. Chem. Int. Ed.*, **2006**, *45*, 1729 – 1733 b) Salman, Z.; Giblin, S. R.; Lan, Y.; Powell, A. K.; Scheuermann, R.; Tingle, R.; Sessoli, R.; Probing the magnetic ground state of the molecular Dysprosium triangle. *Cond. Matt.*, **2010**, *1*, 1 – 5 c) Salman, Z.; Giblin, S. R.; Lan, Y.; Powell, A. K.; Scheuermann, R.; Tingle, R.; Sessoli, R.; Probing the magnetic ground state of the molecular dysprosium triangle with muon spin relaxation. *Phys. Rev. B,* **2010**, *82*, 174427

65. Luzon, J.; Bernot, K.; Hewitt, I. J.; Anson, C. E.; Powell, A. K.; Sessoli, R.; Spin Chirality in a Molecular Dysprosium Triangle: The Archetype of the Noncollinear Ising Model. *Phys. Rev. Lett.*, **2008**, *100*, 247205

66. Liu, C.; Du, M.; Sanudo, C. E.; Echeverria, J.; Hu, M.; Zhang, Q.; Zhou, L.; Fang, S.; A luminescent linear trinuclear DyIII complex exhibiting slow magnetic relaxation of single ion origin. *Dalton Trans.*, **2011**, *40*, 9366 – 9369

67. Anwar, M. U.; Tandon, S. S.; Dawe, L. N.; Habib, F.; Murugesu, M.; Thompson, L. K.; Lanthanide Complexes of Tritopic Bis(hydrazone) Ligands: Single- Molecule Magnet Behavior in a Linear Dy^{III}_3 Complex. *Inorg. Chem.*, **2012**, *51*, 1028 – 1034

68. a) Hewitt, I. J.; Lan, Y.; Anson, C. E.; Luzon, J.; Sessoli. R.; Powell, A. K.; Opening up a dysprosium triangle by ligand oximation. *Chem. Commun.*, **2009**, *45*, 6765 – 6767 b) Guo, F.; Liu, J.; Leng, J.; Meng, Z.; Lin, Z.; Tong, M.; Gao, S.; Ungur, L.; Chibotaru, L. F.; Pure Trinuclear 4f Single-Molecule Magnets: Synthesis, Structures, Magnetism and Ab Initio Investigation. *Chem. Eur. J.*, **2011**, *17*, 2458 – 2466

69. Lin, S.; Zhao, L.; Guo, Y.; Zhang, P.; Guo, Y.; Tang, J.; Two New Dy_3 Triangles with Trinuclear Circular Helicates and Their Single-Molecule Magnet Behavior. Inorg. Chem., 2012, 51, Article ASAP

70. Lin, S.; Guo, Y.; Guo, Y.; Zhao, L.; Zhang, P.; Keab, H.; Tang, J.; Macrocyclic ligand encapsulating dysprosium triangles: axial ligands perturbed magnetic dynamics. *Chem. Commun.*, **2012**, *48*, 6924 – 6926

71. Peng, J.; Ren, Y.; Kong, X.; Long, L.; Huang, R.; Zheng, L.; A series of di-, tri- and tetranuclear lanthanide clusters with slow magnetic relaxation for Dy_2 and Dy_4. *Cryst. Eng. Comm.*, **2011**, *13*, 2084 – 2090

72. Gao, Y.; Xu, G.; Zhao, L.; Tang, J.; Liu, Z.; Observation of Slow Magnetic Relaxation in Discrete Dysprosium Cubane. *Inorg. Chem.*, **2009**, *48*, 11495 – 11497

73. Abbas, G.; Lan, Y.; Kostakis, G. E.; Wernsdorfer, W.; Anson, C. E.; Powell, A. K.; Series of Isostructural Planar Lanthanide Complexes $[Ln^{III}_4(\mu_3\text{-}OH)_2(mdeaH)_2\text{-}(piv)_8]$ with Single Molecule Magnet Behavior for the Dy_4 Analogue. *Inorg. Chem.*, **2010**, *49*, 8067 – 8072

74. Langley, S. K.; Chilton, N. F.; Gass, I. A.; Moubaraki, B.; Murray, K. S.; Planar tetranuclear lanthanide clusters with the Dy_4 analogue displaying slow magnetic relaxation. *Dalton Trans.*, **2011**, *40*, 12656 – 12659

75. Abbas, G.; Kostakis, G. E.; Lan, Y.; Powell, A. K.; Synthesis and characterization of isostructural tetranuclear lanthanide complexes $[Ln_4(\mu_3\text{-}OH)_2(ampdH_4)_2(piv)_{10}]\cdot 4CH_3CN$ (Ln = Sm, Eu, Gd, Tb, Dy, Ho, Er). *Polyhedron*, **2012**, *41*, 1 – 6

76. Gass, I. A.; Moubaraki, B.; Langley, S. K.; Batten, S. R.; Murray, K. S.; A π-π 3D network of tetranuclear μ_2/μ_3-carbonato Dy(III) bis-pyrazolylpyridine clusters showing single molecule magnetism features. *Chem. Commun.*, **2012**, *48*, 2089 – 2091

77. Xue, S.; Zhao, L.; Guo, Y.; Chenc, X.; Tang, J.; Field enhanced thermally activated mechanism in a square Dy_4 aggregate. *Chem. Commun.*, **2012**, *48*, 7031 – 7033

78. Xue, S.; Zhao, L.; Guo, Y.; Tang, J.; A novel windmill-type Dy^{III} [2 ×2] grid exhibiting slow magnetic relaxation. *Dalton Trans.*, **2012**, *41*, 351 – 353

79. Xue, S.; Zhao, L.; Guo, Y.; Deng, R.; Guo, Y.; Tang, J.; A series of tetranuclear lanthanide complexes comprising two edge-sharing triangular units with field-induced slow magnetic relaxation for Dy4 species. *Dalton Trans.*, **2011**, *40*, 8347 – 8352

80. Lin, P.; Korobkov, I.; Wernsdorfer, W.; Ungur, L.; Chibotaru, L. F.; Murugesu, M.; A Rare μ_4-O Centred Dy4 Tetrahedron with Coordination-Induced Local Chirality and Single-Molecule Magnet Behaviour. *Eur. J. Inorg. Chem.*, **2011**, 1535 – 1539

81. Guo, Y.; Xu, G.; Gamez, P.; Zhao, L.; Lin, S.; Deng, R.; Tang, J.; Zhang, H.; Two-Step Relaxation in a Linear Tetranuclear Dysprosium(III) Aggregate Showing Single-Molecule Magnet Behavior. *J. Am. Chem. Soc.*, **2010**, *132*, 8538 – 8539

82. Yang, P.; Gao, X.; Song, H.; Zhang, S.; Mei, X.; Li, L.; Liao, D.; Slow Magnetic Relaxation in Novel Dy_4 and Dy_8 Compounds. *Inorg. Chem.*, **2011**, *50*, 720 – 722

83. Ke,H.; Xu, G.; Guo, Y.; Gamez, P.; Beavers, C. M.; Teat, S. J.; TangJ.; A linear tetranuclear dysprosium(III) compound showing single-molecule magnet behavior. *Chem. Commun.*, **2010**, *46*, 6057 – 6059

84. Yang, P.; Gao, X.; Song, H.; Zhang, S.; Mei, X.; Li, L.; Liao, D.; Slow Magnetic Relaxation in Novel Dy_4 and Dy_8 Compounds. *Inorg. Chem.*, **2011**, *50*, 720 – 722

85. Chen, Y.; Tsai, Y.; Lee. G.; Yang, E.; The synthesis, structure, magnetic and luminescent properties of a new tetranuclear dysprosium (III) cluster. *J. Solid State Chem.*, **2012**, *185*, 166 – 171

86. Zheng, Y.; Lan, Y.; Anson, C. E.; Powell A. K.; Anion-Perturbed Magnetic Slow Relaxation in Planar {Dy_4} Clusters. *Inorg. Chem.*, **2008**, *47*, 10813 – 10815

87. Yan, P.; Lin, P.; Habib, F.; Aharen, T.; Murugesu, M.; Deng, Z.; Li, G.; Sun, W.; Planar Tetranuclear Dy(III) Single-Molecule Magnet and Its Sm(III), Gd(III), and Tb(III) Analogues Encapsulated by Salen-Type and *β*-Diketonate Ligands. *Inorg. Chem.*, **2011**, *50*, 7059 – 7065

88. Lin, S.; Zhao, L.; Ke, H.; Guo, Y.; Tang, J.; Guoa, Y.; Dou, J.; Steric hindrances create a discrete linear Dy_4 complex exhibiting SMM behavior. *Dalton Trans.*, **2012**, *41*, 3248 – 3252

89. Liu, C.; Zhang, D.; Hao, X.; Zhu, D.; Syntheses, Crystal Structures, and Magnetic Properties of Two *p-tert*-Butylsulfonylcalix[4]arene Supported Cluster Complexes with a Totally Disordered $Ln_4(OH)_4$ Cubane Core. *Cryst. Growth Des.*, **2012**, *12*, 2948 – 2954

90. Bi, Y.; Wang, X.; Liao, W.; Wang, X.; Deng, R.; Zhang, H.; Gao, S.; Thiacalix[4]arene-Supported Planar Ln4 (Ln = TbIII, DyIII) Clusters: Toward Luminescent and Magnetic Bifunctional Materials. *Inorg. Chem.*, **2009**, *48*, 11743 – 11747

91. Ritchie, C.; Speldrich, M.; Gable, R. W.; Sorace, L.; Kogerler, P.; Boskovic, C.; Utilizing the Adaptive Polyoxometalate $[As_2W_{19}O_{67}(H_2O)]^{14-}$ To Support a Polynuclear Lanthanoid-Based Single-Molecule Magnet. *Inorg. Chem.*, **2011**, *50*, 7004 – 7014

92. Guo, P.; Liu, J.; Zhang, Z.; Ungur, L.; Chibotaru, L. F.; Leng, J.; Guo, F.; Tong, M.; The First $\{Dy_4\}$ Single-Molecule Magnet with a Toroidal Magnetic Moment in the Ground State. *Inorg. Chem.*, **2012**, *51*, 1233 – 1235

93. Blagg, R. J.; Muryn, C. A.; McInnes, E. J. L.; Tuna, F.; Winpenny, R. E. P.; Single Pyramid Magnets: Dy_5 Pyramids with Slow Magnetic Relaxation to 40K. *Angew. Chem. Int. Ed.*, **2011**, *50*, 6530 – 6533

94. Blagg, R. J.; Tuna, F.; McInnes, E. J. L.; Winpenny, R. E. P.; Pantametallic lanthanide-alkoxide square-based pyramids: high energy barrier for thermal relaxation in a holmium single molecule magnet. *Chem. Commun.*, **2011**, *47*, 10587 – 10589

95. Gamer, M. T.; Lan, Y.; Roesky, P. W.; Powell, A. K.; Clerac, R.; Pentanuclear Dysprosium Hydroxy Cluster Showing Single-Molecule-Magnet Behavior. *Inorg. Chem.*, **2008**, *47*, 6581 – 6583

96. Peng, J.; Kong, X.; Ren, Y.; Long, L.; Huang, R.; Zheng, L.; Trigonal Bipyramidal Dy_5 Cluster Exhibiting Slow Magnetic Relaxation. *Inorg. Chem.*, **2012**, *51*, 2186 – 2190

97. Langley, S. K.; Moubaraki, B.; Forsyth, C. M.; Gass, I. A.; Murray, K. S.; Structure and magnetism of new lanthanide 6-wheel compounds utilizing triethanolamine as a stabilizing ligand. *Dalton Trans.*, **2010**, *39*, 1705 – 1708

98. Langley, S. K.; Moubaraki, B.; Murray, K. S.; Magnetic Properties of Hexanuclear Lanthanide(III) Clusters Incorporating a Central μ_6-Carbonate Ligand Derived from Atmospheric CO_2 Fixation. *Inorg. Chem.*, **2012**, *51*, 3947 – 3949

99. Hewitt, I. J.; Tang, J.; Madhu, N. T.; Anson, C. E.; Lan, Y.; Luzon, J.; Etienne, M.; Sessoli, R.; Powell, A. K.; Coupling Dy_3 Triangles Enhances Their Slow Magnetic Relaxation. *Angew. Chem. Int. Ed.*, **2010**, *49*, 6352 – 6356

100. Tian, H.; Wang, M.; Zhao, L.; Guo, Y.; Guo, Y.; Tang, J.; Liu, Z.; A Discrete Dysprosium Trigonal Prism Showing Single-Molecuel Magnet Behaviour. *Chem. Eur. J.*, **2012**, *18*, 442 – 445

101. Tian, H.; Guo, Y.; Zhao, L.; Tang, J.; Liu, Z.; Hexanuclear Dysprosium(III) Compound Incorporating Vertex- and Edge-Sharing Dy_3 Triangles Exhibiting Single-Molecule-Magnet Behavior. *Inorg. Chem.*, **2011**, *50*, 8688 – 8690

102. Guo, Y.; Chen, X.; Xue, S.; Tang, J.; Molecular Assembly and Magnetic Dynamics of Two Novel Dy_6 and Dy_8 Aggregates. *Inorg. Chem.*, **2012**, *51*, 4035 – 4042

103. Ke, H.; Zhao, L.; Guo, Y.; Tang, J.; A Dy_6 Cluster Displays Slow Magnetic Relaxation with an Edge-to-Edge Arrangement of Two Dy_3 Triangles. *Eur. J. Inorg. Chem.*, **2011**, 4153 – 4156

104. Bi, Y.; Xu, G.; Liao, W.; Du, S.; Deng, R.; Wang, B.; Calixarene-supported hexadysprosium cluster showing single molecule magnet behavior. *Sci. China Chem.*, **2012**, *55*, 967 – 972

105. Sharples, J. W.; Zheng, Y.; Tuna, F.; McInnes, E. J. L.; Collison, D.; Lanthanide discs chill well and relax slowly. *Chem. Commun.*, **2011**, *47*, 7650 – 7652

106. Yang, P.; Gao, X.; Song, H.; Zhang, S.; Mei, X.; Li, L.; Liao, D.; Slow Magnetic Relaxation in Novel Dy_4 and Dy_8 Compounds. *Inorg. Chem.*, **2011**, *50*, 720 – 722

107. Ke, H.; Gamez, P.; Zhao, L.; Xu, G.; Xue, S.; Tang, J.; Magnetic Properties of Dysprosium Cubanes Dictated by the M-O-M Angles of the $[Dy_4(\mu_3\text{-}OH)_4]$ Core. *Inorg. Chem.*, **2010**, *49*, 7549 – 7557

108. Guo, Y.; Chen, X.; Xue, S.; Tang, J.; Molecular Assembly and Magnetic Dynamics of Two Novel Dy_6 and Dy_8 Aggregates. *Inorg. Chem.*, **2012**, *51*, 4035 – 4042

109. Tian, H.; Zhao, L.; Guo, Y.; Guo, Y.; Tang, J.; Liub, Z.; Quadruple-CO_3^{2-} bridged octanuclear dysprosium(III) compound showing single-molecule magnet behavior. *Chem. Commun.*, **2012**, *48*, 708 – 710

110. Guo, F.; Guo, P.; Meng, Z.; Tong, M.; Slow magnetic relaxation in a novel heptanuclear Dy_7 cluster with five edge-sharing Dy_3 triangles. *Polyhedron*, **2011**, *30*, 3079 – 3082

111. Miao, Y.; Liu, J.; Li, J.; Leng, J.; Ou, Y.; Tong, M.; Two novel Dy8 and Dy11 clusters with cubane $[Dy_4(\mu_3\text{-}OH)_4]^{8+}$ units exhibiting slow magnetic relaxation behavior. *Dalton Trans.*, **2011**, *40*, 10229 – 10236

112. Gu, X.; Clérac, R.; Houri, A.; Xue, D.; Slow relaxation of the magnetization in high-nuclearity Ln-complexes. *Inorg. Chim. Acta.*, **2008**, *361*, 3873 – 3876

113. Zhao, L.; Xue, S.; Tang, J.; A Dodecanuclear Dysprosium Wheel Assembled by Six Vertex- Sharing Dy_3 Triangles Exhibiting Slow Magnetic Relaxation. *Inorg. Chem.*, **2012**, *51*, 5994 – 5996

114. Alexandropoulos, D. I.; Mukherjee, S.; Papatriantafyllopoulou, C.; Raptopoulou, C. P.; Psycharis, V.; Bekiari, V.; Christou, G.; Stamatatos, T. C.; A New Family of Nonanuclear Lanthanide Clusters Displaying Magnetic and Optical Properties. *Inorg. Chem.*, **2011**, *50*, 11276 – 11278

115. Ke, H.; Xu, G.; Zhao, L.; Tang, J.; Zhang, X.; Zhang, H.; A Dy10 Cluster Incorporates Two Sets of Vertex-Sharing Dy3 Triangles. *Chem. Eur. J.*, **2009**, *15*, 10335 – 10338

116. Miao, Y.; Liu, J.; Leng, J.; Lina, Z.; Tong, M.; Chloride template formation of {Dy12(OH)16}20+ cluster core incorporating 1,10-phenanthroline-2,9-dicarboxylate. *Cryst. Eng. Comm.*, **2011**, *13*, 3345 – 3348

117. Glerup, J.; Weihe, H.; Magnetic Susceptibility and EPR Spectra of μ-Cyano-bis[pentaamminechromium(III)] Perchlorate. *Acta Chem. Scand.*, **1991**, *45*, 444 – 448

118. Sheldrick, G. M.; A short history of SHELX. *Acta Cryst.*, **2008**, *A64*, 112 – 122

119. Oszlanyi, G.; Suto, A.; *Ab initio* structure solution by charge flipping. *Acta Cryst.*, **2004**, *A60*, 134 – 141